Studies on functions of envelope glycoproteins in replication and pathogenicity of influenza A viruses

（インフルエンザ A ウイルスの複製および病原性発揮における表面糖タンパク質の機能に関する研究）

Daiki Kobayashi

Contents

List of figures and tables

Abbreviations

3'SLN:	3'-sialyl-*N*-acetyllactosamine
AAALAC:	Association for Assessment and Accreditation of Laboratory Animal Care
ABSL:	animal biosafety level
AIV(s):	avian influenza virus(es)
BPL:	*Bauhinia purpurea* lectin
BSA:	bovine serum albumin
CPE:	cytopathic effect
DAPI:	4',6-diamidino-2-phenylindole
DMEM:	Dulbecco's modified Eagle's medium
dpi:	day(s) post-inoculation
ECA:	*Erythrina cristagalli* agglutinin
EEL:	*Euonymus europaeus* lectin
EGFR:	epidermal growth factor
ER:	endoplasmic reticulum
FITC:	fluorescein isothiocyanate
FUT:	fucosyltransferase
Gal:	galactose
GAPDH:	glyceraldehyde-3-phosphate dehydrogenase
GISAID:	Global Initiative on Sharing All Influenza Data
Glc:	glucose
GlcNAc:	*N*-acetylglucosamine
GnTI:	*N*-acetylglucosaminyltransferase I
HA:	hemagglutinin or hemagglutination

HAU:	hemagglutination unit
HEK293 cell(s):	human embryonic kidney 293 cell(s)
HI:	hemagglutination inhibition
HPAIV(s):	high pathogenicity avian influenza virus(es)
hpi:	hour(s) post-infection
HRP:	horseradish peroxidase
HSV-1:	herpes simplex virus type-1
IAV(s):	influenza A virus(es)
IGOT:	isotope-coded glycosylation site-specific tagging
IP:	immunoprecipitation
Km:	Michaelis constant
LacNAc:	galactose-*N*-acetylglucosamine
LC:	liquid chromatography
MAL-I:	*Maackia amurensis* lectin I
MD:	molecular dynamics
MDCK cell(s):	Madin-Darby canine kidney cell(s)
MEM:	Eagle's minimum essential medium
MFE:	minimum free energy
MOI:	multiplicity of infection
MS:	mass spectrometry
MUNANA:	2-(4-methylumbelliferyl)-α-D-*N*-acetylneuraminic acid
NA:	neuraminidase
NAVC:	neuraminidase from *Vibrio cholerae*
NeuAc:	*N*-acetylneuraminic acid
NeuGc:	*N*-glycolylneuraminic acid

NGS:	next generation sequencing
N-glycan(s):	*N*-linked glycan(s)
NP:	nucleoprotein
ORF:	open reading frame
OST:	oligosaccharyltransferase
PBS:	phosphate-buffered saline
PBST:	phosphate-buffered saline containing 0.05% Tween 20
PCR:	polymerase chain reaction
PDB:	Protein Data Bank
PEG:	polyethylene glycol
PNGase F:	peptide *N*-glycosidase F
RCA120:	*Ricinus communis* agglutinin 120
rHA(s):	recombinant hemagglutinin(s)
RT-qPCR:	reverse transcription-quantitative polymerase chain reaction
SDS-PAGE:	sodium dodecyl sulfate-polyacrylamide gel electrophoresis
SD:	standard deviation
SE:	standard error
Sia:	sialic acid
SNA:	*Sambucus Nigra* agglutinin
SSA:	*Sambucus sieboldiana* agglutinin
ST3Gal(s):	β-galactoside α2,3-sialyltransferase(s)
ST6Gal(s):	β-galactoside α2,6-sialyltransferase(s)
TBS:	Tris-buffered saline
TCA:	trichloroacetic acid
$TCID_{50}$:	50% tissue culture infectious dose

TJA-I:	*Trichosanthes japonica* agglutinin I
TJA-II:	*Trichosanthes japonica* agglutinin II
TMB:	3,3',5,5'-tetramethylbenzidine
TRITC:	tetramethyl rhodamine isothiocyanate
UEA-I:	*Ulex europaeus* agglutinin I
UTR:	untranslated region
WFA:	*Wisteria floribunda* agglutinin
WGA:	wheat germ agglutinin

Notes

Contents of the present thesis were published in the following articles:

1. **Kobayashi, D.**, Hiono, T., Adachi, R., Igarashi, M., Matsushita, T., Isoda, N., Sakoda, Y., and Matsuoka, K. Length and density of α2-3 sialyllacose-containing chains on glycopolymers determine receptor binding of avian influenza viruses. *Under submission*

2. **Kobayashi, D.**, Hiono, T., Arakawa, H., Ichikawa, T., Ban, H., Isoda, N., and Sakoda, Y. 2025. Deglycosylation and truncation in the neuraminidase stalk are functionally equivalent in enhancing the pathogenicity of a high pathogenicity avian influenza virus in chickens. *J Virol.,* **99**: e01478-24. DOI: 10.1128/jvi.01478-24

3. **Kobayashi, D.**, Hiono, T., Isoda, N., and Sakoda, Y. Neuraminidase of influenza A viruses induces global desialylation of host cells via its intracellular function. *Under submission*

Preface

Influenza A virus (IAV) has a broad range of hosts, including mammals and birds, and potentially causes acute respiratory infection [1]. The virus is classified into the family *Orthomyxoviridae* and the genus *Alphainfluenzavirus*, and featured by two surface glycoproteins: hemagglutinin (HA) and neuraminidase (NA) [2]. On the basis of antigenic properties of HA and NA, IAVs are classified into 16 HA subtypes (H1–16) and 9 NA subtypes (N1–9) [3–5]. HA is a trimeric type I transmembrane protein and binds to sialylated glycoconjugates with terminal sialic acid (*N*-acetylneuraminic acid [NeuAc] or *N*-glycolylneuraminic acid [NeuGc]: Sia) linked to penultimate galactose (Gal) via α2,3 or α2,6 linkages, facilitating viral attachment to host cells [6]. NA is a tetrameric type II transmembrane protein and is composed of four domains: a short cytoplasmic tail, a transmembrane region, a stalk, and a globular head [7]. The NA-head domain recognizes sialic acids at the non-reducing terminus of glycans and liberates them, leading to viral release from the infected cells [8, 9]. Therefore, the opposing functions of HA and NA during the viral infection must be balanced to maintain IAV infection cycles [10].

IAVs are widely distributed among avian species, including ducks, chickens, various other poultry and wild birds. The viruses cause avian influenza in birds and therefore are also known as avian influenza viruses (AIVs). Since viruses with all known HA and NA subtypes have been isolated from aquatic birds, these species are considered the natural hosts of AIVs [3, 5, 11]. The receptor-binding specificity of viral HA is a primary factor restricting host range [12], and research regarding the glycan specificity of HA has focused on the linkage between Sia and the penultimate Gal at the non-reducing terminus of sialoglycans [13, 14]. AIVs isolated from wild ducks predominantly bind to Siaα2,3Gal, whereas human viruses prefer Siaα2,6Gal [15]. Consistent with these preferences, duck intestinal epithelia are covered by Siaα2,3Gal, whereas human tracheal epithelia predominantly express Siaα2,6Gal [16, 17]. Furthermore, the presence of sialylated *N*-linked glycans (*N*-glycans) with multiple branches and extensions of galactose-*N*-acetylglucosamine (LacNAc) units has been reported in the target organs of IAVs in the host animals [18–21]. Given the complexity of host glycan structures, multivalent interactions of IAVs and complex glycans with various representations have to be assessed. For human influenza viruses, HAs derived from H3N2 IAVs prefer biantennary sialylated glycans with multiple LacNAc repeats. This preference is

facilitated by a bidentate binding mode, in which two receptor-binding pockets of adjacent HA monomers within a trimer engage two branches of a biantennary glycan [22, 23]. In contrast, AIVs are unable to adopt these bidentate binding modes due to the specific orientation of the terminal Sia and Gal [23]. Instead, AIVs bind multiple glycan complexes to facilitate stronger binding, while the multivalent interactions of AIVs with complex glycans with various representations remain poorly understood. Therefore, in Chapter I, the binding specificity of HA and whole virus particles derived from duck-origin AIVs was comprehensively analyzed using a series of sialoglycopolymers with various glycan densities and representations.

AIVs circulating among wild aquatic birds can be transmitted to chickens via intermediate hosts, such as domestic waterfowl and terrestrial birds. These viruses subsequently acquire increased pathogenicity through multiple replication cycles within the chicken population [24]. The insertion of polybasic amino acid residues at the HA cleavage site is necessary for AIVs to obtain the highly pathogenic phenotype in chickens [25], whereas several studies have demonstrated that the presence of these polybasic amino acids alone is insufficient [26, 27]. In addition to the insertion of polybasic amino acids at the HA cleavage site, viruses possessing short-stalk NA exhibit advantages regarding viral growth, pathogenicity, and transmissibility in chickens compared to those with a full-stalk NA [28–30]. In field conditions, viruses with a truncated-stalk NA have been isolated from diseased chickens and turkeys, whereas they have not been found in non-pathogenic viruses circulating in wild aquatic birds [31–34]. Furthermore, viruses harboring short-stalk NA have been selected during the laboratory adaptation of duck-derived viruses to chickens [35–38]. Consequently, the short-stalk NA is considered a hallmark of molecular evolution, reflecting the adaptation of AIVs from wild aquatic birds to chickens. Given that the stalk domain of NA is commonly glycosylated, previous studies have discussed the influence of stalk glycosylation on the biological function of NA and viral pathogenicity in chickens [39–41]. Since potential glycosylation sites in the NA-stalk region can be lost through stalk truncation under field conditions, the functional significance of amino acid deletion and loss of glycosylation in the NA stalk was further investigated in Chapter II. The results of virological assays, alongside site occupancy analyses of glycans on the NA-stalk region of a high pathogenicity avian influenza virus (HPAIV), indicated that the loss of glycosylation in the NA-stalk region contributes to

enhanced viral pathogenicity in chickens. The findings highlight the critical role of *N*-glycosylation in the NA stalk in the pathogenicity of HPAIV in chickens and provide novel insights into the evolutionary strategies of AIVs.

The primary function of NA in the IAV replication cycle is to liberate sialic acid from sialylated glycans as viral receptors during budding, thereby facilitating the efficient release of progeny virions [42]. NA also promotes viral motility on the surface of target cells by reducing the density of sialylated glycans and enabling escape from "decoy" receptors, such as mucins [43–46]. Since both HA and NA recognize the same sialylated glycans, the desialylation of receptor molecules by NA potentially limits superinfection at the cellular level [47, 48]. However, the intracellular maturation and function of NA remain poorly understood. To investigate how NA functions intracellularly, glycans displayed on IAV-infected cells were profiled by lectins, and global glycan desialylation, accompanied by glycan recapping with fucose, was found in the IAV-infected Madin-Darby canine kidney (MDCK) cells in Chapter III. These results suggest that intracellular NA function prepares virus particles for release prior to viral assembly, and potentially reducing the requirement for sialic acid hydrolysis during the final budding process. Furthermore, NA is an attractive target for the development of anti-influenza drugs, such as oseltamivir and zanamivir [49, 50]; however the inhibitory effects of these antivirals on intracellular NA functions were limited. The insights may be further applied to the development of improved antivirals designed to target both intracellular and extracellular NA activities.

Taken together, this study provides a comprehensive understanding of the fundamental functions of envelope glycoproteins that facilitate successful viral replication. By integrating insights into receptor preferences for glycan complexes, adaptation process associated with increased pathogenicity, and intracellular NA functions, this work offers a novel framework for understanding the evolutionary strategies of IAVs.

Chapter I

Length and density of α2-3 sialyllacose-containing chains on glycopolymers determine receptor binding of avian influenza viruses

Introduction

The glycan-binding specificity of HA is a crucial factor in determining host preference for IAV [12]. The binding preference of HA has typically focused on the linkage between terminal Sia and the penultimate Gal at the non-reducing end of glycans [13, 14]. Human influenza virus prefers Siaα2-6Gal, which is predominant on epithelial cells of the human trachea; in contrast AIV preferentially binds to glycans terminating with Siaα2-3Gal, which are commonly observed in the duck colon [16, 17]. Furthermore, respiratory tract tissues in human, swine, and chicken present sialylated *N*-glycans with multiple branches and extensions of LacNAc units [18–21]. Corresponding to the structural complexity of glycans in target tissues, certain HAs derived from human influenza viruses exhibit a preference for biantennary glycans with multiple LacNAc repeats [22, 23, 51]. Specifically, when a glycan contains more than three LacNAc units in its arm, the two sialic acid moieties can simultaneously access the receptor-binding pockets of adjacent HA monomers in a bidentate binding mode [23]. In the case of AIVs, the bidentate binding mode was not taken because of the spatial orientation of the terminal Sia and Gal [23]. Given the presence of complex glycans in host tissues, it is necessary to further characterize the binding preferences of IAVs toward multivalent glycan structures.

A single HA protein binds to the receptor with only millimolar affinity, whereas the multivalent receptor-ligand interactions of an AIV macromolecule allow the virus to attach at much lower concentrations because of the multivalent cluster effect [52]. To evaluate the impact of multivalency, various polyvalent sialoglycans, such as synthetic linear polymers, natural polymers, and dendrimers, have been used for binding analyses with viruses [53–55]. Since the synthesis of glycopolymers with multiple LacNAc units and antennas is laborious and time-consuming, binding analyses between viral particles and these glycopolymers are limited, and their multivalent interactions are poorly understood. In a previous study, LacNAc units in a glycan complex were mimicked by linking the terminal sialyllactose with subsequent polyethylene glycol (PEG) chains to simplify the synthetic procedure [56]. The glycan density was further controlled by polymerizing the glycomonomers with the corresponding number of acrylamide spacers. Using these synthetic polymers, the glycan binding of wheat germ agglutinin (WGA) and the inhibitory effect of glycans against mumps virus entry were assessed [56, 57]. These

studies demonstrated that the local glycan density is a critical factor in binding of WGA and mumps virus. The present study expands upon this work by analyzing glycan binding of HA and AIV particles using the sialoglycopolymers that incorporate various glycan densities and LacNAc repeats. This approach facilitates an assessment of the complex nature of the interactions between AIV particles as macromolecules and glycan clusters.

Materials and Methods

Viruses and cells

An influenza A virus, A/duck/Mongolia/54/2001 (H5N2) (Dk/MNG), was isolated from the fecal sample of a migratory duck in Mongolia [58]. A/duck/Hong Kong/960/1980 (H6N2) (Dk/HK) was kindly provided by Prof. Ken F. Shortridge (University of Hong Kong, Hong Kong SAR; Kikutani *et al*. [26]). Viruses were propagated in 10-day-old embryonated chicken eggs at 35°C for 48 h, and these infectious allantoic fluids were stored at –80°C until use as virus stocks.

HEK293S GnTI–/– cells [60], which lack a functional *N*-acetyl-glucosaminyltransferase I gene, was maintained in pyruvate-free Dulbecco's modified Eagle's medium (DMEM; Thermo Fisher Scientific, Waltham, MA, USA) supplemented with 0.3 mg/mL L-glutamine (Nacalai Tesque, Kyoto, Japan), 100 U/mL penicillin G (Meiji Seika Pharma, Tokyo, Japan), 0.1 mg/mL streptomycin (Meiji Seika Pharma), 8 μg/mL gentamicin (Takata Pharmaceutical, Saitama, Japan), and 10% calf serum (Cambrex Bio Science Walkersville, Walkersville, MD, USA). The cells were maintained at 37°C in a 5% CO_2 atmosphere.

Expression of recombinant HAs (rHAs)

cDNAs encoding the HA genes Dk/MNG and Dk/HK were previously cloned into the pCD5 expression vector [59, 61]. rHAs were expressed in human embryonic kidney 293 (HEK293S GnTI–/–) cells, which lack functional *N*-acetyl-glucosaminyltransferase I gene, and purified from cell culture supernatants as previously described [62].

Glycopolymers

A series of glycopolymers synthesized in previous studies was used [56, 57, 63]. The glycans recognized by AIVs are typically terminated with Siaα2-3Galβ1-4GlcNAc in natural settings, while the synthesis of glycopolymers was carried out by replacing with Siaα2-3Galβ1-4Glc due to the low availability of Siaα2-3Galβ1-4GlcNAc (Figure 1A, B). To mimic the glycans extended with repeating LacNAc units, tri-, hexa-, and nonaethylene glycol linkers corresponding to mono-, di-, and tri-LacNAc repeats were connected to the Siaα2-3Galβ1-4Glc trisaccharide (Figure 1B). To control the local density of glycans on the glycopolymers, the glycosyl monomer was polymerized with or

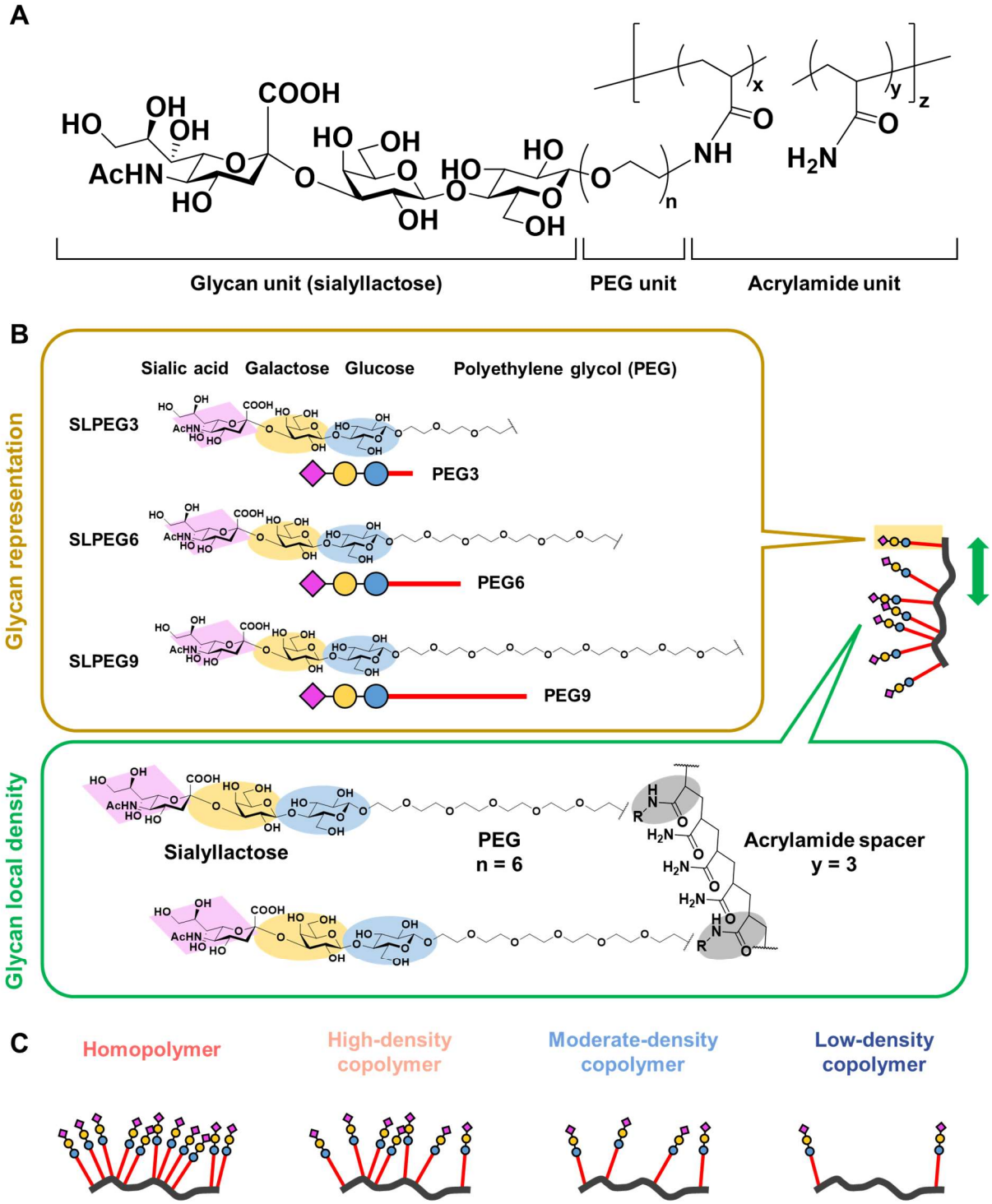

Figure 1. Structure of sialoglycopolymers. (A, B) Structure of a glycan unit containing sialyllactose and a spacer unit adjusting the local density of glycans in a polymer is indicated. (C) Composition of sialoglycopolymers with various glycan densities used in this study. Each polymer is named as a homopolymer, a high-density copolymer, a moderate-density copolymer, and a low-density copolymer based on the ratio of glycan and spacer units and is represented by symbols.

without acrylamide as spacer units. Herein, "SLPEG(n) x:y" indicates the composition of glycopolymers, where n represents the number of PEG units (tri-, hexa-, or nonaethylene glycol), and x:y indicates the average ratio of sugar units and spacer units within the acrylamide chain (Figure 1A, B). Hereafter, SLPEG(n) 1:0 is referred to as a homopolymer, SLPEG(n) 1:4.2–4.6 as high-density, SLPEG(n) 1:12–13 as moderate-density, and SLPEG (n) 1:26–32 as low-density copolymers (Figure 1C). The composition of PEG and acrylamide units in the series of glycopolymers is listed in Table 1. To normalize the amount of Siaα2-3Galβ1-4Glc trisaccharide across the following analyses, the sugar unit content was calculated.

Solid-phase direct binding assay

The glycan-binding specificity of rHAs and viruses was assessed via a solid-phase direct binding assay, as previously described [61], using glycopolymers [57, 63]. In this assay, the concentrations of the glycopolymers with different molecular weights were adjusted to contain equivalent amounts of glycan units. By this means, an equivalent amount of Siaα2-3Galβ1-4Glc trisaccharide with different local densities was immobilized on the plate. Briefly, the concentration of each glycopolymer was adjusted to 1.0 μM based on the content of the sugar unit. Then, 50 μL of two-fold serial dilutions of the glycopolymer solution was added to each well of Nunc Immobilizer Amino C8/F8 96-well strip well microplates (Thermo Fisher Scientific), and the plates were incubated at 37°C for 1 h. Subsequently, each well was blocked with phosphate-buffered saline containing 0.05% Tween 20 (PBST) containing 2% bovine serum albumin (BSA, Merck KGaA, Darmstadt, Germany) at room temperature for 1 h. Next, 5 μg/mL of rHA was precomplexed with Strep-tag mouse monoclonal antibody (IBA Lifesciences GmbH, Göttingen, Germany, 1:2000 dilution) and with goat anti-mouse IgG-horseradish peroxidase (HRP) conjugate (Bio-Rad Laboratories, Hercules, CA, USA, 1:2000 dilution) before incubation for 30 min on ice in PBST containing 0.5% BSA. After washing the plates, 50 μL of complexes were added and incubated at room temperature for 1 h. Following washing, 100 μL of 3,3',5,5'-tetramethylbenzidine (TMB) substrate solution was added to each well. The reaction stopped using 50 μL of 2 N H_2SO_4, and absorbance at 450/630 nm was measured using a MULTISKAN JX (Thermo Fisher Scientific). Data are presented as mean values of three technical replicates with standard errors.

Table 1. Composition of sialoglycopolymers with various glycan representations and densities.

Polymer SLPEG(n) x:y	Polymer composition				Sugar Content	$\overline{Mw}$[a]	$\overline{Mw}$ / $\overline{Mn}$[b]	Sugar unit content
	n	x	y	z	(wt%)	(kDa)		(mol/g)
SLPEG3 1:0	3	1	0	189	100	155	2.61	1.22×10^{-3}
SLPEG3 1:4.2			4.2	245	73	270	2.08	8.95×10^{-4}
SLPEG3 1:12			12	266	49	407	1.16	5.98×10^{-4}
SLPEG3 1:32			32	157	26	407	1.17	3.23×10^{-4}
SLPEG6 1:0	6	1	0	308	100	293	2.02	1.05×10^{-3}
SLPEG6 1:4.3			4.3	270	76	333	1.84	7.96×10^{-4}
SLPEG6 1:12.3			12.3	213	52	354	2.24	5.48×10^{-4}
SLPEG6 1:26.2			26.2	196	34	536	1.39	3.55×10^{-4}
SLPEG9 1:0	9	1	0	148	100	160	2.99	9.23×10^{-4}
SLPEG9 1:4.6			4.6	175	77	239	1.86	7.09×10^{-4}
SLPEG9 1:13			13	193	54	347	1.2	4.98×10^{-4}
SLPEG9 1:26			26	112	37	321	1.19	3.41×10^{-4}

[a] $\overline{Mw}$ indicates weight-average molecular weight.
[b] $\overline{Mn}$ indicates number-average molecular weight.

For the solid-phase direct binding assay using the virus, an influenza virus suspension (16 hemagglutination units [HAU] in phosphate-buffered saline [PBS]), with 10 nM oseltamivir carboxylate (oseltamivir acid; Chemscene, Monmouth Junction, NJ, USA), was added to each well after the blocking step described above. The plates were then incubated at 4°C for 16 h. After washing, mouse H5 and H6 HA monoclonal antibodies (H3/2 has been described by Hiono *et al.* [31]; 85-2-2 was a kind gift from Prof. Ayato Takada and previously established using A/shearwater/South Australia/1/1972 [H6N5], respectively) were added to each well, and the plates were incubated at 4°C for 2 h. The wells were then washed and incubated with a goat anti-mouse IgG-HRP conjugate (Bio-Rad, 1:2000 dilution) at 4°C for 2 h. After washing, the binding of the virus particles was detected using a TMB substrate, and the absorbance was measured using a MULTISKAN JX (Thermo Fisher Scientific), as described above.

Hemagglutination-inhibition (HI) assay

Two-fold serially diluted fetuin (Sigma-Aldrich Co. LLC, Burlington, MA, USA) and SLPEG6 polymers were prepared, and 25 μL of the solutions were dispensed in a 96-well plate with a round bottom (Corning, Corning, NY, USA). An equivalent volume of viral solution containing 4 HAU/50 μL of Dk/HK in PBS was mixed, and the plate was incubated at 4°C for 30 min. Next, 50 μL of 0.5% chicken red blood cells in PBS was added and placed at 4°C for 30 min. Chicken serum against Dk/HK was used as a positive control.

***In silico* structural model of the binding of a trimeric HA of Dk/HK bound to 3'-sialyl-*N*-acetyllactosamine (3'SLN)**

The three-dimensional structure of the H6 HA of Dk/HK was constructed based on the cocrystal structure of trimeric HA of A/Taiwan/2/2013 (H6N1) with 3'SLN (Protein Data Bank [PDB] ID code 4XKE [32]), as described previously [66].

Molecular dynamics (MD) simulation of glycopolymers

The three-dimensional structures of SLPEG6 (1:0 and 1:4) and SLEPG9 (1:0 and 1:5) were constructed using Molecular Operating Environment software (version 2022; Chemical Computing Group, Montreal, Canada). MD simulations were conducted using the Desmond simulation package in the Schrödinger Suite 2022-4 (Schrödinger release

2022-4; DE Shaw Research, New York, NY, USA). The OPLS4 force field was used for the energy minimization and MD simulations. The systems were solvated in a 10 Å cubic box with the simple point charge water together with 0.15 M NaCl to produce the condition of physiological saline. After minimization and relaxation, the production MD simulations of 1 μs were performed for the SLPEG6 and 9 structures in the NpT ensemble at 300 K and 1 bar using Langevin dynamics. The obtained models were visualized using the PyMol software, and the distance between the two oxygen atoms at the C-1 hydroxyl group of glucose (Glc) was measured.

Ethics statements

All experiments involving genetically modified organisms were authorized by the Safety Committee on Genetic Recombination Experiments of Hokkaido University (approval no. 2021-026). This study was approved by the Biosafety Management Committee on Pathogens and Other Hazardous Agents of the Faculty of Veterinary Medicine, Hokkaido University (approval nos. 2024-1-68 and 2024-1-71).

Results

Binding specificity of rHAs derived from two duck-origin AIVs to glycopolymers

The glycan-binding preference of two duck-origin AIVs to glycopolymers terminating with Siaα2-3Galβ1-4Glc triose with various polyethylene glycol (PEG) and acrylamide units was investigated via solid-phase direct binding assay. To assess the glycan binding specificity of AIVs, two duck isolates, A/duck/Hong Kong/960/1980 (H6N2) (Dk/HK) and A/duck/Mongolia/54/2001 (H5N2) (Dk/MNG), were selected for the present study, because rHAs of these strains have exhibited distinct glycan-binding specificities via glycan microarrays: the rHA of Dk/HK accepted α2,3 sialosides with multiple LacNAc without branch via a glycan microarray analysis [59], whereas the rHA of Dk/MNG preferentially bound to biantennary glycans terminating Siaα2-3Gal with multiple LacNAc repeats rather than linear glycans [61]. First, the binding of trimeric rHAs derived from Dk/HK and Dk/MNG to sialoglycopolymers was assessed (Figure 2). Both rHAs bound strongly to the series of SLPEG6 polymers, although binding to the homopolymer and low-density copolymers was slightly weaker than binding to the high- and moderate-density copolymers. However, the binding of these rHAs to the SLPEG9 homopolymer was markedly weaker than that to the other copolymers. The results indicate that these rHAs have preferable combinations of local density and representation of the Siaα2-3Galβ1-4Glc units to achieve stronger binding. In addition, the rHA of Dk/HK showed much weaker binding to low-density SLPEG3 copolymers than to the SLPEG3 homopolymer or high-density SLPEG3 copolymer, whereas the rHA of Dk/MNG was less affected by the local density of SLPEG3 glycopolymers. The binding of the SLPEG3 1:12 polymer to AIV particles and rHAs was lower than that of the other SLPEG3 polymers for unknown reasons. The results indicate that the preferred combination of local density and representation of the Siaα2-3Galβ1-4Glc units may differ among the rHAs.

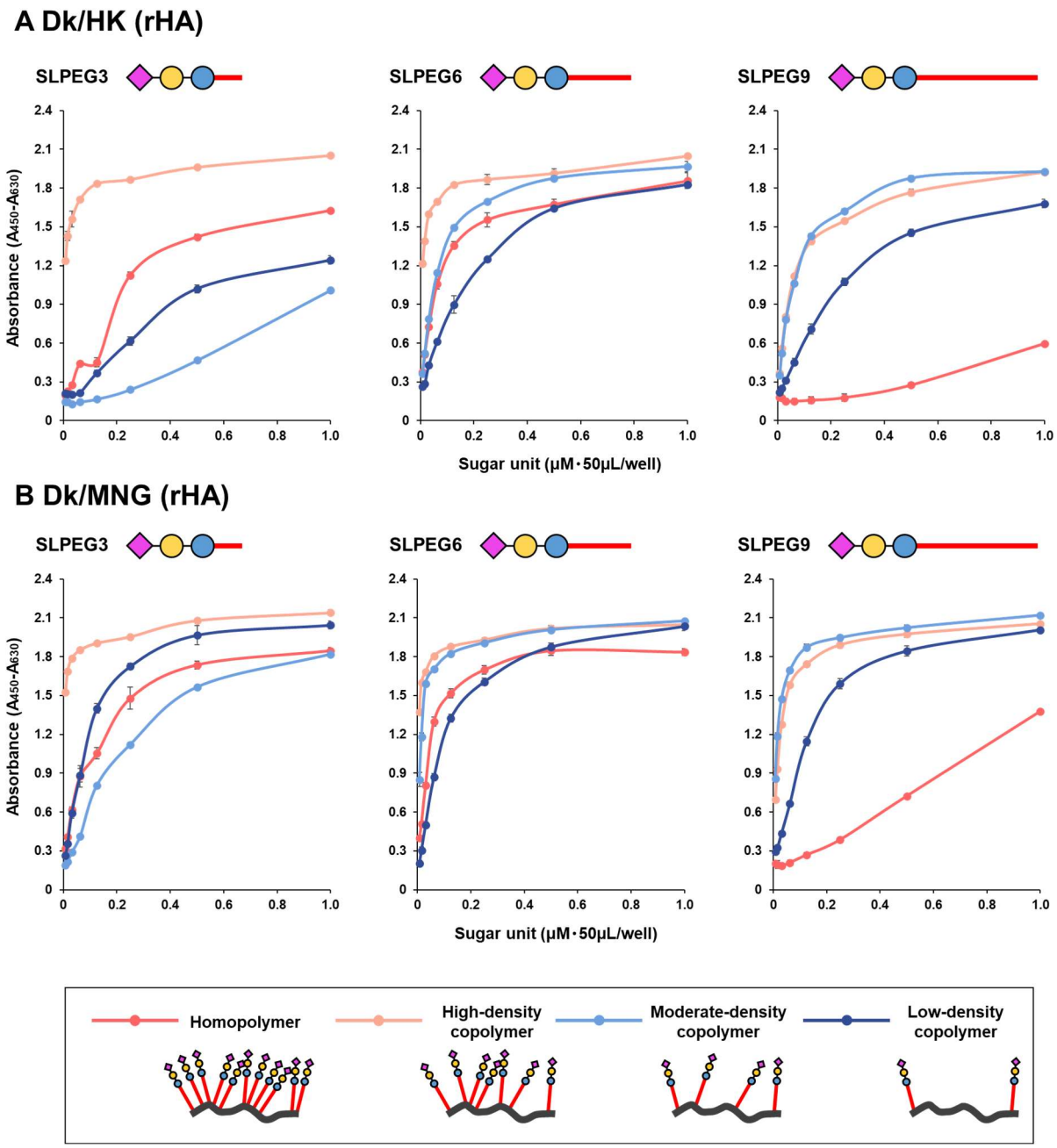

Figure 2. Density-dependent glycan-binding specificity of rHAs of duck-origin AIVs to glycopolymers. Binding of rHAs of Dk/HK (A) and Dk/MNG (B) to glycopolymers. Homopolymer (red), high-density copolymer (orange), moderate-density copolymer (light blue), and low-density copolymer (dark blue) were used for a solid-phase direct binding assay. Data are presented as the mean ± standard error (SE) in triplicate.

High-density glycans of the homopolymer interfered with the binding of HA trimers through steric hindrance

Next, the binding forms of the trimeric HA and sugar units were predicted by *in silico* modeling to determine the structural basis of the specific preference of rHAs for polymers with various sugar unit densities. For this, the structure of a trimeric HA of Dk/HK in complex with Siaα2-3Galβ1-4GlcNAc triose was modeled via homology modeling to measure the distance between two glycan-binding pockets within a single HA trimer. Based on the distance between the two oxygens positioned at the C-1 hydroxyl group of antepenultimate *N*-acetyl glucosamine (GlcNAc) molecules in adjacent monomer models, the distance between two glycan-binding pockets was calculated as 45.3 Å (Figure 3A; PDB accession number 4XKE; Tzarum *et al*. [32]). Because glycans are flexible and dynamic in nature, the distance between two adjacent Siaα2-3Galβ1-4Glc units in a polymer was determined as its average and maximum lengths using MD simulations. To mimic high-density copolymers and homopolymers, the SLPEG6 and 9 units present on the two acrylamide units, with or without spacer units, were used in the simulations. Through the 1000 snapshots of a 1 μs MD simulation trajectory, distances between two Siaα2-3Galβ1-4Glc units in SLPEG6 polymers were calculated to be 18.6 Å on average and 36.6 Å at maximum (with four spacer units) and 16.3 Å on average and 30.4 Å at maximum (without a spacer unit) (Figure 3B, C). These distances in SLPEG9 units were calculated to be 24.9 Å on average and 52.3 Å at maximum (with five spacer units) and 19.9 Å on average and 42.2 Å at maximum (without a spacer unit) (Figure 3D, E). Those average distances were shorter than the distance of Siaα2-3Galβ1-4GlcNAc motifs in two binding pockets in an HA trimer (45.3 Å), except that only a few scenes mimicking high-density SLPEG9 copolymer reached that length. These results indicate that the distance between two adjacent Siaα2-3Galβ1-4Glc units in SLPEG6 and 9 polymers subjected to MD simulations does not reach two binding pockets on a trimeric HA, indicating the unavailability of its bidentate binding with adjacent Siaα2-3Galβ1-4Glc motifs in the polymers. Accordingly, rHAs appear to bind multivalently to glycans rather than a bidentate binding mode. Given that the rHAs exhibited poor binding avidity to the SLPEG9 homopolymer (Figure 2), these results suggest that majority of Siaα2-3Galβ1-4Glc motifs in the homopolymers were not engaged in the interaction with HA. Instead, the high density-glycans likely hindered binding via a negative clustering effect.

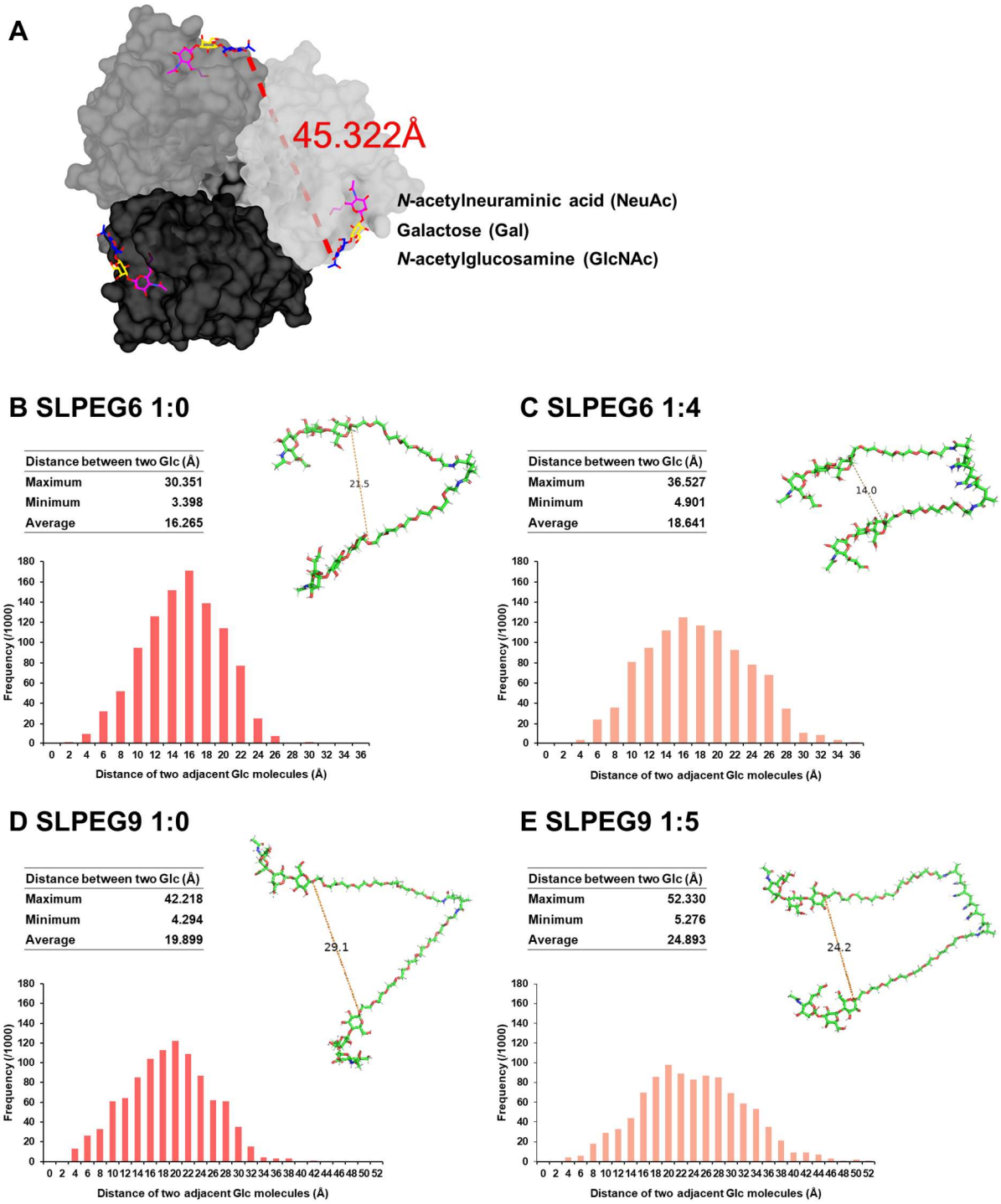

Figure 3. Distance between two glycans interacted with an HA trimer and MD simulations of a unit of sialoglycopolymers. (A) A model of Dk/HK HA with sialyl-LacNAc was constructed based on the cocrystal structure of HA from A/Taiwan/2/2013 (H6N1) with sialyl-LacNAc. The distance between two oxygens at the C-1 hydroxyl group of GlcNAc is indicated with a red broken line. (B–E) The distance between two Siaα2-3Galβ1-4Glc motifs in a glycopolymer was calculated based on the MD simulations. The simulations were performed with glycan units mimicking SLPEG6 1:0 (B), SLPEG6 1:4 (C), SLPEG9 1:0 (D), and SLPEG9 1:5 (E). The frequency of the distance between two oxygens at the C-1 hydroxyl group of Glc was visualized.

Clustering HAs on an AIV particle compensates for weak HA binding to lower-density glycans

As HA does not establish a bidentate binding mode to avian-type receptors [23], the focus of this study was on the cluster effect of lectin-glycan interactions. HA is a weak-affinity lectin monomer; therefore, polyvalent interactions of multiple HAs on a viral particle with a cluster of sialic acids are required for efficient viral attachment to cells, leading to subsequent viral entry [67]. A solid-phase direct binding assay of virus particles was performed to evaluate the contribution of HA clusters to the glycan-binding properties of the virus particles. The assay was conducted at 4°C in the presence of the NA inhibitor oseltamivir carboxylate to eliminate the contribution of NA enzymatic activity. Dk/HK particles bound strongly to high- to low-density SLPEG6 and 9 copolymers, but not to homopolymers with the highest density (Figure 4A). The virus also preferred SLPEG3 low and high-density copolymers but not the SLPEG3 homopolymer and moderate-density copolymer. Because the rHA from Dk/HK exhibited weaker binding to the low-density copolymers independent of the representation of Siaα2-3Galβ1-4Glc motifs (Figure 2A), clustering HAs on a virus particle compensated for their weak binding to low-density glycans by employing multivalent HA-glycan interactions. The Dk/MNG particles exhibited strong binding to high- and moderate-density SLPEG6 copolymers, whereas their binding to the low-density SLPEG6 copolymer and homopolymer was markedly weaker (Figure 4B). Binding to the low-density copolymer reached a plateau at lower concentrations. In contrast, the virus was bound to low- to high-density SLPEG9 copolymers, except for the SLPEG9 homopolymer. Additionally, the Dk/MNG particles also preferred the high-density SLPEG3 copolymer and bound relatively weakly to the low-density SLPEG3 copolymer, whereas binding to the low-density copolymer and homopolymer was clearly low. The glycan density preference of Dk/MNG particles was comparable to that of rHA, indicating that the impact of the HA clusters of Dk/MNG on the glycan-binding properties was limited compared to that of Dk/HK. These results indicate that HA clusters on virus particles contribute to the compensation for weak binding to lower-density sialoglycans, depending on the viral strain.

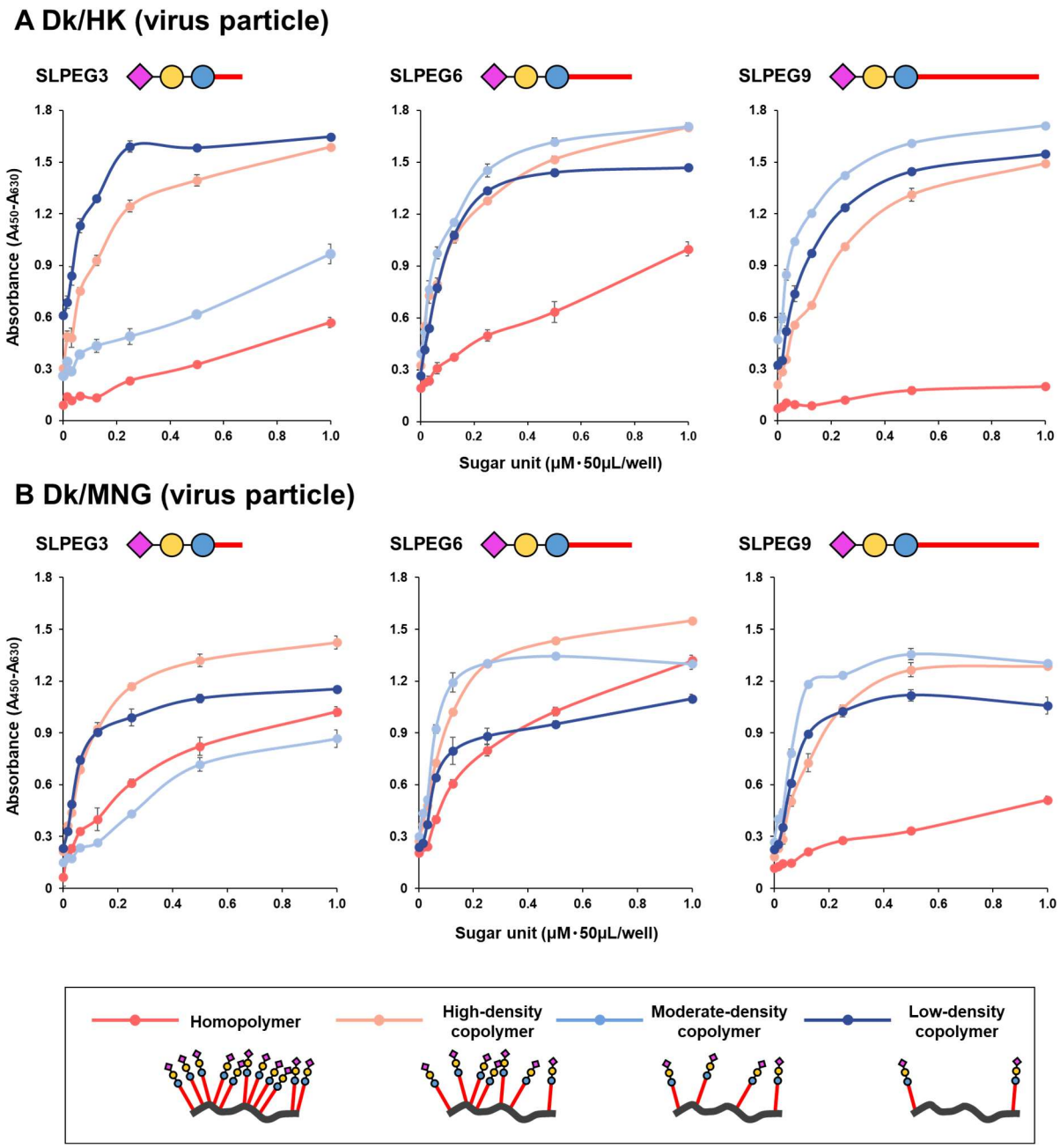

Figure 4. Density-dependent glycan-binding specificity of duck-origin AIVs to glycopolymers. Binding of virus particles of Dk/HK (A) and Dk/MNG (B) to glycopolymers in the presence of an NA inhibitor. Homopolymer (red), high-density copolymer (orange), moderate-density copolymer (light blue), and low-density copolymer (dark blue) were used for solid-phase direct binding assays. Data are presented as the mean ± SE in triplicate.

HI ability of synthetic glycopolymers

Finally, the antiviral potential of these glycopolymers was evaluated via an HI test using the Dk/HK virus and chicken erythrocytes. A series of SLPEG6 glycopolymers showed slight inhibition of hemagglutination in the presence of 10 nM oseltamivir carboxylate, whereas inhibition was not observed when oseltamivir carboxylate was not used (Figure 5). These results suggested that the hydrolysis of glycopolymers via the NA activity of the virus impaired the performance of the sialylglycopolymers in HI test.

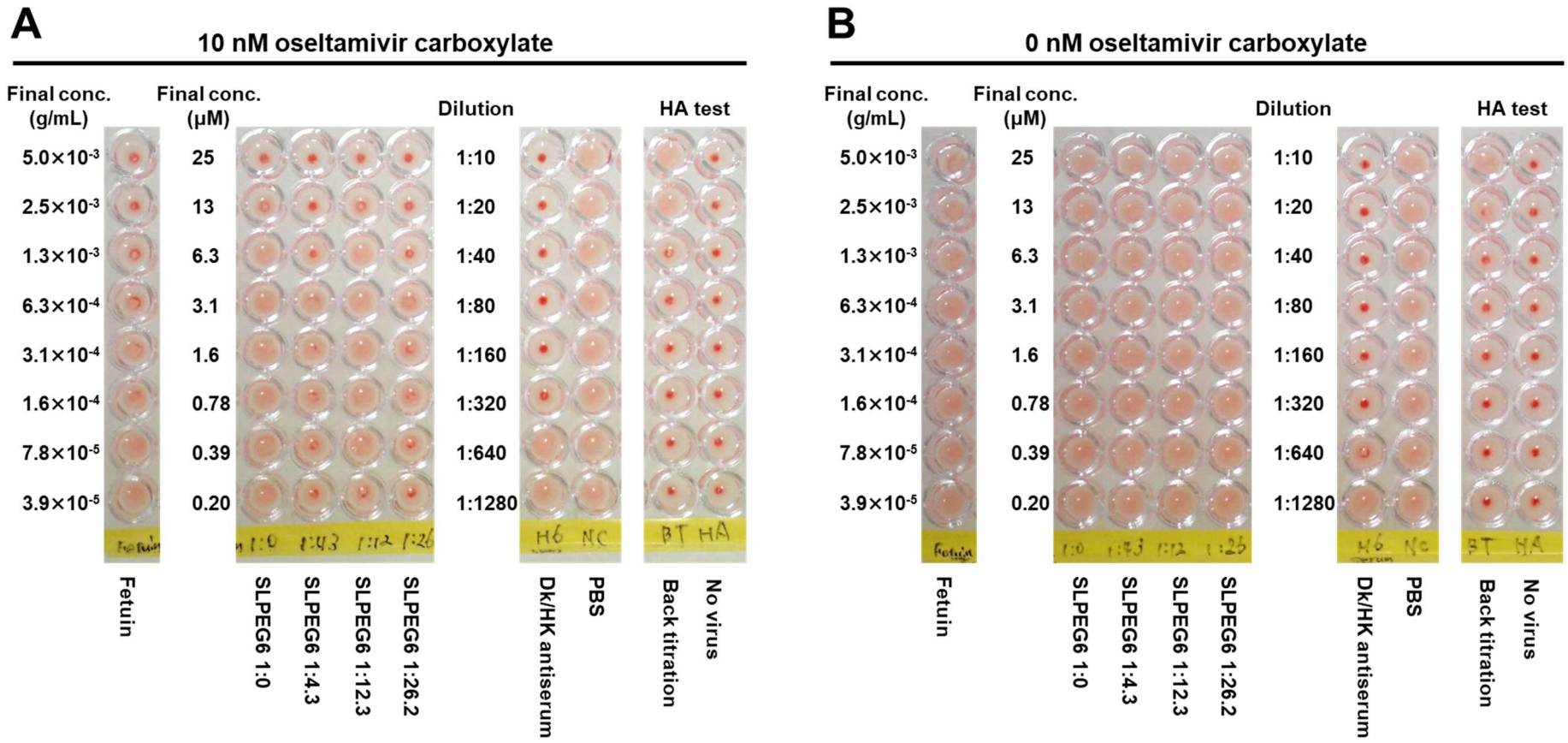

Figure 5. HI ability of synthetic sialylglycopolymers. The antiviral potentials of the glycopolymers were evaluated by HI assays using Dk/HK viral particles. To inhibit the NA activity on viral particles, 10 nM oseltamivir carboxylate was applied to the assay (A), and the inhibitory ability of these polymers was compared to the absence of oseltamivir carboxylate (B).

Discussion

Protein-carbohydrate interactions, such as HA-glycan interactions, are generally weak and require multivalent interactions for biological functions [68, 69]. However, the glycan density that facilitates the receptor binding of HA proteins or virus particles has not been previously understood. To address this, a series of glycopolymers harboring various glycan densities was used for binding analyses of HAs and AIVs in this study. This approach enabled to address the basis of multivalent interactions between glycans and viral particles. These results demonstrate that an extremely high density of glycans negatively affects the binding of rHAs to viral particles. Moreover, it has been suggested that each viral strain has preferred combinations of local density and representation of glycans via HA-glycan interactions.

The HAs of some human influenza viruses, especially recent H3N2 viruses, exclusively require the extension and branching of LacNAc units for their glycan partners, whereas others do not [22, 70]. Similarly, rHA from duck-origin AIVs also showed various binding preferences for extended and/or multiple antennary glycans with poly-LacNAc chains, which were previously assessed using glycan arrays. Specifically, rHA of Dk/HK preferentially binds to extended glycans with poly-LacNAc repeats, whereas that of Dk/MNG prefers multiple antennary glycans to extended glycans [59, 61]. Consistent with observations in glycan arrays, this study demonstrates that the rHA of Dk/HK exhibited much stronger binding to moderate- and low-density SLPEG3 copolymers, as well as SLPEG6 polymers, compared to the SLPEG3 homopolymer and high-density SLPEG3 copolymer. These results indicate that the rHA of Dk/HK necessitates extended glycans rather than higher-density glycans. In contrast, rHA of Dk/MNG generally preferred intermediate-density glycans, such as high- and moderate-density copolymers, and was less affected by glycan extension, indicating that rHA of Dk/MNG was more sensitive to glycan density than to glycan extension. These results suggest that the approach of mimicking the complex backbone of glycans with simple polymers enables to address the glycan density preference of AIVs without requiring an extremely laborious glycan synthesis procedure. These results highlight the differences in glycan preferences between the two rHAs of duck-derived AIVs.

The present study assessed the binding specificity of a series of sialoglycopolymers using both rHAs and viral particles. rHAs were precomplexed with primary and secondary antibodies to enhance the binding between HAs and glycans. Theoretically, the glycan binding of rHAs observed in this study reflects the sum of binding via a maximum of four trimers with multivalency, as rHA-antibody complexes were used for the binding analyses. A previous study using fluorescently labeled HA illustrated that the free HA trimer failed to detect sialosides in a glycan microarray, whereas rHAs pre-complexed with primary and secondary antibodies successfully detected glycans in the array [23]. Free trimeric HA can recognize glycans in tissue sections, highlighting the requirement for substantial glycan density for free trimeric HA [23]. The present study further showed that HA clusters in the glycan-binding properties of AIV particles compensated for the weaker binding of HA to low-density glycans, such as the SLPEG6 low-density copolymer, via positive clustering effects, as observed in natural settings (Figures 2 and 4). Because the contribution of positive clustering effects to HA-glycan binding was different between the two strains, the strain-dependent density or flexibility of HAs on viral particles could reflect these observations. In contrast, HA clusters of particles attenuate viral binding to high-density glycans, such as SLPEG6 and 9 homopolymers, via negative clustering effects. These observations may be related to the number of HAs interacting with sialoglycans or the incompatibility of glycan density with the HA clusters of a viral particle as a macromolecule [68, 71]. These analyses should support further understanding of the nature of interactions between AIVs and sialoglycans.

The potential use of synthetic glycopolymers as antiviral agents against influenza viruses has long been discussed. Glycopolymers bearing sialyllactoses inhibit the hemagglutination of AIV only at high concentrations [72]. In this study, it was expected that the sialyllactose density of the glycopolymer would influence its ability to inhibit hemagglutination. However, in the present study, a series of sialylglycopolymers did not show any inhibition in the absence of an NA inhibitor (Figure 5). Moreover, no obvious difference in the HI ability was observed for polymers with different glycan densities. Thus, glycan hydrolysis by NA may be a cause of the low inhibitory potential of sialoglycopolymers against AIVs as an antiviral agent. Therefore, further improvement of sialoglycopolymers has to be considered to escape NA activity.

In conclusion, the present study assessed the glycan binding of HAs and AIV particles to a series of sialoglycopolymers terminating with Siaα2-3Galβ1-4Glc units with various glycan densities and extensions. This approach illustrated the subtly different glycan-binding preference of HA among virus strains to combinations of local density and representation of Siaα2-3Galβ1-4Glc moieties. These findings imply elaborate protein-carbohydrate interactions via multivalent receptor-ligand binding between AIV particles and sialoglycans. In contrast, sialoglycopolymers had low potential for inhibitory effects against AIVs. Thus, further improvements are needed to reduce the hydrolysis of sialoglycans by NA and to optimize the interactions between AIV particles and sialoglycans for antiviral activity.

Brief summary

Influenza A viruses use host sialoglycans for attachment via HA and hydrolyze them upon budding via NA. The HAs of some human isolates prefer extended and branched glycans for binding; however, the preference of AIVs for these glycans is poorly understood. This study addressed the glycan-binding preferences of HA and AIV particles by using a series of sialoglycopolymers with various glycan representations and densities. Glycan extension was mimicked by linking the terminal sialyllactose with subsequent PEG chains, and glycan density was further controlled by polymerizing the glycomonomers with the corresponding numbers of acrylamide spacers. Recombinant HAs and particles of two AIVs were used in a solid-phase direct binding assay with the aforementioned sialoglycopolymers. Both recombinant HAs preferred higher-density glycans, but did not bind to the homopolymer with the highest density. These observations suggested that most sialyllactoses in the highest-density polymer were not involved in the interaction with HA, whereas extremely high-density sialyllactoses negatively impacted HA binding. Additionally, binding analysis using viral particles demonstrated that HA clusters on the particles compensated for weak binding to low-density glycans by employing multivalent HA-glycan interactions. This approach enabled the evaluation of the complex nature of viral particles as macromolecules in glycan binding and the clustering effect of glycan density in a glycopolymer. These findings suggest elaborate protein-carbohydrate interactions via multivalent receptor-ligand binding between AIV particles and sialoglycans.

Chapter II

Loss of *N*-glycosylation in the neuraminidase stalk contributes to enhancing the pathogenicity of a high pathogenicity avian influenza virus in chickens

Introduction

NA of IAVs is composed of four domains: a short cytoplasmic tail, a transmembrane region, a stalk, and a globular head [7]. The NA-head domain recognizes sialic acids at the non-reducing terminus of glycans and liberates them, leading to viral release from the infected cells [8, 9]. Amino acid truncation in the stalk domain of NA has been identified as a molecular marker for AIVs that acquire a highly pathogenic phenotype in chickens, in addition to the polybasic amino acid sequences at the HA cleavage sites [28–30, 73]. AIVs with truncated NA stalk have been isolated from terrestrial poultry including chickens and turkeys, while have not been found in non-pathogenic viruses circulating in wild aquatic birds [31–34].Viruses with stalk-truncated NA have indeed been isolated as a result of virus passages in quails and chickens [35–38]. Therefore, viruses with short-stalk NA were considered a result of adaptation of AIVs from wild aquatic birds to chickens.

IAVs with short-stalk NA exhibit reduced sialidase activity compared to those with full-stalk NA, but only when tested with bulky substrates like fetuin or erythrocytes [74]. Both short- and full-stalk NA viruses, show similar reactivity to smaller compounds, such as *N*-acetylneuraminyllactose or 2-(4-methylumbelliferyl)-α-D-*N*-acetylneuraminic acid (MUNANA) [28, 74]. This pattern is often explained by the "limited access theory," which posits that short-stalk NA is partially obscured by the HA, which is taller than NA and more abundant on the viral surface, thereby restricting its access to bulky sialylated substrates [74]. In contrast, Durrant *et al.* [75] challenged this theory, arguing that it does not fully account for the reduced sialidase activity of short-stalk NA. They noted that a 20-amino-acid deletion in the NA-stalk leaves approximately 81% of the HA height intact, suggesting that access to the NA globular head domain is unlikely to be significantly impeded by the reduction in stalk height. Furthermore, structural analyses using cryo-electron microscopy have shown that NA forms localized clusters rather than being evenly distributed across the viral surface [76]. These clusters could potentially facilitate substrate access to the catalytic site of the short-stalk NA. Therefore, the impact of stalk deletion on NA biological function remains debaTable.

To explore the molecular mechanisms by which duck-derived, non-pathogenic AIVs acquire high pathogenicity in chickens, several studies have conducted serial

passages of AIVs in chickens [27, 77, 78]. Maruyama *et al.* [27] and later Ichikawa *et al.* [73] performed serial passages of a genetically modified H7N7 non-pathogenic AIV (rgVac2sub-P0) in chickens. Three passages in chick air sacs, followed by four passages in chicken lungs, led to the emergence of an HPAIV (Vac2sub-P3L4) with a 34-amino-acid truncation in the NA stalk under functional coevolution of HA and NA. Their studies revealed that this NA-stalk deletion along with mutations in HA was a crucial adaptation for the virus to acquire a highly pathogenic phenotype in chickens when birds were challenged via intranasal route, in addition to polybasic amino acids at the HA cleavage site. Notably, the deletion site in the NA stalk included five potential *N*-glycosylation sites, while the specific mechanisms by which NA-stalk truncation or deglycosylation contribute to increased viral pathogenicity remain unclear. Protein modification on the stem by *N*-glycans generally modulates the biophysical properties and stability of proteins by adding large hydrophilic carbohydrates [79]. For example, deglycosylation of the HA stem region has been shown to reduce viral replication and pH stability [80]. Consequently, it is hypothesized that the loss of *N*-glycosylations in the NA stalk may influence NA biological function and viral pathogenicity in chickens. To test this hypothesis, the present study rescued a virus with a glycosylation-deficient NA-stalk and evaluated its pathogenicity in chickens. Despite initial genetic instability *in vivo*, a single amino acid substitution corrected this instability and resulted in increased pathogenicity compared with the virus retaining NA-stalk glycosylation. Additionally, viruses with glycosylation-deficient NA-stalk exhibited decreased erythrocyte elution activity, similar to that of a virus with truncated NA-stalk.

Materials and Methods

Viruses and cells

A low pathogenicity AIV, A/duck/Hokkaido/Vac-2/2004 (H7N7) (Vac2; genetic information accession numbers: AB243417–AB243424; [81]) was used. These viruses were propagated in 10-day-old embryonated chicken eggs at 35°C for 48 h, and the infectious allantoic fluids were used as virus stocks.

MDCK cells were maintained in Eagle's minimum essential medium (MEM; Shimadzu Diagnostics Corporation, Tokyo, Japan) supplemented with 0.3 mg/mL L-glutamine (Nacalai Tesque), 100 U/mL penicillin G (Meiji Seika Pharma), 0.1 mg/mL streptomycin (Meiji Seika Pharma), 8 μg/mL gentamicin (Takata Pharmaceutical), and 10% fetal bovine serum (Merck). HEK293T cells were maintained in pyruvate-free DMEM (Thermo Fisher Scientific) supplemented with the above-mentioned antibiotics and 10% fetal bovine serum (Nichirei Biosciences, Tokyo, Japan). Both cell types were maintained at 37°C in a 5% CO_2 atmosphere.

Virus titration

For virus titration, 10-fold dilutions of the virus stocks and organ homogenates were inoculated into confluent monolayers of MDCK cells and incubated at 35°C for 1 h. The virus solution, including unbound viruses, was removed from the cells, and the cells were washed with sterilized PBS. The cells were then cultured in serum-free MEM containing 1.0 μg/mL of acetylated trypsin (Merck) at 35°C for 72 h. The infectious titers of the viruses were expressed as 50% tissue culture infectious dose ($TCID_{50}$), determined using the method reported by Reed and Muench [82], by observing the cytopathic effect (CPE) in virus-infected cells.

Pathogenicity assessment of viruses in chickens

Fertilized eggs of conventional chickens (*Gallus gallus domesticus*) were obtained from Iwamura Poultry (Niigata, Japan) and hatched. Six-week-old chickens were used for the pathogenicity assessment of the viruses. Serum samples were collected from the chickens before the challenge to confirm the absence of specific antibodies against the challenge virus using standard HI test protocols with 25 μL of serum.All chickens were intranasally inoculated with $10^{4.0}$ $TCID_{50}$ of viruses. To observe survival

rates and clinical manifestations, six chickens were challenged with each virus and monitored for 14 days. Once a chicken exhibited severe neurological symptoms, it was euthanized with an overdose of thiopental sodium (Ravonal, 150 mg/kg; Nipro ES Pharma Co., Ltd., Osaka, Japan) administered intravenously, based on a humane endpoint. The number of euthanized chickens was recorded the following day and included in the survival curve. Lung and brain samples were collected from both deceased and euthanized chickens for genetic analysis of the recovered viruses. Additionally, a serum sample was collected from surviving chickens during the experimental period, and HI tests were performed using Vac2 to confirm seroconversion. For virus titration, blood samples were collected from chickens at 3 dpi, and the chickens were subsequently euthanized. Tissue samples from the brain, trachea, lung, liver, kidney, and colon were collected and homogenized using a Multi-Beads Shocker (MB3000, Yasui Kikai Corp., Osaka, Japan) to prepare 10% suspensions in MEM. Infectivity titers for blood and tissue samples were measured using MDCK cells as described above. All infected animals were housed in self-contained isolator units (Tokiwa Kagaku Kikai Co., Ltd., Tokyo, Japan) within an animal biosafety level (ABSL) 3 facility at the Faculty of Veterinary Medicine, Hokkaido University, Hokkaido, Japan.

Reverse genetics

The NA genes of Vac2 mutants were amplified and cloned into the pHW2000 vector [83], using the In-Fusion HD Cloning Kit (Takara Bio Inc., Shiga, Japan), following the manufacturer's protocol. To assess the molecular weight of NA proteins, a nucleotide sequence encoding a FLAG (DYKDDDDK) tag with a single glycine linker (G) was inserted downstream of the C-terminus coding region of NA. This insertion was followed by 157 nucleotides from the 3′ end of the open reading frame (ORF), which includes a noncoding region consisting of a total of 183 nucleotides of the packaging signal [84, 85]. Individual nucleotide substitutions in the NA gene segments were introduced via site-directed mutagenesis using the QuikChange II Site-Directed Mutagenesis Kit (Agilent Technologies, Inc., Santa Clara, CA, USA) or KOD FX Neo DNA Polymerase (Toyobo, Osaka, Japan), according to the manufacturer's instructions. The other seven gene segments from Vac2 and Vac2-P3L4 were previously cloned into pHW2000 [27, 73]. The viruses, for which the gene constellations of all eight segments are listed in Table 2, were rescued via reverse genetics as described previously [83]. The

Table 2. **Recombinant viruses generated by reverse genetics and their usage.**

Virus	Abbreviation	Viral genes								Usage*
		PB2	PB1	PA	HA	NP	NA	M	NS	
rgVac2-P3L4/P0NA	L4/P0NA	P3L4PB2	P3L4PB1	P3L4PA	P3L4HA	P3L4NP	P0NA	P3L4M	P3L4NS	PA
rgVac2-P3L4	L4	P3L4PB2	P3L4PB1	P3L4PA	P3L4HA	P3L4NP	P3L4NA	P3L4M	P3L4NS	PA
rgVac2-P3L4/P0NAΔGlyco	L4/P0NAΔG	P3L4PB2	P3L4PB1	P3L4PA	P3L4HA	P3L4NP	P0NAΔGlyco	P3L4M	P3L4NS	PA
rgVac2-P3L4/P0NA-Y65H	L4/P0NA-65H	P3L4PB2	P3L4PB1	P3L4PA	P3L4HA	P3L4NP	P0NA-Y65H	P3L4M	P3L4NS	PA
rgVac2-P3L4/P0NAΔGlyco-Y65H	L4/P0NAΔG-65H	P3L4PB2	P3L4PB1	P3L4PA	P3L4HA	P3L4NP	P0NAΔGlyco-Y65H	P3L4M	P3L4NS	PA
rgVac2/P0NA	Vac2/P0NA	Vac2PB2	Vac2PB1	Vac2PA	Vac2HA	Vac2NP	P0NA	Vac2M	Vac2NS	EEA, MA, MS
rgVac2/P3L4NA	Vac2/L4NA	Vac2PB2	Vac2PB1	Vac2PA	Vac2HA	Vac2NP	P3L4NA	Vac2M	Vac2NS	EEA, MA
rgVac2/P0NAΔGlyco	Vac2/P0NAΔG	Vac2PB2	Vac2PB1	Vac2PA	Vac2HA	Vac2NP	P0NAΔGlyco	Vac2M	Vac2NS	EEA, MA
rgVac2/P0NA-Y65H	Vac2/P0NA-65H	Vac2PB2	Vac2PB1	Vac2PA	Vac2HA	Vac2NP	P0NA-Y65H	Vac2M	Vac2NS	EEA, MS
rgVac2/P0NAΔGlyco-Y65H	Vac2/P0NAΔG-65H	Vac2PB2	Vac2PB1	Vac2PA	Vac2HA	Vac2NP	P0NAΔGlyco-Y65H	Vac2M	Vac2NS	EEA
rgVac2/P0NAΔGlyco-Q47N	Vac2/P0NAΔG-47N	Vac2PB2	Vac2PB1	Vac2PA	Vac2HA	Vac2NP	P0NAΔGlyco-Q47N	Vac2M	Vac2NS	EEA, MS
rgVac2/P0NAΔGlyco-Q56,57N	Vac2/P0NAΔG-56,57N	Vac2PB2	Vac2PB1	Vac2PA	Vac2HA	Vac2NP	P0NAΔGlyco-Q56,57N	Vac2M	Vac2NS	EEA, MS
rgVac2/P0NAΔGlyco-Q67,68N	Vac2/P0NAΔG-67,68N	Vac2PB2	Vac2PB1	Vac2PA	Vac2HA	Vac2NP	P0NAΔGlyco-Q67,68N	Vac2M	Vac2NS	EEA
rgVac2/P0NA-FLAG	Vac2/P0NA-FLAG	Vac2PB2	Vac2PB1	Vac2PA	Vac2HA	Vac2NP	P0NA-FLAG	Vac2M	Vac2NS	WB, LB
rgVac2/P3L4NA-FLAG	Vac2/L4NA-FLAG	Vac2PB2	Vac2PB1	Vac2PA	Vac2HA	Vac2NP	P3L4NA-FLAG	Vac2M	Vac2NS	WB, LB
rgVac2/P0NAΔGlyco-FLAG	Vac2/P0NAΔG-FLAG	Vac2PB2	Vac2PB1	Vac2PA	Vac2HA	Vac2NP	P0NAΔGlyco-FLAG	Vac2M	Vac2NS	WB, LB

* PA: pathogenicity assessment in chickens, EEA: erythrocyte elution assay, MA: MUNANA assay, MS: mass spectrometry, WB: western blotting, LB: lectin blotting

viruses used for pathogenicity assessment in chickens had a backbone derived from the resultant virus of serial passages in chickens (Vac2sub-P3L4), and the viruses used *in vitro* assays had a backbone of non-pathogenic avian influenza virus (Vac2).

Sanger sequencing of NA genes

Virus RNA was extracted from the allantoic fluid of virus-infected chicken embryos or organ homogenates using TRIzol LS Reagent (Thermo Fisher Scientific), according to the manufacturer's protocol. The extracted RNA was reverse-transcribed with M-MLV Reverse Transcriptase (Promega Corp., Madison, WI, USA) or SuperScript™ III Reverse Transcriptase (Thermo Fisher Scientific) using the Uni 12 primer [86]. The NA segments were then amplified with KOD FX Neo DNA Polymerase (Toyobo) and gene-specific primers [86]. Nucleotide sequences of the polymerase chain reaction (PCR) products and plasmids were determined using the BigDye™ Terminator v3.1 Cycle Sequencing Kit (Thermo Fisher Scientific) and the Applied Biosystems 3500 Genetic Analyzer (Thermo Fisher Scientific). The sequences were analyzed using GENETYX ver. 15 (Nihon Server Corp., Tokyo, Japan).

Whole genome sequence

Whole genomes of viruses recovered from L4/P0NAΔG-inoculated chickens (#31, 33–36) were analyzed. For next-generation sequencing (NGS) of the viruses, the primer sets described by Ip *et al*. [87] were used to amplify the whole genome of AIV for NGS analysis together with three primer sets that specifically improve the yield of PB2, PB1, and PA segments described by Hew *et al*. [88]. Oxford Nanopore libraries were prepared using the NEB Ultra II End Repair/dA-Tailing Module (New England Biolabs, Ipswich, MA, USA) and sequenced on Flongle using the Nanopore Direct cDNA sequencing kit or Ligation Sequencing kit V14 (Oxford Nanopore Technologies, Oxford, England). The obtained reads were mapped and assembled using FluGAS version 2 (World Fusion, Tokyo, Japan). The frequency of minor variants was analyzed based on the sequence data with a minimum coverage of 3,500 reads for NA segment and 500 reads for the other segments.

Immunoprecipitation

One milliliter of infectious allantoic fluid containing viruses was mixed with 200 ng of biotinylated anti-H7HA monoclonal antibodies (224/4; previously established in our laboratory using A/duck/Hokkaido/Vac-2/2004 [H7N7]; [89]). After incubation at 37°C for 1 h, the complexes were captured with Dynabeads MyOne Streptavidin T1 (Thermo Fisher Scientific) at 4°C for 1 h. After washing, virus antigens were eluted from the magnetic beads and disrupted using 100 mM citric acid containing 1% Triton X-100. The supernatant was mixed with an equal volume of ice-cold acetone and incubated at −20°C for 1 h to precipitate proteins. After centrifugation at 13,000 ×*g* at 4°C for 15 min, the pellets were dried at room temperature for 30 min. The pellets were then incubated with 20 μL of denaturation buffer (1 M Tris-HCl [pH 8.6], 1% SDS, 1.5% 2-mercaptoethanol) at 4°C overnight to dissolve them.

Glycosidase digestion

Immunoprecipitated samples were treated with peptide *N*-glycosidase F (PNGase F) to release the *N*-glycans from the NA proteins. The samples were mixed with an equivalent amount of 5% NP-40 for stabilization and incubated at 37°C for 20 min with PNGase F PRIME (N-Zyme Scientifics, Doylestown, PA, USA).

Sodium dodecyl sulfate-polyacrylamide gel electrophoresis (SDS-PAGE) and western blotting

The samples were mixed with an equivalent amount of 2× Laemmli sample buffer (125 mM Tris-HCl [pH 6.8], 4% SDS, 20% glycerol, 0.02% bromophenol blue, 10% 2-mercaptoethanol). SDS-PAGE was performed using a 10% TGX™ FastCast™ Acrylamide gel (Bio-Rad) at a constant voltage of 200 V for 35 min under reducing conditions. The resolved proteins were transferred to an Immobilon-P PVDF membrane (Merck). The membrane was blocked with PVDF Blocking Reagent for Can Get Signal (Toyobo). Subsequently, the membrane was probed with an anti-DDDDK-tag monoclonal antibody (FLA-1, 1:1000 dilution; Medical & Biological Laboratories Co., Ltd., Tokyo, Japan) and a goat anti-mouse IgG antibody conjugated with horseradish peroxidase (1:5000 dilution; Bio-Rad). Proteins were detected using the chemiluminescence substrate ImmunoStar LD (Fujifilm Wako Pure Chemical Corp.,

Osaka, Japan) and visualized with a LuminoGraph I (WSE-6100, Atto Corp., Tokyo, Japan).

Dot blotting

For dot blotting, an Immobilon-P PVDF membrane (Merck) was immersed in methanol and ultrapure water to wet it. Then, 1 μL of immunoprecipitated virus samples was spotted onto the membrane and allowed to dry. The membrane was blocked with PVDF Blocking Reagent for Can Get Signal (Toyobo). Subsequently, the membrane was probed with either an anti-DDDDK-tag monoclonal antibody (FLA-1, 1:1000 dilution; Medical & Biological Laboratories) or an anti-nucleoprotein (NP) monoclonal antibody (183/5, 1:1000 dilution; previously established in our laboratory using A/swine/Hong Kong/10/1998 [H9N2]) as primary antibodies. After incubation with a goat anti-mouse IgG antibody conjugated with horseradish peroxidase (1:5000 dilution; Bio-Rad), proteins were detected using the chemiluminescence method described above. The chemiluminescent density was quantified as previously described by Ohgane and Yoshioka [90].

Site-specific glycosylation analysis via liquid chromatography and mass spectrometry (LC/MS)

The virus particles were collected from 60–80 mL of infectious allantoic fluid from chicken embryonated eggs via ultracentrifugation, followed by a 30% sucrose cushion ultracentrifugation to remove impurities. The pellet was dissolved in 100 μL of PBS with 0.08% sodium azide and then precipitated with acetone (final concentration of 80%) at −20°C overnight. After centrifugation at 13,000 rpm for 15 min, the precipitate was recovered and dissolved in 100 mM Tris-HCl (pH 9.0) containing 12 mM sodium deoxycholate and 12 mM sodium lauroylsarcosinate. The protein samples were treated with dithiothreitol (equal weight of protein, 37°C, 1 h) to reduce disulfide bonds and then alkylated with iodoacetamide (2.5 times the weight of protein, 37°C, 1 h, in the dark) and quenched with dithiothreitol (half the weight of protein, 37°C, 5 min). The proteins were then diluted fourfold with 50 mM ammonium bicarbonate and digested with rLys-C endopeptidase (Promega), followed by treatment with Trypsin Gold (Promega). An aliquot of each digest was treated with PNGase F (Takara Bio) in $H_2{}^{18}O$ to remove *N*-glycans and label glycosylated asparagines with the stable isotope ^{18}O (isotope-coded

glycosylation site-specific tagging [IGOT] method; [91, 92]). The products were lyophilized, redissolved in nonlabeled water, treated with trypsin at 4°C overnight, and purified with MonoTip C18 (GL Sciences, Tokyo, Japan). These labeled peptides were subsequently analyzed using an LC/MS system with a nanoflow LC, UltiMate 3000 RSLCnano (Thermo Fisher Scientific), and an Orbitrap Eclipse Tribrid mass spectrometer (Thermo Fisher Scientific) as described previously for IGOT-LC/MS. Briefly, the peptides were separated using a C18 tip column (Aurora Ultimate, IonOpticks, Australia, 0.075 mm id × 25 cm length) at 300 nL/min with an acetonitrile gradient (3–35% acetonitrile in 0.1% formic acid over 45 min). MS2 spectra were obtained data-dependently (positive mode, cycle time: 3 s, MS1 resolution: 120,000, range: 377–2000, analyzer: Orbitrap, maximum injection time: 100 ms, MS2 resolution: 60,000, range: 135–2000, isolation window: 1.6, analyzer: Orbitrap, activation: HCD, maximum injection time: 200 ms, normalized collision energy: stepped [41, 73, 93]). For site-specific glycosylation analyses, the MS2 spectra were searched using Mascot (ver. 2.8.0.1, Matrix Science, London, UK) with a UniProtKB sequence database (tax id: 9031, including HA sequences). Search conditions were as follows: method: MS/MS ion search, target FDR: 1%, enzyme: semi-trypsin/Lys-C, fixed modification: carbamidomethyl (C), variable modifications: ammonium loss (peptide N-term C), delta:H(1)N(-1)18O(1)(N), Gln>pyroGlu (peptide N-term Q), and Oxidation (M), mass tolerance (MS1): 7 ppm, MS2: 10 ppm, max missed cleavage: 2. All spectra of the target peptides were manually inspected for correct peptide identification and site-specific glycosylation.

Prediction of RNA secondary structure

The RNAfold web server, provided by the ViennaRNA web services (http://rna.tbi.univie.ac.at/; [94]), and the CentroidFold web server (http://rtools.cbrc.jp/centroidfold/; [95]) were used to predict the secondary structure of the RNA sequences of NA-stalk domains. The RNA sequences of partial NA segments (129 nt), including the NA-stalk coding regions, were submitted to either of the above web servers using the default parameters.

Virus elution assay

The function of NA was evaluated by assessing the ability of viruses to elute agglutinated chicken erythrocytes, as previously described by Castrucci and Kawaoka

[96]. The viruses were adjusted to 32 HAU with PBS and serially diluted in borate-buffered saline with calcium (6.8 mM $CaCl_2$, 154 mM NaCl in 20 mM borate buffer, pH 7.2) in technical triplicate. Then, 50 μL of each dilution were incubated with an equivalent volume of 0.5% chicken erythrocytes at 4°C for 1 h in a U-bottom plate (Corning). The plate was then moved to 37°C, and the dissolution of hemagglutination due to NA activity was recorded periodically for 8 h. The elution activity was evaluated as the proportion of wells where hemagglutination was canceled relative to the total number of wells that had been hemagglutinated before incubation at 37°C.

NA enzymatic activity

NA enzymatic activity was measured using MUNANA (Sigma-Aldrich) as a soluble substrate, as described previously [97]. Briefly, the viruses were mixed with serially diluted MUNANA in 96-well black-bottomed plates. The mixture was exerted at 360 nm at 1-min intervals, and the emission signal was periodically monitored for 30 min at 37°C using POWER SCAN 4 (Agilent Technologies). The initial reaction rate under each condition was calculated and plotted to obtain the Michaelis constant, K_m, using R software.

Comparison of NA-stalk domain of N7 AIVs

A total of 1,498 amino acid sequences of N7 NA covering the stalk domain were obtained from the Global Initiative on Sharing All Influenza Data (GISAID, https://gisaid.org/) and aligned using multiple sequence alignment software GENETYX ver. 15 (Nihon Server). Seventy-seven sequences exhibited amino acid deletions in the stalk domain. Each pattern of deletion was categorized based on the original host of each virus as indicated in the strain names. The remaining 1,421 sequences were analyzed to identify amino acid sequences at potential *N*-glycosylation sites within the stalk.

Ethics statements

All animal experiments were authorized by the Institutional Animal Care and Use Committee of the Faculty of Veterinary Medicine, Hokkaido University (approval nos. 13-0108, April 8, 2013; 18-0037, April 4, 2018; 21-0016, April 2, 2021; and 23-0053, March 30, 2023) and were conducted in accordance with the committee's guidelines. The facilities where the animal experiments were performed are certified by the Association

for Assessment and Accreditation of Laboratory Animal Care International (AAALAC International).

All experiments involving genetically modified organisms, including mutant viruses generated via reverse genetics, were authorized by the Safety Committee on Genetic Recombination Experiments of Hokkaido University (approval nos. 2015-019, August 4, 2015; 2020-009, June 2, 2020) and the Ministry of Education, Culture, Sports, Science and Technology, Japan (approval nos. 30-Monkashin-Dai-963, March 28, 2019; 2-Monkashin-Dai-654, September 15, 2020; 4-Monkashin-Dai-142, July 7, 2022). Additionally, the study was authorized by the Biosafety Management Committee on Pathogens and Other Hazardous Agents of the Faculty of Veterinary Medicine, Hokkaido University (approval nos. 2017-1-61, 2018-1-59, 2019-1-62, 2022-1-78, 2023-1-40). The gain-of-function experiments aimed at increasing the pathogenicity of recombinant HPAIVs in chickens were specifically authorized on April 15, 2021, by the same committee, with no concerns regarding dual-use.

Results

Pathogenicity of a recombinant virus with glycosylation-deficient NA stalk in chickens

A previous study performed serial passages of a genetically modified H7N7 duck influenza virus in chick air sacs (P3), followed by four passages in chicken lungs (L4). This adaptation process yielded a high pathogenicity avian influenza virus characterized by a 34-amino-acid deletion in the NA-stalk region. To verify the previous observation that truncation of the amino acids in the NA-stalk domain contributes to increased intranasal pathogenicity in chickens, a pair of viruses harboring a full-length NA stalk (rgVac2-P3L4/P0NA; L4/P0NA) and short NA stalk featuring the 34-amino-acid deletion (rgVac2-P3L4; L4) were used (Figure 6A and Table 2; [73]). Six 6-week-old chickens were intranasally inoculated with $10^{4.0}$ $TCID_{50}$ of each virus, and clinical manifestations were monitored for 14 days. The viral pathogenicity in chickens showed high reproducibility with previous results: all chickens inoculated with L4 died within 4 days post-inoculation (dpi), whereas those inoculated with L4/P0NA exhibited delayed clinical onset and survived for 7 days (Figure 6B). Thus, the truncation of the NA-stalk domain in L4 was proven to increase its pathogenicity in chickens.

Subsequently, to assess the functional significance of the loss of *N*-glycosylations on the stalk domain of NA, N/Q mutations that abrogate *N*-glycosylation sequons (N-X-S/T) were introduced into the NA-stalk domain of P0NA. A virus harboring this NA gene segment (P0NAΔGlyco) with the backbone of the other seven gene segments from L4 was generated (rgVac2-P3L4/P0NAΔGlyco; L4/P0NAΔG; Figure 6A). The virus, L4/P0NAΔG, was intranasally inoculated into chickens to compare its pathogenicity. Interestingly, chickens inoculated with L4/P0NAΔG exhibited various clinical courses (Figure 6B). One chicken died on 4 dpi, and three were euthanized on 4 or 5 dpi due to severe neurological signs. Conversely, another chicken died on 9 dpi, and one survived the 14-day observation period. Furthermore, the surviving chicken seroconverted during the experimental period (8 HI titer). To investigate the cause of the variable pathogenesis of L4/P0NAΔG, NA genes from viruses recovered from the infected chickens were sequenced. Amino acid substitutions or deletions in the NA-stalk domain were observed in all viruses recovered from chickens infected with L4/P0NAΔG (Table 3). Conversely,

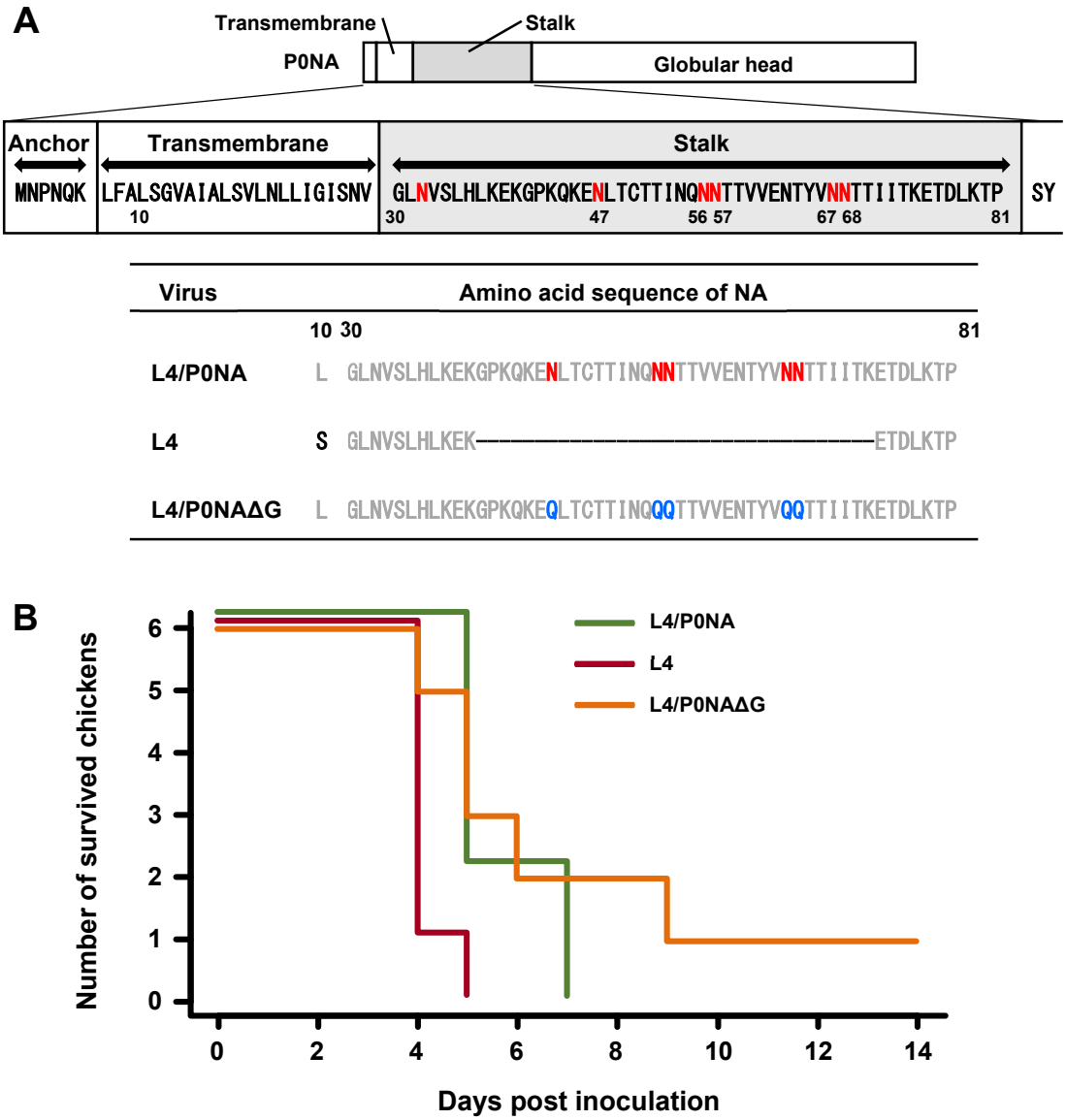

Figure 6. Survival of chickens intranasally inoculated with NA-stalk mutant viruses. (A) NA consists of a membrane anchor, a transmembrane, a stalk, and a globular head. P0NA is a full-stalk NA, whereas P3L4NA, which was derived from serial passages of rgVac2-P0 in chickens, contains a 34-amino-acid deletion in the stalk and one amino acid substitution in the transmembrane. The potential *N*-glycosylation sites in the P0NA are highlighted in red. P0NAΔGlyco was generated by introducing N/Q mutations at the five potential *N*-glycosylation sites in the stalk, which are highlighted in blue. A series of viruses carrying either NA gene and accompanied by the L4 backbone were generated through reverse genetics in this study. (B) Six 6-week-old chickens were intranasally inoculated with 100 µL of each virus at $10^{4.0}$ $TCID_{50}$ and observed for 14 days.

Table 3. Amino acid sequences of recovered viruses from six chickens (#31–36) inoculated with L4/P0NAΔG.

Virus / chicken ID	Clinical course	Organ sample	Amino acid sequence of NA-stalk region[a]
L4/P0NAΔG[b]	Original strain		GLNVSLHLKEKGPKQKEQLTCTTINQQQTTVVENTYVQQTTIITKETDLKTPSY
#31	Euthanized on 4 dpi	Brain	GLNVSLHLKEKGPKQKEQLTCTTINQQQTTVVENTYVQQT----------SY[c]
		Lung	GLNVSLHLKEKGPKQKEQLTCTTINQQQTTVVENTYVQQT----------SY
#32	Seroconversion on 14 dpi	–	No virus rescued
#33	Died on 9 dpi	Brain	GLNVSLHLKEKGPKQKEQLTCTTINQQQTTVVENTHVQQTTIITKETDLKTPSY[d]
		Lung	GLNVSLHLKEKGPKQKEQLTCTTINQQQTTVVENTHVQQTTIITKETDLKTPSY
#34	Euthanized on 5 dpi	Brain	GLNVSLHLKEKGPKQKEQLTCTTINQQQTTVVENTYVQQTTIITKETDLKTPSY GLNVSLHLKEKGPKQKEQLTCTTINQQQTTVVENTHVQQTTIITKETDLKTPSY
		Lung	GLNVSLHLKEKGPKQKEQLTCTTINQQQTTVVENTHVQQTTIITKETDLKTPSY
#35	Died on 4 dpi	Brain	GLNVSLHLKEKGPKQKEQLTCTTINQQQTTVVENTYV----------KTPSY
		Lung	GLNVSLHLKEKGPKQKEQLTCTTINQQQTTVVENTYV----------KTPSY GLNVSLHLKEKGPKQKEQLTCTTINQQQTTVVENTYVQQT----------SY
#36	Euthanized on 4 dpi	Brain	GLNVSLHLKEKGPKQKEQLTCTTINQQQTTVVENTCVQQTTIITKETDLKTPSY
		Lung	GLNVSLHLKEKGPKQKEQLTCTTINQQQTTVVENTCVQQTTIITKETDLKTPSY

[a] Mutations observed in isolates from chickens inoculated with L4/P0NAΔG were determined. The amino acid residues corresponding to the NA-stalk region at positions 30–83 of L4/P0NAΔG are aligned.

[b] L4/P0NAΔG serves as the reference inoculum. The underlined residues indicate the introduction sites of N/Q mutations.

[c] A dash (–) indicates amino acid deletion.

[d] Gray shading highlights amino acid substitutions.

no mutations in the NA-stalk were found in viruses recovered from chickens inoculated with either L4/P0NA or L4, suggesting the genetic instability of L4/P0NAΔG. Although a total of four distinct amino acid mutants were identified among the five individuals, the Y65H mutation was found in viruses recovered from two co-housed chickens in an isolator. Notably, one chicken (#34) showed severe neurological symptoms on 5 dpi, whereas the co-housed one (#33) began to exhibit mild clinical signs on 7 dpi. The observation was supported by whole genome sequencing and the subsequent population analysis of minor variants (Table 4). The population of Y65H mutant was higher in the brain (91.7%) and lung (90.0%) of chicken #33 compared to those of chicken #34 (61.2% in brain and 74.8% in lung). Additionally, a minor variant I621V in PA of chicken #34 (0.7% in brain and 0.9% in lung) turned to be dominant in chicken #33 (88.4% in brain and 73.9% in lung). This suggests that the Y65H mutant was likely transmitted from one chicken (#34) to the other (#33) without further mutation in the NA-stalk. These results indicate that the Y65H mutant appears to be genetically more stable than the original L4/P0NAΔG in chickens.

Genetic stability of Y65H mutant of L4/P0NAΔG

To validate the genetic stability of the Y65H substitution in the NA protein of L4/P0NAΔG, L4/P0NAΔG and the Y65H mutant were serially passaged in embryonated chicken eggs. To achieve this, the Y65H substitution, changing thymidine to cytosine, was introduced into the NA-coding plasmid, and L4/P0NAΔG-65H was rescued via reverse genetics (Figure 7A). Subsequently, two viruses—L4/P0NAΔG and L4/P0NAΔG-65H—were independently passaged three times in chicken embryos. Two distinct variants of L4/P0NAΔG were obtained (Table 5), whereas no mutants were obtained from the descendants of L4/P0NAΔG-65H. This indicates that the Y65H mutation in the NA-stalk seems to stabilize the genetic properties of P0NAΔGlyco.

Since an importance of RNA secondary structures of HA genes in acquisition of serial basic amino acids in the cleavage sites has been proposed [98, 99], RNA secondary structures of NA stalk-coding region can cause slippage of viral polymerase, resulting the genetic instability [100]. To confirm the impact of the Y65H mutation on the genetic stability of the NA stalk-coding region, the RNA secondary structure was predicted through *in silico* analyses and compared. The present study focused on the RNA

Table 4. Amino acid sequences of low-frequent variants recovered from chickens inoculated with L4/P0NAΔG detected by NGS.

Chicken ID	Organ	PB2[a]		PB1		PA				NA				
		280[b]		191		393		621		65			Δ67-78[c]	Δ70-81[c]
		L (CUC)[d]	L (CUA)	**V (GUA)**	V (GUC)	**Y (UAU)**	Y (UAC)	**I (AUU)**	V (GUU)	**Y (UAC)**	H (CAC)	C (UGC)		
#31	Brain	·[e]	–[f]	·	–	·	–	·	–	1.4[g]	–	–	19.6	79.0
	Lung	·	–	·	–	·	–	·	–	1.8	–	–	19.6	78.4
#33	Brain	·	–	·	–	·	–	9.1	88.4	2.7	91.7	–	–	–
	Lung	·	–	·	–	·	–	24.6	73.9	5.2	90.0	–	–	–
#34	Brain	·	–	·	–	·	–	97.6	0.7	34.1	61.2	–	–	–
	Lung	·	–	·	–	·	–	97.5	0.9	20.3	74.8	–	–	–
#35	Brain	6.0	90.7	·	–	7.4	86.2	·	–	0.5	–	–	97.5	2.1
	Lung	39.5	56.8	·	–	37.8	57.8	·	–	5.8	–	–	67.6	26.8
#36	Brain	·	–	7.2	84.7	·	–	·	–	5.2	–	89.3	–	–
	Lung	·	–	9.6	83.8	·	–	·	–	8.6	–	85.9	–	–

[a] Nucleotide mutations were observed in the four gene segments (PB2, PB1, PA, and NA).
[b] Methionine encoded by the AUG start codon is defined as position 1.
[c] Amino acid and its encoding codon harboring mutations which was detected in a consensus sequence by NGS analysis are indicated. The bold letter represents an amino acid of parent virus (L4/P0NAΔG).
[d] Amino acid deletion at positions 67-78 and 70-81.
[e] Period indicates the same amino acid as the parent virus.
[f] En-dush (–) indicates that the population analysis was not performed.
[g] Frequency (%) of the mutations.

A

Virus	Amino acid sequence of NA
	10 30 81
L4/P0NA	L GLNVSLHLKEKGPKQKENLTCTTINQNNTTVVENTYVNNTTIITKETDLKTP
L4	S GLNVSLHLKEK----------ETDLKTP
L4/P0NA-65H	L GLNVSLHLKEKGPKQKENLTCTTINQNNTTVVENTHVNNTTIITKETDLKTP
L4/P0NAΔG-65H	L GLNVSLHLKEKGPKQKEQLTCTTINQQQTTVVENTHVQQTTIITKETDLKTP

B

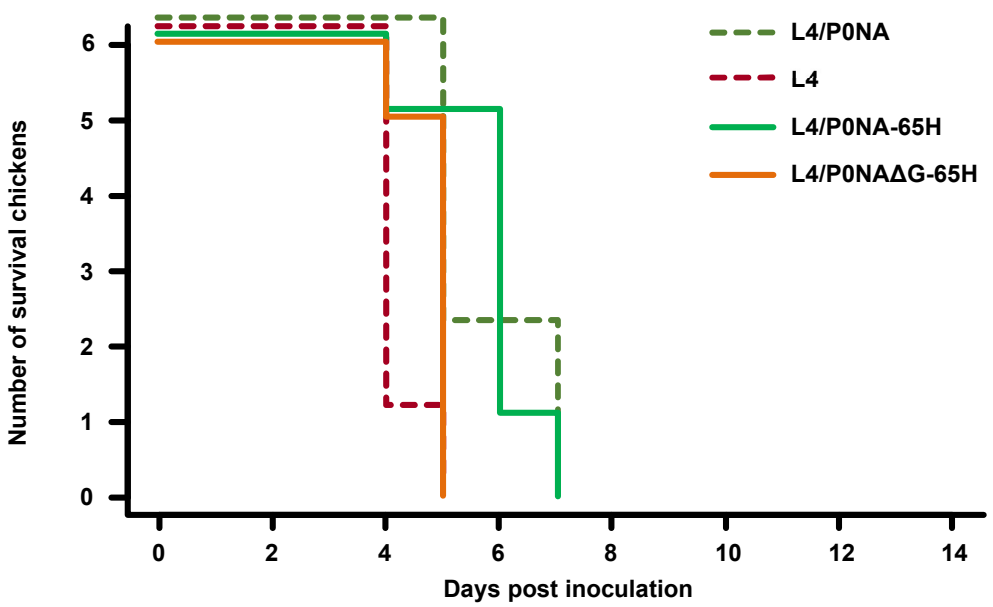

Figure 7. Survival of chickens from chickens intranasally inoculated with L4 mutants harboring Y65H substitution in the NA-stalk domain. (A) Amino acid sequences of Vac2NA mutants with the Y65H mutation are shown. Recombinant viruses L4/P0NA-65H and L4/P0NAΔG-65H were generated using reverse genetics. The potential *N*-glycosylation sites in the P0NA are highlighted in red. P0NAΔGlyco was generated by introducing N/Q mutations at the five potential *N*-glycosylation sites in the stalk, which are highlighted in blue. The position of Y65H substitutions were underlined. (B) Six 6-week-old chickens were intranasally inoculated with 100 μL of each Y65H mutant at $10^{4.0}$ $TCID_{50}$ and observed for 14 days. Survival of chickens inoculated with L4/P0NA and L4 is indicated with break lines for comparison (Figure 6B).

Table 5. Amino acid sequences of viruses passaged in chicken embryo with L4/P0NAΔG.

Passaged virus	Amino acid sequence of NA-stalk region[a]
L4/P0NAΔG[b]	GLNVSLHLKEKGPKQKEQLTCTTINQQQTTVVENTYVQQTTIITKETDLKTPSY
Embryo passage 1-1	GLNVSLHLKEKGPKQKEQLTCTTINQQQTTVVENTYVQQTTIITKETDLKTPSY
	GLNVSLHLKEKGPKQKEQL----------ENTYVQQTTIITKETDLKTPSY[c]
Embryo passage 2-1	GLNVSLHLKEKGPKQKEQL----------ENTYVQQTTIITKETDLKTPSY
Embryo passage 3-1	GLNVSLHLKEKGPKQKEQL----------ENTYVQQTTIITKETDLKTPSY
Embryo passage 1-2	GLNVSLHLKEKGPKQKEQLTCTTINQQQTTVVENTYVQQTTIITKETDLKTPSY
Embryo passage 2-2	GLNVSLHLKEKGPKQKEQLTCTTINQQQTTVVENTYVQQTTIITKETDLKTPSY
Embryo passage 3-2	GLNVSLHLKEKGPKQKEQLTCTTTNQQQTTVVENTYVQQTTIITKETDLKTPSY[d]

[a] Mutations observed in isolates from chickens inoculated with L4/P0NAΔG were determined. The amino acid residues corresponding to the NA-stalk region at positions 30–83 of L4/P0NAΔG are aligned.

[b] L4/P0NAΔG serves as the reference inoculum. The underlined residues indicate the introduction sites of N/Q mutations.

[c] A dash (–) indicates amino acid deletion.

[d] Gray shading highlights amino acid substitutions.

sequences (129 nucleotides) coding the NA-stalk region of P0NAΔGlyco because various mutation patterns were observed in this region of the recovered viruses from chickens. The target region formed a stem-loop structure consisting of 34 nucleotides, as predicted by both minimum free energy (MFE) and centroid structures in RNAfold [94]. Conversely, the stem-loop structure was abolished in the Y65H mutant due to a single substitution from uracil to cytosine (Figure 8). The stem-loop structure was not observed in the RNA sequences of either P0NA or P0NA-Y65H (Figure 8). Predictions made using CentroidFold also suggested stem-loop formation in the stalk-coding region of P0NAΔGlyco (Figure 9). Thus, the presence of the stem-loop structure in the NA-stalk region of P0NAΔGlyco appears to be related to the genetic instability. Conversely, the nucleotide substitution from UAC to CAC (corresponding to Y65H mutation) in P0NAΔGlyco compensates for the instability of the RNA secondary structure in the NA-stalk region. Accordingly, these results support the genetic stability of L4/P0NAΔG-65H.

NA-stalk deglycosylated virus with Y65H mutation (L4/P0NAΔG-65H) shows increased pathogenicity in chickens

The pathogenicity of a pair of genetically stable viruses, L4/P0NA-65H and L4/P0NAΔG-65H, was assessed in chickens to further investigate the functional significance of the loss of glycosylation in the NA-stalk. For this purpose, six 6-week-old chickens were challenged with $10^{4.0}$ $TCID_{50}$ of each virus, and clinical manifestations were monitored. Chickens inoculated with L4/P0NA-65H exhibited similar clinical onsets to those inoculated with L4/P0NA, with no significant difference in the survival curve (p value adjusted using the Bonferroni method following pairwise comparisons using the log-rank test, $p = 1.000$; Figure 7B), suggesting that the Y65H substitution in the NA-stalk did not affect viral pathogenicity in chickens. Conversely, all chickens inoculated with L4/P0NAΔG-65H developed severe neurological signs within 4 dpi and died within 5 days. The time required to affect all individuals inoculated with L4/P0NAΔG-65H was shorter than that for L4/P0NA-65H and no longer than that for L4. The difference in the survival curve was not statistically significant ($p = 0.118$ vs. L4/P0NA-65H; $p = 0.162$ vs. L4, which was compared to $p = 0.023$ for L4/P0NA-65H vs. L4). Notably, no mutations, including substitutions or deletions, were found in the viruses recovered from chickens inoculated with L4/P0NA-65H and L4/P0NAΔG-65H. Chickens were also euthanized on 3 dpi to investigate viral loads in blood and tissue

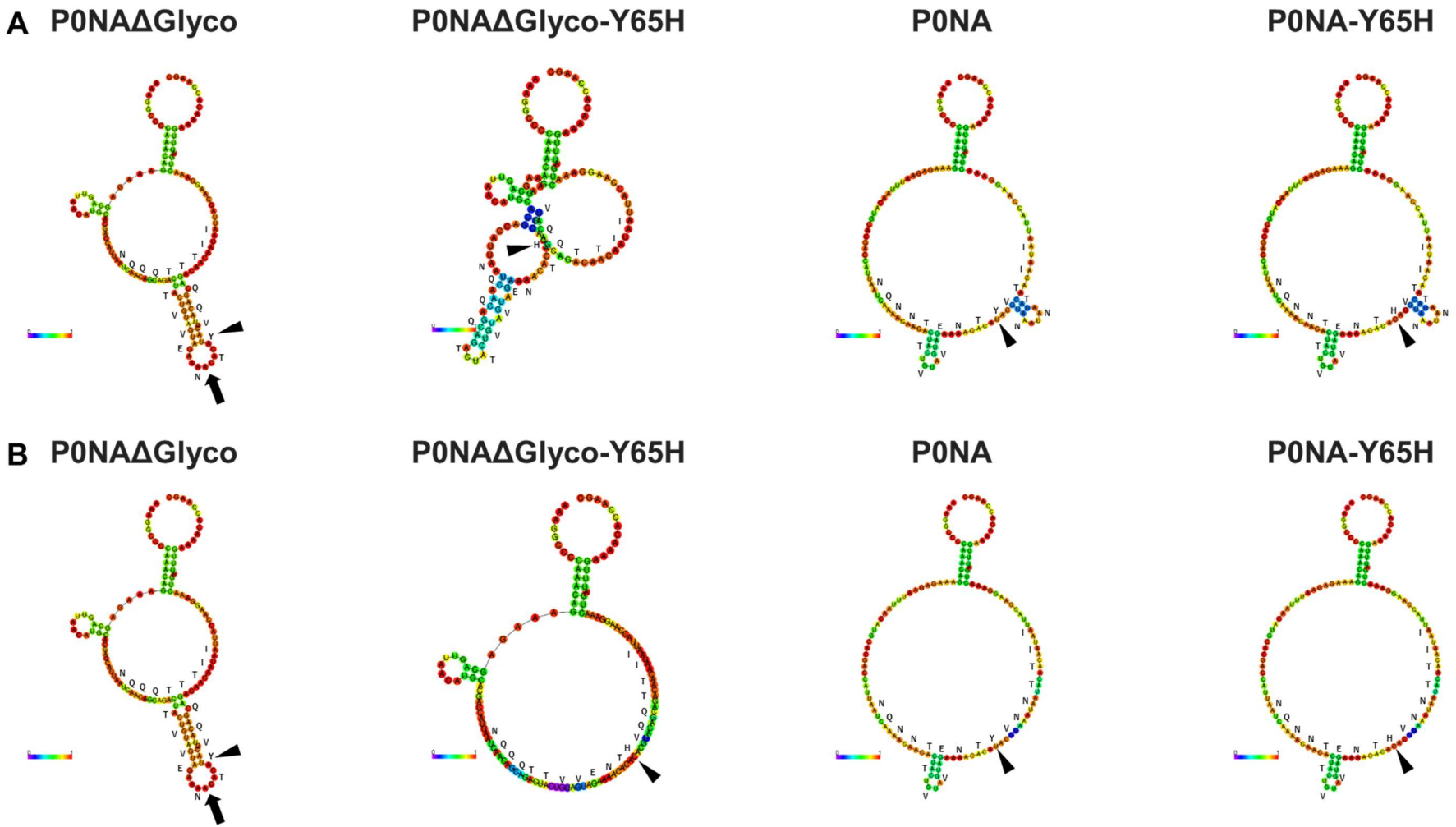

Figure 8. RNA secondary structures predicted using RNAfold WebServer. (A) MFE structure. (B) Centroid structure. Both structures were generated using default settings from the RNAfold WebServer (http://rna.tbi.univie.ac.at//cgi-bin/RNAWebSuite/RNAfold.cgi). Arrowheads indicate the positions of nucleotide substitution from U (coding 65Y) to C (coding 65H). Arrows indicate stem-loop structures within the NA stalk-coding region that exhibit higher base-pair probabilities in the P0NAΔGlyco.

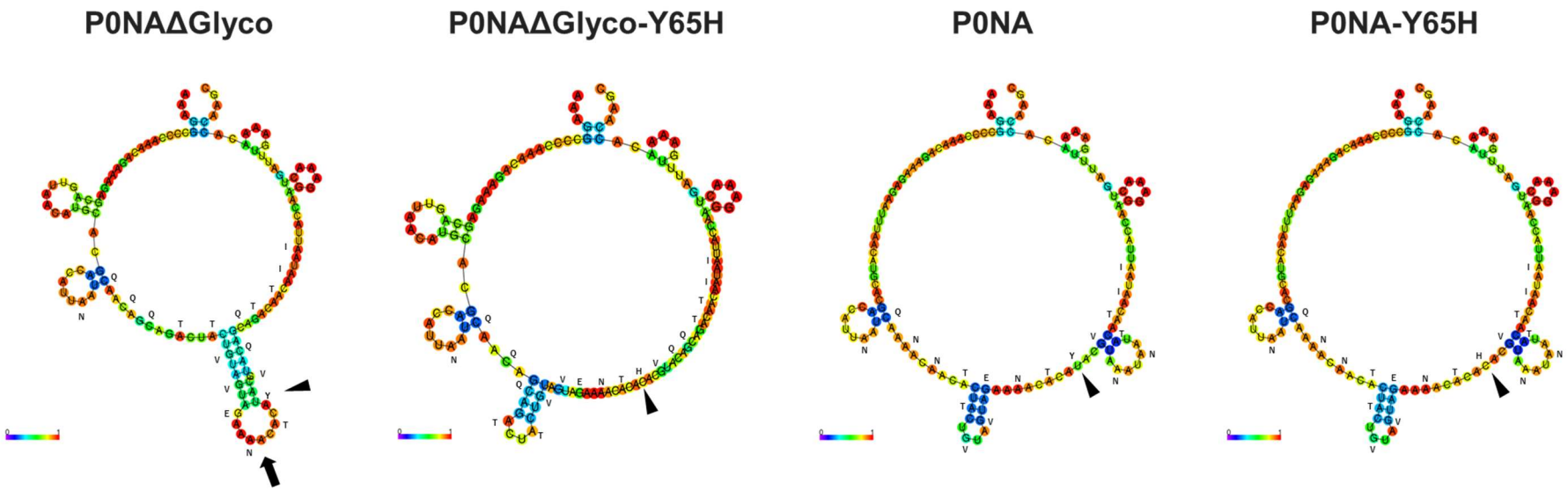

Figure 9. RNA secondary structures predicted using CentroidFold. RNA secondary structures were predicted using CentroidFold (http://rtools.cbrc.jp/cgi-bin/index.cgi) with the default McCaskill (BL) model. Arrowheads indicate the positions of nucleotide substitution from U (coding 65Y) to C (coding 65H). Arrows indicate stem-loop structures within the NA stalk-coding region that exhibit higher base-pair probabilities in the P0NAΔGlyco.

samples. The virus titers in the trachea and lung of L4/P0NAΔG-65H-inoculated chickens were higher than those in chickens inoculated with L4/P0NA-65H (Figure 10). Additionally, higher levels of viremia were confirmed in the blood samples of chickens inoculated with L4/P0NAΔG-65H compared to those inoculated with L4/P0NA-65H. This resulted in higher viral loads in the brain, liver, kidney, and colon. These results demonstrate that the loss of potential *N*-glycosylation sites in the NA-stalk domain contributed to increased viral growth in primary target organs, such as the trachea and lungs, leading to higher viremia on 3 dpi and shortened survival periods for the infected chickens. When comparing L4/P0NAΔG-65H to L4, comparable virus loads were observed in each tissue sample except the brain (Figure 10). This finding supports the notion that the loss of glycosylation in the NA stalk is sufficient for rapid viral growth in chickens and suggests an additional advantage for viruses with short-stalk NA in replicating in the chicken brain.

Loss of glycosylation in the NA stalk reduces the NA function on the virus particles

Loss of glycosylation in the NA-stalk region in L4/P0NA-65H enhanced viral pathogenicity in chickens, the NA function was assessed based on erythrocyte elution activity. Previous studies have demonstrated that viruses with a short NA stalk have reduced elution activity against chicken erythrocytes, which is consistent with their higher pathogenicity in chickens compared to viruses with a full NA stalk [38, 73, 96]. Thus, this study aimed to address the contribution of deglycosylation in the NA-stalk to erythrocyte elution activity. Viruses with an L4 backbone could not achieve high HA titers (<2 HAU) in eggs due to their exceptionally high lethality to chicken embryos. Therefore, a set of viruses—Vac2/P0NA, Vac2/L4NA, and Vac2/P0NAΔG—using the backbone of a nonpathogenic AIV (Vac2) were generated and used for the erythrocyte elution assay as previously described (Table 2; [96]). As expected, the virus with full-stalk NA, Vac2/P0NA, efficiently eluted chicken erythrocytes, whereas the virus with short-stalk NA, Vac2/L4NA, did not elute erythrocytes within 8 hours (Figure 11A). Similarly, the NA-stalk deglycosylated virus, Vac2/P0NAΔG, also failed to elute chicken erythrocytes, suggesting that the loss of *N*-glycosylation in the NA-stalk domain, rather than stalk truncation, reduces the erythrocyte elution activity of the virus. Since Arai *et al*. [39] reported that the deglycosylation or truncation in the NA stalk domain has a minor effect on the substrate-binding affinity of the catalytic site, the NA activity was also

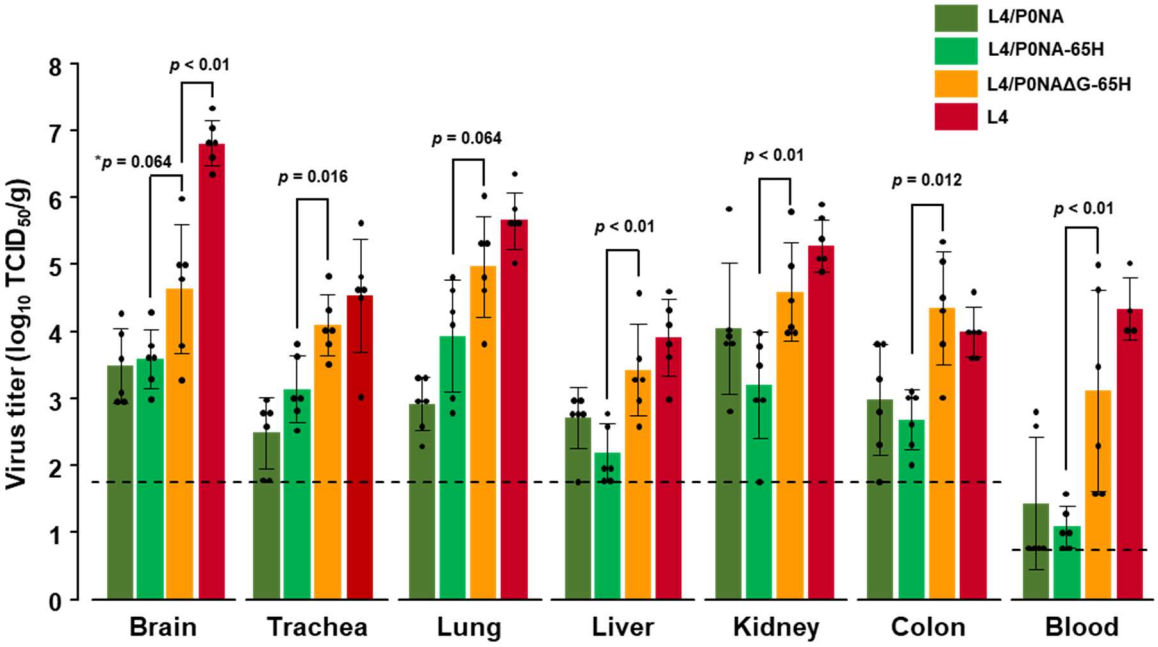

Figure 10. Virus recovery from chickens intranasally inoculated with L4 mutants harboring Y65H substitution in the NA-stalk domain. Virus titers in the organs of chickens intranasally inoculated with each virus were evaluated 3 days post-inoculation. The dotted line indicates the threshold for virus titration (<1.8 $\log_{10}$ $TCID_{50}$/g for organ samples and <0.8 $\log_{10}$ $TCID_{50}$/g for blood). *Statistical analysis was performed using the Mann–Whitney U test between L4/P0NA-65H (light green) and L4/P0NAΔG-65H (orange). Virus titers below the detection limit were considered as 1.8 $\log_{10}$ $TCID_{50}$/g for tissue samples and 0.8 $\log_{10}$ $TCID_{50}$/g for blood for statistical analysis.

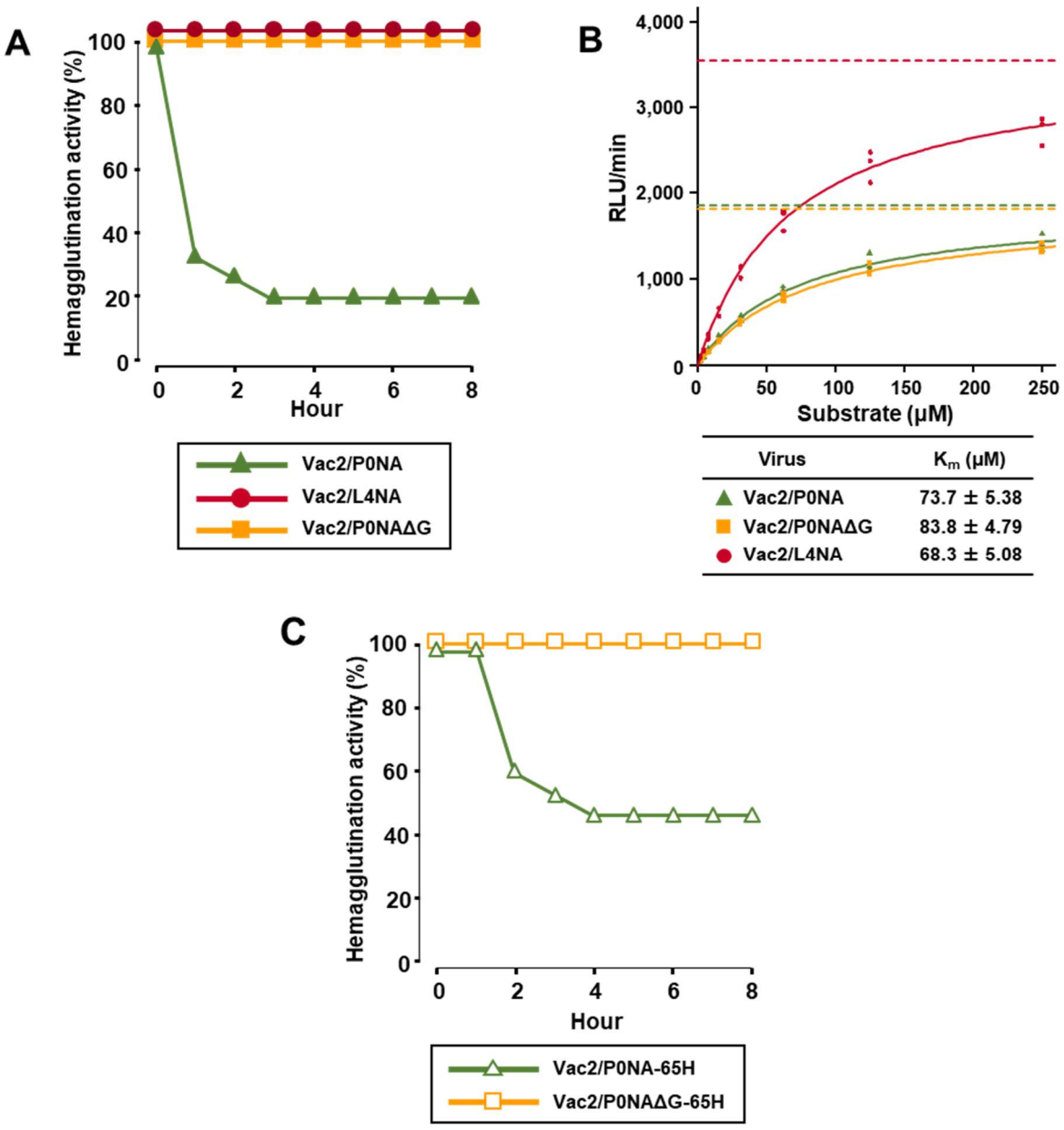

Figure 11. Biological characteristics of Vac2 mutants with or without glycosylation in the NA-stalk domain. (A) Erythrocyte elution activity of Vac2/P0NA, Vac2/L4NA, and Vac2/P0NAΔG was assessed. These mutants harbor full-stalk NA, short-stalk NA, and glycan-deficient-stalk NA, respectively. (B) Sialidase activity of Vac2/P0NA, Vac2/L4NA, and Vac2/P0NAΔG to MUNANA was assessed. The initial reaction rate at each condition was plotted to calculate the K_m. The data were represented as the mean ± SE of three independent experiments. (C) Erythrocyte elution activity of Vac2 mutants with partially glycosylated NA in the stalk was assessed.

evaluated using a small compound, MUNANA. The data were fitted to the Michaelis-Menten equation via non-linear regression, and the Michaelis constant (K_m) was calculated for each of the viruses. The K_m values were 73.7 ± 5.38 μM for Vac2/P0NA, 83.8 ± 4.79 μM for Vac2/P0NAΔG and 68.3 ± 5.08 μM for Vac2/L4NA, indicating that their comparable affinities with the small substrate (Figure 11B). Although the maximum velocity of the reaction (V_{max}) for Vac2/L4NA was higher than the others, this rather reflects the higher input of viruses in the assay. These results demonstrate that while the deglycosylation and truncation in the NA stalk domain do not affect its sialidase activity to small substrates, they remarkably affect the erythrocyte elution activity, suggesting the reduction of activity to bulky substrates.

Next, the effect of the Y65H mutation on elution activity using a pair of Y65H mutants (Vac2/P0NA-65H and Vac2/P0NAΔG-65H; Figure 11C) was assessed. The erythrocyte elution activity of Vac2/P0NA-65H was relatively lower than that of Vac2/P0NA, whereas the phenotypic change induced by glycosylation deficiency was evident in the elution activity of Vac2/P0NAΔG-65H. Thus, the impact of the Y65H mutation in the NA-stalk domain was limited to the erythrocyte elution activity of the viruses.

Potential *N*-glycosylation sites on the NA stalk of rgVac2-P0NA were occupied

Given that the loss of potential *N*-glycosylation sites in the NA-stalk domain decreased erythrocyte elution activity, two hypotheses arose: a reduction in the NA molecules on the virus particles or functional changes in NA resulting from the loss of glycosylations at the stalk. First, the amount of NA incorporated into the virus particles was assessed. To detect NA proteins using a commercial antibody, plasmids coding FLAG (DYKDDDDK)-tagged NA proteins were generated as described by Hiono and Kuno ([85]; Figure 12A). A set of plasmids encoding FLAG-tagged NA (Vac2/P0NA-FLAG, Vac2/P0NAΔG-FLAG, and Vac2/L4NA-FLAG) was used for virus rescue with the Vac-2 backbone to obtain higher titers of these viruses. The relative NA/NP ratios of the glycosylation-deficient virus and NA-stalk truncated virus were compared to the virus harboring full-stalk NA via dot blotting. The relative NA incorporation was calculated as 1.48 for Vac2/P0NAΔG-FLAG and 0.74 for Vac2/L4NA-FLAG. These values did not correlate with the NA function as evaluated by erythrocyte elution activity (Figure 12B).

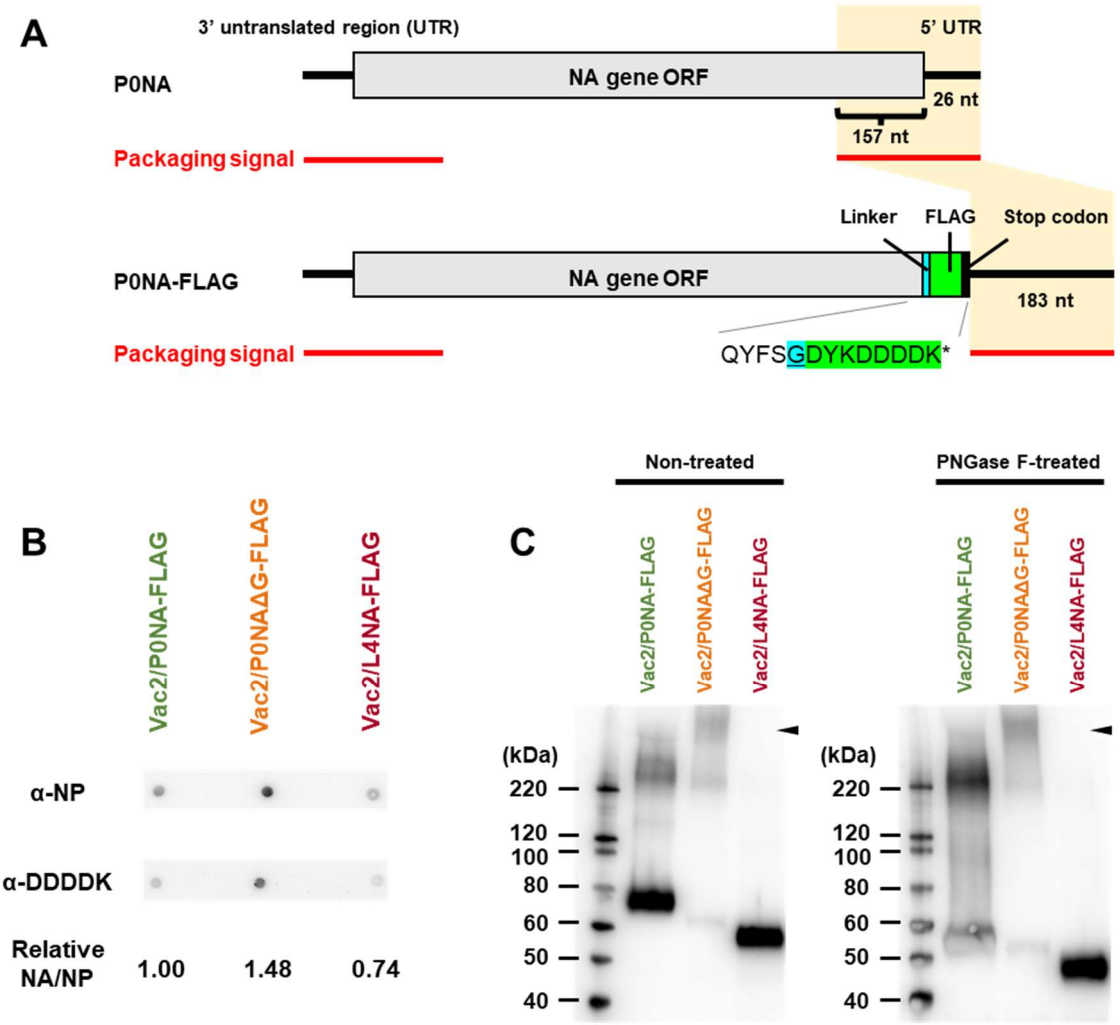

Figure 12. Gene construction for the FLAG-fused NA protein and comparison of NA intake in virus virions among Vac2 mutants. (A) Schematic representation of the gene construction for generating the FLAG (DYKDDDDK)-fused NA protein. (B) NA intake in the virus virions of Vac2 mutants was assessed by comparing NA/NP ratios of the virus virions immunoprecipitated with an anti-HA antibody. The relative intensity of three spots was calculated and normalized to Vac2/P0NA. (C) Molecular weight of the NA proteins was compared to assess glycosylation of the NA-stalk domains under nontreated and PNGase F-treated conditions. Arrowhead indicates the aggregates of NA proteins of Vac2/P0NAΔG on the top of resolving gel.

Second, to validate the glycan occupancy of the NA-stalk domain, the molecular weights of NA proteins were compared via western blotting (Figure 12C). The molecular weight of Vac2/P0NA-FLAG was larger than that of Vac2/P0NAΔG-FLAG under nontreated conditions. In contrast, after treatment with PNGase F, which removes *N*-glycans from the NA proteins, the electrophoretic mobility of Vac2/P0NA-FLAG and Vac2/P0NAΔG-FLAG was comparable. It should be noted that the faint band was obtained at approximately 65 kDa in Vac2/P0NAΔG-FLAG without PNGase F treatment because this NA was prone to be aggregated due to the deglycosylation, which was also supported by the presence of another band at the top of the resolving gel. These results indicate that the stalk domain of P0NA-FLAG is glycosylated with at least one *N*-glycan.

Potential *N*-glycosylation sites on the NA stalk of rgVac2-P0NA were occupied

To comprehensively investigate site-specific glycan occupancy on the NA-stalk domain, IGOT-LC/MS analysis was performed. Among the tryptic digests identified, all five potential *N*-glycosylation sites were included in a single peptide (QKENLTCTTINQNNTTVVENTYVNNTTIITK). In the IGOT analysis, glycan-liberated asparagines were converted into ^{18}O-containing aspartic acids by digestion with PNGase F in $H_2{}^{18}O$. Therefore, glycosylated peptides could be differentiated from nonglycosylated peptides by a molecular mass shift of 2.988261 Da per glycosylation site. In the peptides derived from P0NA, three or four sites were generally occupied among five N-!P-S/T (!P = any amino acid except proline) sites, and peptides with fewer than three *N*-glycans were not identified. In MS1 spectra, a total of six distinct peptides covering the five potential *N*-glycosylation sites of P0NA were identified via Mascot searching (Figures 13–18). In a peptide glycosylated with three asparagine residues, the *N*-glycosylations on N47, N56, and N67 were confirmed by the b and y ions in MS2 spectra (Figure 13A, B). Subsequently, a monoisotopic peak for non- or less-glycosylated peptides, which have a smaller molecular mass than the glycosylated peptide by 2.988261 Da, was searched for in MS1 spectra. However, no specific ions corresponding to less-glycosylated peptides were obtained in the MS1 spectra, indicating that peptides with two glycans were not identified (Figure 13C, D). Moreover, two peptides with four IGOT labels were identified through database searching using Mascot, and double glycosylation at either of the NNTT sequons was suspected in these peptides.

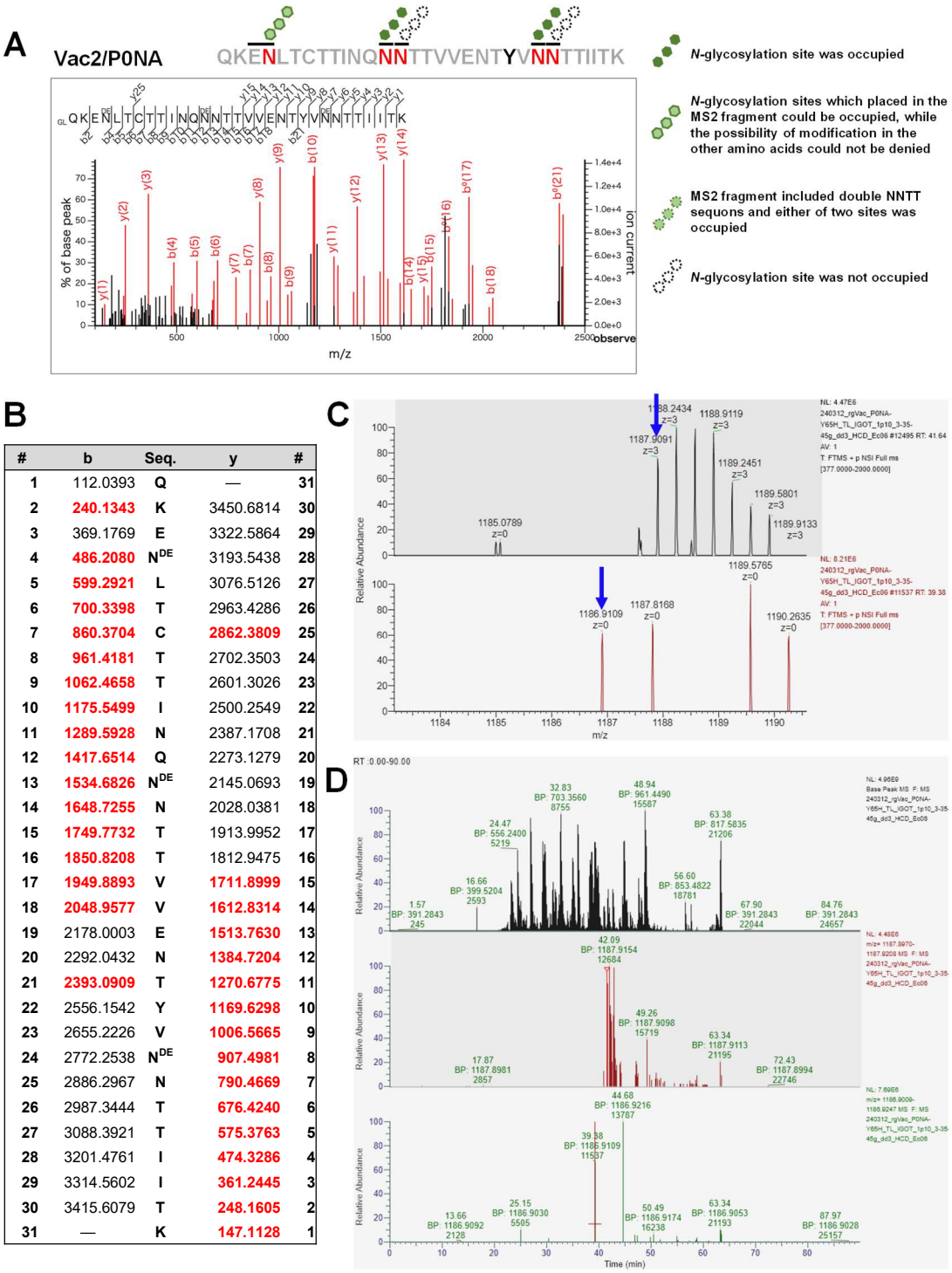

#	b	Seq.	y	#
1	112.0393	Q	—	31
2	240.1343	K	3450.6814	30
3	369.1769	E	3322.5864	29
4	486.2080	N^{DE}	3193.5438	28
5	599.2921	L	3076.5126	27
6	700.3398	T	2963.4286	26
7	860.3704	C	2862.3809	25
8	961.4181	T	2702.3503	24
9	1062.4658	T	2601.3026	23
10	1175.5499	I	2500.2549	22
11	1289.5928	N	2387.1708	21
12	1417.6514	Q	2273.1279	20
13	1534.6826	N^{DE}	2145.0693	19
14	1648.7255	N	2028.0381	18
15	1749.7732	T	1913.9952	17
16	1850.8208	T	1812.9475	16
17	1949.8893	V	1711.8999	15
18	2048.9577	V	1612.8314	14
19	2178.0003	E	1513.7630	13
20	2292.0432	N	1384.7204	12
21	2393.0909	T	1270.6775	11
22	2556.1542	Y	1169.6298	10
23	2655.2226	V	1006.5665	9
24	2772.2538	N^{DE}	907.4981	8
25	2886.2967	N	790.4669	7
26	2987.3444	T	676.4240	6
27	3088.3921	T	575.3763	5
28	3201.4761	I	474.3286	4
29	3314.5602	I	361.2445	3
30	3415.6079	T	248.1605	2
31	—	K	147.1128	1

Figure 13. MS2 spectrum of the peptide of P0NA with three glycans at N47, N56 and N67, and mass chromatograms of precursor ions to identify site occupancy. (A) MS2 spectrum of the peptide of P0NA containing three glycans. (B) Molecular mass of b and y ion fragments derived from the peptide of P0NA. Red and black letters indicate b and y ion fragments detected and calculated based on the amino acid sequence, respectively. (C) MS1 spectra of a peptide with three glycans in upper panel and that with two glycans in lower panel were compared. The monoisotopic peak of MS1 corresponding to the less-glycosylated peptide (blue arrow in the bottom panel) was not observed. (D) Base peak mass spectrum (black) and mass chromatogram of the precursor ions corresponding to the peptide with three glycans (red) and two glycans (green). The less-glycosylated peptide was not detected.

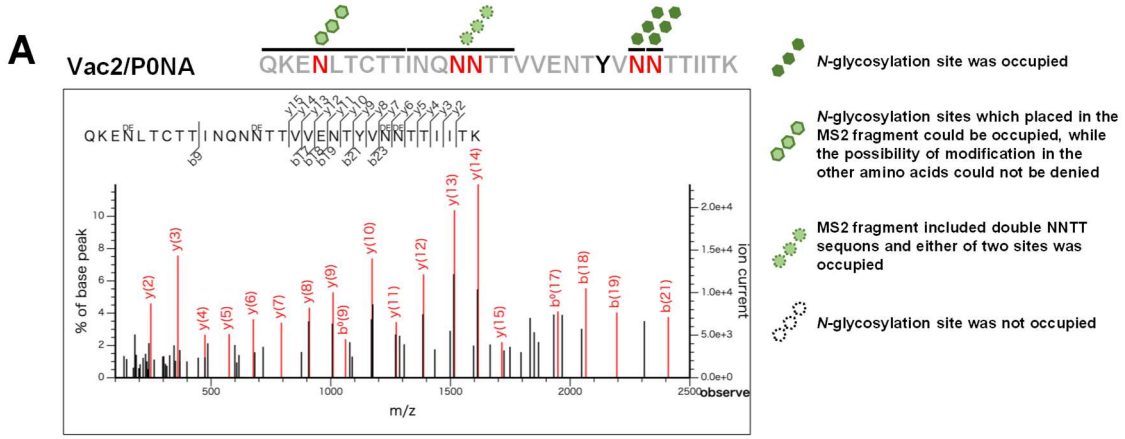

Figure 14. MS2 spectrum of the peptide of P0NA with four glycans at N47, N56/57, N67 and N68, and mass chromatograms of precursor ions to identify site occupancy. (A) MS2 spectrum of the peptide of P0NA containing four glycans.

B

#	b	Seq.	y	#
1	129.0659	Q	—	31
2	257.1608	K	3453.6697	30
3	386.2034	E	3325.5747	29
4	503.2346	N	3196.5321	28
5	616.3187	L	3079.5009	27
6	717.3663	T	2966.4168	26
7	877.3970	C	2865.3692	25
8	978.4447	T	2705.3385	24
9	1079.4923	T	2604.2908	23
10	1192.5764	I	2503.2432	22
11	1306.6193	N	2390.1591	21
12	1434.6779	Q	2276.1162	20
13	1548.7208	N	2148.0576	19
14	1665.7520	N	2034.0147	18
15	1766.7997	T	1916.9835	17
16	1867.8474	T	1815.9358	16
17	1966.9158	V	1714.8881	15
18	2065.9842	V	1615.8197	14
19	2195.0268	E	1516.7513	13
20	2309.0697	N	1387.7087	12
21	2410.1174	T	1273.6658	11
22	2573.1807	Y	1172.6181	10
23	2672.2492	V	1009.5548	9
24	2789.2803	N^{DE}	910.4863	8
25	2906.3115	N^{DE}	793.4552	7
26	3007.3592	T	676.4240	6
27	3108.4069	T	575.3763	5
28	3221.4910	I	474.3286	4
29	3334.5750	I	361.2445	3
30	3435.6227	T	248.1605	2
31	—	K	147.1128	1

C

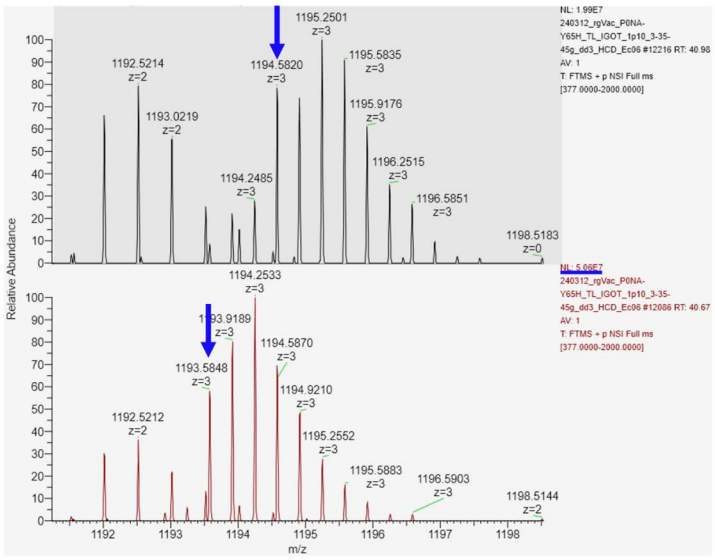

D

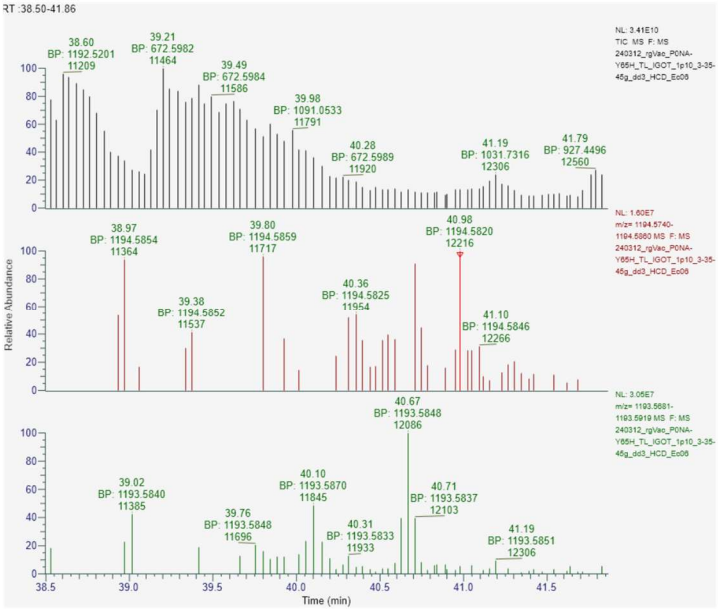

Figure 14 (*cont*)**. MS2 spectrum of the peptide of P0NA with four glycans at N47, N56/57, N67 and N68, and mass chromatograms of precursor ions to identify site occupancy.** (B) Molecular mass of b and y ion fragments derived from the peptide of P0NA with four glycans. Red and black letters indicate b and y ion fragments detected and calculated based on the amino acid sequence, respectively. (C) The monoisotopic peak of MS1 corresponding to the less-glycosylated peptide, which had a smaller molecular mass by 2.99 Da (m/z 0.997 [z = +3]; two blue arrows), was observed. (D) Mass chromatogram of precursor ions shows that the less-glycosylated peptide with three glycans (40.67 min; green) had a shorter LC retention time compared to the peptide with four glycans (40.98 min; red).

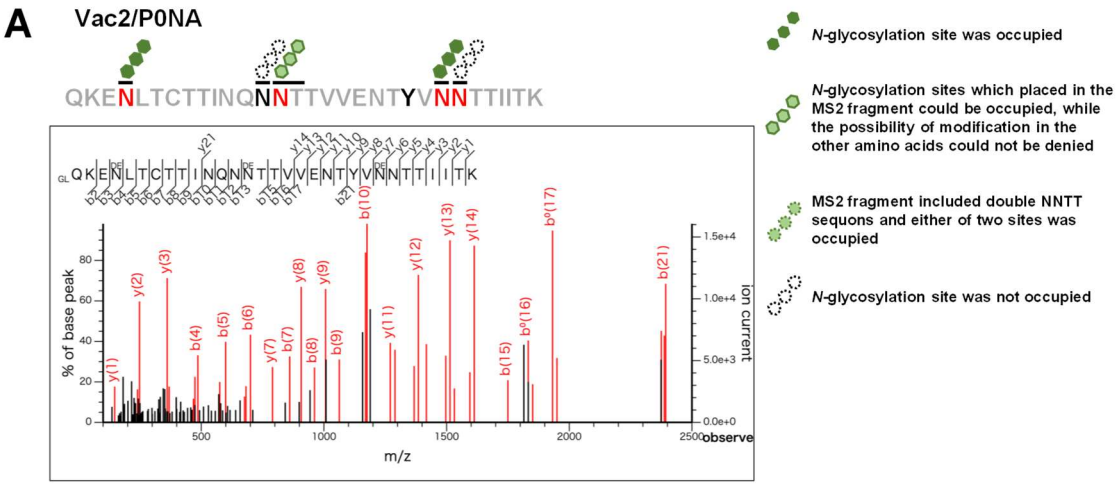

B

#	b	Seq.	y	#
1	112.0393	Q	—	31
2	240.1343	K	3450.6814	30
3	369.1769	E	3322.5864	29
4	486.2080	N^{DE}	3193.5438	28
5	599.2921	L	3076.5126	27
6	700.3398	T	2963.4286	26
7	860.3704	C	2862.3809	25
8	961.4181	T	2702.3503	24
9	1062.4658	T	2601.3026	23
10	1175.5499	I	2500.2549	22
11	1289.5928	N	2387.1708	21
12	1417.6514	Q	2273.1279	20
13	1531.6943	N	2145.0693	19
14	1648.7255	N^{DE}	2031.0264	18
15	1749.7732	T	1913.9952	17
16	1850.8208	T	1812.9475	16
17	1949.8893	V	1711.8999	15
18	2048.9577	V	1612.8314	14
19	2178.0003	E	1513.7630	13
20	2292.0432	N	1384.7204	12
21	2393.0909	T	1270.6775	11
22	2556.1542	Y	1169.6298	10
23	2655.2226	V	1006.5665	9
24	2772.2538	N^{DE}	907.4981	8
25	2886.2967	N	790.4661	7
26	2987.3444	T	676.4240	6
27	3088.3921	T	575.3763	5
28	3201.4761	I	474.3286	4
29	3314.5602	I	361.2445	3
30	3415.6079	T	248.1605	2
31	—	K	147.1128	1

C

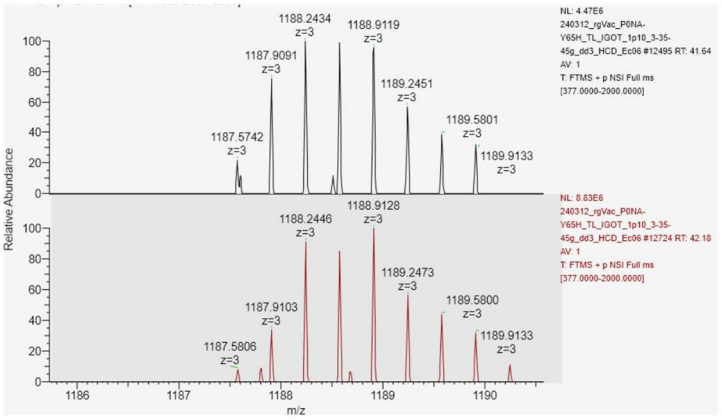

Figure 15. MS2 spectrum of the peptide of P0NA with three glycans at N47, N57 and N67. (A) MS2 spectrum of the peptide of P0NA containing three glycans. (B) Molecular mass of b and y ion fragments derived from the peptide of P0NA with three glycans. Red and black letters indicate b and y ion fragments detected and calculated based on the amino acid sequence, respectively. (C) The monoisotopic peak of MS1 corresponding to the less-glycosylated peptide was not observed.

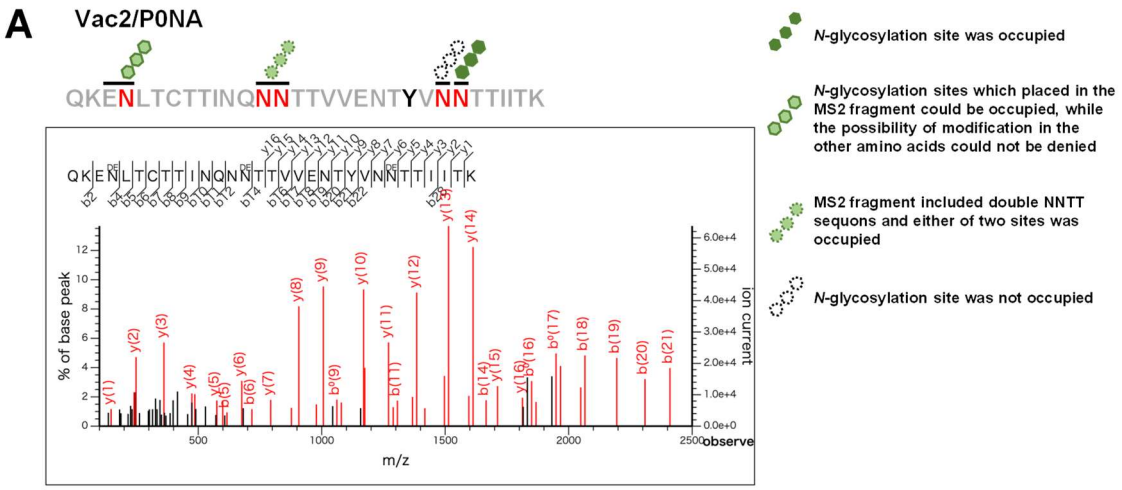

Figure 16. MS2 spectrum of the peptide of P0NA with three glycans at N47, N56/57, and N68, and confirmation of no peptide with two glycans. (A) MS2 spectrum of the peptide of P0NA containing three glycans.

B

#	b	Seq.	y	#
1	129.0659	Q	—	31
2	257.1608	K	3450.6814	30
3	386.2034	E	3322.5864	29
4	503.2346	N^{DE}	3193.5438	28
5	616.3181	L	3076.5126	27
6	717.3663	T	2963.4286	26
7	877.3970	C	2862.3809	25
8	978.4441	T	2702.3503	24
9	1079.4923	T	2601.3026	23
10	1192.5764	I	2500.2549	22
11	1306.6193	N	2387.1708	21
12	1434.6779	Q	2273.1279	20
13	1548.7208	N	2145.0693	19
14	1665.7520	N^{DE}	2031.0264	18
15	1766.7997	T	1913.9952	17
16	1867.8474	T	1812.9475	16
17	1966.9158	V	1711.8999	15
18	2065.9842	V	1612.8314	14
19	2195.0268	E	1513.7630	13
20	2309.0691	N	1384.7204	12
21	2410.1174	T	1270.6775	11
22	2573.1807	Y	1169.6298	10
23	2672.2492	V	1006.5665	9
24	2786.2921	N	907.4981	8
25	2903.3233	N^{DE}	793.4552	7
26	3004.3710	T	676.4240	6
27	3105.4186	T	575.3763	5
28	3218.5027	I	474.3286	4
29	3331.5868	I	361.2445	3
30	3432.6344	T	248.1605	2
31	—	K	147.1128	1

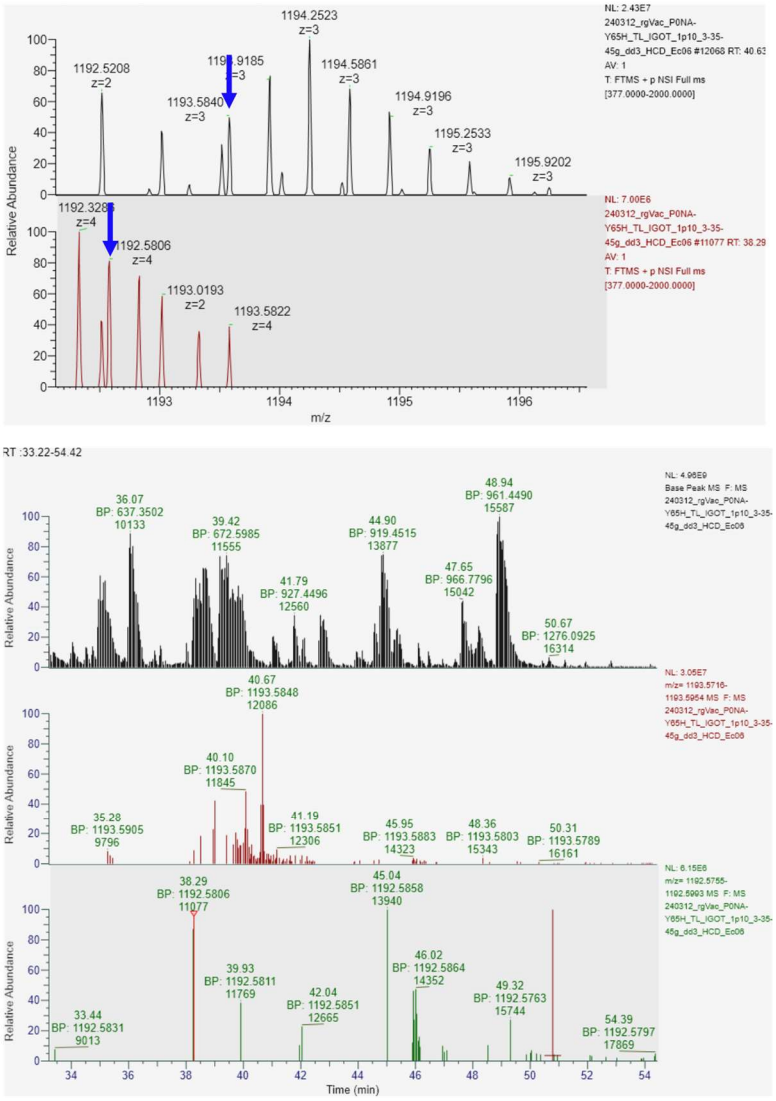

Figure 16 (*cont*)**. MS2 spectrum of the peptide of P0NA with three glycans at N47, N56/57, and N68, and confirmation of no peptide with two glycans.** (B) Molecular mass of b and y ion fragments derived from the peptide of P0NA with three glycans. Red and black letters indicate b and y ion fragments detected and calculated based on the amino acid sequence, respectively. (C) The monoisotopic peak of MS1 corresponding to the suspicious less-glycosylated peptide, which had a smaller molecular mass by 2.99 Da (m/z 0.997 [z = +3]; two blue arrows), was not an ideal peak but a noise. (D) Mass chromatogram of precursor ions indicates that there was no peptide with two glycans.

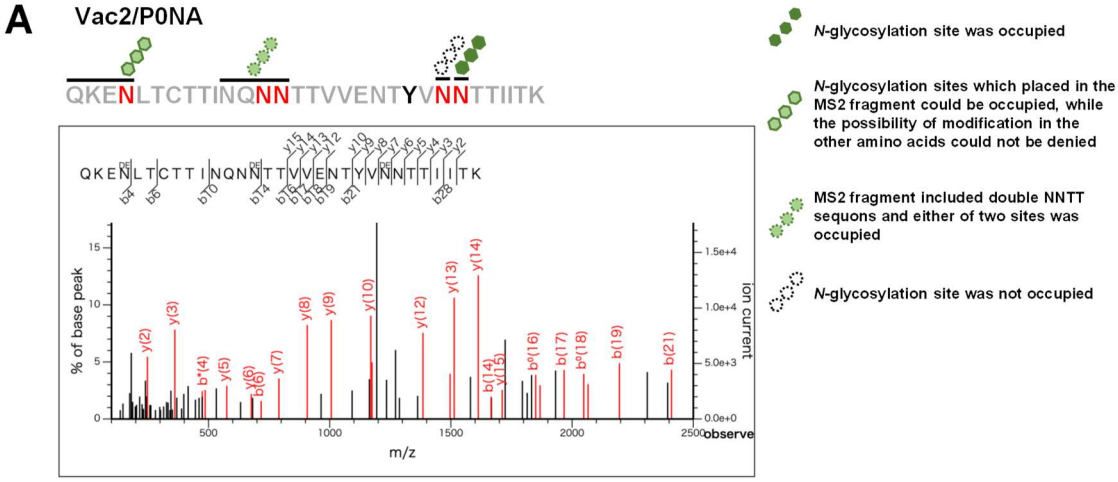

B

#	b	Seq.	y	#
1	129.0659	Q	—	31
2	257.1608	K	3450.6814	30
3	386.2034	E	3322.5864	29
4	503.2346	N^{DE}	3193.5438	28
5	616.3187	L	3076.5126	27
6	717.3663	T	2963.4286	26
7	877.3970	C	2862.3809	25
8	978.4447	T	2702.3503	24
9	1079.7923	T	2601.3026	23
10	1192.5764	I	2500.2549	22
11	1306.6193	N	2387.1708	21
12	1434.6779	Q	2273.1279	20
13	1548.7208	N	2145.0693	19
14	1665.7520	N^{DE}	2031.0264	18
15	1766.7997	T	1913.9952	17
16	1867.8474	T	1812.9475	16
17	1966.9158	V	1711.8999	15
18	2065.9842	V	1612.8314	14
19	2195.0268	E	1513.7630	13
20	2309.0697	N	1384.7204	12
21	2410.1174	T	1270.6775	11
22	2573.1807	Y	1169.6298	10
23	2672.2492	V	1006.5665	9
24	2789.2803	N^{DE}	907.4981	8
25	2903.3233	N	790.4669	7
26	3004.3710	T	676.4240	6
27	3105.4186	T	575.3763	5
28	3218.5027	I	474.3286	4
29	3331.5868	I	361.2445	3
30	3432.6344	T	248.1605	2
31	—	K	147.1128	1

C

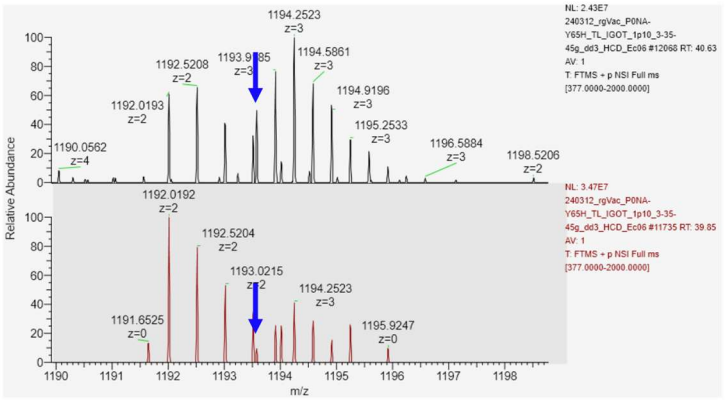

Figure 17. Identification of multiple peptides of P0NA with three glycans at N47, N56/57, and N68. (A) MS2 spectrum of the peptide of P0NA containing three glycans. (B) Molecular mass of b and y ion fragments derived from the peptide of P0NA with three glycans. Red letters indicate b and y ion fragments detected in this analysis, whereas black letters refer to the calculated molecular weights based on the amino acid sequence. (C) The monoisotopic peak of MS1 corresponding to the peptide with three glycans (Figure 15) had the same molecular mass, indicating the same peptide.

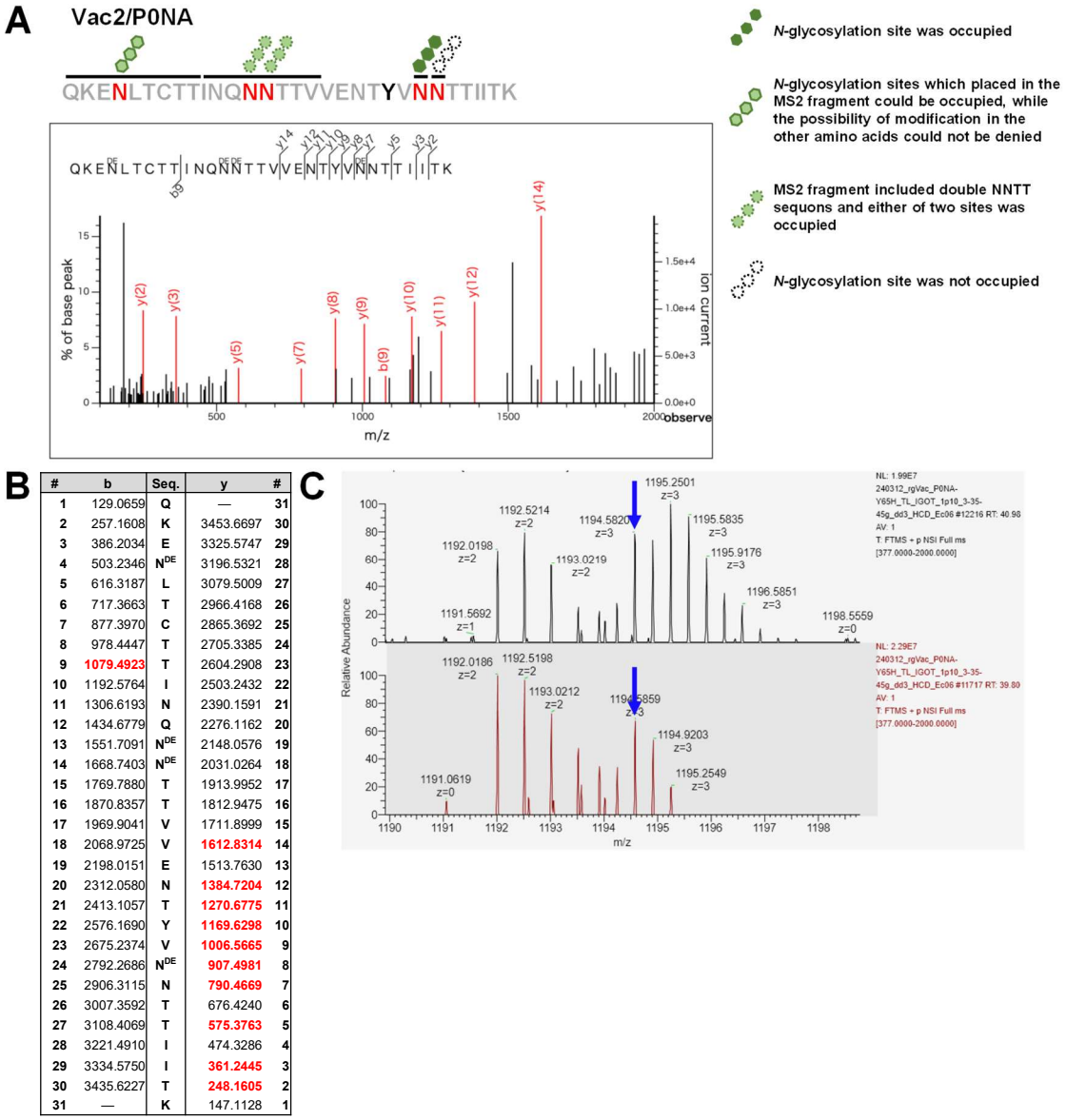

#	b	Seq.	y	#
1	129.0659	Q	—	31
2	257.1608	K	3453.6697	30
3	386.2034	E	3325.5747	29
4	503.2346	N^{DE}	3196.5321	28
5	616.3187	L	3079.5009	27
6	717.3663	T	2966.4168	26
7	877.3970	C	2865.3692	25
8	978.4447	T	2705.3385	24
9	1079.4923	T	2604.2908	23
10	1192.5764	I	2503.2432	22
11	1306.6193	N	2390.1591	21
12	1434.6779	Q	2276.1162	20
13	1551.7091	N^{DE}	2148.0576	19
14	1668.7403	N^{DE}	2031.0264	18
15	1769.7880	T	1913.9952	17
16	1870.8357	T	1812.9475	16
17	1969.9041	V	1711.8999	15
18	2068.9725	V	1612.8314	14
19	2198.0151	E	1513.7630	13
20	2312.0580	N	1384.7204	12
21	2413.1057	T	1270.6775	11
22	2576.1690	Y	1169.6298	10
23	2675.2374	V	1006.5665	9
24	2792.2686	N^{DE}	907.4981	8
25	2906.3115	N	790.4669	7
26	3007.3592	T	676.4240	6
27	3108.4069	T	575.3763	5
28	3221.4910	I	474.3286	4
29	3334.5750	I	361.2445	3
30	3435.6227	T	248.1605	2
31	—	K	147.1128	1

Figure 18. Identification of multiple peptides of P0NA with four glycans at N47, N56, N57, and N67. (A) MS2 spectrum of the peptide of P0NA containing four glycans. (B) Molecular mass of b and y ion fragments derived from the peptide of P0NA with four glycans. Red letters indicate b and y ion fragments detected in this analysis, whereas black letters refer to the calculated molecular weights based on the amino acid sequence. (C) The monoisotopic peak of MS1 corresponding to the multiple peptides with four glycans had identified.

In one of the two peptides, consecutive glycosylations at N67 and N68 were identified based on the y ion fragments in the MS2 spectrum, whereas N47 and either N56 or N57 were occupied in the peptide (Figure 14A, B). In the other peptide, the b and y ion fragments were not observed at the NNTT sequon; therefore, the site-specific glycan occupancy of N56 and N57 was not confirmed (Figure 18). To estimate the abundance ratio of peptides with three versus four *N*-glycans, the mass chromatograms of the precursor ions were analyzed. A monoisotopic peak with m/z 1194.5820 (z = +3) was obtained, which was assigned to the peptide with four glycans, whereas a larger peak with m/z 1193.5848 (z = +3), corresponding to the peptide with three glycans, was also detected (Figure 14C). The latter signal exhibited a shorter LC retention time, confirming it as the peak of the glycosylated peptide with three glycans (Figure 14D). The ratio of peak intensities of monoisotopic ions in the MS1 spectra indicated that peptides with four *N*-glycans (1.99 E7; Figure 14C) constituted 40% of those with three glycans (5.06 E7; Figure 14C). These results demonstrate that the NA-stalk domain of P0NA is occupied by three or four *N*-glycans. Additionally, at least one of the asparagine residues in the NNTT sequons, observed in N56/57 and N67/68, was glycosylated.

The site-specific glycan occupancy was also assessed for P0NA-Y65H to confirm the effect of the Y65H mutation on glycosylation in the NA-stalk. As observed with P0NA, three or four of the five potential *N*-glycosylation sites were occupied, and peptides with fewer than three *N*-glycans were not detected (Figures 19–23). Moreover, the ratio of peak intensities of precursor ions corresponding to triple and quadruple glycosylated peptides indicated that peptides with four glycans reached a level comparable to those with three glycans (Figures 19–22).

These results indicate that the potential *N*-glycosylation sites on the NA-stalk domain of P0NA were occupied. Furthermore, the Y65H mutation did not affect the overall glycosylation of the NA-stalk domain.

Various contributions of *N*-glycosylations to NA function among the sites

Because three or four of the five potential *N*-glycosylation sites in the stalk domain of P0NA were occupied with *N*-glycans, the functional contribution of each *N*-glycosylation site (amino acids 47, 56, 57, 67, and 68) to erythrocyte elution activity was assessed. To this end, mutant viruses with partially restored *N*-glycosylation sequons

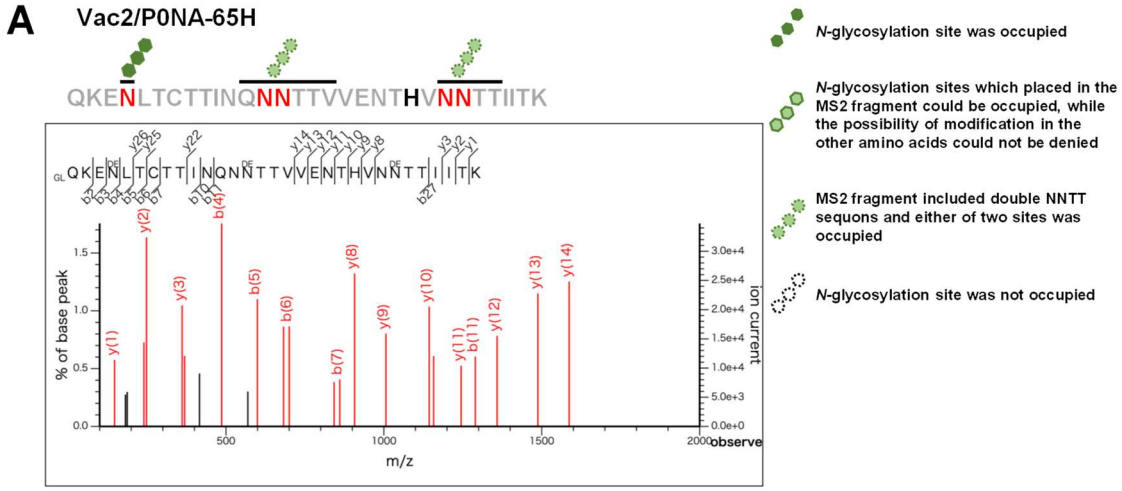

Figure 19. MS2 spectrum of the peptide of P0NA-65H with three glycans at N47, N56/57 and N67/68, and confirmation of no peptide with two glycans. (A) MS2 spectrum of the peptide of P0NA-65H containing three glycans.

B

#	b	Seq.	y	#
1	112.0393	Q	—	31
2	240.1343	K	3424.6770	30
3	369.1769	E	3296.5820	29
4	486.2080	N^{DE}	3167.5394	28
5	599.2921	L	3050.5082	27
6	700.3398	T	2937.4242	26
7	860.3704	C	2836.3765	25
8	961.4181	T	2676.3458	24
9	1062.4658	T	2575.2982	23
10	1175.5499	I	2474.2505	22
11	1289.5928	N	2361.1664	21
12	1417.6514	Q	2247.1235	20
13	1531.6943	N	2119.0649	19
14	1648.7255	N^{DE}	2005.0220	18
15	1749.7732	T	1887.9908	17
16	1850.8208	T	1786.9431	16
17	1949.8893	V	1685.8954	15
18	2048.9577	V	1586.8270	14
19	2178.0003	E	1487.7586	13
20	2292.0432	N	1358.7160	12
21	2393.0909	T	1244.6731	11
22	2530.1498	Y	1143.6254	10
23	2629.2182	V	1006.5665	9
24	2743.2611	N	907.4981	8
25	2860.2923	N^{DE}	793.4552	7
26	2961.3400	T	676.4240	6
27	3062.3877	T	575.3763	5
28	3175.4717	I	474.3286	4
29	3288.5558	I	361.2445	3
30	3389.6035	T	248.1605	2
31	—	K	147.1128	1

C

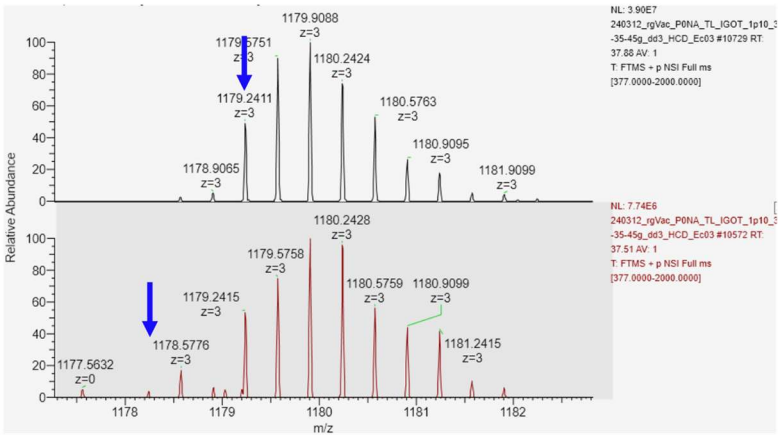

D

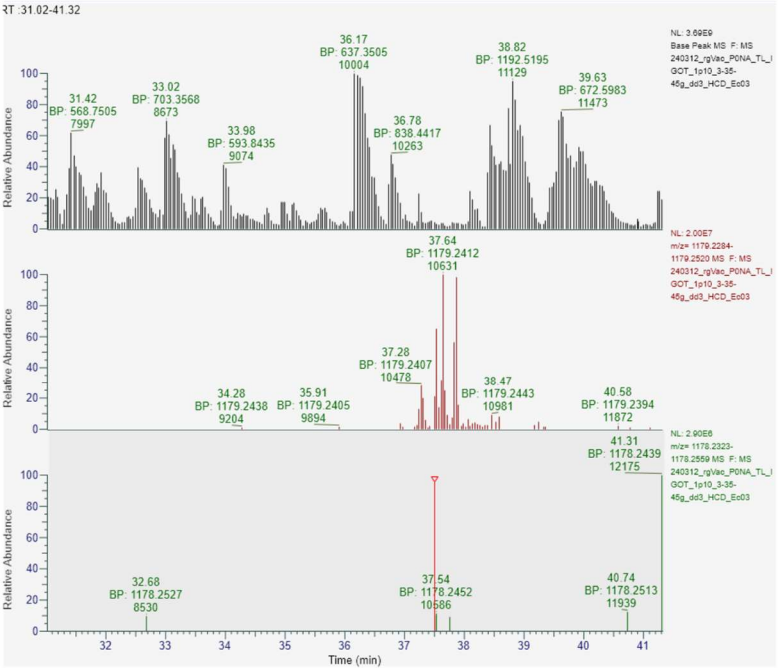

Figure 19 (*cont*)**. MS2 spectrum of the peptide of P0NA-65H with three glycans at N47, N56/57 and N67/68, and confirmation of no peptide with two glycans.** (B) Molecular mass of b and y ion fragments derived from the peptide of P0NA-Y65H with three glycans. Red and black letters indicate b and y ion fragments detected and calculated based on the amino acid sequence, respectively. (C) The monoisotopic peak of MS1 corresponding to the suspicious less-glycosylated peptide, which had a smaller molecular mass by 2.99 Da (m/z 0.997 [z = +3]; two blue arrows), was not found. (D) Mass chromatogram of precursor ions indicates that there was no peptide with two glycans.

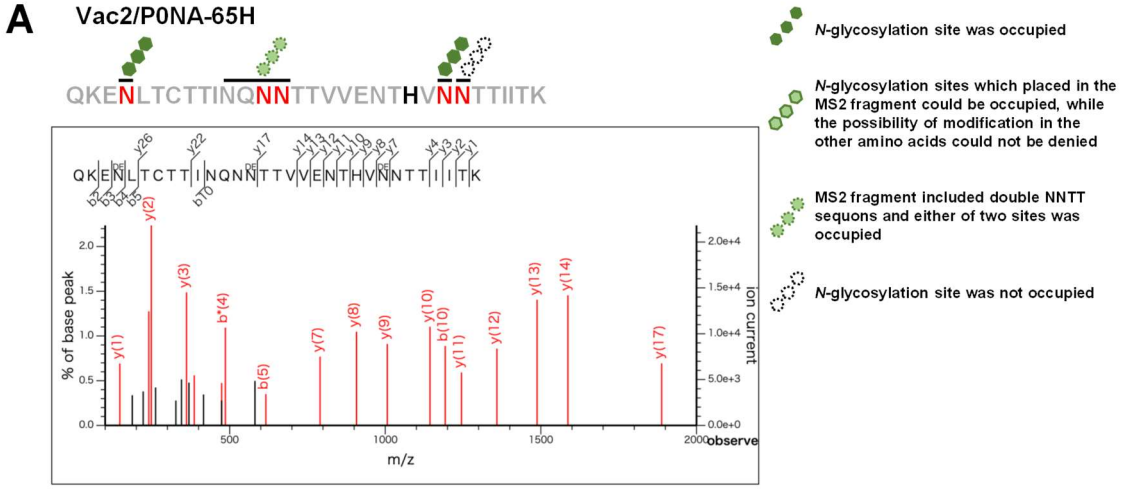

Figure 20. MS2 spectrum of the peptide of P0NA-65H with three glycans at N47, N56/57 and N67, and confirmation of no peptide with two glycans. (A) MS2 spectrum of the peptide of P0NA-65H containing three glycans.

B

#	b	Seq.	y	#
1	129.0659	Q	—	31
2	257.1608	K	3424.6770	30
3	386.2034	E	3296.5820	29
4	503.2346	N^{DE}	3167.5394	28
5	616.3187	L	3050.5082	27
6	717.3663	T	2937.4242	26
7	877.3970	C	2836.3765	25
8	978.4447	T	2676.3458	24
9	1079.4923	T	2575.2982	23
10	1192.5764	I	2474.2505	22
11	1306.6193	N	2361.1664	21
12	1434.6779	Q	2247.1235	20
13	1548.7208	N	2119.0649	19
14	1665.7520	N^{DE}	2005.0220	18
15	1766.7997	T	1887.9908	17
16	1867.8474	T	1786.9431	16
17	1966.9158	V	1685.8954	15
18	2065.9842	V	1586.8270	14
19	2195.0268	E	1487.7586	13
20	2309.0697	N	1358.7160	12
21	2410.1174	T	1244.6731	11
22	2547.1763	Y	1143.6254	10
23	2646.2447	V	1006.5665	9
24	2763.2759	N^{DE}	907.4981	8
25	2877.3189	N	790.4669	7
26	2978.3665	T	676.4240	6
27	3079.4142	T	575.3763	5
28	3192.4983	I	474.3286	4
29	3305.5823	I	361.2445	3
30	3406.6300	T	258.1605	2
31	—	K	147.1128	1

C

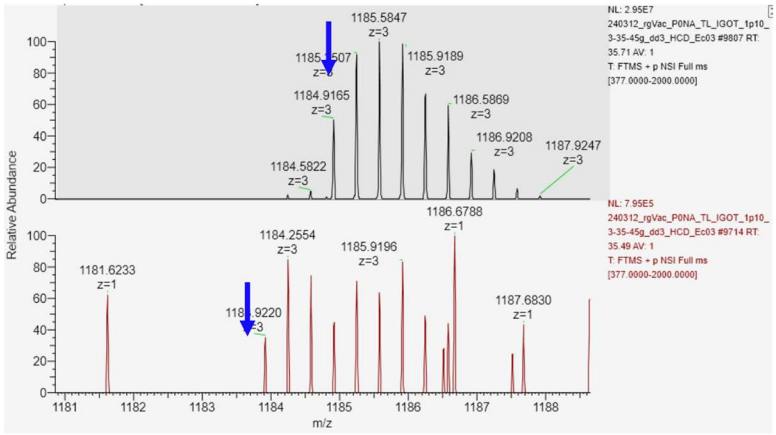

D

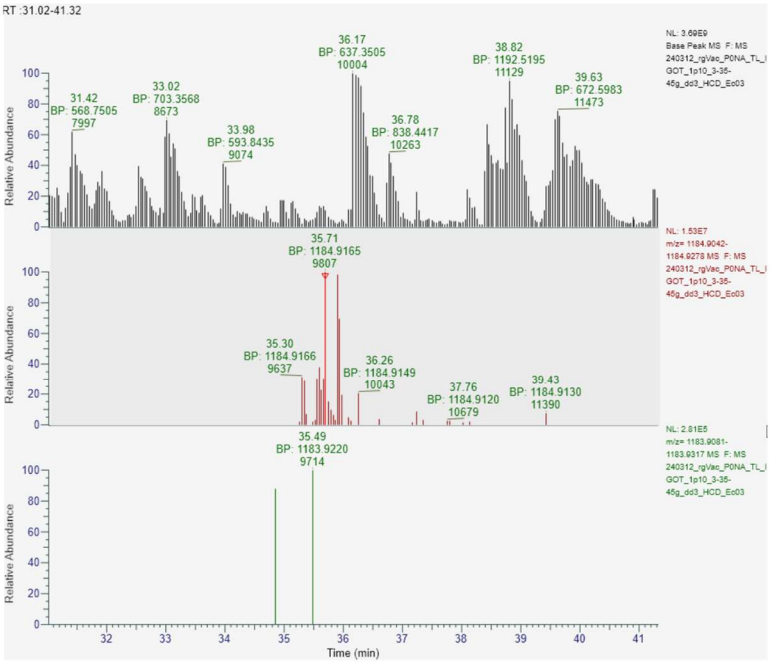

Figure 20 (*cont*)**. MS2 spectrum of the peptide of P0NA-65H with three glycans at N47, N56/57 and N67, and confirmation of no peptide with two glycans.** (B) Molecular mass of b and y ion fragments derived from the peptide of P0NA-Y65H with three glycans. Red and black letters indicate b and y ion fragments detected and calculated based on the amino acid sequence, respectively. (C) The monoisotopic peak of MS1 corresponding to the suspicious less-glycosylated peptide, which had a smaller molecular mass by 2.99 Da (m/z 0.997 [z = +3]; two blue arrows), was not found. (D) Mass chromatogram of precursor ions indicates that there was no peptide with two glycans.

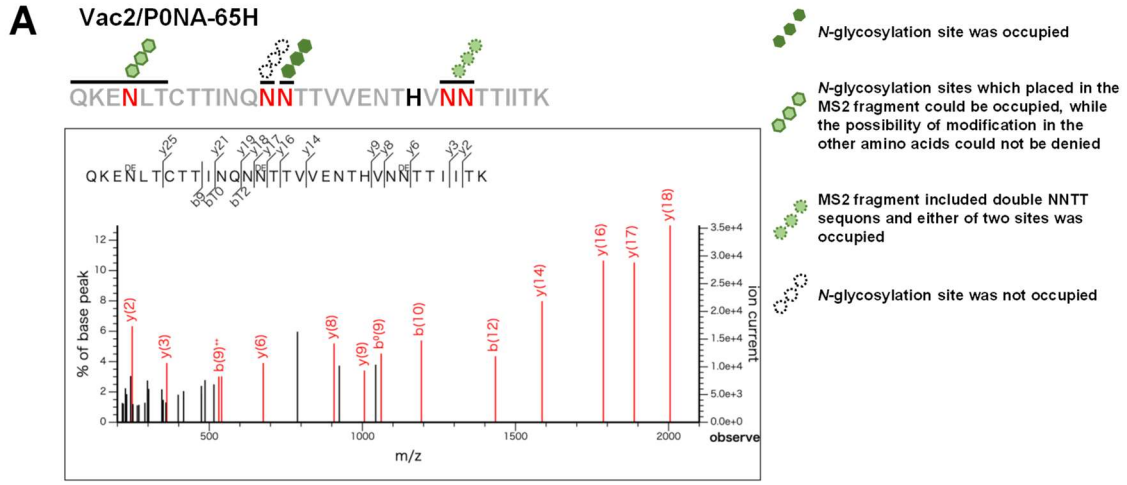

Figure 21. MS2 spectrum of the peptide of P0NA-65H with three glycans at N47, N57 and N67/68, and confirmation of no peptide with two glycans. (A) MS2 spectrum of the peptide of P0NA-65H containing three glycans.

B

#	b	Seq.	y	#
1	129.0659	Q	—	31
2	257.1608	K	3424.6770	30
3	386.2034	E	3296.5820	29
4	503.2346	N^{DE}	3167.5394	28
5	616.3187	L	3050.5082	27
6	717.3663	T	2937.4242	26
7	877.3970	C	2836.3765	25
8	978.4447	T	2676.3458	24
9	1079.4923	T	2575.2982	23
10	1192.5764	I	2474.2505	22
11	1306.6193	N	2361.1664	21
12	1434.6779	Q	2247.1235	20
13	1548.7208	N	2119.0649	19
14	1665.7520	N^{DE}	2005.0220	18
15	1766.7997	T	1887.9908	17
16	1867.8474	T	1786.9431	16
17	1966.9158	V	1685.8954	15
18	2065.9842	V	1586.8270	14
19	2195.0268	E	1487.7586	13
20	2309.0697	N	1358.7160	12
21	2410.1174	T	1244.6731	11
22	2547.1763	Y	1143.6254	10
23	2646.2447	V	1006.5665	9
24	2760.2877	N	907.4981	8
25	2877.3189	N^{DE}	790.4669	7
26	2978.3665	T	676.4240	6
27	3079.4142	T	575.3763	5
28	3192.4983	I	474.3286	4
29	3305.5823	I	361.2445	3
30	3406.6300	T	258.1605	2
31	—	K	147.1128	1

C

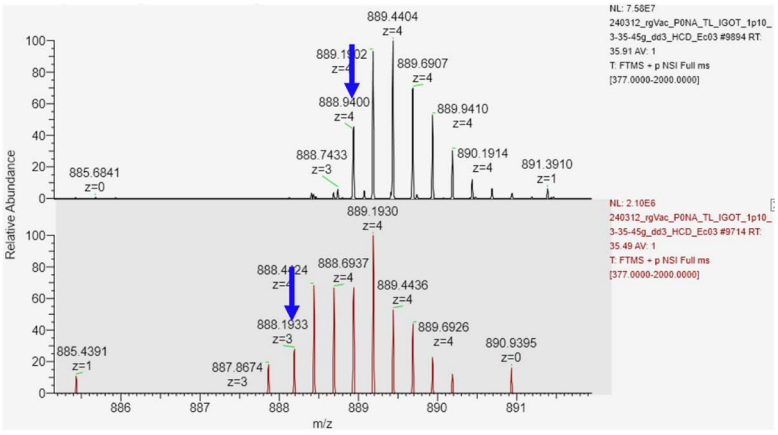

D

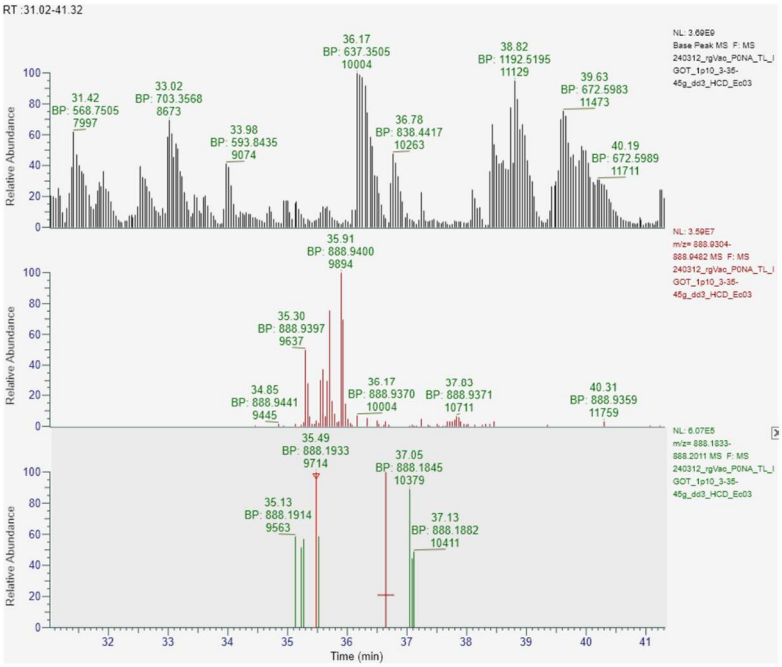

Figure 21 (*cont*)**. MS2 spectrum of the peptide of P0NA-65H with three glycans at N47, N57 and N67/68, and confirmation of no peptide with two glycans.** (B) Molecular mass of b and y ion fragments derived from the peptide of P0NA-65H with three glycans. Red and black letters indicate b and y ion fragments detected and calculated based on the amino acid sequence, respectively. (C) The monoisotopic peak of MS1 corresponding to the suspicious less-glycosylated peptide, which had a smaller molecular mass by 2.99 Da (m/z 0.747 [z = +4]; two blue arrows), was not an ideal peak but a noise. (D) Mass chromatogram of precursor ions indicates that there was no peptide with two glycans.

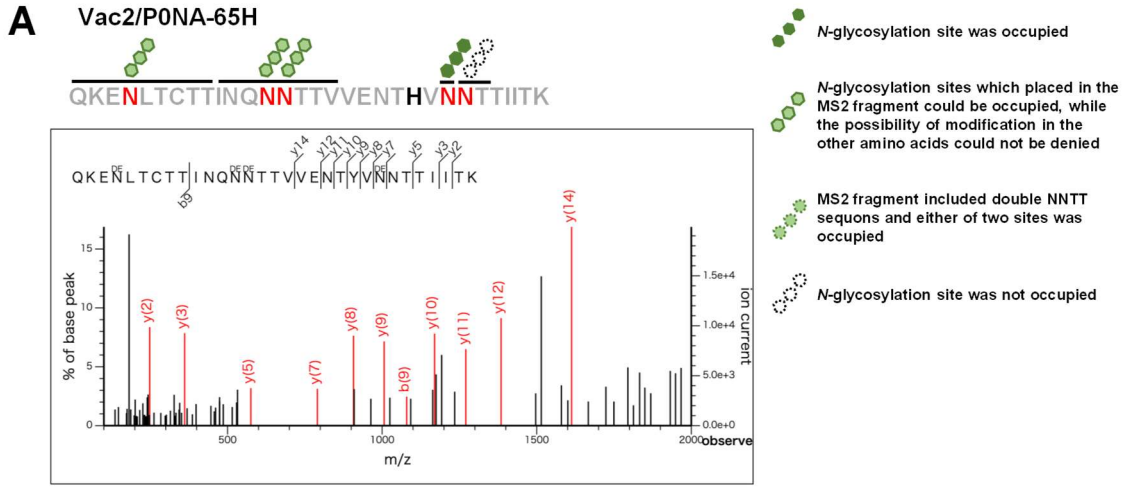

Figure 22. MS2 spectrum of the peptide of P0NA-65H with four glycans at N47, N56, N57 and N67, and mass chromatograms of precursor ions to identify site occupancy. (A) MS2 spectrum of the peptide of P0NA-65H containing four glycans.

B

#	b	Seq.	y	#
1	129.0659	Q	—	31
2	257.1608	K	3427.6652	30
3	386.2034	E	3299.5703	29
4	503.2346	N^{DE}	3170.5277	28
5	616.3187	L	3053.4965	27
6	717.3663	T	2940.4124	26
7	877.3970	C	2839.3647	25
8	978.4447	T	2679.3341	24
9	1079.4923	T	2578.2864	23
10	1192.5764	I	2477.2387	22
11	1306.6193	N	2364.1547	21
12	1434.6779	Q	2250.1117	20
13	1548.7208	N^{DE}	2122.0532	19
14	1665.7520	N^{DE}	2008.0102	18
15	1766.7997	T	1890.9791	17
16	1867.8474	T	1789.9314	16
17	1966.9158	V	1688.8837	15
18	2065.9842	V	1589.8153	14
19	2195.0268	E	1490.7469	13
20	2309.0697	N	1361.7043	12
21	2410.1174	T	1247.6613	11
22	2547.1763	Y	1146.6137	10
23	2646.2447	V	1009.5548	9
24	2763.2759	N^{DE}	910.4863	8
25	2880.3071	N	793.4552	7
26	2981.3548	T	676.4240	6
27	3082.4025	T	575.3763	5
28	3195.4865	I	474.3286	4
29	3308.5706	I	361.2445	3
30	3409.6183	T	248.1605	2
31	—	K	147.1128	1

C

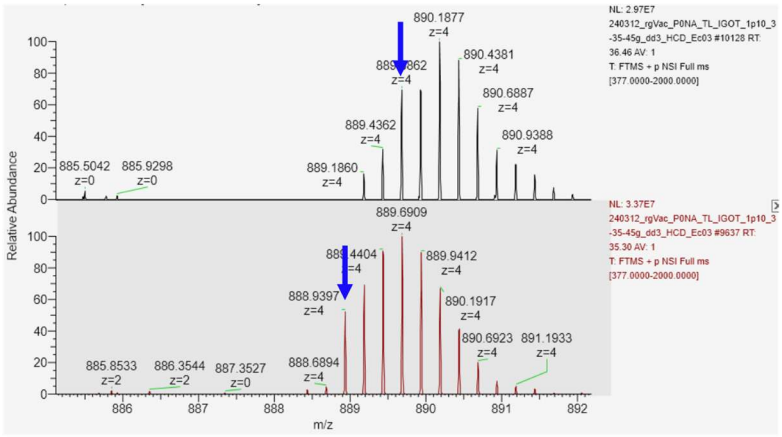

D

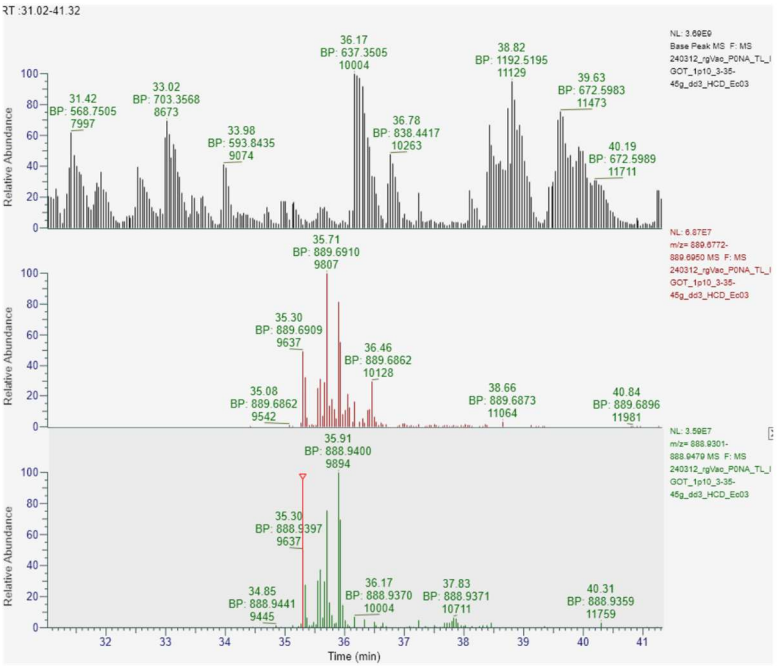

Figure 22 (*cont*)**. MS2 spectrum of the peptide of P0NA-65H with four glycans at N47, N56, N57 and N67, and mass chromatograms of precursor ions to identify site occupancy.** (B) Molecular mass of b and y ion fragments derived from the peptide of P0NA-65H with four glycans. Red and black letters indicate b and y ion fragments detected and calculated based on the amino acid sequence, respectively. (C) The monoisotopic peak of MS1 corresponding to the less-glycosylated peptide, which had a smaller molecular mass by 2.99 Da (m/z 0.747 [z = +4]; two blue arrows), was observed. (D) Mass chromatogram of precursor ions shows that the less-glycosylated peptide with three glycans (35.30 min; green) had a shorter LC retention time compared to the peptide with four glycans (36.46 min; red).

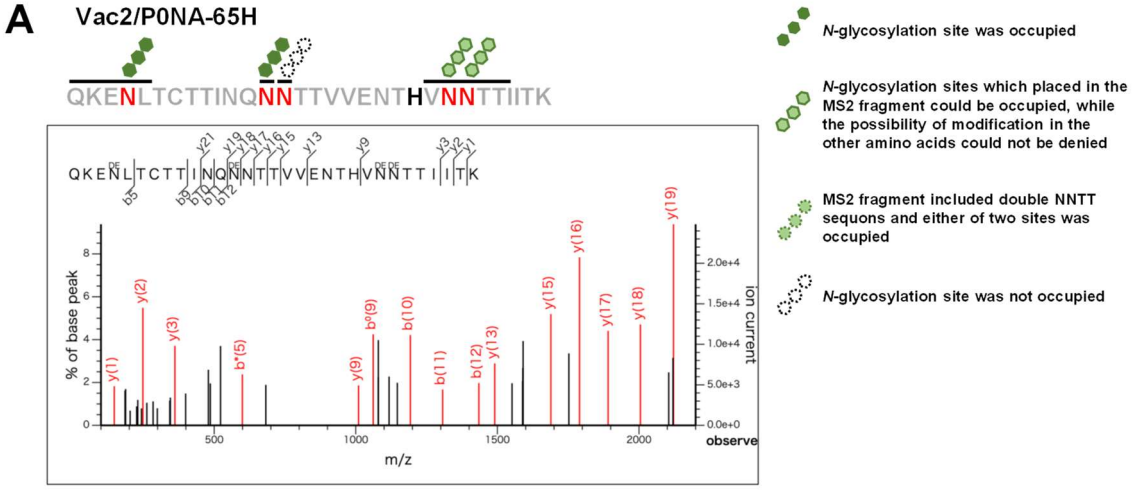

B

#	b	Seq.	y	#
1	129.0659	Q	—	31
2	257.1608	K	3427.6652	30
3	386.2034	E	3299.5703	29
4	503.2346	N^{DE}	3170.5277	28
5	616.3187	L	3053.4965	27
6	717.3663	T	2940.4124	26
7	877.3970	C	2839.3647	25
8	978.4447	T	2679.3341	24
9	1079.4923	T	2578.2864	23
10	1192.5764	I	2477.2387	22
11	1306.6193	N	2364.1547	21
12	1434.6779	Q	2250.1117	20
13	1551.7091	N^{DE}	2122.0532	19
14	1665.7520	N	2005.0220	18
15	1766.7997	T	1890.9791	17
16	1867.8474	T	1789.9314	16
17	1966.9158	V	1688.8837	15
18	2065.9842	V	1589.8153	14
19	2195.0268	E	1490.7469	13
20	2309.0697	N	1361.7043	12
21	2410.1174	T	1247.6613	11
22	2547.1763	Y	1146.6137	10
23	2646.2447	V	1009.5548	9
24	2763.2759	N^{DE}	910.4863	8
25	2880.3071	N^{DE}	793.4552	7
26	2981.3548	T	676.4240	6
27	3082.4025	T	575.3763	5
28	3195.4865	I	474.3286	4
29	3308.5706	I	361.2445	3
30	3409.6183	T	248.1605	2
31	—	K	147.1128	1

C

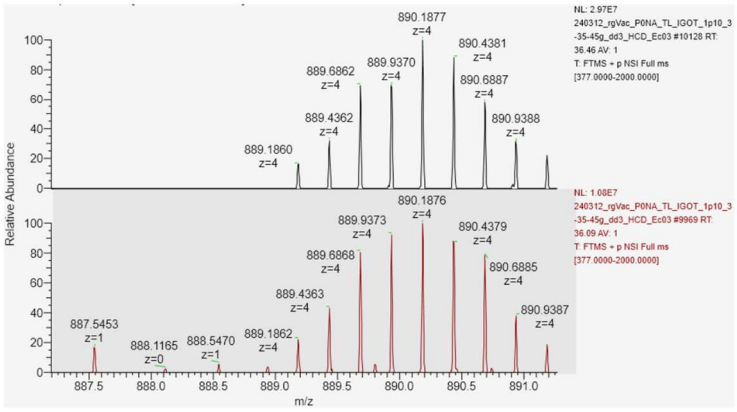

Figure 23 Identification of multiple peptides of P0NA-65H with four glycans at N47, N56, N67 and N68. (A) MS2 spectrum of the peptide of P0NA-65H containing four glycans. (B) Molecular mass of b and y ion fragments derived from the peptide of P0NA-65H with four glycans. Red letters indicate b and y ion fragments detected in this analysis, whereas black letters refer to the calculated molecular weights based on the amino acid sequence. (C) The monoisotopic peak of MS1 corresponding to the multiple peptides with four glycans had identified.

through Q/N substitution in P0NAΔG were rescued (Figure 24A). The virus harboring potential glycosylation sites at N56 and N57, Vac2/P0NAΔG-56,57N, showed comparable erythrocyte elution activity to the virus with full-stalk NA, rgVac2/P0NA (Figure 24B). Conversely, the virus harboring potential glycosylation sites at N67 and N68, Vac2/P0NAΔG-67,68N, did not elute erythrocytes, and the virus with one glycosylation site at N47, Vac2/P0NAΔG-47N, showed intermediate elution activity over 8 hours (Figure 24B). These results indicate that the potential *N*-glycosylation sites at N56 and N57 significantly contribute to the high erythrocyte elution activity of the virus, whereas the site at N47 less contributed to this activity. In addition, the results implied that the presence or absence of glycans at N67 and N68 does not affect the erythrocyte elution activity. Accordingly, it was speculated that the glycan occupancy at N47 and N56/57 of the mutants affects erythrocyte elution activity and therefore, the site-specific glycan occupancy of two mutants, Vac2/P0NAΔG-47N and Vac2/P0NAΔG-56,57N, was assessed via LC-MS/MS. The b and y ion fragments corresponding to *N*-glycosylation at N47 of the NA-stalk derived from Vac2/P0NAΔG-47N were not identified via MS/MS. However, the precursor ion obtained in the MS1 spectrum indicated an ^{18}O label in a mono-asparagine residue in the peptide, suggesting that the potential *N*-glycosylation site at N47 of P0NAΔG-47N was occupied (Figure 25). Additionally, the nonglycosylated peptide was not identified in the mass chromatogram, indicating that glycan occupancy at N47 of P0NAΔG-47N reached 100%. Moreover, peptides with one or two *N*-glycans in the NA-stalk domain of P0NAΔG-56,57N were detected via MS/MS (Figures 26–28). Among these peptides, glycosylation at N56 was identified, but there was no evidence of single glycosylation at N57. Precursor ions corresponding to nonglycosylated peptides were detected, with their peak intensity being 20% of that of the single-glycosylated peptides. Furthermore, the intensity of ion peaks corresponding to double-glycosylated peptides was 40% lower than that of single-glycosylated peptides (Figures 26–28). These results indicate that the potential *N*-glycosylation sites at N47 of P0NAΔG-47N, and N56 and/or N57 of P0NAΔG-56,57N were generally occupied. Thus, the functional difference in erythrocyte elution activity was not due to glycan occupancy alone. Rather, *N*-glycosylation at each site contributed differently to erythrocyte elution activity: glycosylation deficiency at N56 and N57 greatly reduced elution activity, whereas

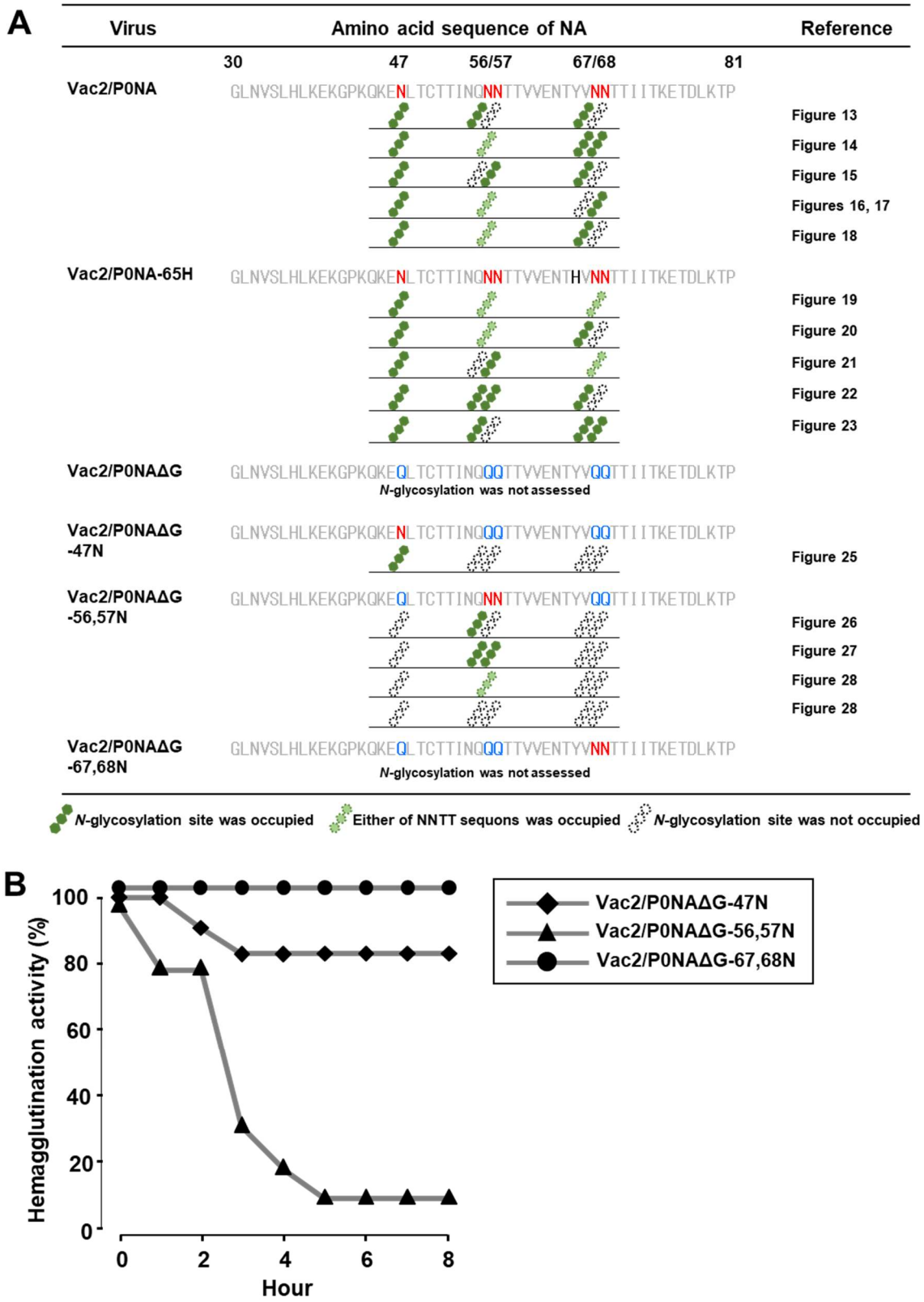

Figure 24. Glycosylation patterns of potential *N*-glycosylation sites in the NA-stalk domain of Vac2 mutants. (A) Amino acid sequences of the NA-stalk domain for the viruses constructed in this study are listed. Glycosylation patterns were summarized based on LC-MS/MS analysis. (B) Erythrocyte elution activity of Vac2 mutants with the Y65H substitution in the NA was assessed.

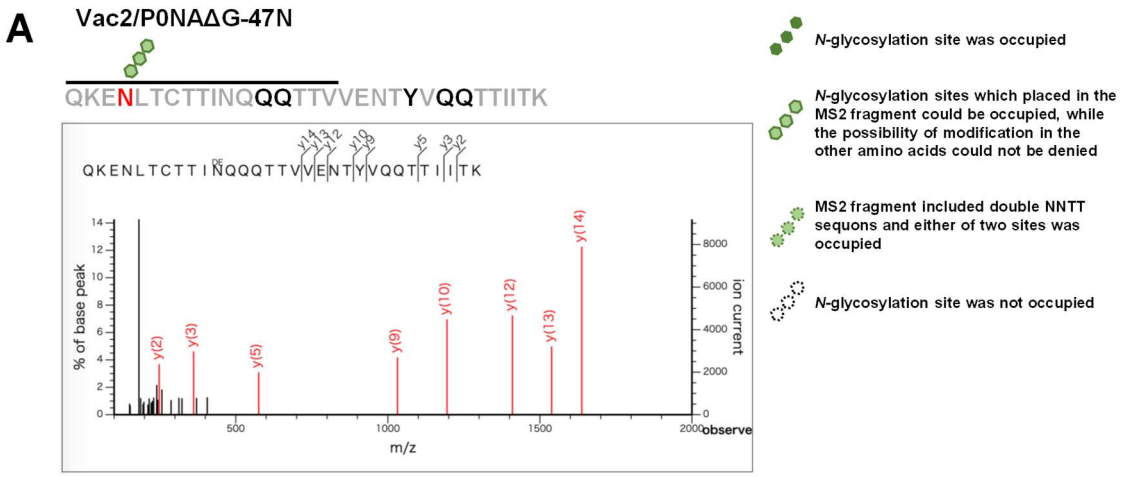

Figure 25. MS2 spectrum of the peptide of P0NAΔG-47N with a glycan and confirmation of no peptide without the glycan. (A) MS2 spectrum of the peptide of P0NAΔG-47N harboring a glycan.

B

#	b	Seq.	y	#
1	129.0659	Q	—	31
2	257.1608	K	3500.7675	30
3	386.2034	E	3372.6725	29
4	500.2463	N^{DE}	3243.6299	28
5	613.3304	L	3129.5870	27
6	714.3781	T	3016.5029	26
7	874.4087	C	2915.4552	25
8	975.4564	T	2755.4246	24
9	1076.5041	T	2654.3769	23
10	1189.5882	I	2553.3292	22
11	1306.6193	N	2440.2452	21
12	1434.6779	Q	2323.2140	20
13	1562.7365	Q	2195.1554	19
14	1690.7951	Q	2067.0968	18
15	1791.8428	T	1939.0383	17
16	1892.8904	T	1837.9906	16
17	1991.9588	V	1736.9429	15
18	2091.0273	V	1637.8745	14
19	2220.0699	E	1538.8061	13
20	2334.1128	N	1409.7635	12
21	2435.1605	T	1295.7205	11
22	2598.2238	Y	1194.6729	10
23	2697.2922	V	1031.6095	9
24	2825.3508	Q	932.5411	8
25	2953.4094	Q	804.4825	7
26	3054.4570	T	676.4240	6
27	3155.5047	T	575.3763	5
28	3268.5888	I	474.3286	4
29	3381.6728	I	361.2445	3
30	3482.7205	T	248.1605	2
31	—	K	147.1128	1

C

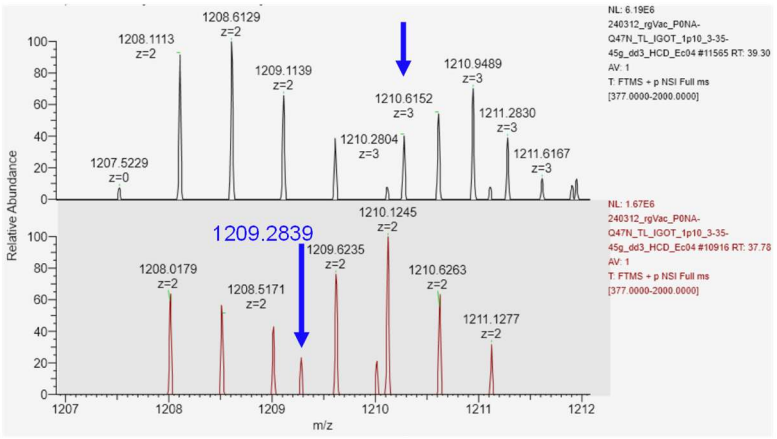

D

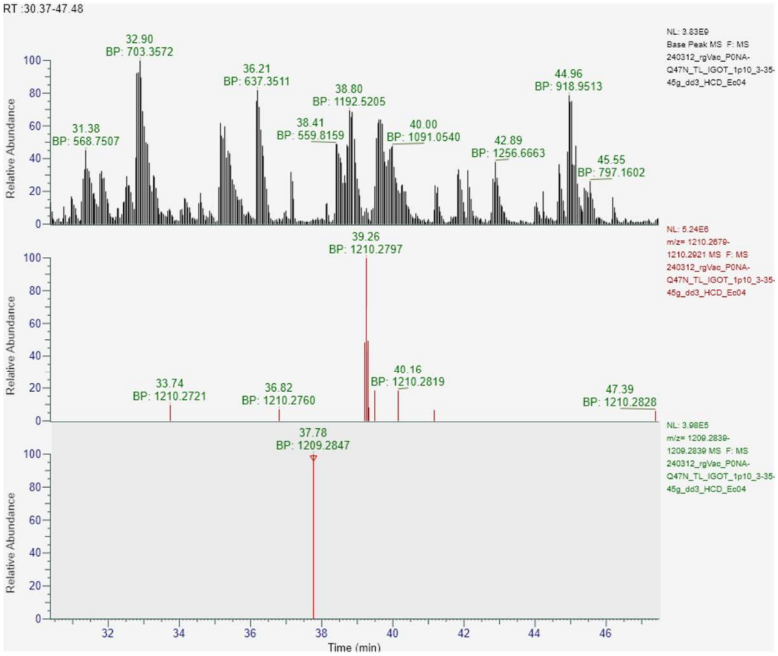

Figure 25 (*cont*)**. MS2 spectrum of the peptide of P0NAΔG-47N with a glycan and confirmation of no peptide without the glycan.** (B) Molecular mass of b and y ion fragments derived from the peptide of P0NAΔG-47N with a glycan. Red and black letters indicate b and y ion fragments detected and calculated based on the amino acid sequence, respectively. (C) The monoisotopic peak of MS1 corresponding to the suspicious non-glycosylated peptide, which had a smaller molecular mass by 2.99 Da (m/z 0.997 [z = +3]; two blue arrows), was not an ideal peak but a noise. (D) Mass chromatogram of precursor ions indicates that there was no non-glycosylated peptide.

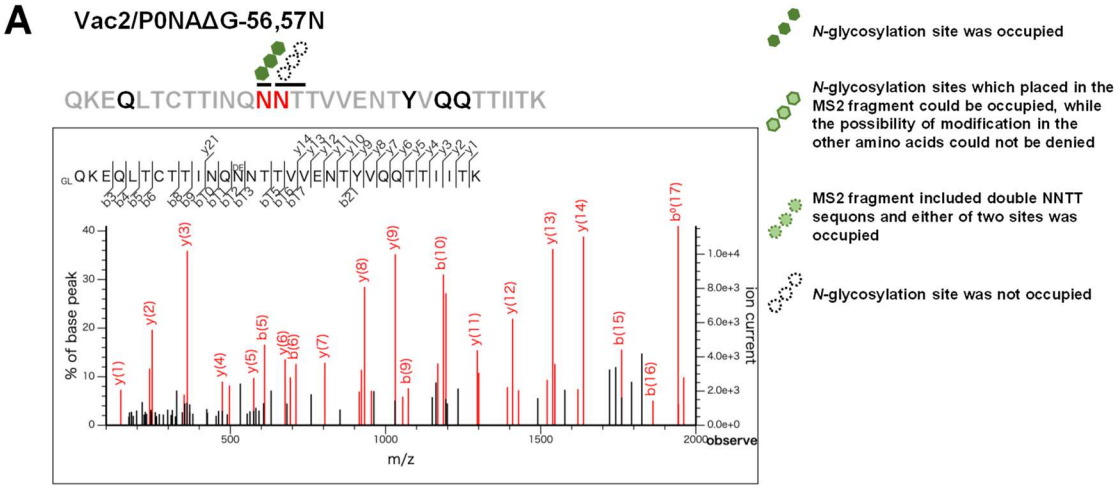

Figure 26. MS2 spectrum of the peptide of P0NAΔG-56,57N with a glycan at N56 and confirmation of no peptide without the glycan. (A) MS2 spectrum of the peptide of P0NAΔG-56,57N containing a glycan.

B

#	b	Seq.	y	#
1	112.0393	Q	—	31
2	240.1343	K	3486.7518	30
3	369.1769	E	3358.6569	29
4	497.2354	Q	3229.6143	28
5	610.3195	L	3101.5557	27
6	711.3672	T	2988.4716	26
7	871.3978	C	2887.4239	25
8	972.4455	T	2727.3933	24
9	1073.4932	T	2626.3456	23
10	1186.5773	I	2525.2979	22
11	1300.6202	N	2412.2139	21
12	1428.6788	Q	2298.1709	20
13	1545.7099	N^{DE}	2170.1124	19
14	1659.7529	N	2053.0812	18
15	1760.8006	T	1939.0383	17
16	1861.8482	T	1837.9906	16
17	1960.9166	V	1736.9429	15
18	2059.9851	V	1637.8741	14
19	2189.0277	E	1538.8061	13
20	2303.0706	N	1409.7635	12
21	2404.1183	T	1295.7205	11
22	2567.1816	Y	1194.6729	10
23	2666.2500	V	1031.6095	9
24	2794.3086	Q	932.5411	8
25	2922.3672	Q	804.4825	7
26	3023.4148	T	676.4240	6
27	3124.4625	T	575.3763	5
28	3237.5466	I	474.3286	4
29	3350.6306	I	361.2445	3
30	3451.6783	T	248.1605	2
31	—	K	147.1128	1

C

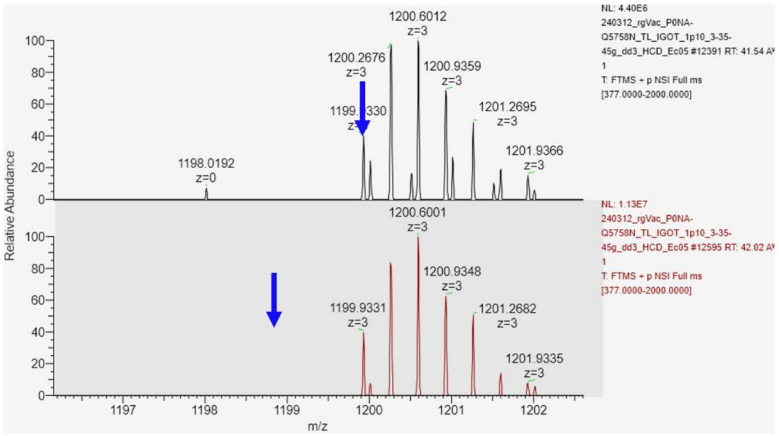

D

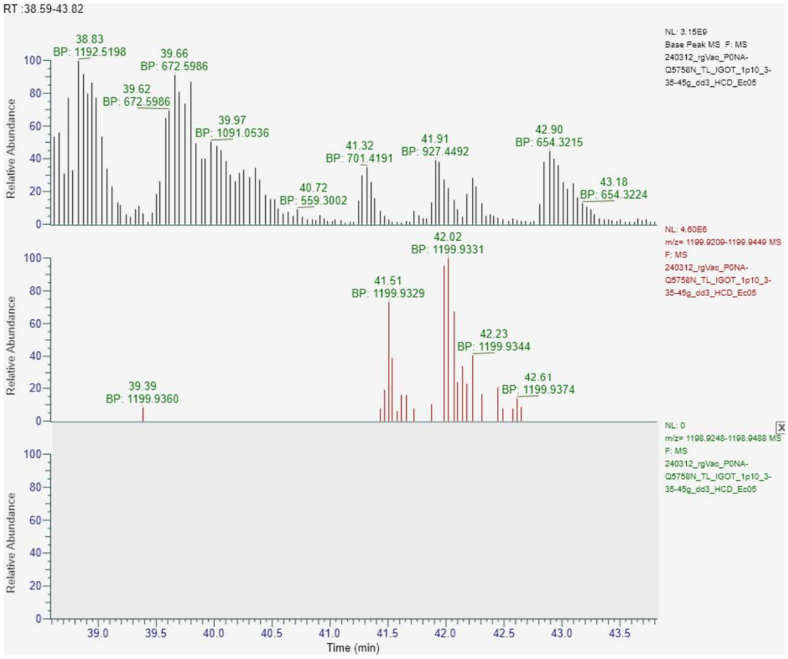

Figure 26 (*cont*)**. MS2 spectrum of the peptide of P0NAΔG-56,57N with a glycan at N56 and confirmation of no peptide without the glycan.** (B) Molecular mass of b and y ion fragments derived from the peptide of P0NAΔG-56,57N with a glycan. Red and black letters indicate b and y ion fragments detected and calculated based on the amino acid sequence, respectively. (C) The monoisotopic peak of MS1 corresponding to the suspicious non-glycosylated peptide, which had a smaller molecular mass by 2.99 Da (m/z 0.997 [z = +3]; two blue arrows), was not identified. (D) Mass chromatogram of precursor ions indicates that there was no non-glycosylated peptide.

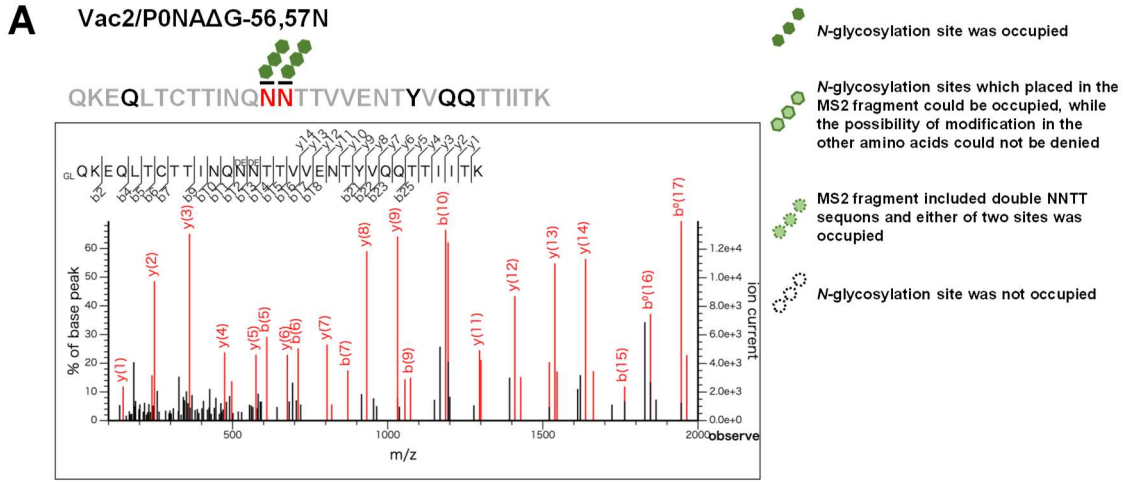

Figure 27. MS2 spectrum of the peptide of P0NAΔG-56,57N with two glycans and mass chromatograms of precursor ions to identify site occupancy. (A) MS2 spectrum of the peptide of P0NAΔG-56,57N containing two glycans.

B

#	b	Seq.	y	#
1	112.0393	Q	—	31
2	240.1343	K	3489.7401	30
3	369.1769	E	3361.6451	29
4	497.2354	Q	3232.6025	28
5	610.3195	L	3104.5439	27
6	711.3672	T	2991.4599	26
7	871.3978	C	2890.4122	25
8	972.4455	T	2730.3816	24
9	1073.4932	T	2629.3339	23
10	1186.5773	I	2528.2862	22
11	1300.6202	N	2415.2021	21
12	1428.6788	Q	2301.1592	20
13	1545.7099	N^{DE}	2173.1006	19
14	1662.7411	N^{DE}	2056.0694	18
15	1763.7888	T	1939.0383	17
16	1864.8365	T	1837.9906	16
17	1963.9049	V	1736.9429	15
18	2062.9733	V	1637.8745	14
19	2192.0159	E	1538.8061	13
20	2306.0588	N	1409.7635	12
21	2407.1065	T	1295.7205	11
22	2570.1698	Y	1194.6729	10
23	2669.2383	V	1031.6095	9
24	2797.2968	Q	932.5411	8
25	2925.3554	Q	804.4825	7
26	3026.4031	T	676.4240	6
27	3127.4508	T	575.3763	5
28	3240.5348	I	474.3286	4
29	3353.6189	I	361.2445	3
30	3454.6666	T	248.1605	2
31	—	K	147.1128	1

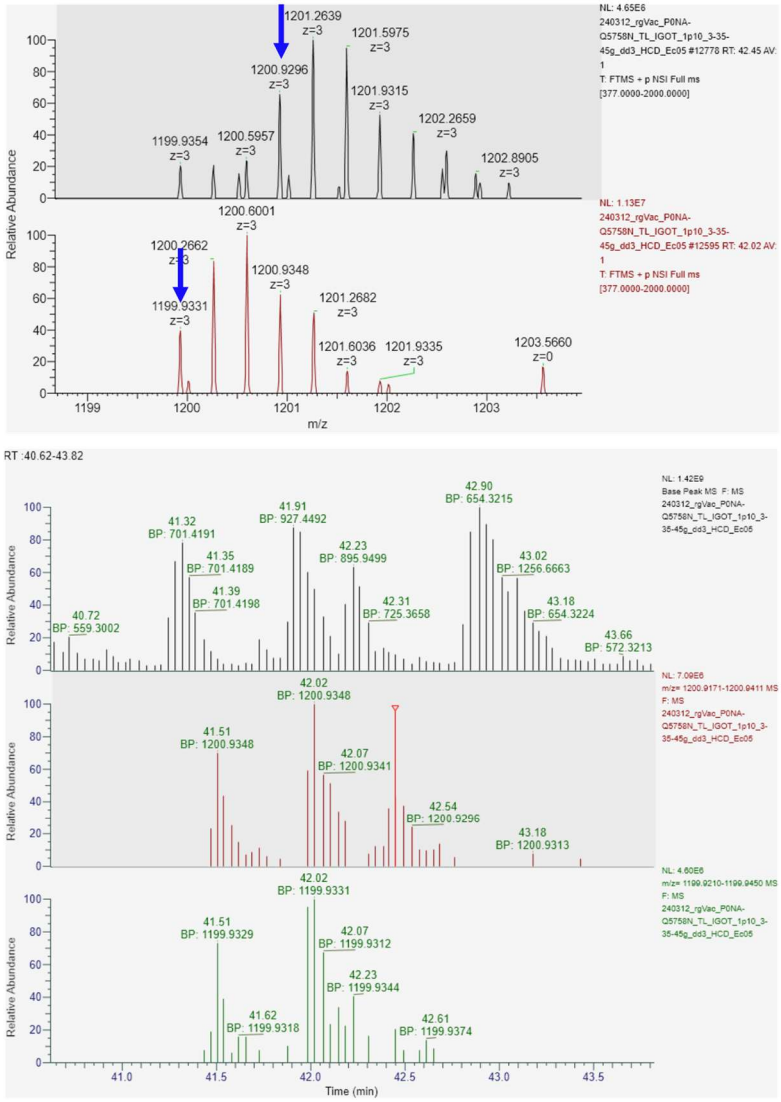

Figure 27 (*cont*)**. MS2 spectrum of the peptide of P0NAΔG-56,57N with two glycans and mass chromatograms of precursor ions to identify site occupancy.** (B) Molecular mass of b and y ion fragments derived from the peptide of P0NAΔG-56,57N with two glycans. Red and black letters indicate b and y ion fragments detected and calculated based on the amino acid sequence, respectively. (C) The monoisotopic peak of MS1 corresponding to the less-glycosylated peptide, which had a smaller molecular mass by 2.99 Da (m/z 0.997 [z = +3]; two blue arrows), was observed. (D) Mass chromatogram of precursor ions shows that the less-glycosylated peptide with one glycan (42.02 min; green) had a shorter LC retention time compared to the peptide with two glycans (42.54 min; red).

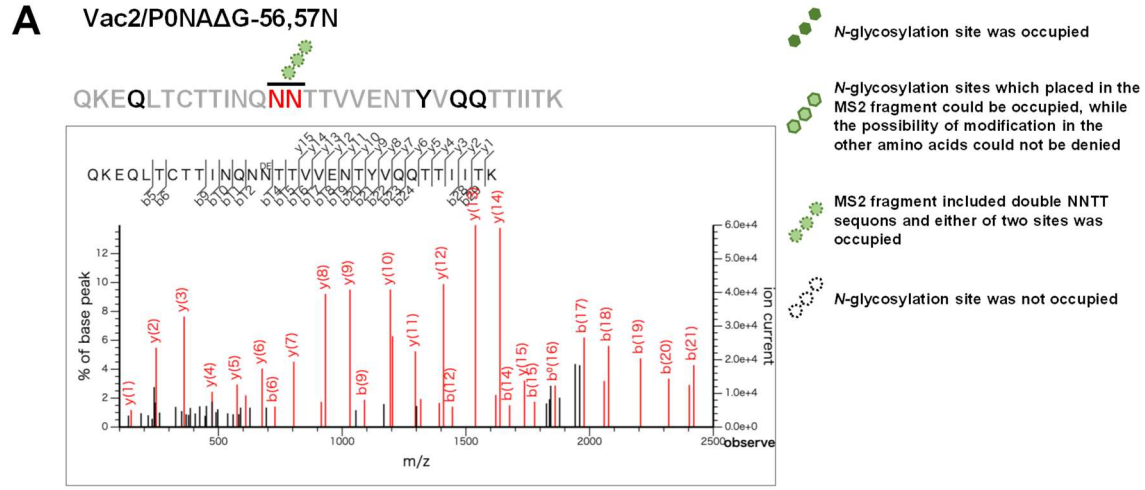

Figure 28. MS2 spectrum of the peptide of P0NAΔG-56,57N with a glycan at N56/57 and a small amount of non-glycosylated peptide was identified. (A) MS2 spectrum of the peptide of P0NAΔG-56,57N containing a glycan.

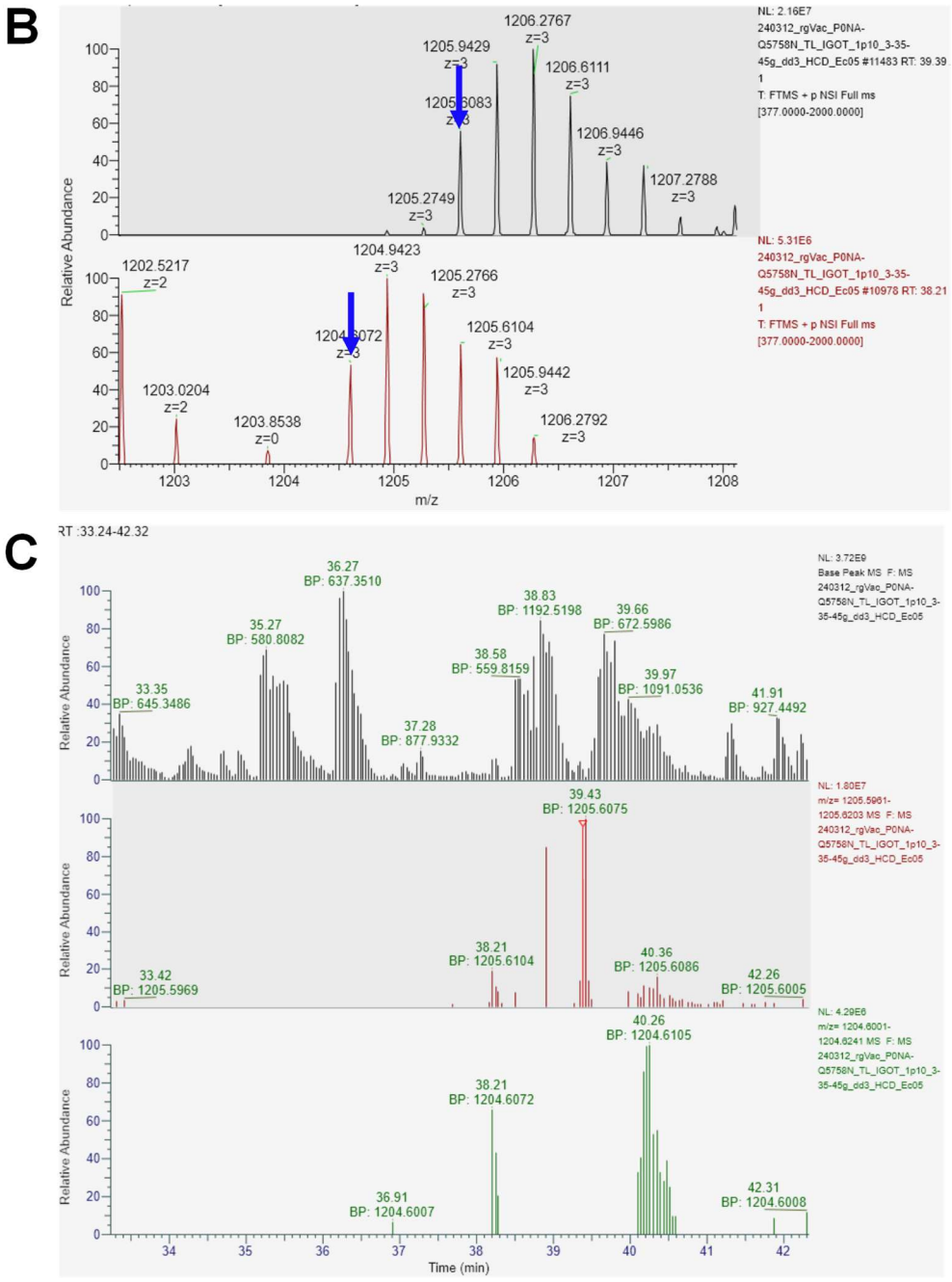

Figure 28 (*cont*)**. MS2 spectrum of the peptide of P0NAΔG-56,57N with a glycan at N56/57 and a small amount of non-glycosylated peptide was identified.** (B) The monoisotopic peak of MS1 corresponding to the non-glycosylated peptide, which had a smaller molecular mass by 2.99 Da (m/z 0.997 [z = +3]; two blue arrows), was observed. (C) Mass chromatogram of precursor ions shows that the non-glycosylated peptide with one glycan (38.21 min; green) had a shorter LC retention time compared to the peptide with two glycans (39.43 min; red).

deficiency at N47 had a milder effect, and deficiency at N67 and N68 did not reduce erythrocyte elution activity.

Comparison of NA-stalk domain of N7 NA AIVs

Lastly, the potential *N*-glycosylation motifs in the NA-stalk domain were compared among field-isolated N7 NA AIVs. A previous study has shown that NA-stalk deletion in AIVs reduces erythrocyte elution activity, which correlates with increased viral pathogenicity in chickens [29]. In the present study, *N*-glycosylations at N56 and N57 were found to contribute most significantly to erythrocyte elution activity among the five potential sites. Therefore, it was hypothesized that the loss of *N*-glycosylations at these positions might have a greater impact on the adaptation of N7 NA to chickens. Amino acid sequences of the NA stalk regionfrom field strains were obtained from GISAID database and aligned with the P0NA sequence (Figure 29). In the comparison of stalk-truncated strains, four of the five potential glycosylation sites missing in P3L4NA (specifically at positions N56/57 and N67/68) were consistently located within the deletion regions, despite the varying truncation positions and lengths observed across 16 distinct patterns. Interestingly, those viruses harboring short-stalk NAs were predominantly isolated from chickens rather than wild ducks. Conversely, a few strains lost the potential glycosylation sites at N47 due to amino acid substitutions of the full-stalk NAs. Notably, at least one potential site in either of the two adjacent glycosylation sites (NNTT sequons) observed in N56/57 and N67/68 was conserved among the full-stalk NAs. These results suggest that stalk truncation, which results in the loss of potential *N*-glycosylation sites at N56/57 and N67/68 in the NA stalk, is beneficial for viral adaptation to Galliformes in natural settings. Taken together with the functional analysis of the Vac2 strains, these stalk truncations of N7 NA result in loss of glycosylation of the stalk and enhanced viral pathogenicity in chickens.

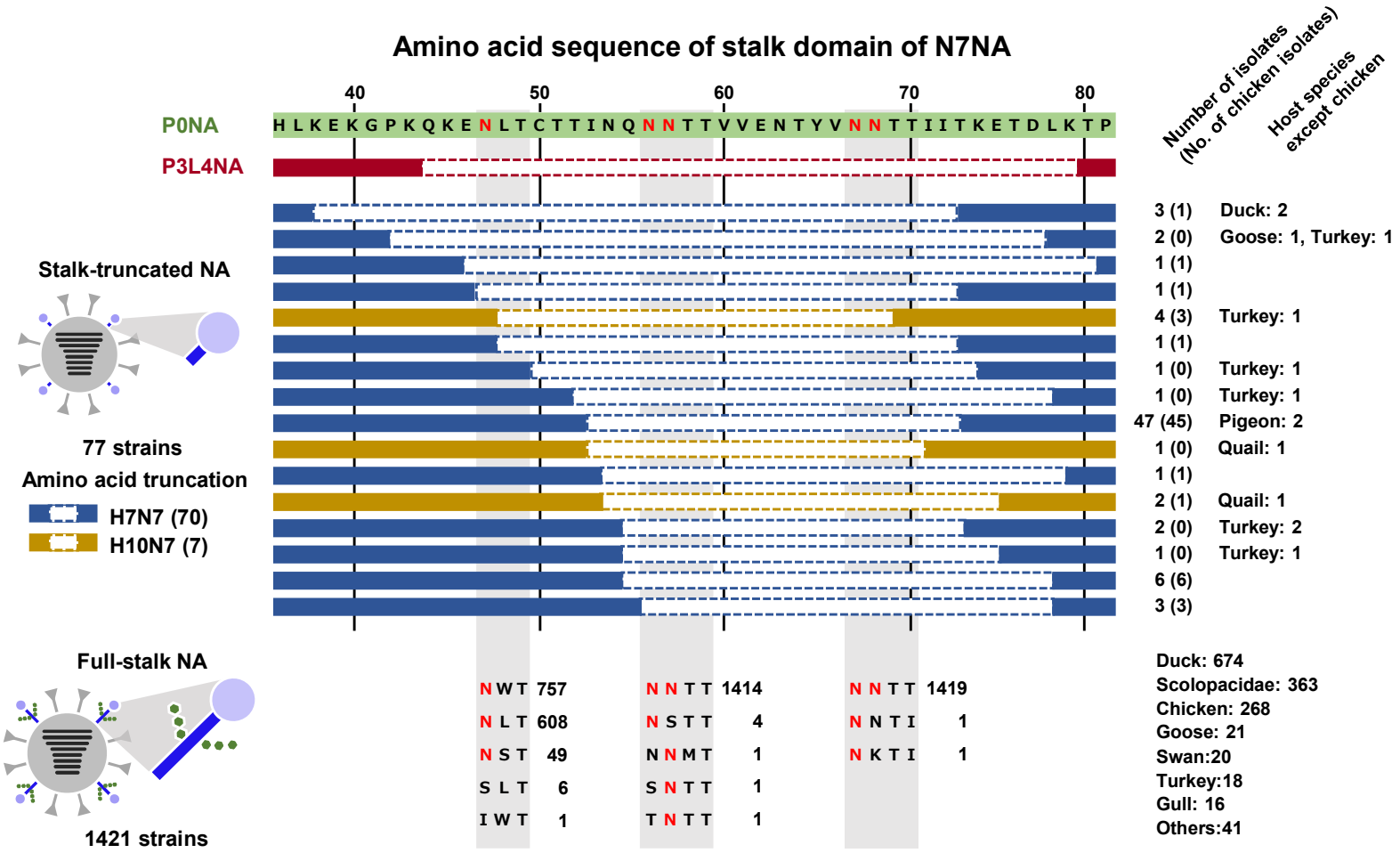

Figure 29. Overview of multiple potential *N*-glycosylation sites in the NA-stalk domain of N7 NA and patterns of amino acid truncation in natural isolates. Amino acid sequences of N7 NA were obtained from the GISAID database (https://gisaid.org/) and the stalk region was aligned with P0NA and P3L4NA. The positions and lengths of stalk truncations in 77 short-stalk NA viruses are represented by bars (blue for H7N7 and ocher for H10N7). Additionally, amino acid variations at the *N*-glycosylation sites of full-stalk NAs across 1,421 strains were counted. Red letters indicate potential *N*-glycosylation sites at the corresponding positions. Hosts of the isolates were listed.

Discussion

For certain decades, the “limited access theory” has been believed to explain the reduced sialidase activity of short-stalk NAs. According to this theory, the shorter height of the NA stalk compared to HA restricts access to cellular sialylated glycans, impeding the enzymatic ability to interact with "bulky" substrates [74]. This theory aligns with observations that viruses with stalk-truncated NA exhibit low erythrocyte elution activity [73, 96]. In contrast, recent research suggests that the limited access theory may not fully account for the reduced NA activity of short-stalk NA proteins [75]. The present study found that the loss of glycosylation in the NA-stalk domain, in addition to the shortened height of the NA stalk, led to decreased elution activity against bulky substrates like chicken erythrocytes without alteration of NA enzymatic activity to a small compound. The observation agreed with the results of MUNANA assays with NA stalk-truncated or deglycosylated strains in several studies [39, 41, 101]. Perhaps, the affinity of NA head to bulky substrates was affected by the NA-stalk modification. Generally, protein glycosylation can decrease root-mean-square fluctuations, enhance global protein mobility, or increase protein dynamics and flexibility [79, 102–104]. A molecular dynamics simulation of an NA protein has demonstrated that glycans on the protein, in general, decrease the protein rigidity. However, the effects of glycosylation on the protein stability may not be consistent throughout the protein and may differentially affect the two functional domains; for example, the glycosylation of NA stabilizes the NA head domain while minimally affecting the stalk domain [105]. Likewise, deglycosylation at the stalk domain can reduce the stability of NA head domain. Thus, the loss of glycosylation in the NA-stalk plays a critical role in increasing fluctuation of the NA head and reducing the enzymatic activity to balky substrates.

Deglycosylation or truncation encompassing potential *N*-glycosylation sites at the NA stalk mainly contributes to decreasing erythrocyte elution activity of the virus [39, 40, 106], while the functional contribution of *N*-glycosylations on the NA stalk was still controversial due to the less information of the site-specific glycosylation. The present study highlighted the site-specific contributions of *N*-glycosylations on the NA-stalk to the erythrocyte elution activity of viruses. Glycosylation at N56 and N57 was associated with higher elution activity, whereas glycosylation at N68 and N69, which are closer to the head domain, did not affect elution activity. Additionally, glycosylation

at N47, located near the transmembrane domain, contributed intermediate effects to erythrocyte elution activity. These observations suggest that the position of *N*-glycosylation sites influences the stability of the NA head, thereby affecting its activity on bulky substrates. These results underscore the importance of structural and functional analyses of NA glycans to understand how NA-stalk deletion affects viral sialidase activity and its implications for the emergence of HPAIVs.

Amino acid deletions in the NA-stalk domain, including some potential *N*-glycosylation sites, have been observed in several isolates of N1–3 and N5–7 subtypes from terrestrial birds such as chickens and turkeys [34, 93]. In N7 NA, all patterns of amino acid deletions in the NA-stalk domain of natural isolates included more than one potential *N*-glycosylation site, although the lengths of the deletion sites varied among strains. Conversely, only a few strains lost a potential *N*-glycosylation site due to amino acid substitutions in the stalk. These observations suggest that the loss of glycosylation in the NA-stalk domain in natural settings is primarily achieved through amino acid deletions rather than substitutions. Kawasaki *et al*. [107] found that the frequency of insertions/deletions was 10 times lower than that of nonsynonymous mutations in the coding regions of NA genes over 15 passages *in vitro* of an influenza A virus. The finding supports the idea that a single amino acid deletion in the NA-stalk domain, rather than multiple nonsynonymous mutations, is more likely to result in the loss of glycosylation in field isolates. Once a nucleotide deletion in the NA-stalk coding region occurs and a NA-stalk truncated virus emerges during replication in chicken respiratory tracts, the NA-stalk truncated virus is likely to become dominant due to its advantage in viral proliferation potentially via higher affinity to sialoglycans representing on the target cells or higher potential in escaping from decoy receptors like mucins within the chicken host.

The functional balance between glycan binding by HA and cleaving by NA is also considered in the host specificity of AIVs [34, 40, 106]. During the passage to obtain the L4 mutant, amino acid substitutions in HA were also observed, in addition to the stalk truncation in NA [73]. It should be noted that no further mutation in HA genes was obtained from the recovered viruses in the experimental inoculation with the L4 mutant in the present study. The mutations E227G and I388T in HA observed in the previous study were essential for the intravenous pathogenicity in chickens and E227G

especially contributed to the reduced receptor binding avidity [73]. The reduction of binding to the receptor by the mutation in HA was perhaps later balanced with the reduced function of NA by deglycosylation or truncation in the stalk domain, leading to the efficient replication of L4 and L4/P0NAΔG in chickens. In theory, lower NA activity compared with the receptor binding avidity by HA reduces the moving of the virions on sialic acid-coated surface *in vitro* [45]. Since the repertoire of sialic acid-containing glycans varies between species, further studies are needed to address how the reduced function of NA benefits viral replication in chickens.

In conclusion, the present study proposes a novel theory that the loss of glycosylation in the stalk domain of NA enhances viral pathogenicity in chickens. This theory is supported by a combination of site-specific *N*-glycosylation analysis and virological assays. In natural settings, amino acid truncation in the NA-stalk occurs more frequently than multiple amino acid substitutions at potential glycosylation sites. Consequently, viruses with glycosylation-deficient or truncated NA stalks are likely selected due to their enhanced replication ability in chickens. However, the precise mechanisms by which reduced NA activity contributes to increased viral pathogenicity in chickens remain to be fully elucidated. Further studies are needed to determine how the loss of glycosylation in NA stalks enhance virus attachment or replication in chickens.

Brief summary

Influenza A viruses with fewer amino acids in the NA stalk domain are primarily isolated from chickens rather than wild ducks, indicating that a shortened NA stalk is considered an adaptation marker of AIVs to chickens. Experimental passages of an H7N7 nonpathogenic AIV (rgVac2-P0) in chickens resulted in a highly pathogenic variant (Vac2-P3L4) with a 34-amino-acid deletion in the NA stalk, encompassing five potential *N*-glycosylation sites. To investigate how amino acid truncation and deglycosylation in the NA stalk contribute to increased pathogenicity, a virus with glycosylation-deficient mutations at these sites (rgVac2-P3L4/P0NAΔGlyco) was constructed. Contrary to expectations, chickens inoculated with rgVac2-P3L4/P0NAΔGlyco exhibited variable clinical outcomes, attributed to the genetic instability of the virus. A single mutation stabilized the virus and the mutant (rgVac2-P3L4/P0NAΔGlyco-Y65H) resulted in higher pathogenicity compared to a virus with restored glycosylation (rgVac2-P3L4/P0NA-Y65H). Glycan occupancy analysis revealed 3–4 glycans at the five potential sites. In functional analysis, glycosylation-deficient mutants, similar to the short-stalk NA virus, showed significantly reduced erythrocyte elution activity. Additionally, mutational analysis indicated variable contributions of *N*-glycans to elution activity across the sites. Moreover, the functionally most contributing sites of the five potential *N*-glycosylation motifs were consistently included in the amino acid deletions of the stalk-truncated NA in N7-subtyped field isolates, despite the varying truncation position or length. These findings suggest that the loss of glycosylation is functionally equivalent to a reduction in amino acids and it plays a crucial role in enhancing pathogenicity in chickens and affecting NA function.

Chapter III

Neuraminidase of influenza A viruses induces global desialylation of host cells via its intracellular function

Introduction

HA and NAof IAVs are essential for viral attachment, entry and budding. The main function of NA is to destroy viral receptors upon IAV budding, facilitating efficient viral release from infected cells, and spreading the infection to other cells [42]. The NA also promotes viral movement on target cells by reducing the density of sialylated glycans and removing "decoy" receptors [43–46]. As both HA and NA recognize the same sialylated glycans during viral replication, destruction of receptor molecules by NA potentially limits superinfection and reassortment of IAVs at the cellular level [47, 48]. As a virus-specific enzyme, NA is an attractive target for the development of anti-influenza drugs such as oseltamivir and zanamivir [49, 50]. These drugs aggregate virus particles at the cellular surface of infected cells [108], leading to the indispensability of viral NA function during the IAV lifecycle, especially upon virus budding.

IAV envelope and host proteins are glycosylated by *N*-glycans via co- or post-translational modification. During *N*-glycan synthesis, en bloc transfer of an *N*-glycan progenitor to N-!P-S/T sequon motif undergoes in the endoplasmic reticulum (ER) membrane. Glycans are sequentially processed in the ER or Golgi lumen by host glycosidases and glycosyltransferases [109]. Viral infection sometimes induces atypical glycan modification of the host cells, as well as of viral proteins, by modulating host glycan synthesis machinery. For example, herpes simplex virus type-1 (HSV-1) infection upregulates fucosyltransferase (FUT3, FUT5, and FUT6) genes via the NFκB signaling pathway, leading to the high level of sialyl Lewis X on infected cells [110, 111]. In contrast, *N*-glycans in IAV-infected cells and viral glycoproteins are broadly desialylated due to viral NA activity [112]. Recent glycobiological approaches using lectins have suggested global glycome alterations in IAV-infected cells [113, 114]. Glycans displayed on IAV particles propagated in MDCK cell lines and those on IAV-infected cells have been recognized by EEL (*Euonymus europaeus* lectin; specific for α1-3 galactose) or TJA-II (*Trichosanthes japonica* agglutinin II; specific for α1-2 fucose), in addition to ECA (*Erythrina cristagalli* agglutinin; specific for terminal LacNAc), suggesting alternative recapping of glycan terminals [113–115]. These unique glycan profiles have also been confirmed by a glycomic analysis using LC/MS, which indicates α1-3 galactosylation and α1-2 fucosylation at the non-reducing terminus of glycans on HA and NA [116]. Because α1-3 galactosyltransferases and α1-2 fucosyltransferases are localized

in Golgi apparatus and function to non-sialylated glycans [117, 118], two hypotheses may support the molecular mechanisms underlying the IAV infection-induced glycosylation alterations; i) IAV infections disrupt the normal harmony of glycan synthesis machinery in host cells to upregulate α1-3 galactosyltransferase and/or α1-2 fucosyltransferase genes, or ii) NA intracellularly liberate the terminal sialic acids to generate the terminal LacNAc, as acceptor of α1-3 galactosyltransferase and/or α1-2 fucosyltransferases [114].

To demonstrate the intracellular function of NA in IAV-infected cells, the present study first focused on the glycan profiles of IAV-infected MDCK cells and demonstrated glycan recapping by α1-2 fucose on IAV-infected cells, which was supported by the glycan profiles of NA-expressing cells. Functional analyses indicated that glycan recapping was induced by the intracellular function of NA in IAV-infected cells, highlighting the novel mechanisms of fundamental NA functions in promoting virus release from cells. Moreover, this study demonstrated the potential contribution of NA functions to superinfection exclusion of IAVs. The findings provide a novel insight into NA functions in the evolutional strategy of IAVs.

Materials and Methods

Viruses and cells

The IAVs A/Puerto Rico/8/1934 (H1N1) (PR8), A/duck/Mongolia/47/2001 (H7N1), A/duck/Mongolia/54/2001 (H5N2), A/duck/Hokkaido/84/2002 (H5N3), A/duck/Hokkaido/95/1981 (H8N4), A/duck/Hokkaido/66/2001 (H12N5), A/duck/England/1/1956 (H11N6), A/duck/Ukraine/1/1963 (H3N8), and A/duck/Hokkaido/W245/2004 (H11N9) were used. A recombinant IAV, Vac2/P0NA-FLAG (Vac2-FLAG), which was generated in Chapter II via reverse genetics from a plasmid encoding FLAG-tagged NA with the backbone of A/duck/Hokkaido/Vac-2/2004 (H7N7), was used. Viruses were propagated in 10-day-old embryonated chicken eggs at 35°C for 48 h, and these infectious allantoic fluids were stored at –80°C until use as virus stocks.

MDCK and MDCK-FUT cells [64] were maintained in MEM (Shimadzu Diagnostics) supplemented with 0.3 mg/mL L-glutamine (Nacalai Tesque), 100 U/mL penicillin G (Meiji Seika Pharma), 0.1 mg/mL streptomycin (Meiji Seika Pharma), 8 μg/mL gentamicin (Takata Pharmaceutical), and 10% fetal bovine serum (Merck) in an incubator at 37°C with 5% CO_2. A549 and Vero E6 cells were maintained in DMEM (Thermo Fisher Scientific) supplemented with 0.3 mg/mL L-glutamine (Nacalai Tesque), 100 U/mL penicillin G (Meiji Seika Pharma), 0.1 mg/mL streptomycin (Meiji Seika Pharma), 8 μg/mL gentamicin (Takata Pharmaceutical), and 10% fetal bovine serum (Nichirei Biosciences) in an incubator at 37°C with 5% CO_2.

Antibodies and lectins

Anti-PR8 HA monoclonal antibodies (2F1A7 and 016) were purchased from Sino Biological (11684-MM03 and 11684-R016; Beijing, China), and biotinylated anti-DDDDK-tag monoclonal antibody (FLA-1) was purchased from Medical & Biological Laboratories (M185-6). The HA antibody was purified using a MonoSpin ProG column (GL Sciences) and then biotinylated using a Biotin Labeling Kit – NH_2 (Dojindo Laboratories, Kumamoto, Japan) for immunoprecipitation of PR8 HA, as previously described by Hiono *et al*. [114]. For detection of HA derived from AIVs, H5 and H7 HA monoclonal antibodies previously established (64/1 has been described by Soda *et al*.

[119] and 253/1 has been described by Manzoor *et al*. [120], respectively) were used. In addition, H3 HA monoclonal antibody (D17/4) established using A/duck/Hokkaido/8/1980 (H3N2), H8 HA monoclonal antibody (66/B8) established with A/turkey/Ontario/6118/1968 (H8N4), H11 HA monoclonal antibody (1C6/2/1) established with A/duck/England/1/1956 (H11N6), and H12 HA monoclonal antibody (146/5/1) established with A/duck/Alberta/60/1976 (H12N5) were kindly provided from Prof. Ayato Takada. An anti-NP monoclonal antibody (183/5) was previously established using A/swine/Hong Kong/10/1998 (H9N2) [121]. The anti-sialyl Lewis X antibody (KM93) was purchased from Kyowa Kirin (Tokyo, Japan) and anti-β-actin monoclonal antibody (BA3R) was purchased from Applied Biological Materials (Richmond, BC, Canada). Fluorescein (FITC)-conjugated SNA (*Sambucus Nigra* agglutinin; FL-1301-2) and biotinylated UEA-I (*Ulex europaeus* agglutinin I; B-1065-2) were purchased from Vector Laboratories (Burlingame, CA, USA). FITC-conjugated ECA was purchased from EY Laboratories (F-5901-5; San Mateo, CA, USA). Two fluorescently labeled streptavidin-Alexa Fluor 488 and 555 conjugates were purchased from Thermo Fisher Scientific and horseradish peroxidase (HRP)-conjugated streptavidin was purchased from Jackson ImmunoResearch (West Grove, PA, USA). Chicken polyclonal antisera against PR8 or Vac2 were also used for immunostaining of NA-overexpressing cells. The secondary antibodies used were anti-mouse IgG-Alexa Fluor 568, anti-rabbit IgG-Alexa Flour 555, anti-rabbit IgG-Alexa Flour 594 (Thermo Fisher Scientific), anti-chicken IgG-tetramethyl rhodamine (TRITC) (Abnova; Taipei, Taiwan), anti-mouse IgG-FITC (Rockland Immunochemicals Inc., Pottstown, PA, USA), anti-mouse IgG-HRP (Bio-Rad), and anti-FITC-HRP (Southern Biotech, Birmingham, AL, USA) were used.

Virus titration

Ten-fold dilutions of the virus stocks and cellular supernatants were inoculated into confluent monolayers of MDCK cells and incubated at 35°C for 1 h. The viral solution, including unbound viruses, was removed from the cells, and the cells were washed with serum-free MEM. Cells were cultured in serum-free MEM containing 1.0 μg/mL of acetylated trypsin (Merck) at 35°C for 72 h. The infectious titers of the viruses were expressed as $TCID_{50}$, determined using the method reported by Reed and Muench (1938) [82] by observing the cytopathic effect in virus-infected cells.

Assessment of inhibitory effects of NA inhibitors on virus growth

Confluent monolayers of MDCK cells seeded in 24-well plates were inoculated with PR8 at 100 $TCID_{50}$/well and incubated at 35°C for 1 h. The viral solution, including unbound viruses, was removed from the cells, and the cells were washed with serum-free MEM. The cells were then cultured in serum-free MEM containing 1.0 μg/mL of acetylated trypsin (Merck) and the corresponding dose of each NA inhibitor, laninamivir (MedChemExpress, Monmouth Junction, NJ, USA), laninamivir octanoate (Merck), oseltamivir carboxylate (ChemScene) at 35°C for 48 h. Culture supernatants were collected and the virus titers were determined.

Cloning of NA expression plasmids

The NA gene of PR8 was amplified and independently cloned into the pGEM-T Easy Vector (Promega) by ligation with T4 DNA Ligase (Promega). A nucleotide sequence encoding a FLAG (DYKDDDDK) tag with a single glycine linker (G) and stop codon was inserted into the C-terminal coding region of each NA gene using the KOD Plus Mutagenesis Kit (Toyobo), and the construct was designated pGEM-T-PR8NA-FLAG. The pGEM-T-PR8NA-FLAG and a pCXN2-empty vectors were digested with *Eco*RI (Toyobo) at 37°C for 1 h and the NA-coding fragments were cloned into the pCXN2 expression vector [122, 123] using DNA Ligation kit <Mighty Mix> (Takara Bio) and designated as pCXN2-PR8NA-FLAG. The Vac2NA-coding fragments were amplified from pHW2000-Vac2NA-FLAG, which was constructed in Chapter II to rescue an infectious virus, and cloned into the pCXN2 vector (pCXN2-Vac2NA-FLAG) using an In-Fusion HD Cloning Kit (Takara Bio).

To generate the catalytic-dead NA-coding plasmids, a nucleotide mutation encoding an amino acid substitution of E119V (GAG to GTG) [124], D151G (GAC to GGC) [125] and I222L (ATA to CTA) [126] in PR8 NA was individually introduced into pCXN2-PR8NA-FLAG. The mutations were introduced by site-directed mutagenesis using KOD One DNA polymerase (Toyobo) and complementary primer sets for each substitution.

Establishment of NA stably overexpressed MDCK cells

MDCK cells cultured on a 12-well plate were transfected with 1 μg of pCXN2-PR8NA-FLAG or pCXN2-Vac2NA-FLAG using Lipofectamine 3000 (Thermo Fisher Scientific) and maintained in a culture medium with 500 μg/mL of G418 sulfate (FUJIFILM Wako Pure Chemical). To establish cloned NA-expressing cells, the transfected cells were passaged seven times and G418-resistant clones were isolated and transferred to 12-well plates. Each clone was passaged four times in the presence of G418 sulfate and frozen to prepare the cell stock.

For establishment of catalytic-dead NA expressing cells, 1 μg of pCXN2-PR8NA-FLAG or its mutants was mixed with Lipofectamine 3000 (Thermo Fisher Scientific) in a 12-well plate. A suspension of MDCK cells was then added to the plate and incubated in Opti-MEM (Thermo Fisher Scientific) at 37°C for 48 h in the presence of two TBK1 inhibitors, 1 μM of BX795 (Merck) and 1.5 μM of amlexanox (Tokyo Chemical Industry, Tokyo, Japan) [127]. The cells were maintained in culture medium containing 500 μg/mL of G418 sulfate (FUJIFILM Wako Pure Chemical Corp.). The resulting G418-resistant cell populations were passaged twice and subjected to lectin staining.

Lectin and immunofluorescent staining

Confluent monolayers of MDCK, MDCK-FUT, MDCK-PR8NA, and MDCK-Vac2NA cells were seeded on glass chamber slides (Matsunami Glass), washed with PBS, and fixed for 10 min in cold methanol or 4% paraformaldehyde in PBS. For staining of IAV-infected cells, MDCK cells were infected with either PR8 or Vac2 at multiplicity of infections (MOI) of 0.1, 1, or 100, and then fixed. For functional analyses of NA, virus-infected MDCK cells were maintained in serum-free MEM supplemented with acetylated trypsin, laninamivir (MedChemExpress), laninamivir octanoate (Merck), oseltamivir carboxylate (ChemScene), or baloxavir acid (BXA; Shionogi, Osaka, Japan). For assessment of extracellular NA function, confluent monolayers of MDCK cells were cultured in serum-free MEM supplemented with equivalent units of neuraminidase from *Vibrio cholerae* (Merck, N7885) at 37°C for 16 h. Before staining, the cells were washed three times with PBS. To detect viral antigens and glycan epitopes, the cells were incubated with the corresponding primary antibody (anti-NP, anti-HA, or anti-DDDDK monoclonal antibody) together with lectin (FITC-SNA or biotinylated UEA-I) at 4°C

overnight. After washing three times with PBS, the cells were incubated with the appropriate fluorescent-labeled secondary antibodies or streptavidin at room temperature for 2 h. After washing three times with PBS, the cells were counterstained with 4',6-diamidino-2-phenylindole (DAPI; Dojindo). The cells were mounted using the SlowFade Diamond Antifade Mountant (Thermo Fisher Scientific) and observed under a fluorescence microscope (Axiovert 200; Carl Zeiss, Oberkochen, Germany). The signal intensities of fluorescent images staining with lectins were quantitated by ImageJ software version 1.54g [128]. The data are represented as mean signals of three fields of view ±standard deviations (SD). The mean of signal intensities were statistically analyzed by Student's t-test or one-way ANOVA with Dunnet's post hoc test via EZR software version 1.63 [129].

Lectin microarray analysis

Lectin microarray analyses were performed as previously described with some modifications [114, 130, 131]. Briefly, for virus-infected cells, confluent MDCK cells were inoculated with PR8 at MOI = 1 or PBS as mock and cultured at 35°C for 1 h. The cells were then washed and cultured in serum-free MEM containing 1.0 μg/mL of acetylated trypsin at 35°C for 12 h. The IAV-infected cells and NA-expressing cells were washed with ice-cold PBS three times and labeled with 1 mg/mL of EZ-Link Sulfo-NHS-Biotin (Thermo Fisher Scientific) at 4°C for 1 h. The cells were then washed with Tris-buffered saline (TBS) to quench the remaining biotin-labeling reagents and lysed with TBS containing 1% Nonidet P-40, 0.5% sodium deoxycholate, 0.1% SDS, and an EDTA-free protease inhibitor (cOmplete ULTRA Tablets, Mini, EDTA-free; Roche, Basel, Switzerland). Protein samples were diluted with probing buffer (TBS containing 1% Triton X-100, 500 mM glycine, 1 mM $CaCl_2$, and 1 mM $MnCl_2$) and applied to an activated LecChip (Ver.1.0; Precision System Science Co., Ltd., Chiba, Japan; Table 6). The array glass slides were incubated at 20°C overnight. After washing, slides were overlaid with streptavidin and Alexa Fluor 555 conjugate (Thermo Fisher Scientific). After washing, the slides were scanned using an evanescent field excitation fluorescence imager (GlycoStation Reader 1200, Precision System Science; Chiba, Japan). Luminance obtained from the images was measured using GlycoStation ToolsPro Suite ver. 2 (Precision System Science). The data are mean-normalized and represented as mean signals of three spots ±SD.

Table 6. List of 45 lectins used in lectin microarray analyses and those glycan specificities.

No.	Name	Origin	Reported glycan specificity[a]	Classification by specificity
1	LTL	*Lotus tetragonolobus*	Fucα1-3GlcNAc, Lewis X, sialyl Lewis X	Fucose
2	PSA	*Pisum sativum*	Fucα1-6GlcNAc , α-Man	Fucose
3	LCA	*Lens culinaris*	Fucα1-6GlcNAc , α-Man, α-Glc	Fucose
4	UEA-I	*Ulex europaeus*	Fucα1-2Galβ1-4GlcNAc	Fucose
5	AOL	*Aspergillus oryzae*	Terminal αFuc, Lewis X, sialyl Lewis X	Fucose
6	AAL	*Aleuria auranti*	Terminal αFuc, Lewis X, sialyl Lewis X	Fucose
7	MAL-I	*Maackia amurensis*	Siaα2-3Gal	Sialic acid
8	SNA	*Sambucus nigra*	Siaα2-6Gal/GalNAc	Sialic acid
9	SSA	*Sambucus sieboldiana*	Siaα2-6Gal/GalNAc	Sialic acid
10	TJA-I	*Trichosanthes japonica*	Siaα2-6Galβ1-4GlcNAc	Sialic acid
11	PHA-L	*Phaseolus vulgaris*	Tri/tetra-antennary complex-type *N*-glycan	LacNAc
12	ECA	*Erythrina cristagalli*	Lac/LacNAc	LacNAc
13	RCA120	*Ricinus communis*	Lac/LacNAc	LacNAc
14	PHA-E	*Phaseolus vulgaris*	Bi-antennary complex-type *N*-glycan with outer Gal and bisecting GlcNAc	LacNAc
15	DSA	*Datura stramonium*	Chitin, poly LacNAc, LacNAc	LacNAc
16	GSL-II	*Griffonia simplicifolia*	Agalactosylated tri/tetra antennary *N*-glycan	—
17	NPA	*Narcissus pseudonarcissus*	High-Mannose including Manα1-6Man	Mannose
18	ConA	*Canavalia ensiformis*	High-Mannose including Manα1-6(Manα1-3)Man	Mannose
19	GNA	*Galanthus nivalis*	High-Mannose including Manα1-3Man	Mannose
20	HHL	*Hippeastrum* hybrid	High-Mannose including Manα1-3Man or Manα1-6Man	Mannose
21	ACG	*Agrocybe cylindracea*	Siaα2-3Galβ1-4GlcNAc	—
22	TxLC-I	*Tulipa gesneriana*	Manα1-3(Manα1-6)Man, bi/tri-antennary complex-type *N*-glycan, GalNAc	—
23	BPL	*Bauhinia purpurea*	Galβ1-3GalNAc, tri/tetra-antennary complex-type *N*-glycan with outer Gal	Galactose

Table 6 (*cont*)**. List of 45 lectins used in lectin microarray analyses and those glycan specificities.**

No.	Name	Origin	Reported glycan specificity	Classification by specificity
24	TJA-II	*Tanthes japonica*	Fucα1-2Galβ1/GalNAcβ1, tri/tetra-antennary complex-type *N*-glycan with outer Gal	Galactose
25	EEL	*Euonymus europaeus*	Galα1-3[Fuc α1-2 Gal], Gal α1-3 Gal	Galactose
26	ABA	*Agaricus bisporus*	Galβ1-3GalNAcα-Thr/Ser (T) and sialyl-T	Galactose
27	LEL	*Lycopersicon esculentum*	Chitin, poly LacNAc	Chitin
28	STL	*Solanum tuberosum*	Chitin, poly LacNAc	Chitin
29	UDA	*Urtica dioica*	Chitin, poly LacNAc	Chitin
30	PWM	*Phytolacca americana*	Chitin, poly LacNAc	Chitin
31	Jacalin	*Artocarpus integrifolia*	Galβ1-3GalNAcα-Thr/Ser (T) and GalNAcα-Thr/Ser (Tn)	*O*-glycan
32	PNA	*Arachis hypogaea*	Galβ1-3GalNAcα-Thr/Ser (T)	*O*-glycan
33	WFA	*Wisteria floribunda*	GalNAcβ1-4GlcNAc (LacdiNAc), terminal GalNAc	*O*-glycan
34	ACA	*Amaranthus caudatus*	Galβ1-3GalNAcα-Thr/Ser (T)	*O*-glycan
35	MPA	*Maclura pomifera*	Galβ1-3GalNAcα-Thr/Ser (T) and GalNAcα-Thr/Ser (Tn)	*O*-glycan
36	HPA	*Helix pomatia*	Terminal GalNAc	*O*-glycan
37	VVA	*Vicia villosa*	α- or β-linked terminal GalNAc and GalNAcα-Thr/Ser (Tn)	*O*-glycan
38	DBA	*Dolichos biflorus*	GalNAcα-Thr/Ser (Tn) and GalNAcα1-3GalNAc	*O*-glycan
39	SBA	*Glycine max*	Terminal GalNAc	*O*-glycan
40	Calsepa	*Calystegia sepium*	Man, Maltose	—
41	PTL-I	*Psophocarpus tetragonolobus*	α-GalNAc, Gal	—
42	MAH	*Maackia amurensis*	Siaα2-3Galβ1-3(Siaα2-6)GalNAc (disialyl-T)	—
43	WGA	*Triticum aestivum*	Chitin, multicalent Sia	—
44	GSL-I-A4	*Griffonia simplicifolia*	α-GalNAc, GalNAcα-Thr/Ser (Tn)	—
45	GSL-I-B4	*Griffonia simplicifolia*	α-Gal	—

[a] Specificity data of lectins were obtained from LfDB (Lectin Frontier Database; https://acgg.asia/db/lfdb/).

Immunoprecipitation

Confluent MDCK cells were inoculated with PR8 at MOI = 1 or PBS as mock and cultured at 35°C for 1 h. Cells were washed and cultured in serum-free MEM containing 1.0 μg/mL of acetylated trypsin at 35°C for 24 h. Then, 1 mL of infectious cell culture supernatants was mixed with trichloroacetic acid (TCA, FUJIFILM Wako Pure Chemical) and incubated at 4°C for 3 h to precipitate proteins in cellular supernatant. After centrifugation, TCA was removed, and the pellet was washed with cold acetone. The protein samples were centrifuged and the pellet was resolved in 1 M Tris-HCl (pH 8.6) containing 1% SDS and 1.5% 2-mercapt ethanol. The samples were subjected to sodium dodecyl sulfate-polyacrylamide gel electrophoresis, western blotting, and lectin blotting of the cell supernatant (Sup). The original cellular supernatant was also immunoprecipitated to enrich HA proteins as immunoprecipitated samples (IP). Biotinylated anti-HA monoclonal antibodies (200 ng; Sino Biological). After incubation at 37°C for 1 h, the complexes were captured with Dynabeads MyOne Streptavidin T1 (Thermo Fisher Scientific) at 4°C for 1 h. After washing, viral antigens were eluted from the magnetic beads by disruption with 100 mM citric acid containing 1% Triton X-100. Biotinylated antibodies contaminated into the eluted samples were depleted by incubation with Dynabeads MyOne Streptavidin T1 at 4°C for 1 h. The culture supernatant of mock-infected cells was used as a negative control.

SDS-PAGE, silver staining, western and lectin blotting

Samples were mixed with an equivalent amount of 2× Laemmli sample buffer (125 mM Tris-HCl [pH 6.8], 4% SDS, 20% glycerol, 0.02% bromophenol blue and 10% 2-mercaptoethanol). SDS-PAGE was conducted using a 4–15% Mini-PROTEAN TGX Precast Protein Gel (Bio-Rad) at a constant voltage of 200 V for 35 min under reducing conditions. For silver staining, the proteins on the gel were stained with EzStain Silver (AE-1360; Atto) following the commercial protocol. For Western and lectin blotting, the resolved proteins were transferred to Immobilon-P PVDF membranes (Merck). The membrane was blocked with a PVDF Blocking Reagent for Can Get Signal (Toyobo). To detect viral HA or NA, the membrane was probed with an anti-PR8 HA monoclonal antibody (2F1A7, 1:2000 dilution, Sino Biological) or an anti-DDDDK tag monoclonal antibody (FLA-1, 1:2000 dilution, Medical & Biological Laboratories), and then a goat

anti-mouse IgG monoclonal antibody conjugated with HRP (1:10000 dilution; Bio-Rad). For loading control, the membrane was probed with an anti-β-actin monoclonal antibody (BA3R, 1:2000 dilution; Applied Biological Materials), followed by the mouse-IgG HRP conjugate (1:10000 dilution). For lectin blotting, the membrane was probed with FITC-labeled ECA (1:2000 dilution; EY Laboratories), biotinylated UEA-I (1:2000 dilution; Vector Laboratories) or FITC-labeled SNA (1:2000 dilution; Vector Laboratories), and appropriate HRP-conjugates, goat anti-FITC antibody (1:10000 dilution; Southern Biotech), or HRP-streptavidin (1:10000 dilution; Thermo Fisher Scientific), respectively. Proteins were detected using a chemiluminescent substrate, ImmunoStar LD (FUJIFILM Wako Pure Chemical) or Immobilon Crescendo Western HRP substrate (Merck), and visualized using LuminoGraph I (WSE-6100, Atto).

Reverse transcription-quantitative polymerase chain reaction (RT-qPCR) of glycosyltransferases

Lysates of PR8-infected cells and NA-expressing cells were collected and subjected to quantification of FUT1 and FUT2 genes, with the glyceraldehyde-3-phosphate dehydrogenase (GAPDH) gene as a housekeeping gene. Total RNA was extracted from cellular lysates using TRIzol Reagent (Thermo Fisher Scientific) in triplicate and reverse-transcribed into cDNA using ReverTra Ace (Toyobo). Subsequently, qPCR was performed with the KOD SYBR qPCR Mix (Toyobo) using the Applied Biosystems StepOnePlus real-time PCR system (Thermo Fisher Scientific). The primer sequences used for qPCR are listed in Table 7 [132]. Specific amplification of the fucosyltransferase and GAPDH genes was confirmed using melting curve analysis. The relative mRNA expression levels of target genes were calculated by comparative Ct method and presented as $2^{-\Delta\Delta Ct}$ with a housekeeping gene encoding GAPDH as an internal control. The data are represented as mean expression level of biological triplicates ±SD.

Assessment of superinfection exclusion

Confluent monolayers of MDCK cells seeded on glass chamber slides (Matsunami Glass) were inoculated with either PR8 or Vac2-FLAG at an MOI of 1, and incubated at 35°C for 30 min. The viral solution, including unbound viruses, was removed from the cells, and the cells were washed with serum-free MEM. The cells were then

Table 7. Primer list used for RT-qPCR of glycosyltransferase genes.

Gene	Direction	Primer sequence	Reference
FUT1	Forword	GATGTGGGCTGCACTTGC	Designed in this paper
	Reverse	GAAGACGGCTGAAAGAACACAG	
FUT2	Forword	CTGGGCGGTTCTGATTTTTGAG	Designed in this paper
	Reverse	ATGGGGAAGAAAGACACCTGAC	
GAPDH	Forword	TTCCACGGCACAGTCAAG	Menzes-Souza *et al*. [132]
	Reverse	ACTCAGCACCAGCATCAC	

cultured in serum-free MEM containing 1.0 μg/mL of acetylated trypsin (Merck) at 35°C until the secondary infection. After washing with serum-free MEM, PR8 or Vac2-FLAG was inoculated into the cells at an MOI of 1 and further incubated at 35°C for 30 min. The viral solution was removed from the cells, and the cells were washed once with serum-free MEM. The cells were then cultured in serum-free MEM containing 1.0 μg/mL of acetylated trypsin (Merck) at 35°C until 8 h post primary viral infection. The cells were then washed with PBS and fixed with 4% paraformaldehyde in PBS at room temperature for 10 min. Viral antigens on the cells were stained using the abovementioned immunofluorescence staining method.

Ethics statements

All experiments using genetically modified organisms, including mutant viruses generated by reverse genetics, were authorized by the Safety Committee on Genetic Recombination Experiments of Hokkaido University (approval no. 2020-009, June 2, 2020) and the Ministry of Education, Culture, Sports, Science, and Technology, Japan (approval no. 4-Monkashin-Dai-142, July 7, 2022). This study was approved by the Biosafety Management Committee on Pathogens and Other Hazardous Agents of the Faculty of Veterinary Medicine, Hokkaido University (approval nos. 2022-1-82, 2023-1-43 and 2024-1-70).

Results

Changes in the glycan profiles on the surface of MDCK cells infected with an IAV

To validate previously observed glycome alterations in MDCK cells infected with IAV [113, 114, 116], glycan structures on the surface of MDCK cells infected with IAV, A/Puerto Rico/8/1934 (H1N1) (PR8), were profiled using a lectin microarray. Briefly, the cellular surface of MDCK cells inoculated with PR8 or mock-infected cells was labeled with hydrophilic biotin-NHS analogs, and the cell lysates were subjected to lectin microarray analysis to assess the reactivity of a series of lectins [114, 131]. Cell surface glycan profiles were enriched by detecting biotin-labeled proteins using fluorescently labeled streptavidin (Figure 30). Lectins specific to sialylated glycans (MAL-I [*Maackia amurensis* lectin I], SNA, SSA [*Sambucus sieboldiana* agglutinin], and TJA-I [*Trichosanthes japonica* agglutinin I]) exhibited low signal intensities in PR8-infected MDCK cells. In contrast, ECA, RCA120 [*Ricinus communis* agglutinin 120], BPL [*Bauhinia purpurea* lectin], and WFA [*Wisteria floribunda* agglutinin], which preferentially recognize the terminal LacNAc or its cluster [133], exhibited higher signal intensities in PR8-infected cells than mock-infected cells. These results indicated desialylation on the surface of PR8-infected MDCK cells. Next, glycans terminating with α1-3 galactose or α1-2 fucose were examined because previous reports noted that these have been observed in IAV-infected MDCK cells but rarely detected in non-infected cells [114, 116]. Although α1-3 galactose had been observed from whole cell lysates of PR8-infected MDCK cells [114], the EEL signal intensity was not high in the PR8-infected MDCK cells compared to the mock-infected ones in this study (Figure 30). In contrast, the higher signal intensity of TJA-II, specific for α1-2 fucose, was observed in PR8-infected cells, consistent with previous studies [114, 116]. These results indicate that IAV-infected cells display glycans terminating with α1-2 fucose instead of sialic acids, suggesting a unique glycan profile on IAV-infected cells.

Global desialylation and α1-2 fucosylation on the surface of PR8-infected MDCK cells

For further validation of whether glycome alteration was specifically observed in virus-infected cells, fluorescent staining was performed with lectins specific for terminal sialic acids (SNA) and α1-2 fucose (UEA-I), in parallel with immunostaining using an

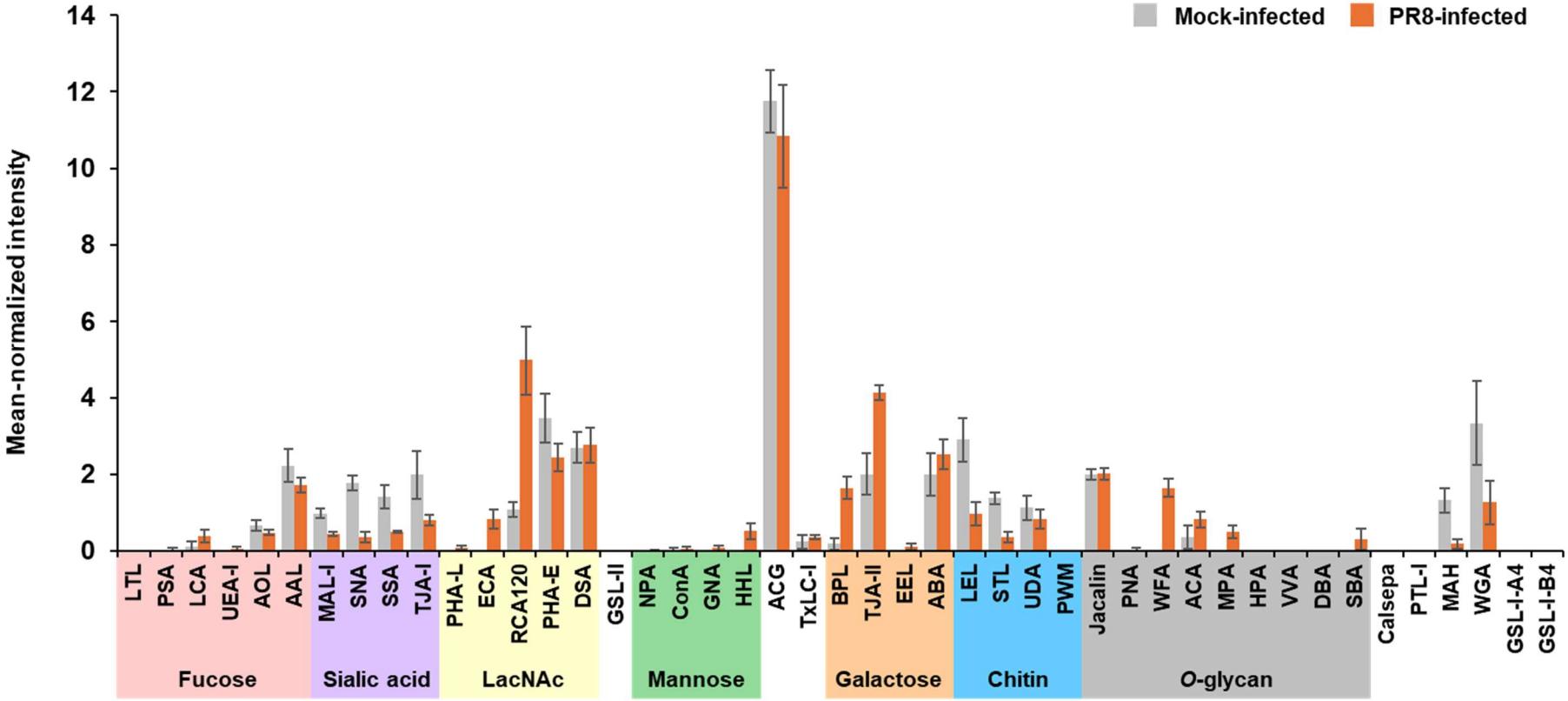

Figure 30. Alterations in glycan profiles on the surface of MDCK cells infected with PR8. The surface of MDCK cells infected with mock (gray bars) and PR8 (orange bars) were labeled with biotin and the whole cell lysates were placed on lectin microarray slides to incubate with a set of lectins. The interactions of glycans displayed on the cellular surfaces and lectins were detected with a fluorescent-labeled secondary antibody. The data are mean-normalized and represented as mean signals of three spots ±SD.

anti-PR8 HA antibody. The surface of HA-positive cells was not stained by SNA (Figure 31B, C), while the mock-infected HA-negative cells were strongly stained by SNA (Figure 31A, C), indicating desialylation on the surface of HA-positive cells. Conversely, UEA-I signal intensity was higher on the surface of HA-positive cells than HA-negative cells (Figure 31D–F). These results demonstrated desialylation and glycan recapping with α1-2 fucose on the HA-positive MDCK cells after PR8 infection.

α1-2 fucosylation is induced on the surface of MDCK cells by a broad range of IAV strains

To investigate whether the changes in glycan profiles in MDCK cells during PR8 infection are commonly observed by other IAV infections, the reactivities of SNA and UEA-I were tested in MDCK cells infected with duck-origin IAVs with NA subtypes from N1 to N9. Eight strains (N1–6, N8 and N9 subtypes) are non-pathogenic AIVs isolated from ducks and a N7 strain is a recombinant virus, Vac2-FLAG, whose NA was tagged with FLAG (DYKDDDDK) for detection of NA expression in the infected cells. The infection of cells was confirmed by staining with corresponding anti-HA monoclonal antibodies. Fluorescent intensities of SNA in AIV-infected cells varied among the strains. Especially, the signals were drastically diminished in cells infected with N1, N4, and N6–8 viruses (Figure 32). In contrast, marked increase in UEA-I signal was observed in all cells infected with AIVs except an N3 virus (Figure 33). It was noted that the growth of the N3 virus, A/duck/Hokkaido/84/2002 (H5N3), was low in MDCK cells, possibly causing slight increase of UEA-I signal in the infected cells without significant difference. These results suggest that the changes in glycan profiles with increased α1-2 fucose can be commonly observed in IAV-infected MDCK cells.

IAV infection induces desialylation without terminal recapping with fucose in A549 and Vero E6 cells

Because IAVs leads a global decrease in sialic acid and an increase in α1-2 fucose on the surface of infected MDCK cells, a similar assay was attempted using A549 and Vero E6 cell lines. Since PR8 protein expression was not high in those cells, lectin fluorescent staining showed an obvious decrease in SNA signal intensity for both PR8 and Vac2 infections (Figure 34A–C, G–I). In contrast, an increase in UEA-I signals was not observed (Figure 34D–F, J–L). Thus, hydrolysis of sialic acid by NA was induced

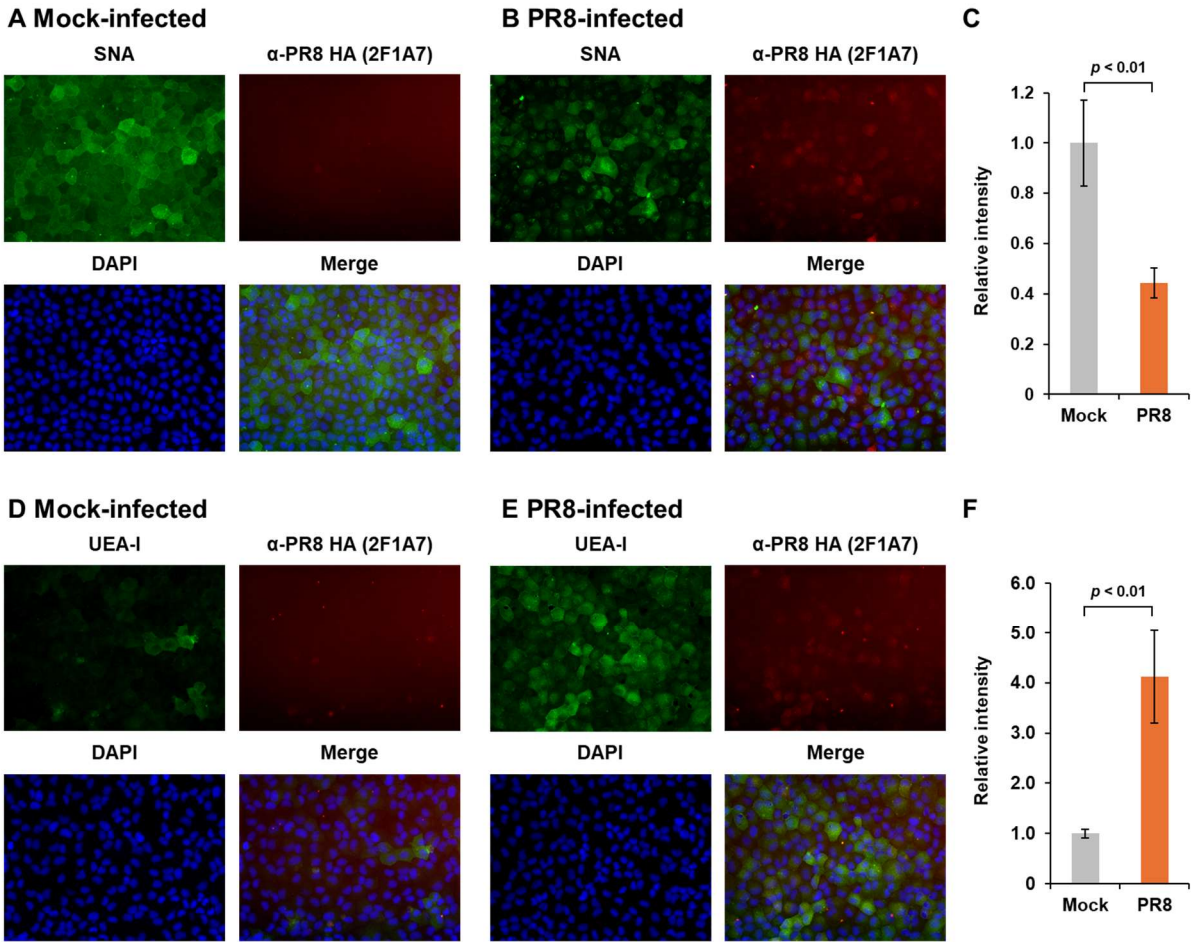

Figure 31. PR8 infection induces desialylation and fucosylation in MDCK cells. (A, B) Lectin and immunofluorescence staining of mock- or PR8-infected MDCK cells at 8 hpi. Cells were stained with SNA (green) and an anti-PR8 HA monoclonal antibody (red), and counterstained with DAPI (blue). (C) Fluorescent intensities derived from SNA in an average of three fields of view were compared between mock- and PR8-infected cells. The signal intensity of PR8-infected cells was significantly lower than that of mock-infected ones ($p < 0.01$, Student's t-test)**.** (D, E) Cells were stained with UEA-I (green) and an anti-PR8 HA monoclonal antibody (red), and counterstained with DAPI (blue). (F) Fluorescent intensities derived from UEA-I in an average of three fields of view were compared between mock- and PR8-infected cells. The signal intensity of PR8-infected cells was significantly higher than that of mock-infected ones ($p < 0.01$, Student's t-test)**.**

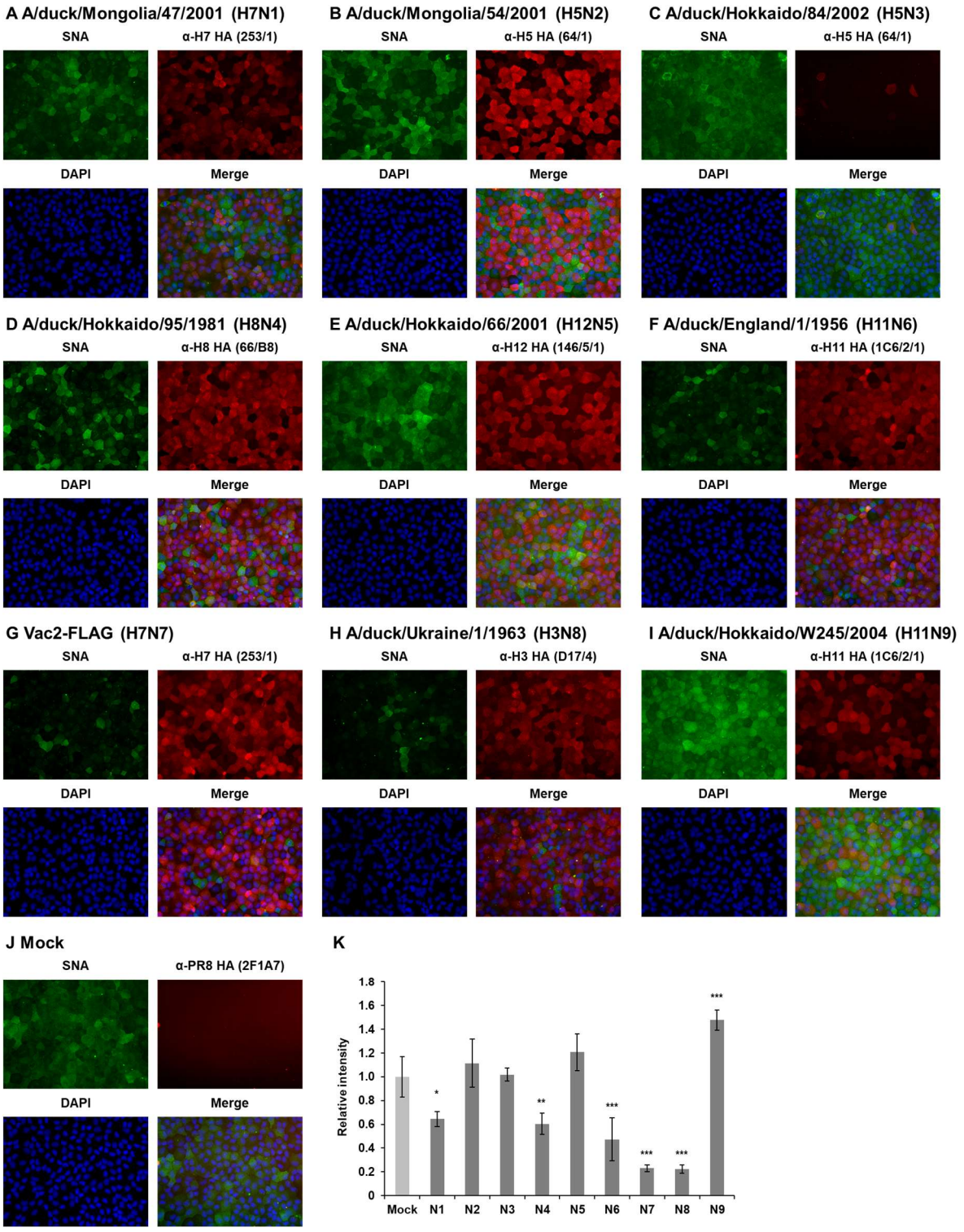

Figure 32. SNA staining of MDCK cells infected with various AIVs. (A–J) Lectin and immunofluorescence staining of AIV (N1–9 subtypes) or mock-infected MDCK cells at 8 hpi. (K) Fluorescent intensities derived from SNA in an average of three fields of view were compared. The signal intensities of IAV-infected cells compared to that of mock-infected ones were statistically analyzed by one-way ANOVA with Dunnett's post hoc test (*: $p < 0.05$, **: $p < 0.01$, ***: $p < 0.001$).

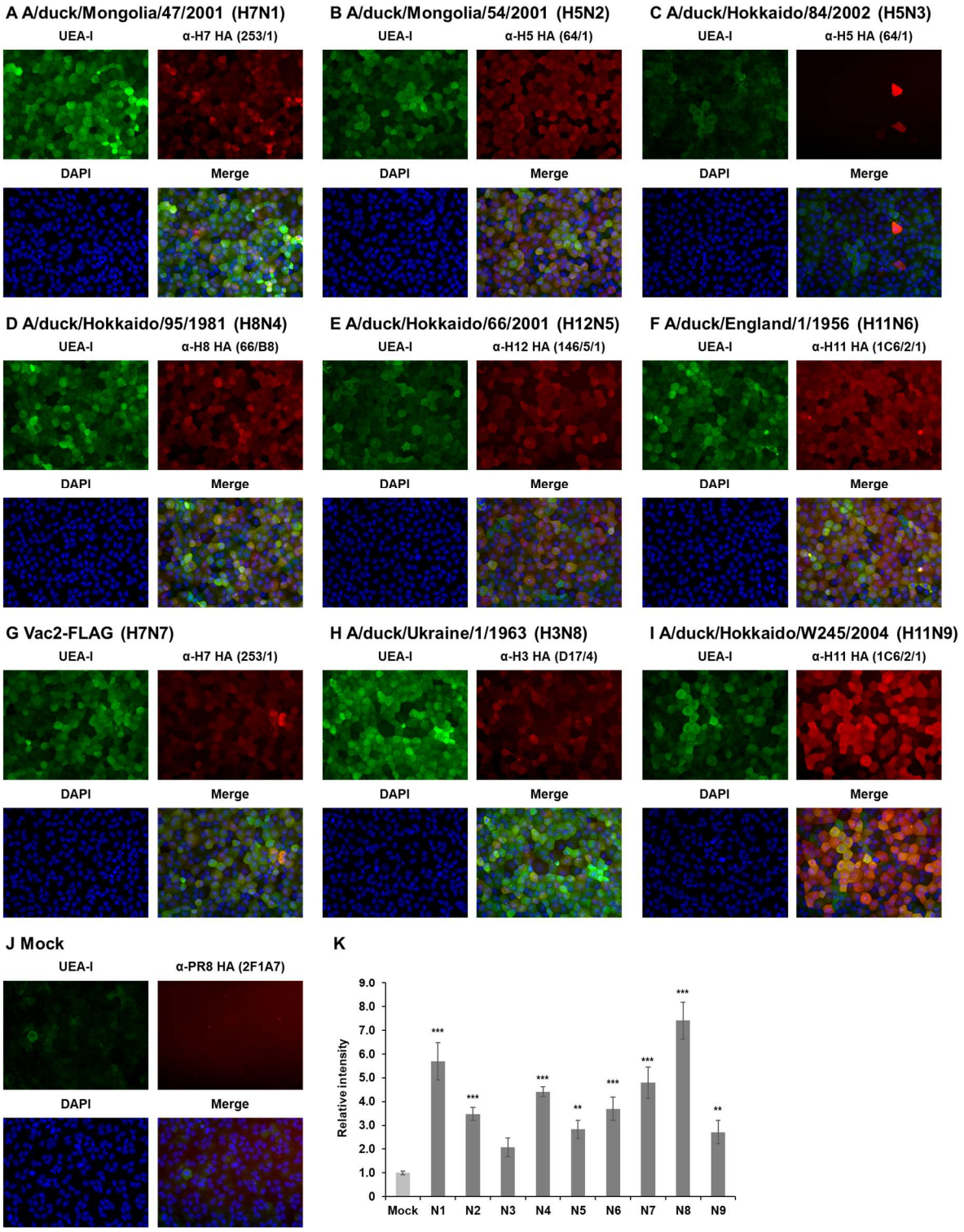

Figure 33. UEA-I staining of MDCK cells infected with various AIVs. (A–J) Lectin and immunofluorescence staining of AIV (N1–9 subtypes) or mock-infected MDCK cells at 8 hpi. (K) Fluorescent intensities derived from UEA-I in an average of three fields of view were compared. The signal intensities of IAV-infected cells compared to that of mock-infected ones were statistically analyzed by one-way ANOVA with Dunnett's post hoc test (*: $p < 0.05$, **: $p < 0.01$, ***: $p < 0.001$).

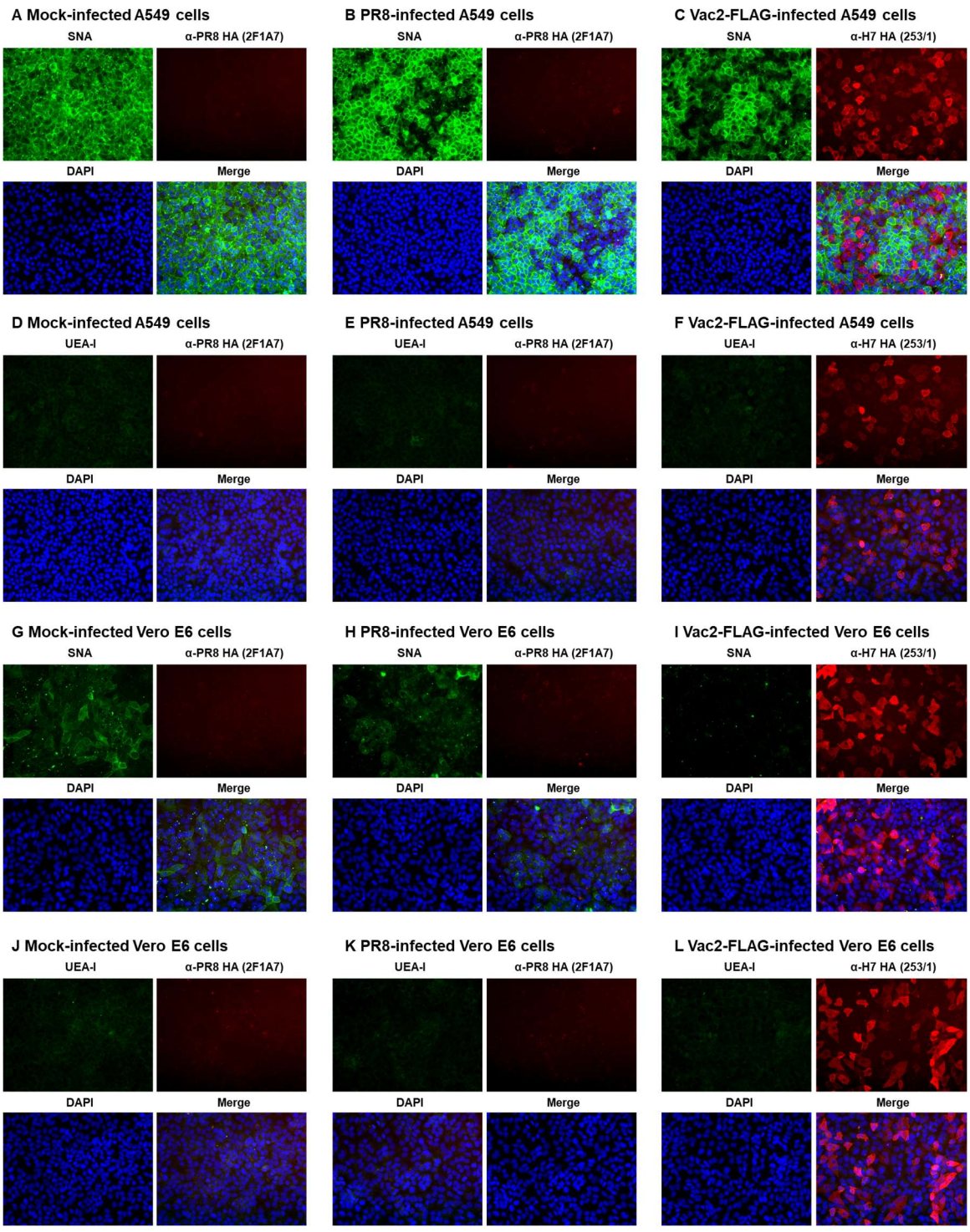

Figure 34. Lectin staining of A549 and Vero E6 cells infected with PR8 or Vac2 virus. (A–F) Lectin and immunofluorescence staining of IAV or mock-infected A549 cells at 8 hpi. (G–L) Lectin and immunofluorescence staining of IAV or mock-infected Vero E6 cells at 8 hpi.

after IAV infection in various types of cells, whereas glycan recapping appears to be highly dependent on the cell-specific glycan synthesis machinery.

Glycan alterations are induced in both viral and host proteins by IAV infection

The present study further examined whether the changes in glycan profiles were specific to either viral or host proteins. To assess this, culture supernatants and whole cell lysates of mock- or PR8-infected cells were subjected to lectin and western blot analyses (Figure 35). The total protein concentration in whole-cell lysates was approximately adjusted using the band intensities of silver staining. Viral HA was enriched via immunoprecipitation using an anti-HA antibody. A band of approximately 65 kDa (arrowhead) detected by the anti-HA antibody in the immunoprecipitated sample of the PR8-infected cells was observed by lectin blotting with both lectins specific for LacNAc (ECA) and α1-2 fucose (UEA-I). In contrast, HA protein was not detected in the immunoprecipitated sample with lectin specific for terminal sialic acids (SNA). This demonstrated that desialylation and glycan recapping with α1-2 fucose are observed on the viral HA. Moreover, lectin blotting of whole-cell lysates and culture supernatants of PR8-infected cells exhibited several higher-intensity bands than those of mock-infected cells using ECA and UEA-I, in addition to a high-intensity band of HA, while the band intensity of SNA in whole-cell lysates was lower in PR8-infected cells. It should be noted that several bands were observed in the culture supernatant of PR8-infected cells when blotting with SNA. This reflects a higher degree of protein contamination in the supernatant of virus-infected cells compared to that of mock-infected cells. These results suggested some host proteins, as well as viral HA, were globally desialylated and α1-2 fucosylated during PR8 infection in MDCK cells.

α1-2 fucosylation in IAV-infected cells are induced by the latter part of a viral replication cycle

Since PR8 infection induced global changes in the glycome of virus-infected-MDCK cells, the displays of sialic acids and α1-2 fucose on the cells were monitored by time-course analysis from the viral infection (Figure 36A, B). The cells infected with PR8 at a MOI of 1 showed a decrease in SNA signals at 3 h post-infection (hpi), and the signals decreased at 6 and 9 hpi (Figure 36A, C). Conversely, the proportion of cells recognized by UEA-I increased at 6 hpi and showed high-intensity signals in the perinuclear space at

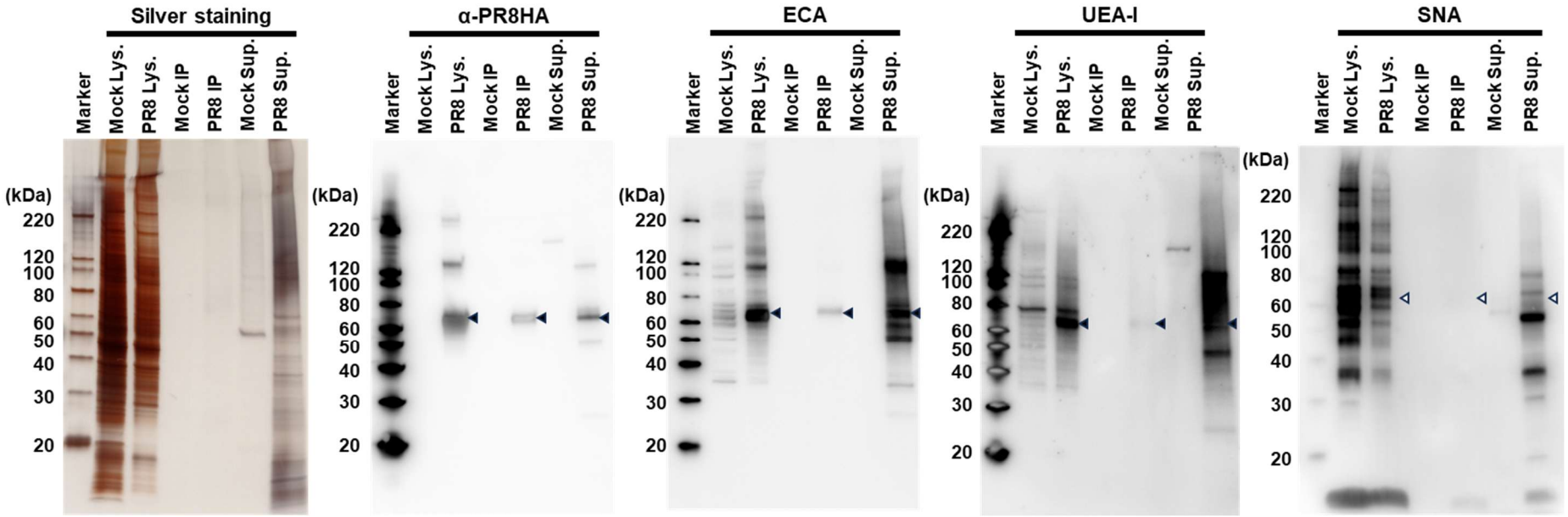

Figure 35. PR8 infection induces desialylation and fucosylation on viral glycoproteins and host proteins. Whole cell lysates (Lys.) and supernatant (Sup.) of mock- and PR8-infected MDCK cells were collected for western blotting and lectin blotting. Whole cell lysates were immunoprecipitated with the anti-PR8 HA antibody (IP). Those samples were analyzed by SDS-PAGE with silver staining, western blotting with the anti-PR8 HA antibody, and lectin blotting with ECA, UEA-I, and SNA. The filled arrowheads indicate a size of 65 kDa, which is considered HA proteins of PR8. The opened arrowheads indicate around 65 kDa, while the clear bands were not observed.

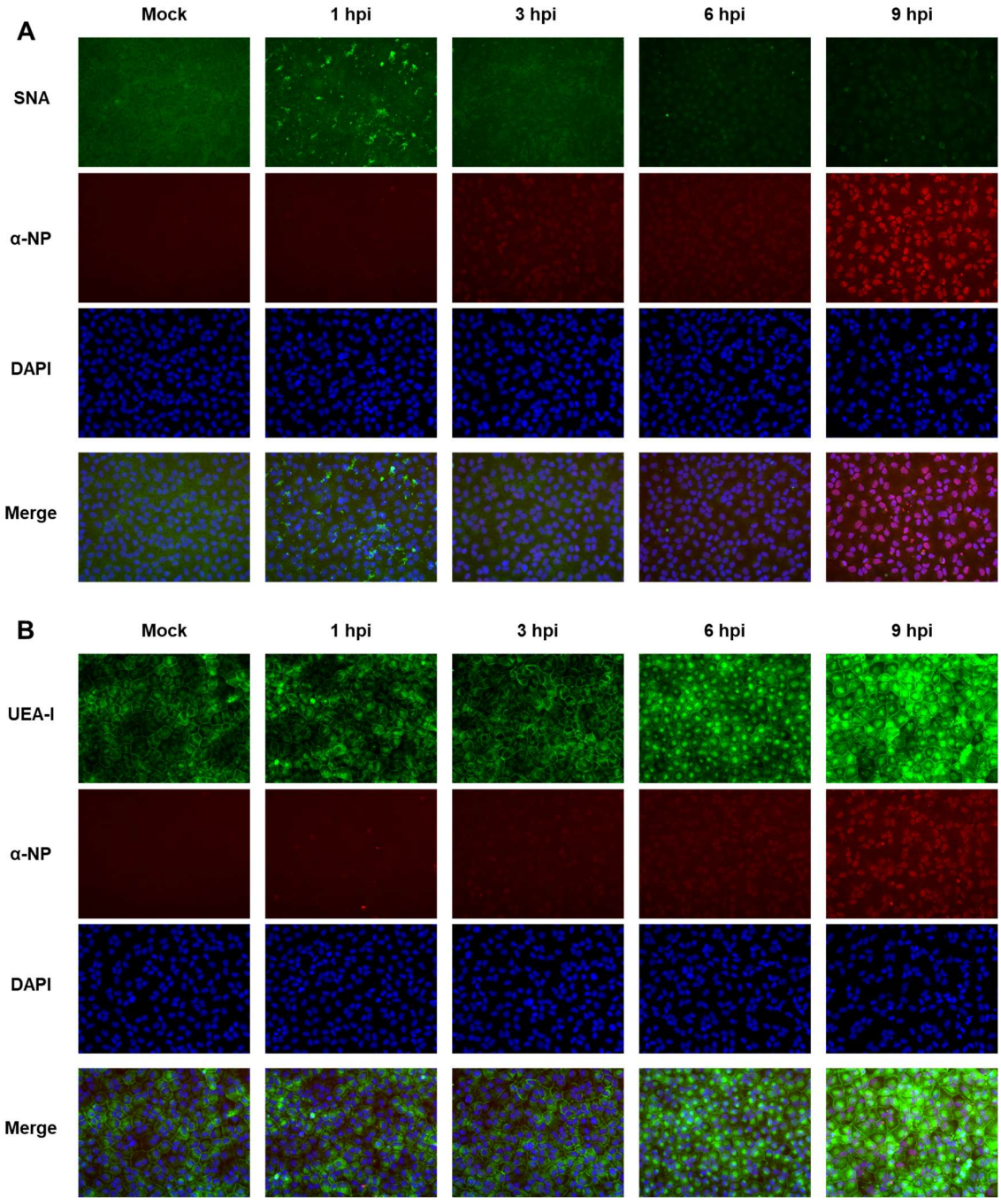

Figure 36. Glycome alterations associated with desialylation and α1-2 fucosylation were induced by the latter stage of PR8 replication cycle. (A, B) PR8-infected MDCK cells were fixed with methanol at multiple time points of 1, 3, 6, and 9 hpi, and lectin stained with SNA or UEA-I (green) together with immunostaining with an anti-NP monoclonal antibody (red). Cells were also counterstained with DAPI (blue).

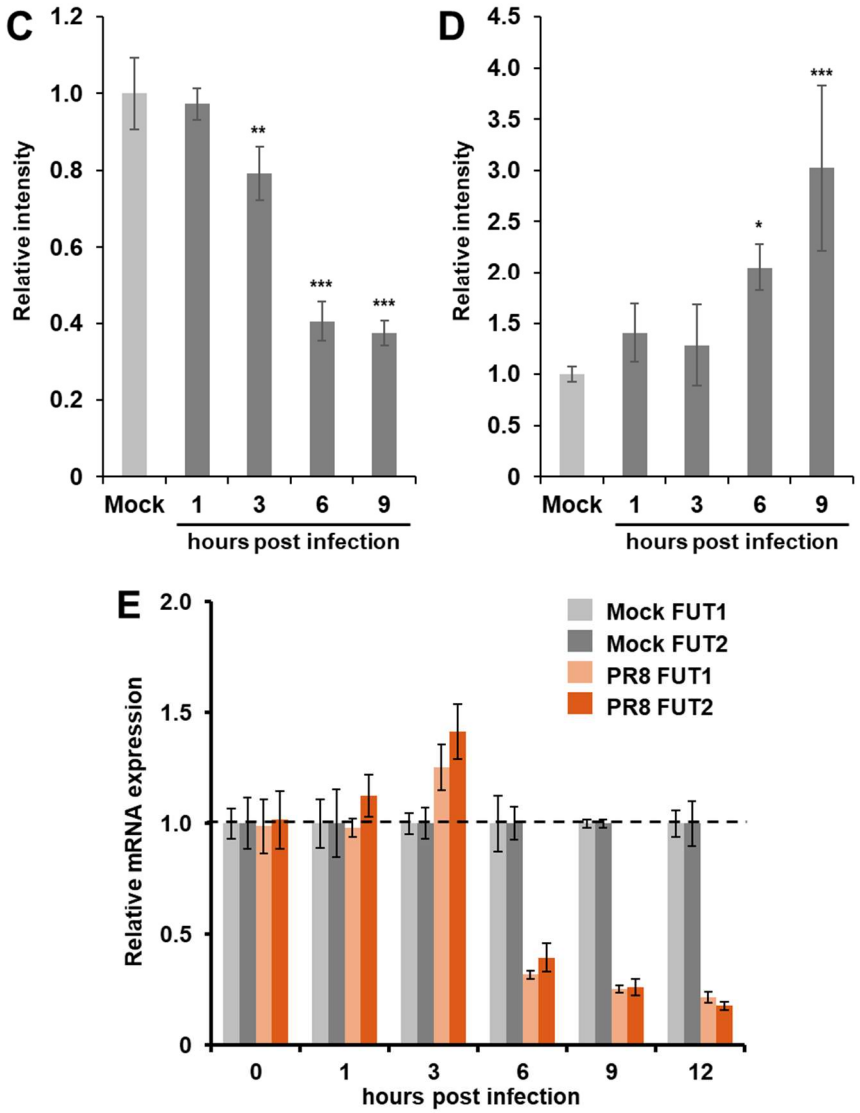

Figure 36 (*cont*)**. Glycome alterations associated with desialylation and α1-2 fucosylation were induced by the latter stage of PR8 replication cycle.** (C) Fluorescent intensities derived from SNA in an average of three fields of view were compared between mock- and PR8-infected cells by one-way ANOVA with Dunnett's post hoc test (*: $p < 0.05$, **: $p < 0.01$, ***: $p < 0.001$). (D) Fluorescent intensities derived from UEA-I in an average of three fields of view were compared between mock- and PR8-infected cells by one-way ANOVA with Dunnett's post hoc test (*: $p < 0.05$, **: $p < 0.01$, ***: $p < 0.001$). (E) mRNA expression levels of α1-2 fucosyltransferase (FUT1 and FUT2) genes were quantified via RT-qPCR. The relative mRNA levels of FUT1 and FUT2 genes were normalized based on the expression level of GAPDH gene as a house keeping gene and were compared between mock- and PR8-infected MDCK cells at multiple time points. The data are presented as mean expression level of biological triplicates ±SD.

6 and 9 hpi (Figure 36B, D). Corresponding to these signal changes in SNA and UEA-I, immunostaining with an anti-NP antibody indicated that viral NP was localized in the nucleus of the infected cells at 3 hpi, whereas nuclear export of NP was confirmed at 6 hpi in the latter stage of the IAV replication cycle, corresponding to the timeline for viral protein expression. These results suggested that the latter part of the viral replication cycle, including viral protein expression and assembly, induces glycome alterations in IAV-infected MDCK cells. Next, expression levels of endogenous fucosyltransferase (FUT1 and FUT2) genes, which are responsible for α1-2 fucosylation, were quantified via RT-qPCR in a time course after PR8 infection in MDCK cells. The mRNA levels of both FUT1 and FUT2 increased slightly at 3 hpi, with no significant difference; thereafter, the expression levels remained low until 12 hpi, potentially due to the host protein shutoff by PR8 infection (Figure 36E). Thus, the increased glycan recapping by α1-2 fucose at 6 hpi or later in the IAV-infected cells could not be due to the upregulation of endogenous FUT1 or FUT2 gene expression.

The association between glycome alteration in IAV-infected cells and viral protein expression was investigated. Lectin staining was performed on IAV-infected MDCK cells maintained in the presence of a cap-dependent endonuclease inhibitor, BXA, to suppress the mRNA synthesis of viral proteins and their subsequent expression [134, 135]. All PR8-infected cells showed a decrease in SNA signal intensity, regardless of treatment dose of BXA, compared to the mock-infected cells (Figure 37A–D). Cells that were faintly stained with an anti-PR8 HA antibody under 1000 nM of BXA remained low signal intensity of UEA-I by lectin staining (Figure 37E). Conversely, HA-positive cells treated with lower concentrations (100, 10, and 1 nM) of BXA exhibited higher UEA-I signal intensities (Figure 37F–H). These results emphasize that glycome alterations were not caused by IAV entry but at a later stage of the replication cycle, including viral genome transcription, protein expression, or assembly. A similar trend was observed in Vac2-infected MDCK cells, suggesting that these glycome alterations are mediated by a conserved mechanism across IAV strains (Figure 38). To elucidate the mechanism underlying these glycome changes, the present study focused on the expression and function of NA in IAV-infected cells.

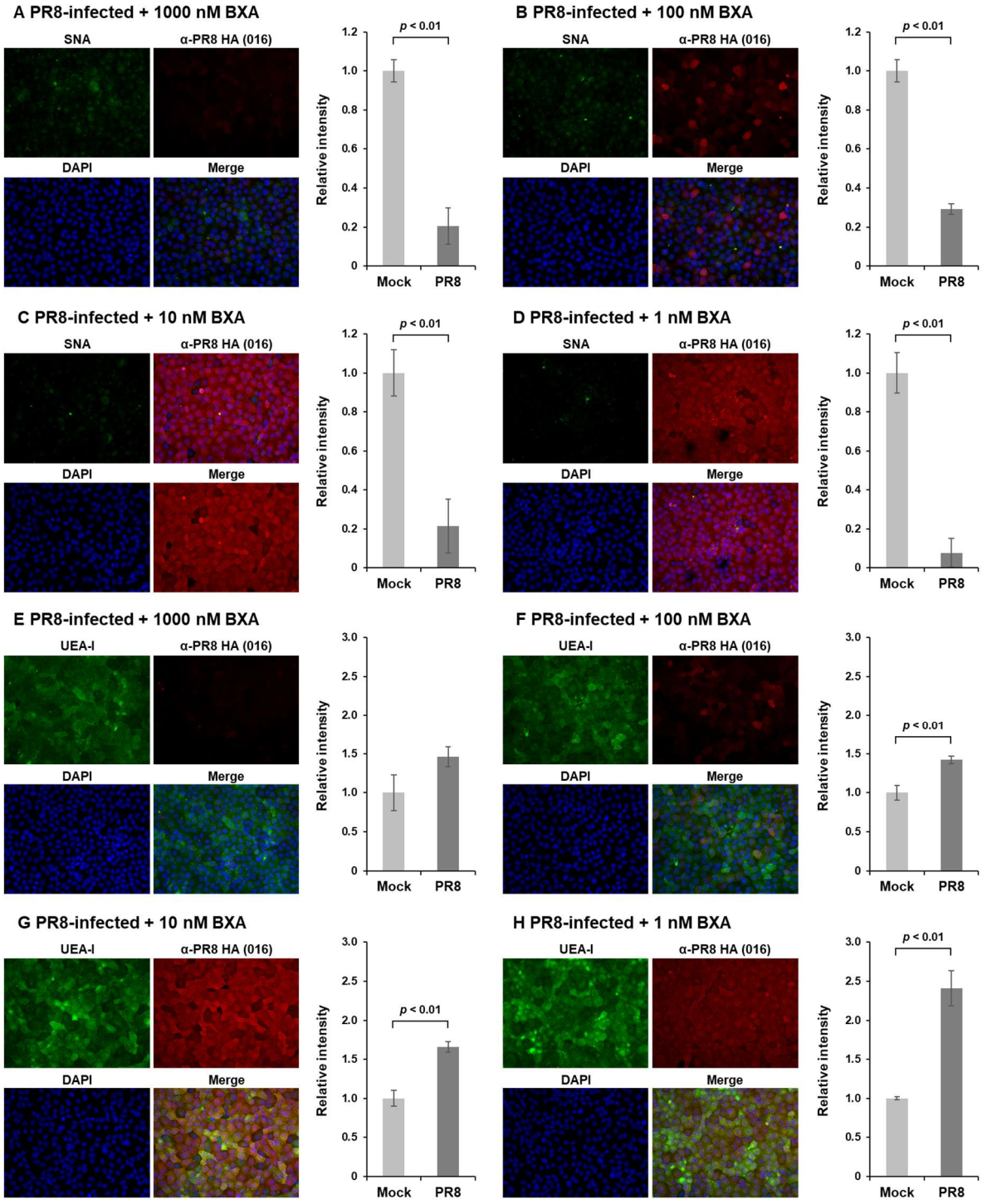

Figure 37. Inhibitory effect of BXA on glycan alterations on PR8-infected MDCK cells. MDCK cells infected with PR8 were cultured in the presence of 1–1000 nM of BXA for 8h and subjected to lectin and immunofluorescence staining. (A–D) The cells were stained with SNA (A–D; green) or UEA-I (E-H; green) and an anti-PR8 HA monoclonal antibody (red), and counterstained with DAPI (blue). Fluorescent intensities derived from SNA or UEA-I in an average of three fields of view were compared between mock- and PR8-infected cells. The statistical analysis was performed with Student's t-test.

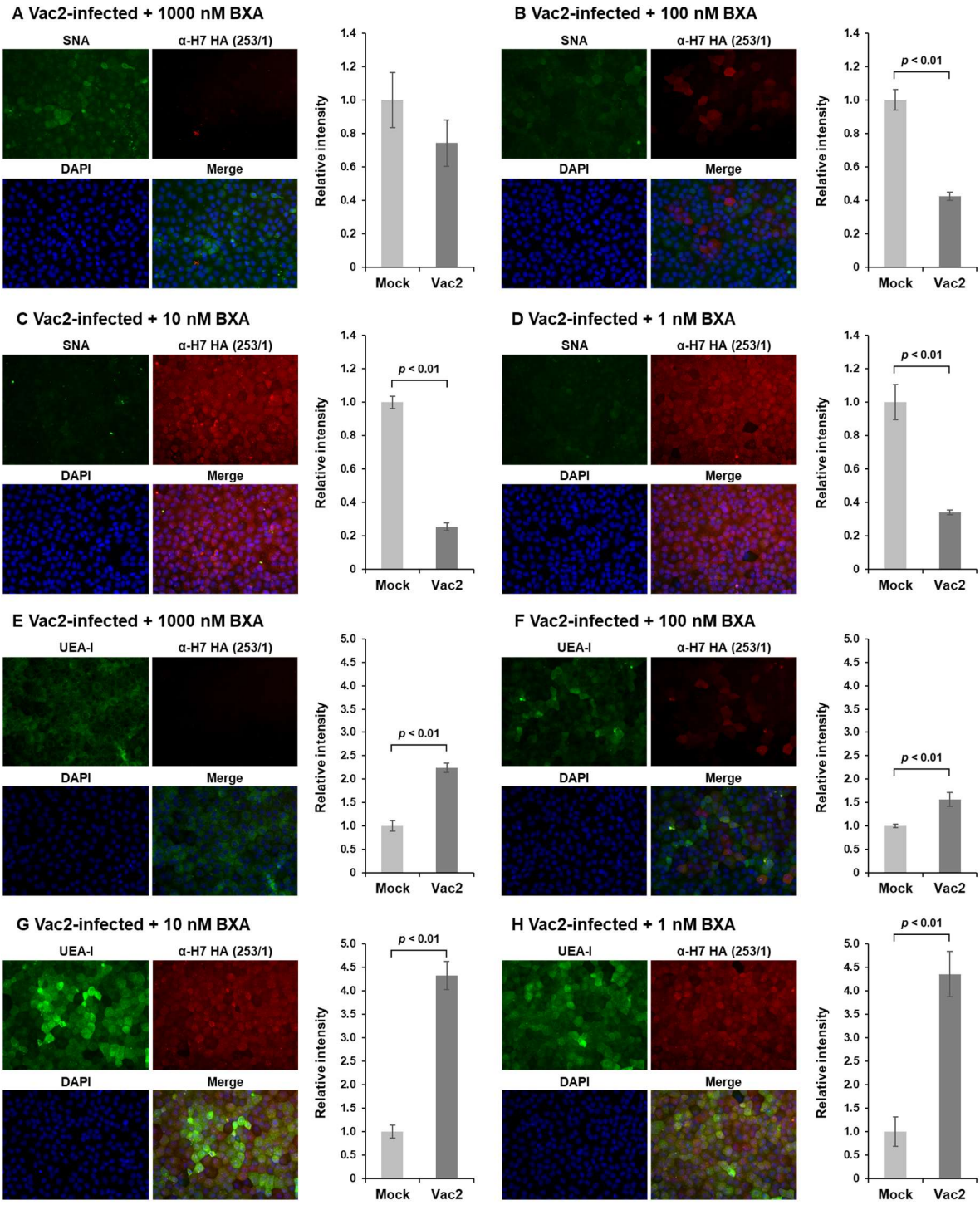

Figure 38. Inhibitory effect of BXA on glycan alterations on Vac2-infected MDCK cells. MDCK cells infected with Vac2 were cultured in the presence of 1–1000 nM of BXA for 8h and subjected to lectin and immunofluorescence staining. (A–D) The cells were stained with SNA (A–D; green) or UEA-I (E–H; green) and an anti-H7 HA monoclonal antibody (red), and counterstained with DAPI (blue). Fluorescent intensities derived from SNA or UEA-I in an average of three fields of view were compared between mock- and Vac2-infected cells. The statistical analysis was performed with Student's t-test.

NA expression in MDCK cells induced desialylation and glycan recapping with α1-2 fucose

To investigate the contribution of NA to glycome alterations in IAV-infected cells, MDCK cells stably expressing PR8 NA (MDCK-PR8NA) or Vac2 NA (MDCK-Vac2NA) were established. NA expression in MDCK cells was confirmed by detecting FLAG-fused NA proteins by western blotting with an anti-DDDDK-tag monoclonal antibody (Figure 39A). A band of either 55 kDa for PR8 NA or 75 kDa for Vac2 NA was detected in each NA-expressing cells via western blotting, indicating the expression of the designed NA in each cloned cells.

The glycan structures on the surface of NA-expressing cells were profiled using a lectin microarray. These NA-expressing cells exhibited glycan profiles similar to those of PR8-infected cells (Figures 30 and 39B). In particular, lectins specific for sialylated glycans (MAL-I, SNA, SSA) showed low signal intensities for NA-expressing cells, whereas lectins specific for α1-2 fucose (TJA-II), as well as those specific for terminal LacNAc or its clusters (ECA, RCA120, BPL, WFA), exhibited higher signal intensities for NA-expressing cells than parental MDCK cells. Subsequently, glycome alterations in MDCK-PR8NA or MDCK-Vac2NA cells were also assessed by lectin staining with SNA and UEA-I (Figures 39C–H and 40). Both NA-expressing MDCK cells exhibited lower intensity SNA signals and higher intensity UEA-I signals than parental cells. Although the signal intensities of UEA-I were low for both PR8-infected and NA-expressing MDCK cells via lectin microarray, they might have been affected by the orientation or representation of the glycan recognition epitope of this lectin on the microarray slide. Furthermore, the glycan structures recognized by UEA-I were further validated by α1-2 fucosidase pretreatment prior to lectin staining (Figure 41). To this end, parental MDCK cells, MDCK cells overexpressing α1,3/4 fucosyltransferases (MDCK-FUT cells), and MDCK-PR8NA cells were used [64]. The signal intensities of an anti-sialyl Lewis X antibody against MDCK-FUT cells were consistent regardless of pretreatment with α1-2 fucosidase as a negative control (Figure 41C, D). In contrast, the signal intensities of UEA-I in MDCK-PR8NA cells were higher than those in parental cells (Figure 41A, E). Moreover, the signal intensity decreased by α1-2 fucosidase pretreatment (Figure 41E, F), supporting the presence of α1-2 fucose on MDCK-PR8NA cells. Overall, the NA-expressing MDCK cells have the same glycome alterations of desialylation and glycan

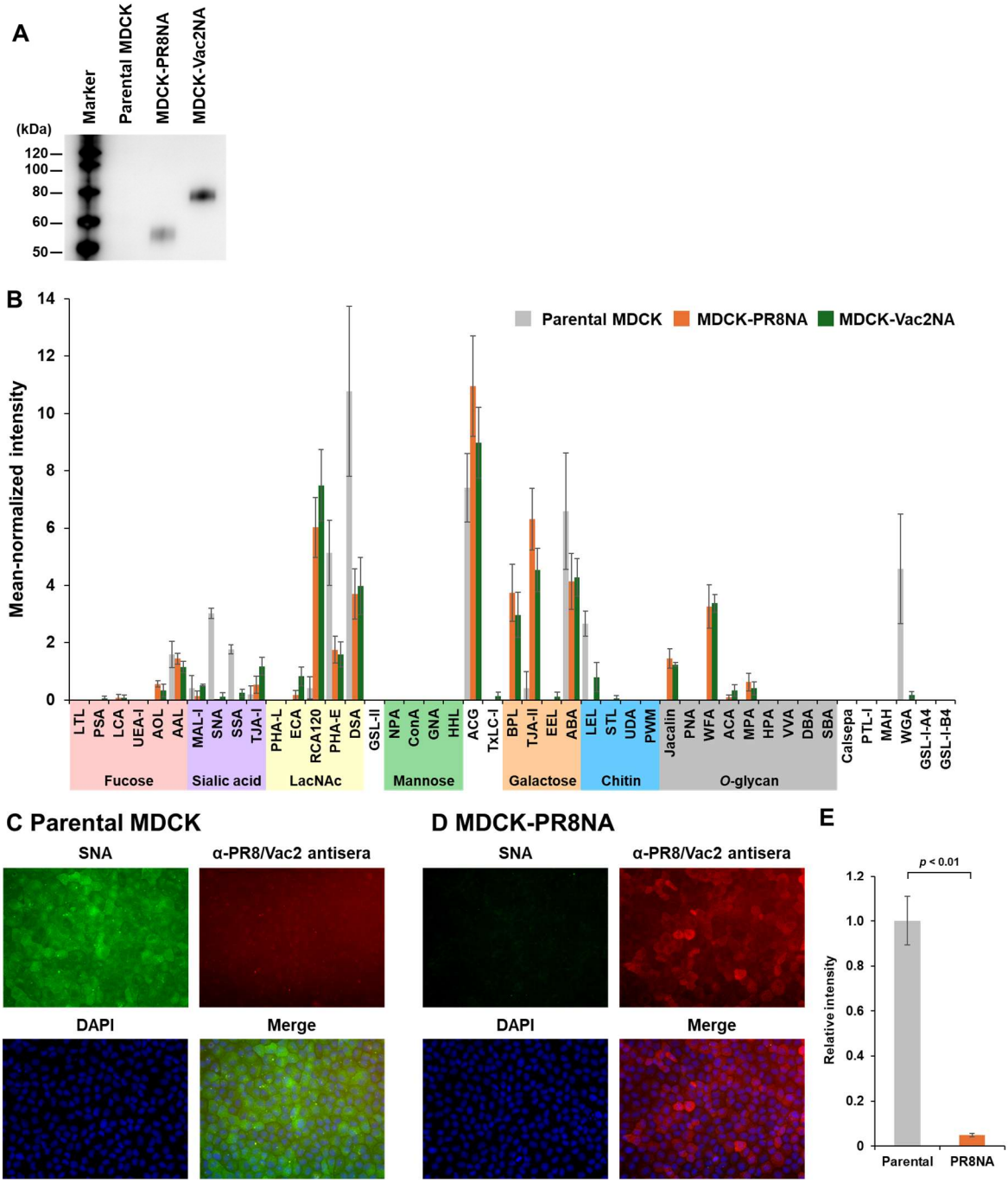

Figure 39. Glycome alterations in MDCK cells stably expressed NA protein of PR8 or Vac2 virus. (A) Expression of each FLAG-tagged NA protein derived from PR8 or Vac2 was confirmed via SDS-PAGE with western blotting using an anti-DDDDK-tag monoclonal antibody. (B) The surface of NA-expressing MDCK cells was labeled with biotin and whole cell lysates were placed on lectin microarray slides to incubate with a set of lectins. The interactions of glycans displayed on the cellular surfaces and lectins were detected with a fluorescent-labeled secondary antibody. The data are mean-normalized and presented as mean signals of three spots ±SD. (C, D) The wild type and PR8 NA-expressing MDCK cells were stained with SNA (green) and immunostained with a mixture of PR8 and Vac2 chicken antisera (red) and counterstained with DAPI (blue). (E) Fluorescent intensities derived from SNA in an average of three fields of view were compared between wild type and PR8 NA-expressing cells. The statistical analysis was performed with Student's t-test.

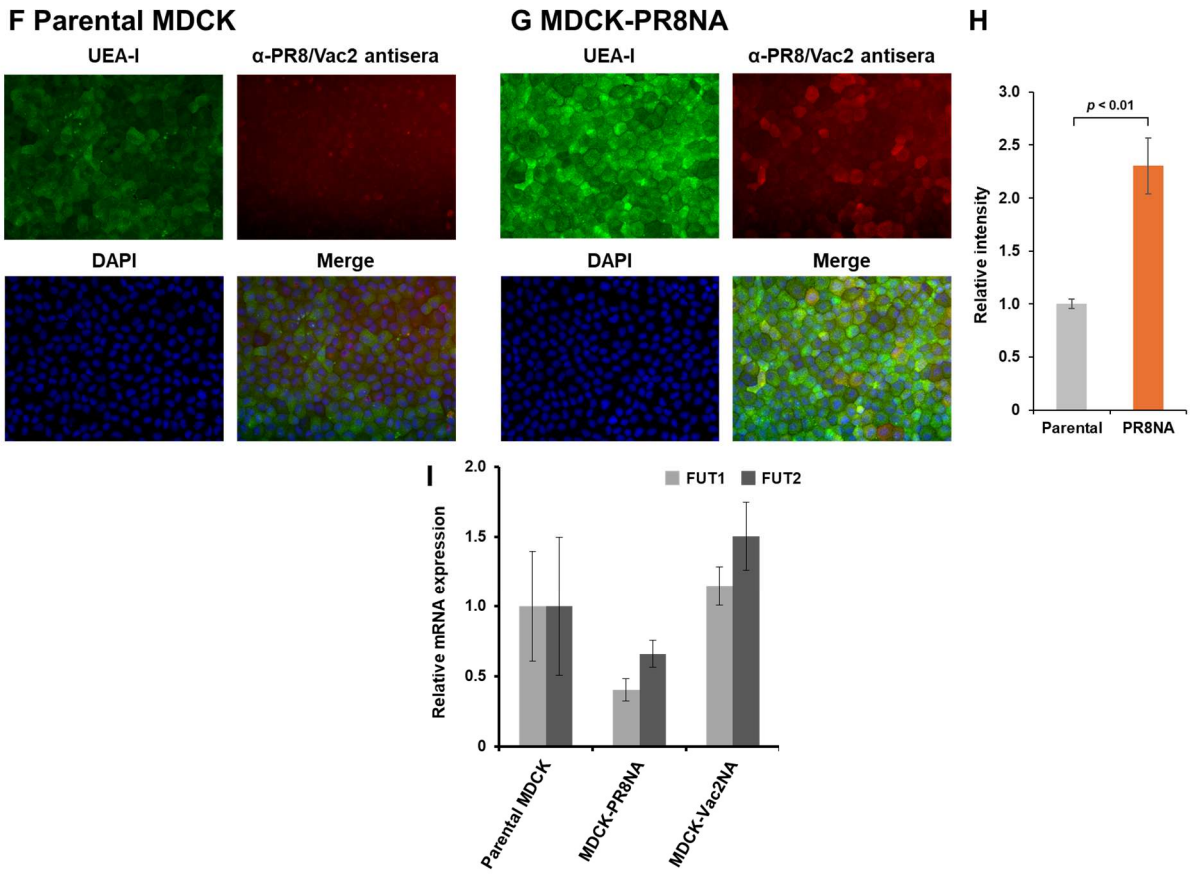

Figure 39 (*cont*)**. Glycome alterations in MDCK cells stably expressed NA protein of PR8 or Vac2 virus.** (F, G) The wild type and PR8 NA-expressing MDCK cells were stained with SNA (green) and immunostained with a mixture of PR8 and Vac2 chicken antisera (red) and counterstained with DAPI (blue). (H) Fluorescent intensities derived from SNA in an average of three fields of view were compared between mock- and PR8-infected cells. The statistical analysis was performed with Student's t-test. (I) mRNA expression levels of FUT1 and FUT2 genes in the NA-expressing cells were quantified via RT-qPCR. The relative mRNA levels of FUT1 and FUT2 genes were normalized based on the expression level of GAPDH gene as a house keeping gene and were compared between wild type and PR8 NA-expressing cells. The data are presented as mean expression level of biological triplicates ±SD.

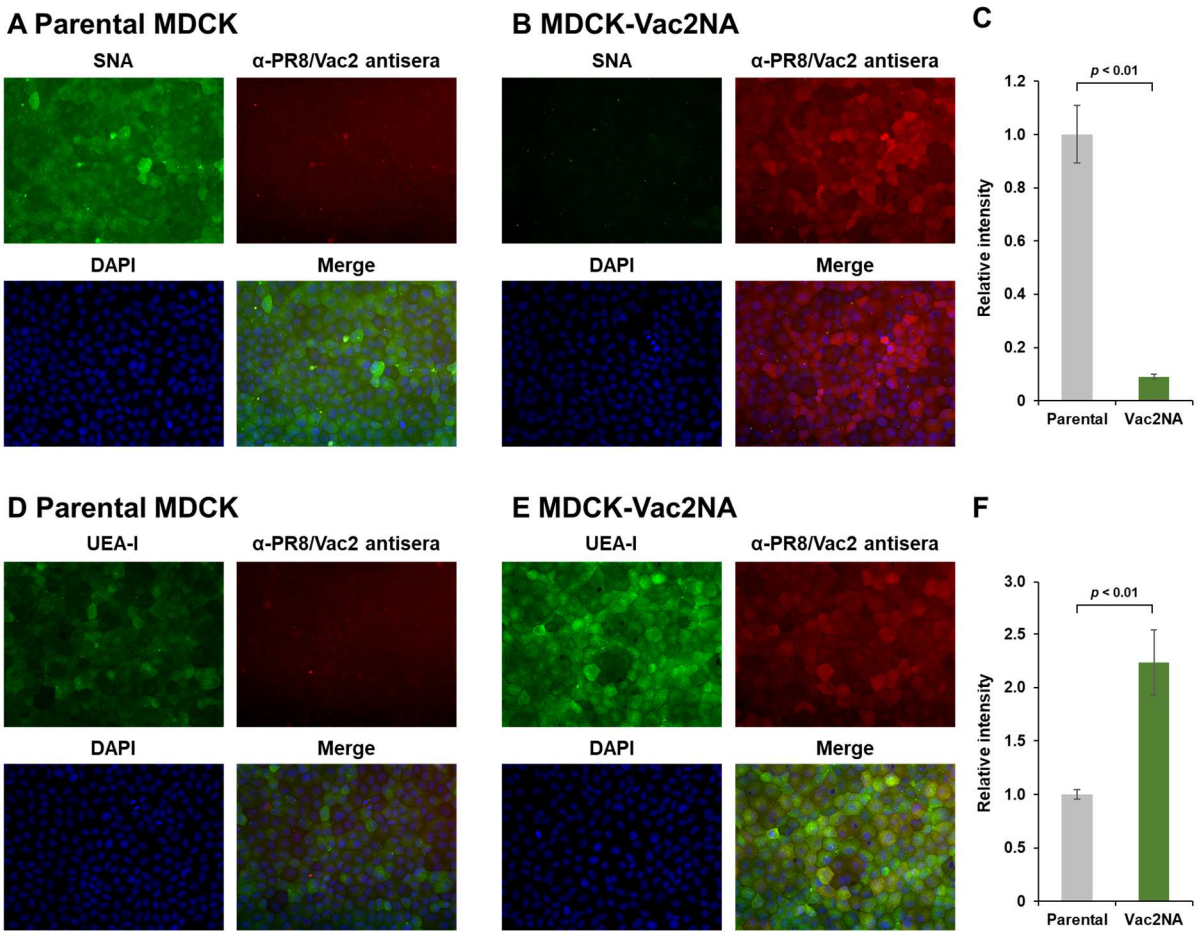

Figure 40. Desialylation and α1-2 fucosylation in MDCK cells stably expressed NA protein of Vac2 virus. (A, B) The wild type and Vac2 NA-expressing MDCK cells were stained with SNA (green) and immunostained with a mixture of PR8 and Vac2 chicken antisera (red) and counterstained with DAPI (blue). (C) Fluorescent intensities derived from SNA in an average of three fields of view were compared between mock- and Vac2-infected cells. The statistical analysis was performed with Student's t-test. (D, E) The wild type and Vac2 NA-expressing MDCK cells were stained with UEA-I (green) and immunostained with a mixture of PR8 and Vac2 chicken antisera (red) and counterstained with DAPI (blue). (F) Fluorescent intensities derived from UEA-I in an average of three fields of view were compared between mock- and Vac2-infected cells. The statistical analysis was performed with Student's t-test.

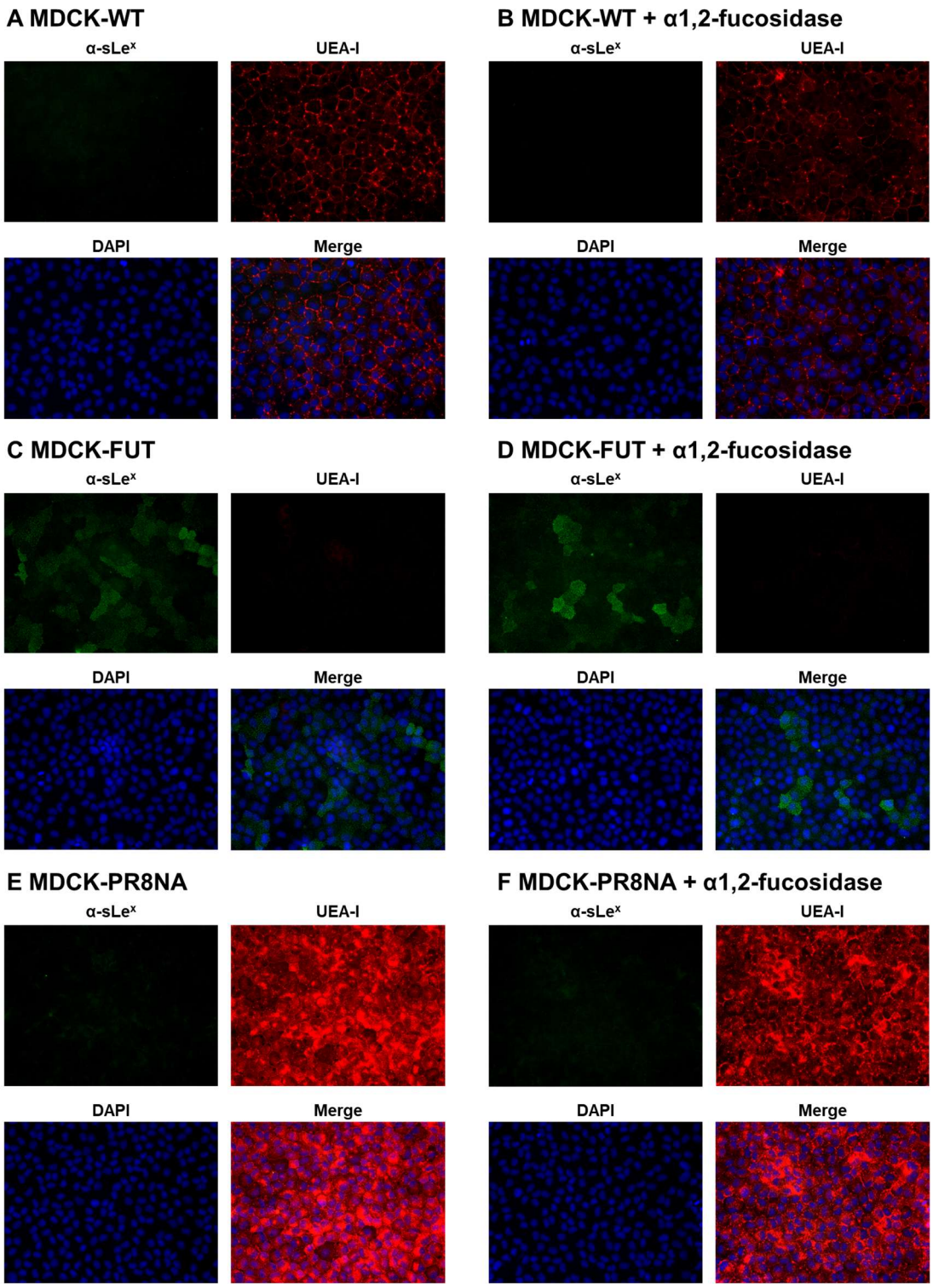

Figure 41. Expression of NA protein induced α1-2 fucosylation without upregulation of sialyl Lewis X antigen. (A, B) Wild-type MDCK cells were co-stained with an anti-sialyl Lewis X monoclonal antibody (green) and UEA-I (red) with (B) or without (A) pretreatment with α1-2 fucosidase. MDCK cells overexpressing a chicken fucosyltransferase (cFUT3/5/6) gene (C, D) and NA-expressing MDCK cells (E, F) were also costained with the anti-sialyl Lewis X antibody (green) and UEA-I (red) with or without pretreatment with α1-2 fucosidase and also counterstained with DAPI (blue).

recapping with α1-2 fucose, which were observed in IAV-infected MDCK cells.

The mRNA expression of α1-2 fucosyltransferase genes in the NA-expressing MDCK cells were also evaluated by RT-qPCR to exclude the possibility of the increased expression of these genes (Figure 39I). The results demonstrated that endogenous expression levels of FUT1 and FUT2 in MDCK-PR8NA cells were relatively lower, and *vice versa,* those in MDCK-Vac2NA cells were slightly higher, compared to parental MDCK cells with no significant difference. Accordingly, α1-2 fucosylation observed on the NA-expressing MDCK cells were not regulated by FUT1 or FUT2 gene.

Catalytic activity of NA is necessary for desialylation and glycan recapping with α1-2 fucose

NA expression in MDCK cells led to desialylation and glycan recapping, suggesting that the catalytic activity of NA is required for this glycan alteration. To test this hypothesis, catalytic-dead mutants of PR8 NA (E119V, D151G, and I222L) were expressed in MDCK cells [124–126], and the resulting bulk G418-resistant populations were subjected to lectin staining. As biologically independent NA-expressing cells showed variability in the signal intensities of SNA and UEA-I, the mean of three biological replicates was analyzed. Cells expressing wild-type PR8 NA (WT) exhibited lower SNA signal intensities than parental MDCK cells but higher intensities than the cloned MDCK-PR8NA cells (Figure 42A, B). Both E119V and D151G mutant-expressing cells retained the SNA signal intensities, while the effect of the I222L mutation was limited (Figure 42B, C). In contrast, UEA-I signal intensities in mutant NA-expressing cells were lower than those in WT-expressing cells (Figure 42D). Specifically, E119V- and D151G-expressing cells exhibited much lower UEA-I signal intensities than I222L-expressing cells (Figure 42E, F). Additionally, UEA-I signal and NA (detected by antiserum) merged in WT- and I222L-expressing cells, but not in E119V- or D151G-expressing cells (Figure 42D), suggesting that the impairment of NA function by the E119V and D151G mutations contributed to the lower UEA-I signals in MDCK cells. Taken together, these results demonstrate that the catalytic activity of NA is required for desialylation and glycan recapping with α1-2 fucose in MDCK cells.

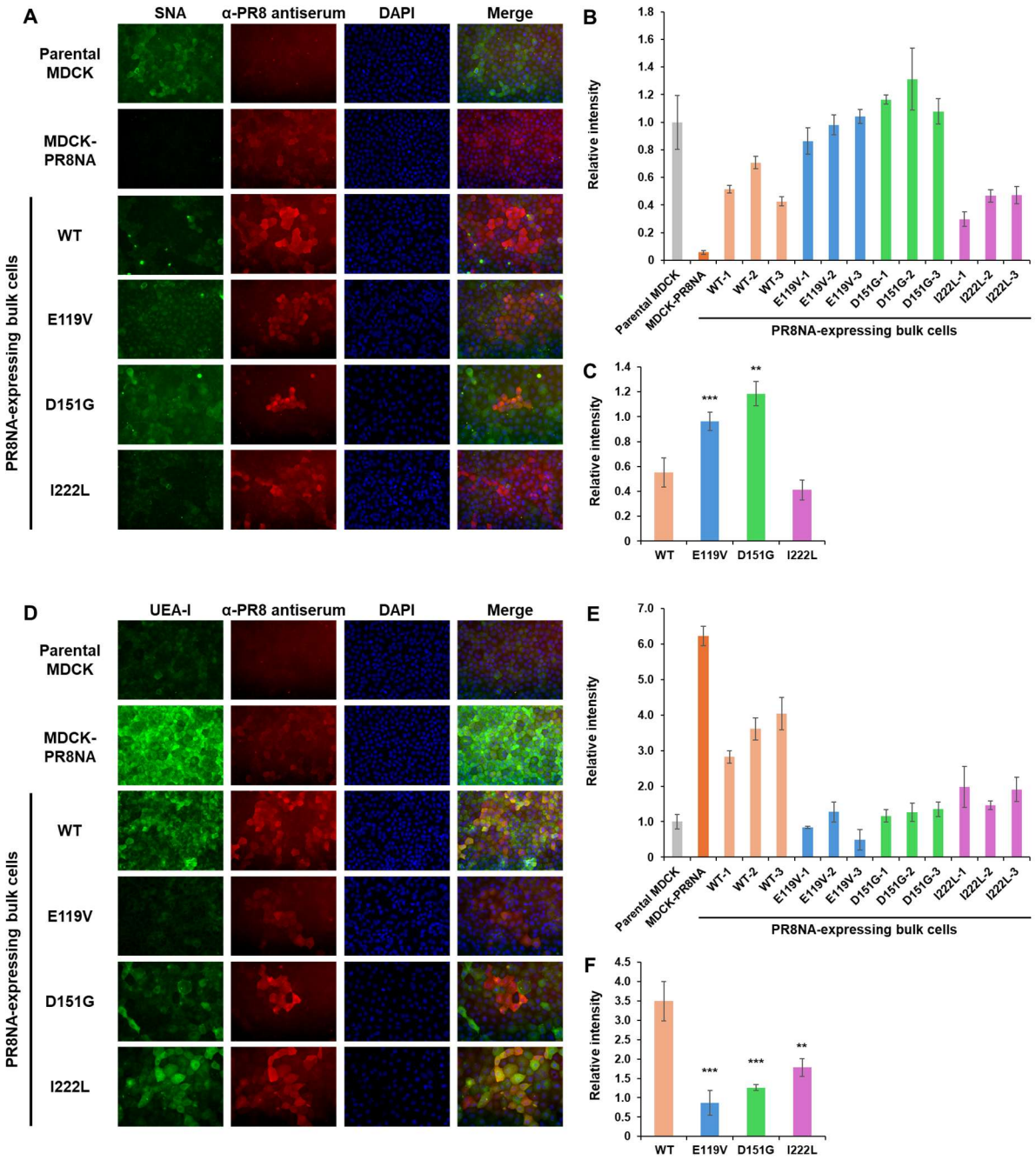

Figure 42. Glycan alterations in MDCK cells expressing catalytic-dead NA. MDCK cells were transfected with wild-type (WT) or catalytic-dead mutants (E119V, D151G, and I222L) of PR8 NA, and G418-resistant populations were analyzed. (A) Representative images of SNA staining. (B) Fluorescence intensities of SNA were quantified from the average of three fields of view per sample across three biologically independent replicates. (C) Mean SNA signal intensities from three biological replicates were compared between WT and each mutant. Statistical analysis was performed using one-way ANOVA followed by Dunnett's post hoc test (*: $p < 0.05$, **: $p < 0.01$, ***: $p < 0.001$). (D) Representative images of UEA-I staining. (E) Fluorescence intensities of UEA-I were quantified from the average of three fields of view per sample across three biologically independent replicates. (F) Mean UEA-I signal intensities from three biological replicates were compared between WT and each mutant. Statistical analysis was performed using one-way ANOVA followed by Dunnett's post hoc test (*: $p < 0.05$, **: $p < 0.01$, ***: $p < 0.001$).

Intracellular NA function is crucial for glycan recapping with α1-2 fucose in the IAV-infected cells

Since α1-2 fucosyltransferases are localized at the Golgi apparatus in host cells [117], glycan recapping with α1-2 fucose observed in NA-expressing and IAV-infected cells suggests that NA liberates sialic acids from non-reducing terminus of glycans and serves LacNAc as an acceptor for α1-2 fucosyltransferases intracellularly. Thus, the focus of this study was to determine whether intracellular or extracellular functions of NA predominantly contribute to glycome alterations in cells. To inhibit extracellular NA activity in MDCK-PR8NA and -Vac2NA cells, cells were cultured in the presence of either of the three NA inhibitors, laninamivir, laninamivir octanoate, or oseltamivir carboxylate. Then, the reactivities of SNA and UEA-I were evaluated by lectin staining. The tests were performed with 200 μM of NA inhibitors, which inhibit growth of PR8 virus in MDCK cells (Figure 43A), and no influence of NA inhibitors on an increase of sialic acid or a decrease of α1-2 fucose was confirmed in advance (Figure 43B–K). When the NA-expressing MDCK cells were treated with NA inhibitors, signal intensity of SNA was higher compared to the cells incubated without the inhibitor (Figures 44A–E and 45A–E). The signal intensity of UEA-I remained high in laninamivir and oseltamivir carboxylate-treated cells, whereas the intensity decreased in laninamivir octanoate-treated cells (Figures 44 F–J and 45 F–J). Since laninamivir octanoate could be taken up by cells and transformed into the activate form in the cells [136], a decrease in the UEA-I signal intensity could be reflected by inhibition of NA function, intracellularly. These results indicated that inhibition of extracellular NA activity did not influence the glycan recapping by α1-2 fucose in NA-expressing MDCK cells, while inhibition of intracellular NA activity led to a decrease of α1-2 fucose on the cells.

To assess extracellular and intracellular NA functions in IAV-infected cells, MDCK cells were inoculated with an extremely high titer of PR8 (MOI = 100) premixed with BXA and stained with lectins. The signal intensity of SNA in the PR8-infected cells with or without BXA treatment decreased at 3 hpi (Figure 46A–D). In particular, the cells cultured without BXA treatment showed a remarkable decrease in the SNA signal intensity at 6 and 9 hpi. On the other hand, an increase in UEA-I signal intensity was observed in the virus-infected cells cultured without BXA from 6 hpi, while the UEA-I signal remained low in the BXA-treated cells as well as the non-infected cells (Figure

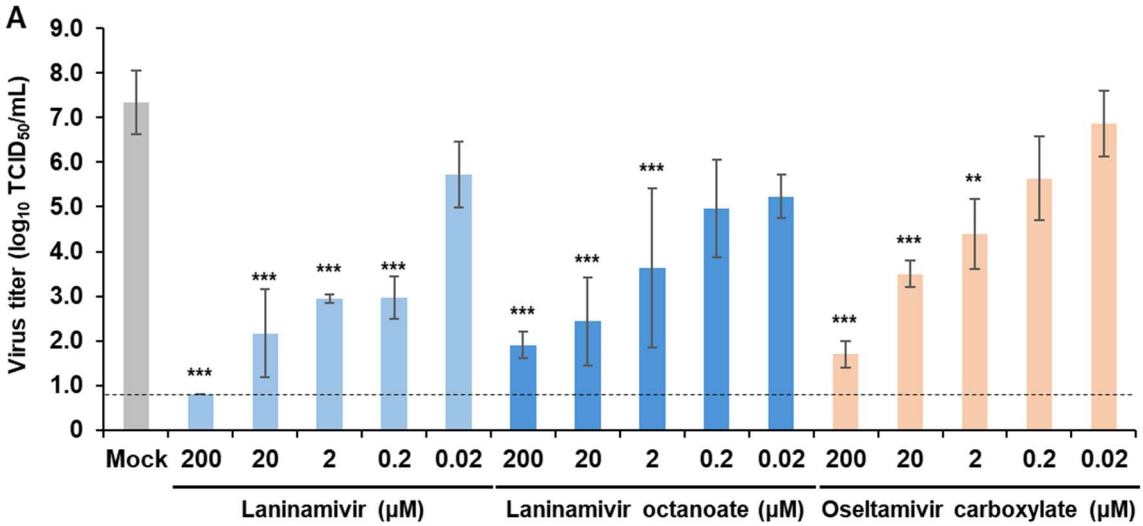

Figure 43. Treatment with NA inhibitors did not induce glycan alterations in MDCK cells. (A) Antiviral effect of NA inhibitors (laninamivir, laninamivir octanoate, oseltamivir carboxylate) was assessed by culturing the PR8-infected cells in the presence of several concentrations of the inhibitors. The dotted line indicates the threshold for virus titration (<0.8 log_{10} $TCID_{50}$/mL). To compare the viral titers between mock- and NA inhibitor-treated groups, statistical analysis was performed using the one-way ANOVA with Dunnett's post hoc test (*: $p < 0.05$, **: $p < 0.01$, ***: $p < 0.001$). Virus titers below the detection limit were considered as 0.8 log_{10} $TCID_{50}$/mL for statistical analysis.

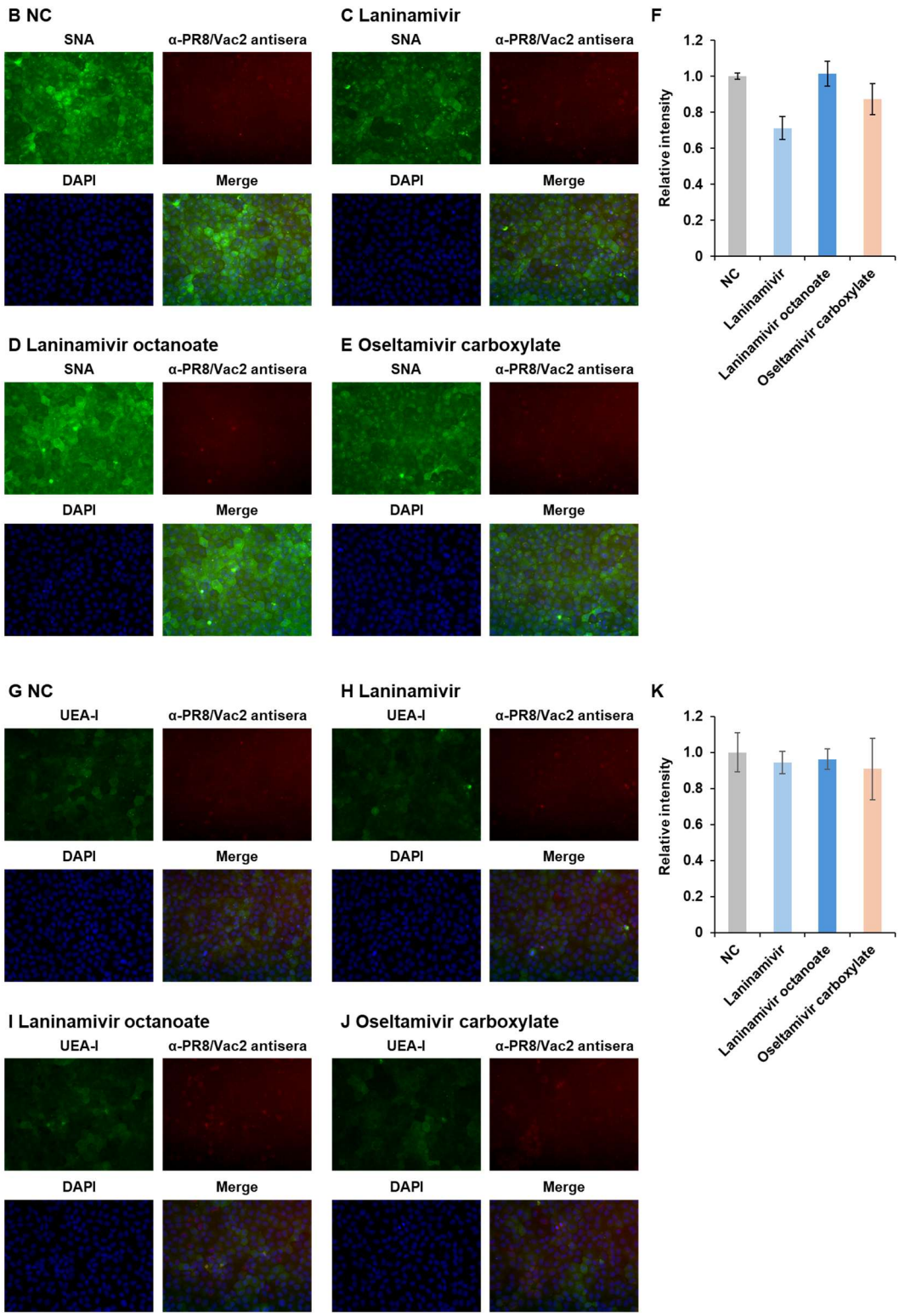

Figure 43 (*cont*)**. Treatment with NA inhibitors did not induce glycan alterations in MDCK cells.** (B–E) MDCK cells treated with NA inhibitor were stained with SNA. (G–J) MDCK cells treated with NA inhibitor were stained with UEA-I. Fluorescent intensities derived from SNA (F) and UEA-I (K) in an average of three fields of view were compared to non-treated control (NC). The statistical analysis was performed using the one-way ANOVA with Dunnett's post hoc test (*: $p < 0.05$, **: $p < 0.01$, ***: $p < 0.001$).

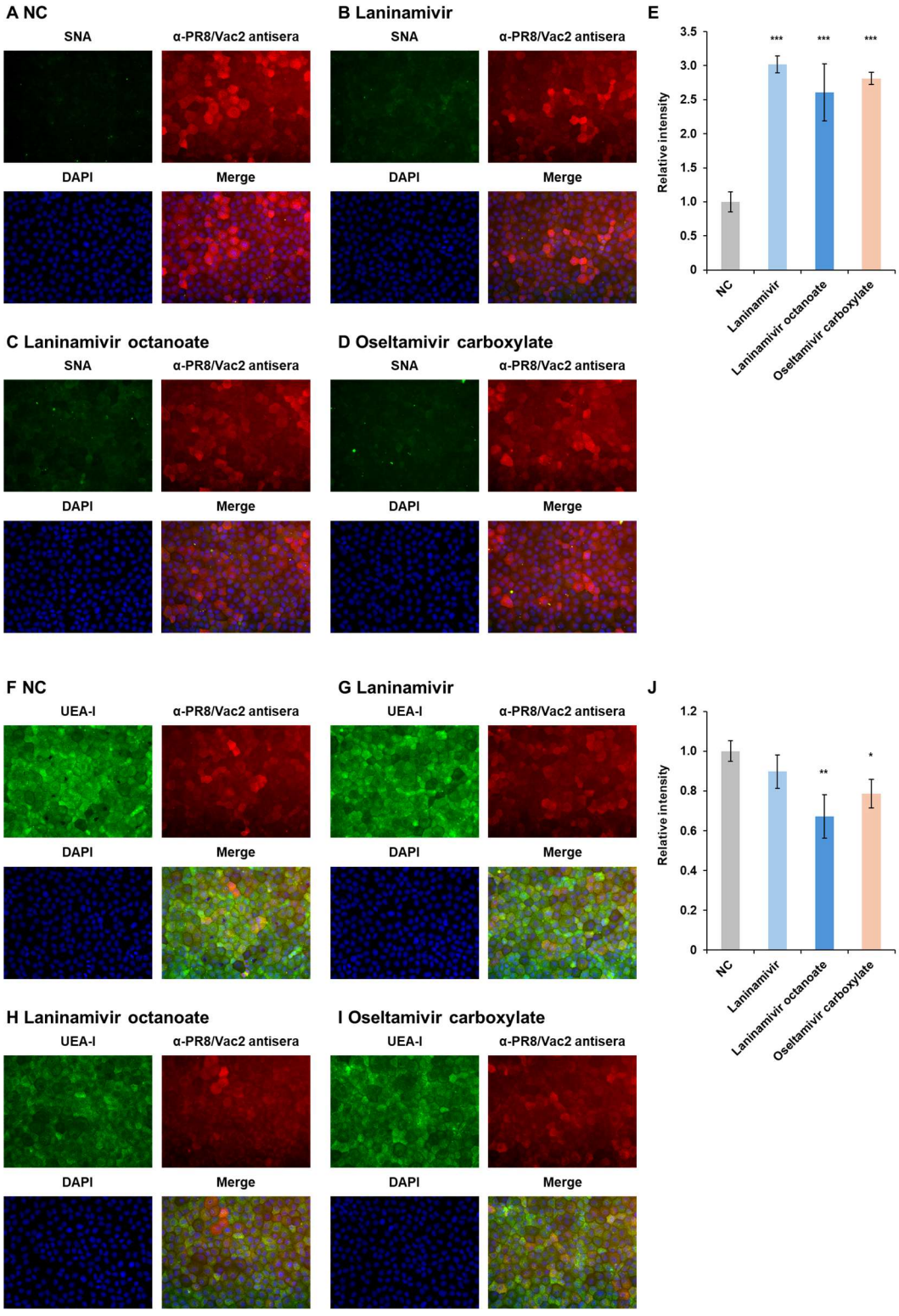

Figure 44. Glycan alterations induced by treatment with NA inhibitors in MDCK-PR8NA cells. (A–D) MDCK-PR8NA cells treated with NA inhibitor were stained with SNA. (F–I) MDCK-PR8NA cells treated with NA inhibitor were stained with UEA-I. Fluorescent intensities derived from SNA (E) and UEA-I (J) in an average of three fields of view were compared to non-treated control (NC). The statistical analysis was performed using the one-way ANOVA with Dunnett's post hoc test (*: $p < 0.05$, **: $p < 0.01$, ***: $p < 0.001$).

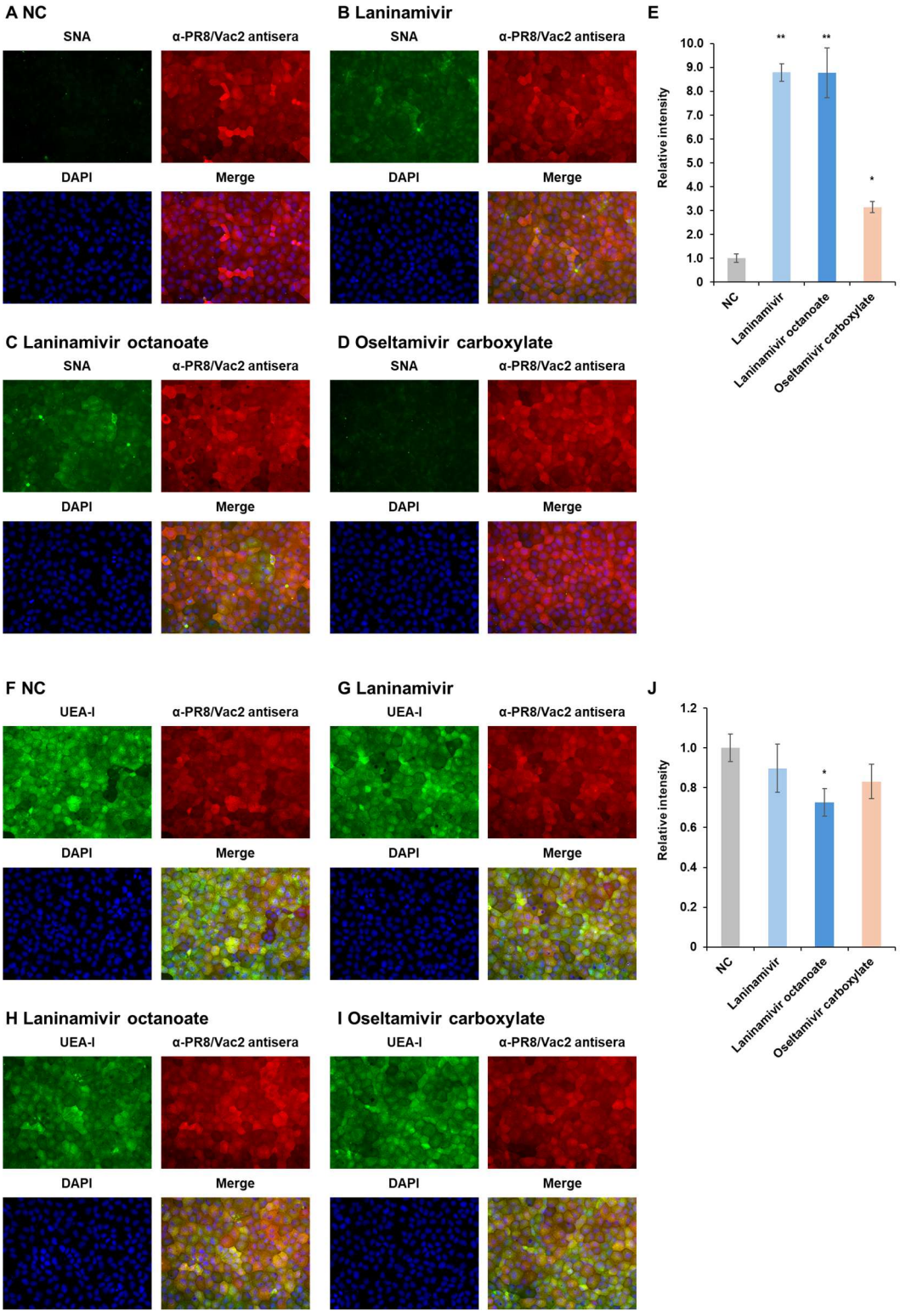

Figure 45. Glycan alterations induced by treatment with NA inhibitors in MDCK-Vac2NA cells. (A–D) MDCK-Vac2NA cells treated with NA inhibitor were stained with SNA. (F–I) MDCK-Vac2NA cells treated with NA inhibitor were stained with UEA-I. Fluorescent intensities derived from SNA (E) and UEA-I (J) in an average of three fields of view were compared to non-treated control (NC). The statistical analysis was performed using the one-way ANOVA with Dunnett's post hoc test (*: $p < 0.05$, **: $p < 0.01$, ***: $p < 0.001$).

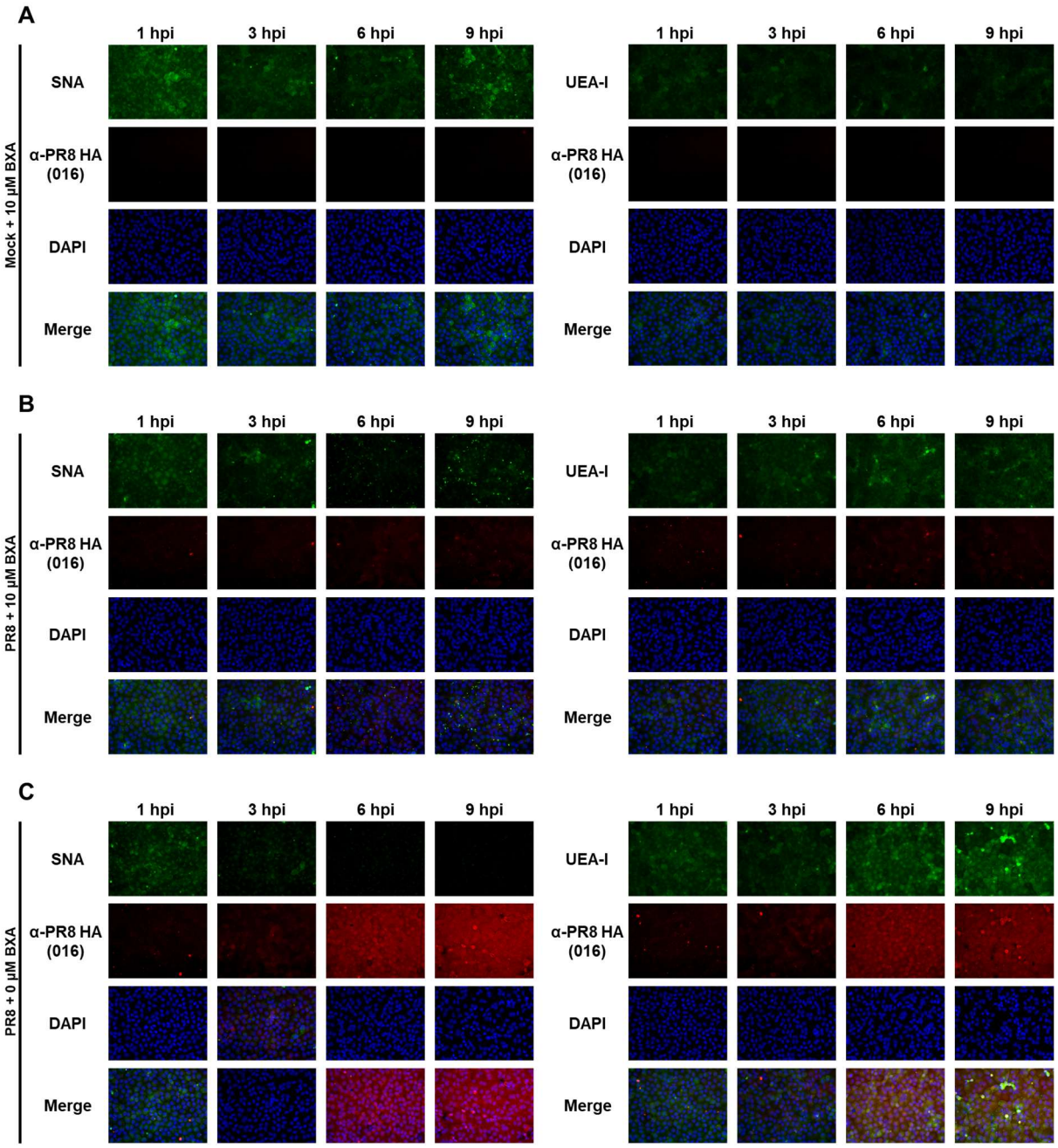

Figure 46. BXA treatment in the PR8-infected cells did not influence on desialylation of glycans while inhibited representation of α1-2 fucose. MDCK cells were infected with an extremely high titer of PR8 (MOI = 100) and cultured in the presence (B) or absence (C) of 10 μM BXA. Mock-infected MDCK cells were also treated with10 μM BXA as a control. The cells were fixed with 4% paraformaldehyde at multiple time points of 1, 3, 6 or 9 hpi. The cells were then lectin stained with SNA or UEA-I (green) together with immunostaining with an anti-PR8 HA monoclonal antibody (red) and also counterstained with DAPI (blue).

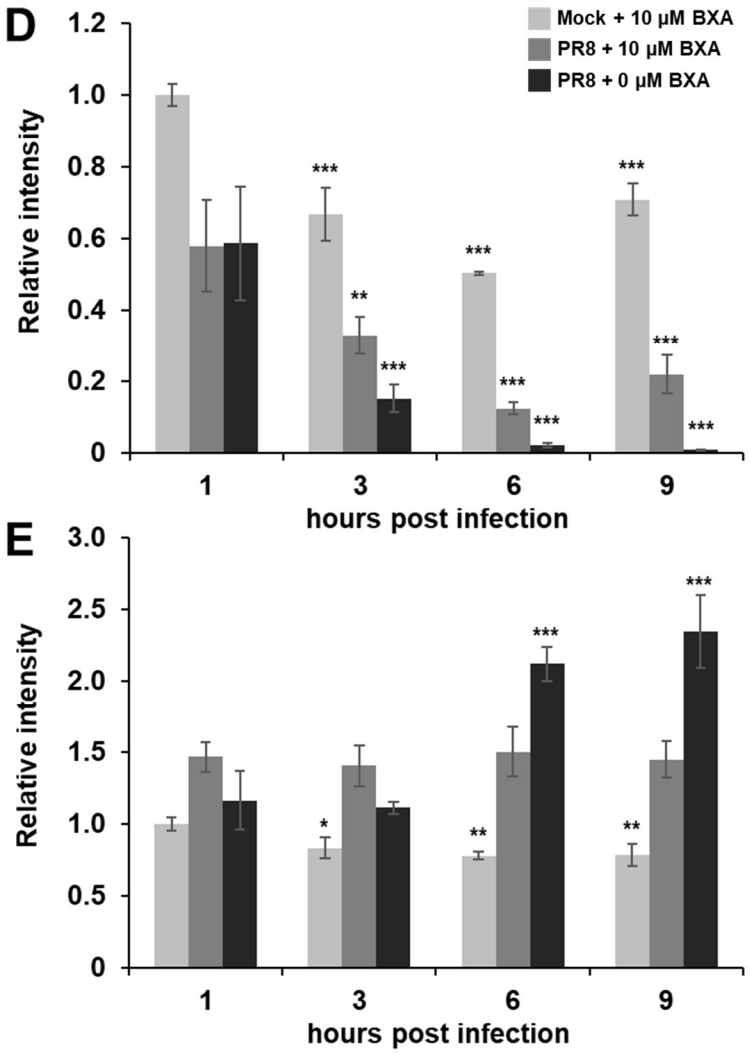

Figure 46 (*cont*)**. BXA treatment in the PR8-infected cells did not influence on desialylation of glycans while inhibited representation of α1-2 fucose.** (D) Time-dependent fluorescent intensities derived from SNA in an average of three fields of view were compared. The data were represented by calculating relative intensities compared to 1 hpi of mock-infected group. The statistical analysis was performed by one-way ANOVA with Dunnett's post hoc test in comparison to 1 hpi as a control within a group (*: $p < 0.05$, **: $p < 0.01$, ***: $p < 0.001$). (E) Time-dependent fluorescent intensities derived from UEA-I in an average of three fields of view were compared. The data were represented by calculating relative intensities compared to 1 hpi of mock-infected group. The statistical analysis was performed by one-way ANOVA with Dunnett's post hoc test in comparison to 1 hpi as a control within a group (*: $p < 0.05$, **: $p < 0.01$, ***: $p < 0.001$).

46C–E). To further assess the influence of extracellular NA activity on glycan alterations, MDCK cells were cultured with recombinant neuraminidase from *Vibrio cholerae* (NAVC) and subjected to lectin staining. The treatment with bacterial neuraminidase markedly decreased the signal intensity of SNA, whereas no increase in UEA-I signal was observed (Figure 47). Consistent with the observations using NA-expressing cells, these results demonstrate that intracellular NA function is necessary for glycan recapping with α1-2 fucose. Conversely, NA on viral particles hydrolyzes sialylated glycans; however, extracellular NA functions cannot induce glycan recapping in IAV-infected cells.

NA function contributes to superinfection exclusion of IAVs

Since sialic acid-containing glycans serve as initial receptors for IAVs on host cells, desialylation of IAV-infected cells by intracellular NA is likely to interfere with secondary IAV infection. To test this hypothesis, a superinfection experiment with IAVs was performed in MDCK cells at several time intervals between primary and secondary infections. MDCK cells infected with PR8 or Vac2-FLAG were inoculated with the other virus. After fixing the cells 8 h post primary IAV infection, PR8 HA and Vac2 NA proteins were detected by immunofluorescent staining. The proportion of Vac2 NA-positive cells per PR8-primarily infected cell decreased when Vac2 was inoculated at a 2 h or longer interval after PR8 infection, and Vac2 NA-positive cells were not detected when there was a 5 or 6 h-interval from primary PR8 infection to secondary Vac2 inoculation (Figure 48A). The time intervals required for the inhibition of 2 h and blocking superinfection for 5 h were similar, even when PR8 was inoculated into Vac2-primarily infected MDCK cells (Figure 48B). To validate desialylation and α1-2 fucosylation on IAV-infected cells, PR8 or Vac2-FLAG virus was inoculated into MDCK cells at the same experimental condition of MOI with superinfection assay and the glycan profiles were monitored until 6 hpi by lectin staining and blotting (Figures 49–51). SNA signal intensities in IAV-infected cells decreased from 3 hpi and UEA-I signal intensities increased from 5 hpi (Figure 49C, D and 50C, D). In addition, the NA expression in Vac2-FLAG-infected cells was confirmed slightly at 4 hpi and obviously at 5 hpi by western blotting, together with increase in band intensities by lectin blotting with UEA-I (Figure 51). Taking account of the impact of desialyoltion and α1-2 fucosylation on IAV-infected MDCK cells after 5 hpi (Figures 49–52), the complete superinfection exclusions by 5 h-

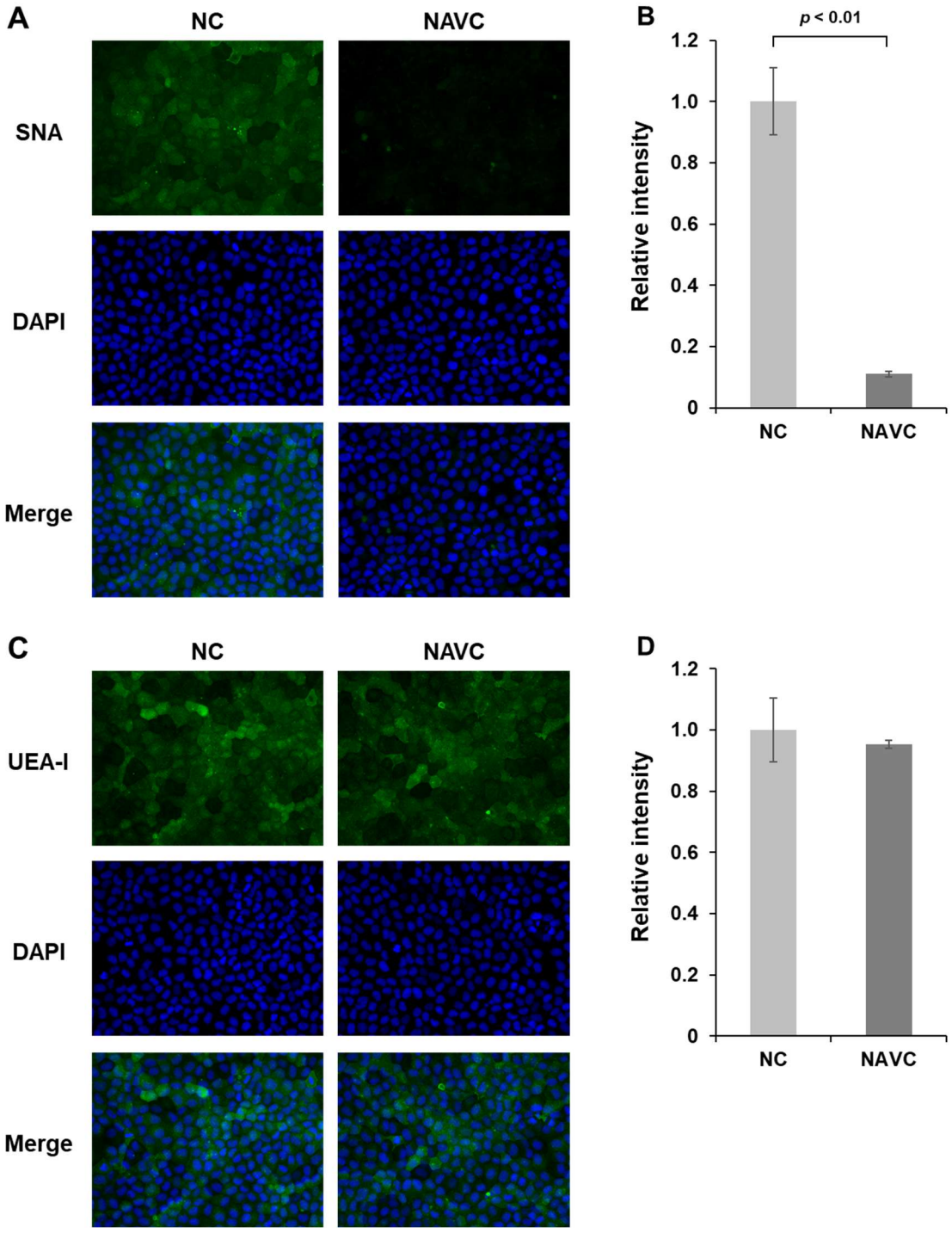

Figure 47. Bacterial neuraminidase treatment in MDCK cells diminished sialic acids while it did not upregulate representation of α1-2 fucose. (A, C) MDCK cells were treated with recombinant neuraminidase derived from *Vibrio cholerae* (NAVC). The cells were stained with SNA and UEA-I (green) and counterstained with DAPI (blue). (B, D) The signal intensities of each lectin in the neuraminidase-treated cells were compared with those in the non-treated cells (NC). The statistical analysis was performed with Student's t-test.

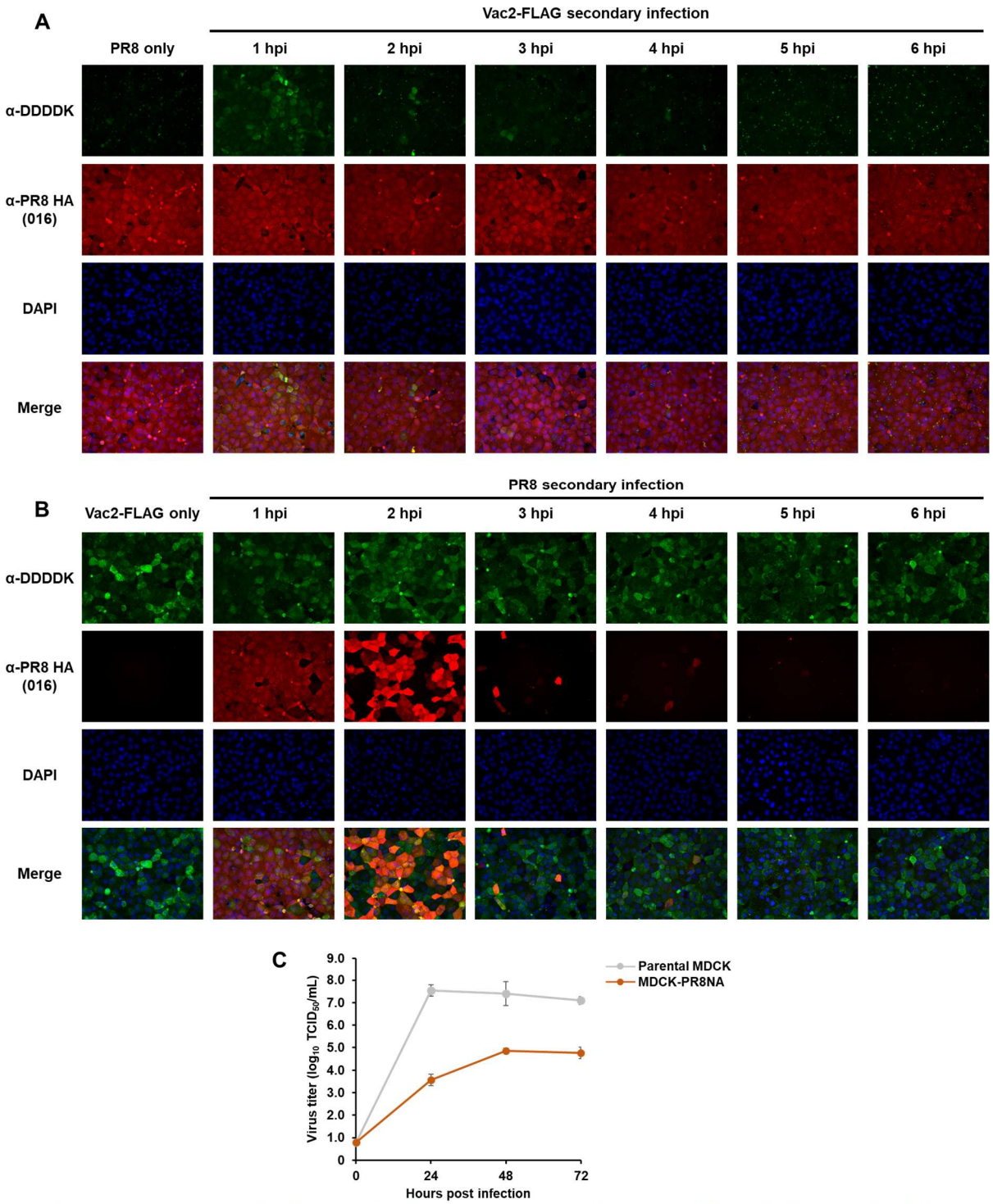

Figure 48. Superinfection exclusion was observed in *MDCK* cells infected with an IAV. (A) MDCK cells primarily infected with PR8 at MOI = 1 were secondarily inoculated with Vac2-FLAG at MOI = 1 at different time intervals. The cells were fixed in 4% paraformaldehyde at 8 hpi from the primary infection. Viral protein expression was detected by an anti-PR8 HA monoclonal antibody (red) or an anti-DDDDK monoclonal antibody for Vac2 NA (green) via immunofluorescent staining. (B) MDCK cells primarily infected with Vac2-FLAG at MOI = 1 were secondarily inoculated with PR8 at MOI = 1 at different time intervals. (C) Virus growth kinetics of PR8 in MDCK-PR8NA cells were compared with those in MDCK-WT cells. The culture supernatants were collected and the infectious titer in the samples were calculated using MDCK cells.

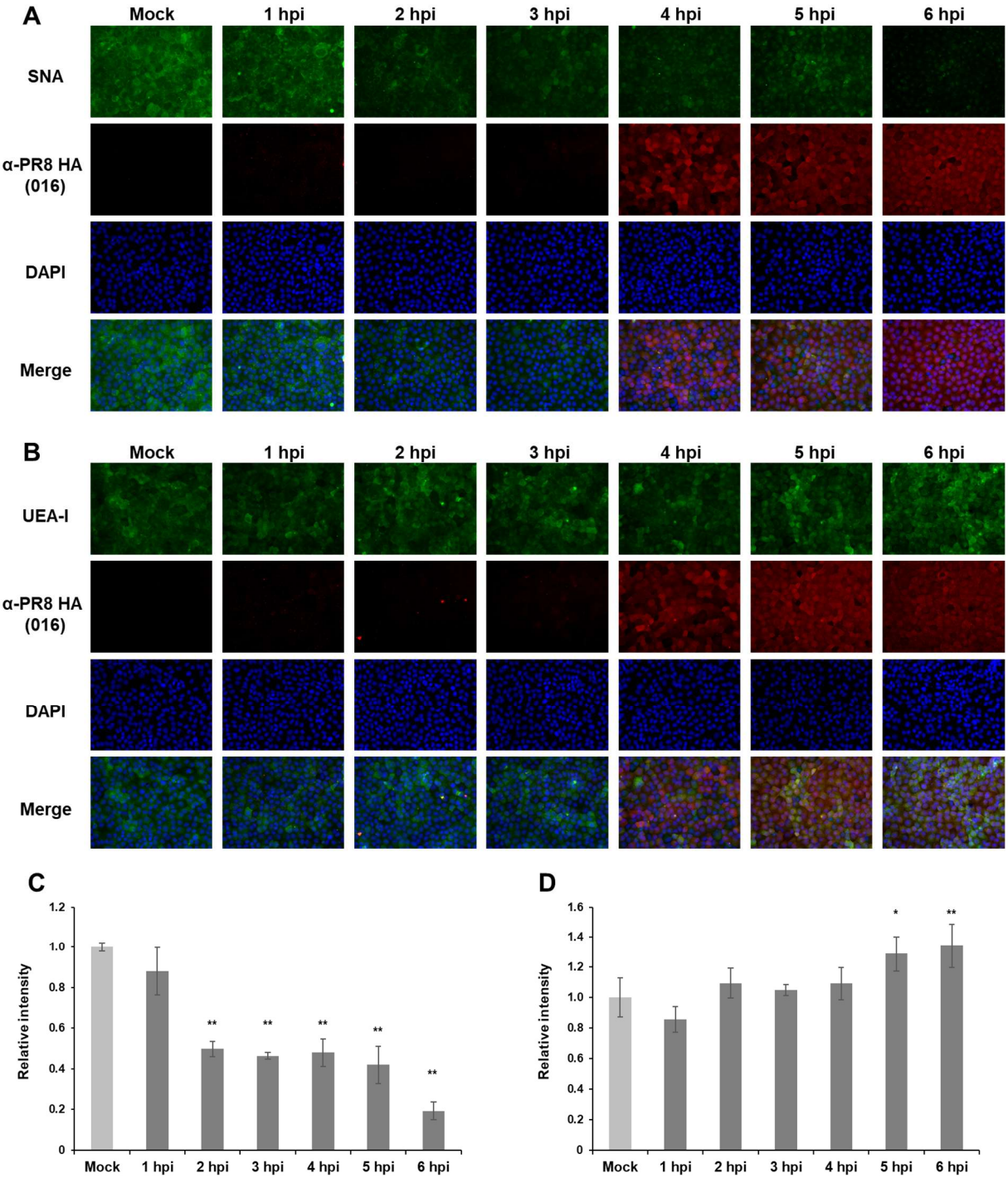

Figure 49. Glycan profile changes observed on the surface of MDCK cells during PR8 infection. MDCK cells infected with PR8 at an MOI of 1 were fixed in 4% paraformaldehyde for 3–6 hpi. The cells were then stained with either SNA (A) or UEA-I (B) for glycan profiling (green), and HA protein expression was detected using an anti-PR8 HA monoclonal antibody (red) and also counterstained with DAPI (blue). (C, D) The signal intensities of the lectins were statistically analyzed by one-way ANOVA with Dunnett's post hoc test (*: $p < 0.05$, **: $p < 0.01$, ***: $p < 0.001$).

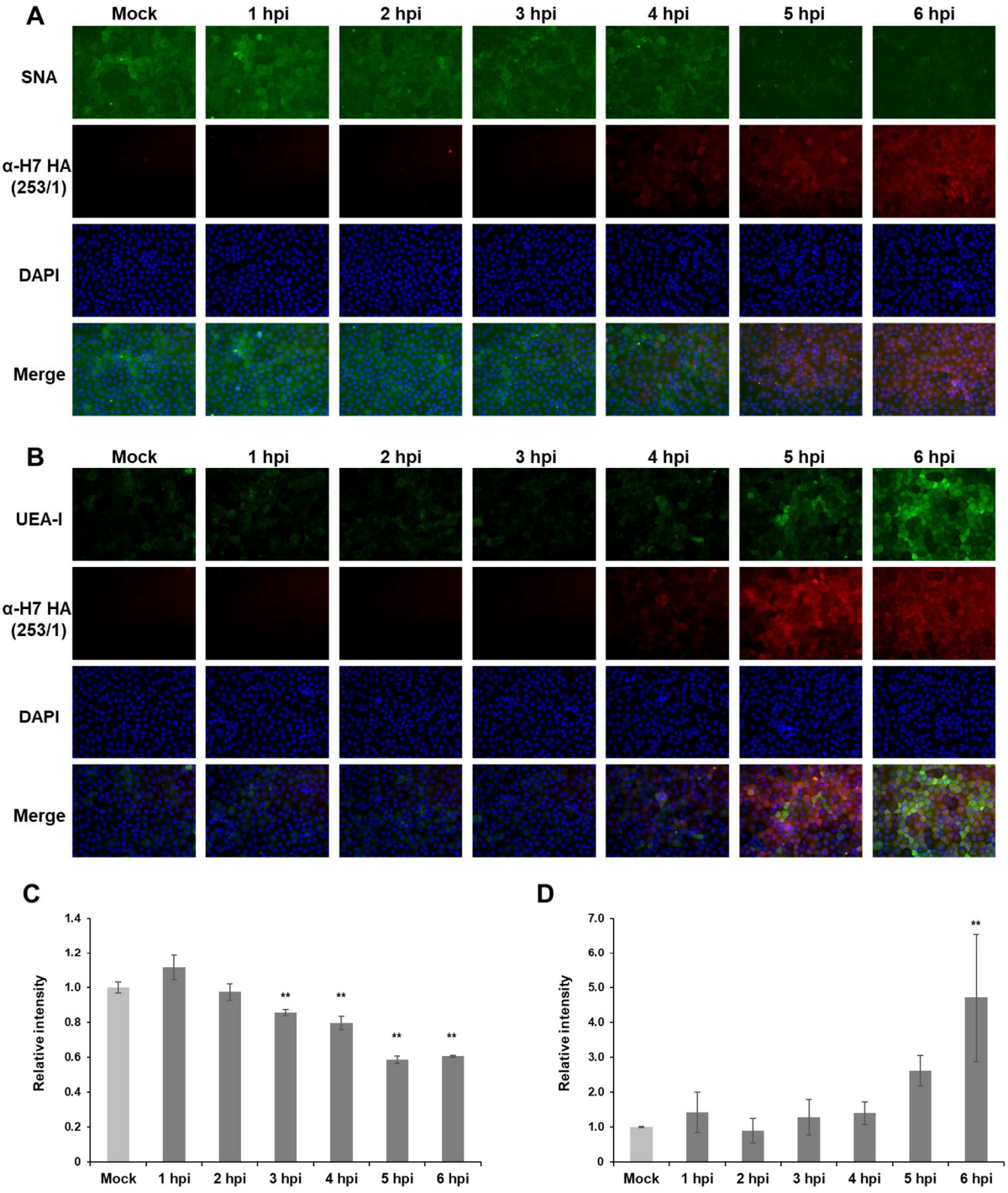

Figure 50. Glycan profile changes observed on the surface of MDCK cells during Vac2 infection. MDCK cells infected with Vac2-FLAG at an MOI of 1 were fixed in 4% paraformaldehyde for 3–6 hpi. The cells were stained with either SNA (A) or UEA-I (B) for glycan profiling (green), and the expression of NA proteins was detected using an anti-DDDDK-tag monoclonal antibody (red). and also counterstained with DAPI (blue). (C, D) The signal intensities of the lectins were statistically analyzed by one-way ANOVA with Dunnett's post hoc test (*: $p < 0.05$, **: $p < 0.01$, ***: $p < 0.001$).

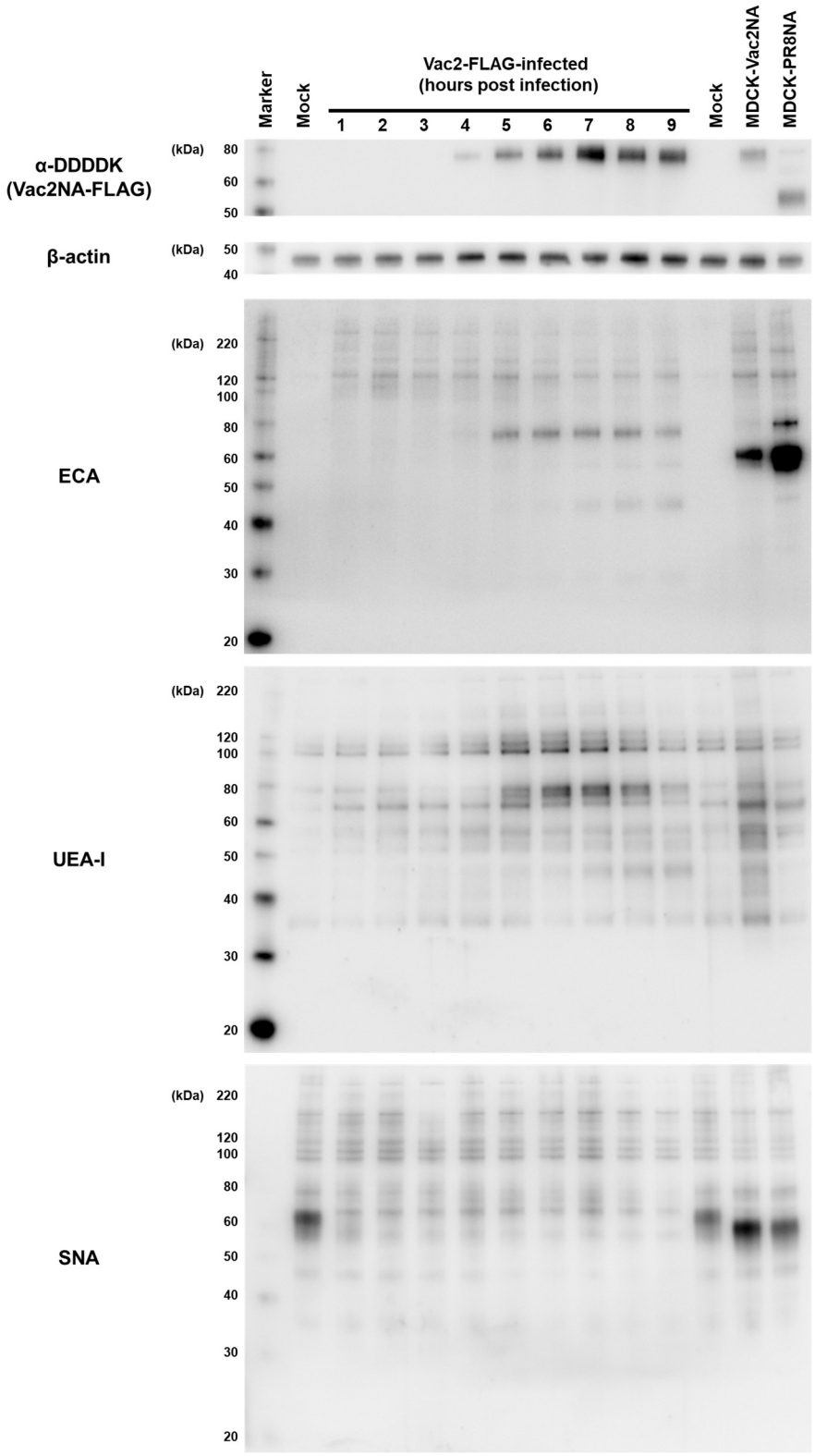

Figure 51. Time-dependent NA protein expression and glycan alterations in MDCK cells infected with Vac2-FLAG. Whole lysates of Vac2-FLAG-infected MDCK cells were assessed by western blotting and lectin blotting. NA protein and β-actin expressed in MDCK cells were detected with anti-DDDDK and β-actin antibodies, respectively.

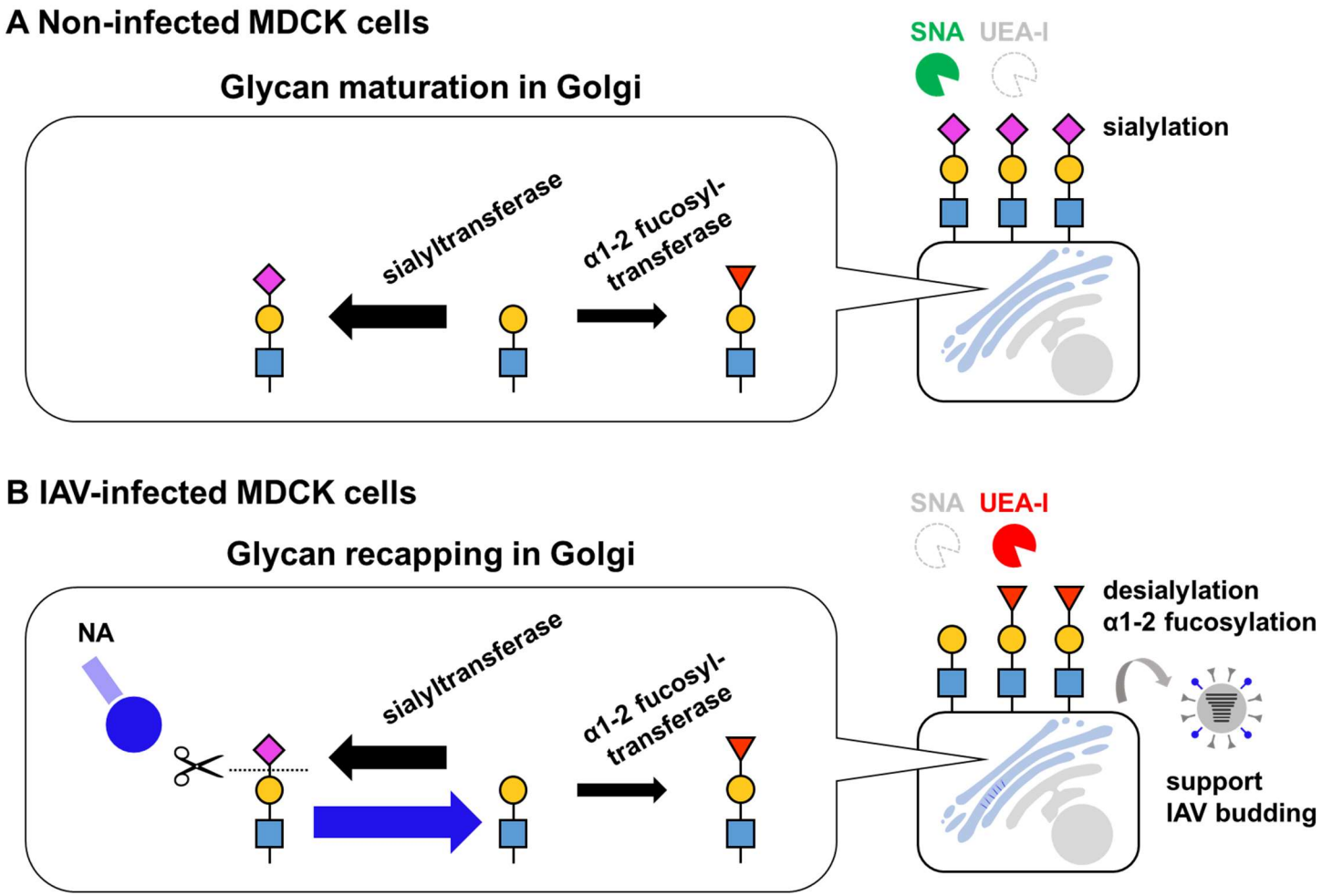

Figure 52. Glycome alterations observed in IAV-infected MDCK cells. (A) Sialylation of glycans is induced by sialyltransferases in the Golgi apparatus of non-infected MDCK cells and terminal sialic acids displayed on the cell surface can be recognized by SNA. (B) Since NA obtains its function intracellularly during IAV infection, desialylation in the Golgi apparatus by the intracellular NA function induces glycan recapping with α1-2 fucose. The intracellular NA function blocks re-sialylation, contributing to efficient IAV budding.

interval between two IAV infections were likely due to the lack of sialic acids on the cell surface.

The ability of PR8 to replicate MDCK-PR8NA cells, which established by cell cloning and express similar amount of NA with IAV-infected cells at 5–6 hpi (Figure 51), was also assessed. MDCK-PR8NA cells infected with PR8 did not exhibit any cytopathic effects for up to 72 hpi. In parallel, the viral titer in the supernatant was 10^4- fold lower than that in parental MDCK cells at 24 hpi and remained lower until 72 hpi (Figure 48C). These results suggested that NA expression in host cells restricted IAV infection.

Discussion

The present study found that virus-infected cells displayed α1-2 fucose-capping glycans instead of sialylated ones, in agreement with previous studies [113, 114, 116]. The global glycome alteration with desialylation and α1-2 fucosylation was also observed in NA-expressing MDCK cells without upregulation of FUT1 and FUT2 gene expressions. Since FUT1 and FUT2 were localized in Golgi apparatus [117], the mechanisms of glycan recapping by α1-2 fucose observed in IAV-infected cells can be explained by intracellular NA functions: viral NA has obtained its catalytic activity in the Golgi apparatus and it provides acceptors for α1-2 fucosyltransferases as a competitor of sialyltransferases. Moreover, the occupation of the glycan terminus by α1-2 fucose on both host and viral proteins, as a result of intracellular NA functions, limits the opportunities of re-sialylation. Hence, in addition to the conventional theory that NA functions cleave sialic acids on the cellular surface during viral release, intracellular NA functions provide an advantage for virus release by reducing sialoglycan traps. These findings highlighted a novel mechanism of NA action that supports viral budding in IAV-infected cells.

Glycan capping with sialic acids in host cells is regulated by β-galactoside α2,3-sialyltransferases (ST3Gals) and α2,6-sialyltransferases (ST6Gals) [137]. A previous study revealed that knocking out either ST3Gals or ST6Gals (KO) in MDCK cells increased the proportion of Siaα2,6Gal in ST3Gals-KO cells and Siaα2,3Gal in ST6Gals-KO cells [130]. In contrast, double KO cells, as well as sialic acid transporter (SLC35A1)-KO cells, showed a lack of sialylated glycans. Corresponding to the global desialylation, these cells reacted remarkably strongly to UEA-I, TJA-II, and EEL in the lectin microarray. Taken together with glycan recapping observed with IAV-infected cells in this study, these observations indicate that intracellular global desialylation is a trigger of glycan recapping with α1-2 fucose and/or α1-3 galactose in MDCK cells. Although α1-2 fucose on the IAV-infected cells is likely to be a consequence of intracellular NA activity, the unique glycan structure may have an unknown role in differentiating IAV-infected cells from non-infected ones. It is of interest that glycan recapping by α1-3 galactose was not detected in this study, dissimilar from previous studies [113, 114, 116]. The MDCK cells originating from canine possess the functional α1-3 galactosyltransferase gene required for synthesizing α1-3 galactose at non-reducing terminus of glycans [138]. Since

the monosaccharides used in the enzymatic glycosylation rely heavily on the sugar intake of cells [139], differences in culture conditions or components of the cell culture medium, such as fetal bovine serum, might influence the glycome of IAV-infected MDCK cells.

Lectin staining of A549 and Vero E6 cells revealed desialylation following IAV infection. Additionally, lectin staining of respiratory tissues from IAV-infected animals showed no binding of recombinant HA in their epithelia, especially in the cells that were positive for IAV antigens [121], suggesting the desialylation by the NA function following the IAV infection. In contrast, α1-2 fucosylation could not be detected in other cell lines except MDCK cells. Consistent with this observation, previous lectin microarray analysis demonstrated that virus particles propagated in A549 and Vero E6 cells strongly reacted with chitin-binding lectins, suggesting higher representations of poly-LacNAc structures rather than recapping with α1-2 fucose [114]. These observations suggested that intracellular NA functions can contribute to the desialylation in the IAV-infected cells, while the glycan recapping process heavily dependent on the glycan synthesis machinery in the host cells. The present study could assess the intracellular NA functions by detecting α1-2 fucose on the cellular surface, because the α1-2 fucosylation proceeds exclusively on glycan capping with sialic acid in the Golgi of host cells. However, differentiation of intracellular and extracellular NA functions by observing glycan structures on the IAV-infected cells is still challenging without the unique glycan structures exclusively present on the glycan terminus, including α1-2 fucose or α1-3 galactose. Accordingly, the present study could not prove the intracellular NA activity in other cell lines except MDCK cells.

In agreement with low PR8 replication in the NA-expressing cells in this study, the sialic acid transporter SLC35A1-knockout MDCK cells or sialyltransferase (all ST3Gal and ST6Gal series)-deficient MDCK cells exhibited significantly decreased IAV replication ability [130]. Since the intracellular NA activity in NA-expressing cells competes for sialyltransferases and induces a similar glycome as the SLC35A1-knockout or sialyltransferase-deficient cells, low IAV growth in these cells suggests that sialic acids on the cell surface are required for efficient IAV replication but are not necessary for infection. These observations correspond to the theory that functional receptors, such as epidermal growth factor (EGFR) or calcium channels (CaV1.2), are required for IAV entry into cells via clathrin-mediated endocytosis or micropinocytosis, although IAVs use

sialosides for cell attachment [140–142]. Indeed, the absence of sialic acids in cells reduced interactions between IAVs and EGFR, inducing fewer downstream signals and clathrin-mediated endocytosis [143]. Thus, global desialylation of IAV-infected cells could reduce the opportunities for secondary infecting viruses to access functional receptors, thereby potentially shaping the window for superinfection. The mechanism, in combination with liberation of sialic acid by extracellular NA expressed on the plasma membrane, facilitates the latter phase of superinfection exclusion. Moreover, the short window for superinfection in advancing budding may be beneficial for IAVs to facilitate a viral replication cycle using sufficient intracellular resources and produce progeny virions at the cellular level.

In conclusion, this study indicated that the NA protein obtains its catalytic function intracellularly and induces glycome alterations in infected MDCK cells. The intracellular NA function contributes to global desialylation and glycan recapping with α1-2 fucose, leading to efficient virus release from host cells. This demonstrated a novel theory that intracellular NA activity, in addition to extracellular activity, hydrolyzes sialosides and blocks interactions between progeny virus particles and the virus receptor to advance virus budding. Consequently, glycan recapping induced by the NA functions potentially restricts secondary IAV infection in cells, resulting in a strict window of superinfection. These findings provide insights into the evolutionary strategies of IAVs by maintaining a balance between successful replication and reassortment under limited superinfection opportunities controlled by the NA functions.

Brief summary

The NA of IAVs plays a role in the release of viruses from infected cells. NA on viral particles hydrolyzes sialylated glycans on the cell surface for viral budding. However, the maturation and intracellular functions of NA are poorly understood. To investigate how NA functions intracellularly, glycans displayed on IAV-infected MDCK cells were profiled by lectins and global glycome alterations, accompanied by exposed terminal galactose and glycan recapping with α1-2 fucose, were found in the virus-infected MDCK cells. Since α1-2 fucosyltransferases are localized in the Golgi, these unique structures suggest a potential NA function in the IAV-infected cells. Functional analyses using antivirals and NA-expressing cells indicate that intracellular NA function is necessary for the glycome alterations. Time-course analyses in IAV-infected cells revealed that global desialylation and α1-2 fucosylation could be observed 5 h post-infection, corresponding to the timeframe of viral protein expression. These observations provide a novel theory of NA functions that NA obtains its enzymatic activity intracellularly before virus assembly and serves desialylated glycans for competitive glycosyltransferases, including α1-2 fucosyltransferases, as their acceptors, resulting in glycan recapping with α1-2 fucose. Hence, intracellular NA blocks the re-sialylation of glycans, promoting efficient virus release from infected cells by inhibiting the interaction between progeny virions and sialosides. This study further demonstrated the potential NA functions of limiting secondary IAV infection. These findings provide insights into the evolutionary strategies of IAVs for shaping the strict window of superinfection by NA functions under a balance between successful replication and reassortment.

Conclusion

IAVs infect various animal species among mammals and birds. The viruses pose a risk to humans through acute respiratory infections, a significant economic loss in poultry industries, and huge mortality cases in wildlife, especially due to HPAIV infections. Accordingly, understanding the mechanisms of IAV replication and pathogenesis is necessary for controlling influenza virus infections.

Two surface glycoproteins of IAVs, HA and NA, have primary functions in viral attachment and release in a replication cycle, respectively. These two proteins have opposing roles in the viral replication cycle; HA binds to sialosides on the surface of target cells and initiates viral infection, whereas NA hydrolyzes the sialic acid at the non-reducing terminus, leading to the viral release from the infected cells. Since interactions between HA and glycans are generally weak, multivalent HA-glycan interactions are required in the natural setting. To assess the complex nature of glycan-binding specificity of AIVs via multivalent interactions, Chapter I used glycopolymers harboring various representations and densities of Siaα2-3Galβ1-4Glc, which mimicked AIV receptors. The results demonstrated differences in binding preference of HAs among duck-origin AIVs based on the local glycan density and representation of Siaα2-3Galβ1-4Glc moiety. Moreover, the glycan-binding preference of AIV particles revealed a compensation for weak HA-glycan binding by employing multivalent HA-glycan interactions.

The functions of surface glycoproteins are also known to be associated with AIV pathogenesis in chickens. Herein, Chapter II focused on the molecular basis of amino acid truncation of the NA-stalk domain of an HPAIV to the viral pathogenicity in chickens. A previous study passaged a genetically modified non-pathogenicity AIV in chickens and resulted in an HPAIV with a 34-amino-acid deletion in the NA stalk, encompassing five potential *N*-glycosylation sites [78]. The subsequent pathogenicity assessment *in vivo*, as well as functional and glycan occupancy analyses of NA *in vitro*, revealed that the loss of glycosylation was functionally equivalent to amino acid truncation in enhancing pathogenicity in chickens, in addition to reducing the NA activity to chicken erythrocytes.

Chapter III demonstrated that intracellular NA functions of IAVs were involved in global desialylation and glycan recapping in the virus-infected MDCK cells. Contrary to the conventional theory that NA liberates sialic acid on the cell surface upon virus

release from the cell, this study revealed that NA also functions intracellularly to induce the global desialylation in infected cells prior to viral budding. Based on these observations, IAV particles are poised to be released from infected cells at viral budding without the barrier of HA-glycan interactions. The findings provide insights into the evolutionary strategies of IAVs that enable efficient release from infected cells and limit the window for superinfection. The mechanisms further contribute to promote successful replication and restrict reassortant opportunities. Moreover, the results support the design of more effective and rational antiviral drugs by targeting the intracellular NA function.

In conclusion, the present study highlights novel functions of envelope glycoproteins in the replication and pathogenesis of IAVs. These improved understandings of the molecular basis of IAVs contribute to a better understanding of the molecular evolution and strengthen countermeasures against IAVs.

Acknowledgements

The author would like to acknowledge Prof. Y. Sakoda, Laboratory of Microbiology, Department of Disease Control, Faculty of Veterinary Medicine, Hokkaido University (Sapporo, Japan) for his guidance and encouragement during the course of this work.

Great appreciation is extended to Specially Appointed Prof. H. Kariwa, Laboratory of Public Health, Department of Preventive Veterinary Medicine, Faculty of Veterinary Medicine, Hokkaido University and Assoc. Prof. K. Matsuno, Division of Risk Analysis and Management, International Institute for Zoonosis Control, Hokkaido University for their critical review of the manuscripts.

The author is profoundly grateful to Assoc. Prof. T. Hiono, One Health Research Center, Hokkaido University and Assoc. Prof. N. Isoda, Laboratory of Microbiology, Department of Disease Control, Faculty of Veterinary Medicine, Hokkaido University for their continuous support, valuable advice, and encouragements throughout this study.

The author heartily thanks Prof. H. Kaji and Dr. H. Arakawa, Institute for Glyco-core Research (iGCORE), Nagoya University (Nagoya, Japan); Prof. K. Matsuoka, Dr. T. Matsushita, and Mr. R. Adachi, Graduate School of Engineering, Saitama University (Saitama, Japan); Assoc. Prof. M. Igarashi, Division of Global Epidemiology, International Institute for Zoonosis Control, Hokkaido University; Ms. A. Ohkawara, Mr. T. Ichikawa and Ms. H. Ban, Laboratory of Microbiology, Department of Disease Control, Faculty of Veterinary Medicine. Hokkaido University for their excellent contribution and support for the present study.

The author thanks Prof. A. Takada, Division of Global Epidemiology, International Institute for Zoonosis Control, Hokkaido University for sharing valuable monoclonal antibodies; and Prof. K. F. Shortridge, University of Hong Kong, Hong Kong, SAR for kindly providing viruses.

The author greatly appreciates all members and colleagues of Laboratory of Microbiology, Department of Disease Control, Faculty of Veterinary Medicine, Hokkaido University for their invaluable help and support.

The Japan Society for the Promotion of Science (JSPS) Research Fellowship for Young Scientists supported this work. The Japan Science and Technology Agency SPRING and the World-leading Innovative and Smart Education Program (1801) from Ministry of Education, Culture, Sports, Science, and Technology also supported the present study.

The author expresses profound sorrow for all the animals sacrificed for the present study.

References

1. Horimoto, T. and Kawaoka, Y. 2005. Influenza: lessons from past pandemics, warnings from current incidents. *Nat Rev Microbiol*. **3**: 591–600.

2. Walker, P. J., Siddell, S. G., Lefkowitz, E. J., Mushegian, A. R., Adriaenssens, E. M., Alfenas-Zerbini, P., Davison, A. J., Dempsey, D. M., Dutilh, B. E., García, M. L., Harrach, B., Harrison, R. L., Hendrickson, R. C., Junglen, S., Knowles, N. J., Krupovic, M., Kuhn, J. H., Lambert, A. J., Łobocka, M., Nibert, M. L., Oksanen, H. M., Orton, R. J., Robertson, D. L., Rubino, L., Sabanadzovic, S., Simmonds, P., Smith, D. B., Suzuki, N., Van Dooerslaer, K., Vandamme, A. M., Varsani, A. and Zerbini, F. M. 2021. Changes to virus taxonomy and to the International Code of Virus Classification and Nomenclature ratified by the International Committee on Taxonomy of Viruses (2021). *Arch Virol*. **166**: 2633–2648.

3. Fouchier, R. A. M., Munster, V., Wallensten, A., Bestebroer, T. M., Herfst, S., Smith, D., Rimmelzwaan, G. F., Olsen, B. and Osterhaus, A. D. M. E. 2005. Characterization of a novel influenza A virus hemagglutinin subtype (H16) obtained from black-headed gulls. *J Virol*. **79**: 2814–2822.

4. Röhm, C., Zhou, N., Süss, J., Mackenzie, J. and Webster, R. G. 1996. Characterization of a novel influenza hemagglutinin, H15: Criteria for determination of influenza A subtypes. *Virology*. **217**: 508–516.

5. Webster, R. G., Bean, W. J., Gorman, O. T., Chambers, T. M. and Kawaoka, Y. 1992. Evolution and ecology of influenza A viruses. *Microbiol Rev*. **56**: 152–179.

6. Rogers, G. N. and Paulson, J. C. 1983. Receptor determinants of human and animal influenza virus isolates: Differences in receptor specificity of the H3 hemagglutinin based on species of origin. *Virology*. **127**: 361–373.

7. Varghese, J. N., Laver, W. G. and Colman, P. M. 1983. Structure of the influenza virus glycoprotein antigen neuraminidase at 2.9 Å resolution. *Nature*. **303**: 35–40.

8. Benton, D. J., Martin, S. R., Wharton, S. A. and McCauley, J. W. 2015. Biophysical measurement of the balance of influenza A hemagglutinin and neuraminidase activities. *J Biol Chem*. **290**: 6516–6521.

9. Reiter-Scherer, V., Cuellar-Camacho, J. L., Bhatia, S., Haag, R., Herrmann, A., Lauster, D. and Rabe, J. P. 2019. Force spectroscopy shows dynamic binding of influenza hemagglutinin and neuraminidase to sialic acid. *Biophys J*. **116**: 1037–1048.

10. Wagner, R., Matrosovich, M. and Klenk, H. D. 2002. Functional balance between haemagglutinin and neuraminidase in influenza virus infections. *Rev Med Virol*. **12**: 159–166.

11. Kida, H., Yanagawa, R. and Matsuoka, Y. 1980. Duck influenza lacking evidence of disease signs and immune response. *Infect Immun*. **30**: 547–553.

12. de Graaf, M. and Fouchier, R. A. M. 2014. Role of receptor binding specificity in influenza A virus transmission and pathogenesis. *EMBO J*. **33**: 823–841.

13. Matrosovich, M. N., Gambaryan, A. S., Teneberg, S., Piskarev, V. E., Yamnikova, S. S., Lvov, D. K., Robertson, J. S. and Karlsson, K. A. 1997. Avian influenza A viruses differ from human viruses by recognition of sialyloligosaccharides and gangliosides and by a higher conservation of the HA receptor-binding site. *Virology*. **233**: 224–234.

14. Stevens, J., Blixt, O., Glaser, L., Taubenberger, J. K., Palese, P., Paulson, J. C. and Wilson, I. A. 2006. Glycan microarray analysis of the hemagglutinins from modern and pandemic influenza viruses reveals different receptor specificities. *J Mol Biol*. **355**: 1143–1155.

15. Matrosovich, M., Tuzikov, A., Bovin, N., Gambaryan, A., Klimov, A., Castrucci, M. R., Donatelli, I. and Kawaoka, Y. 2000. Early alterations of the receptor-binding properties of H1, H2, and H3 avian influenza virus hemagglutinins after their introduction into mammals. *J Virol*. **74**: 8502–8512.

16. Ito, T., Couceiro, J. N. S. S., Kelm, S., Baum, L. G., Krauss, S., Castrucci, M. R., Donatelli, I., Kida, H., Paulson, J. C., Webster, R. G. and Kawaoka, Y. 1998. Molecular basis for the generation in pigs of influenza A viruses with pandemic potential. *J Virol*. **72**: 7367–7373.

17. Shinya, K., Ebina, M., Yamada, S., Ono, M., Kasai, N. and Kawaoka, Y. 2006. Influenza virus receptors in the human airway. *Nature*. **440**: 435–436.

18. Bateman, A. C., Karamanska, R., Busch, M. G., Dell, A., Olsen, C. W. and Haslam, S. M. 2010. Glycan analysis and influenza A virus infection of primary swine respiratory epithelial cells. *J Biol Chem*. **285**: 34016–34026.

19. Sriwilaijaroen, N., Kondo, S., Yagi, H., Takemae, N., Saito, T., Hiramatsu, H., Kato, K. and Suzuki, Y. 2011. *N*-glycans from porcine trachea and lung: Predominant NeuAcα2-6Gal could be a selective pressure for influenza variants in favor of human-type receptor. *PLoS One*. **6**: e16302.

20. Suzuki, N., Abe, T. and Natsuka, S. 2022. Structural analysis of *N*-glycans in chicken trachea and lung reveals potential receptors of chicken influenza viruses. *Sci Rep*. **12**: 2081.

21. Walther, T., Karamanska, R., Chan, R. W. Y., Chan, M. C. W., Jia, N., Air, G., Hopton, C., Wong, M. P., Dell, A., Peiris, J. S. M., Haslam, S. M. and Nicholls, J. M. 2013. Glycomic analysis of human respiratory tract tissues and correlation with influenza virus infection. *PLoS Pathog*. **9**: e1003223.

22. Peng, W., de Vries, R. P., Grant, O. C., Thompson, A. J., McBride, R., Tsogtbaatar, B., Lee, P. S., Razi, N., Wilson, I. A., Woods, R. J. and Paulson, J. C. 2017. Recent H3N2 viruses have evolved specificity for extended branched human-type receptors conferring potential for increased avidity. *Cell Host Microbe*. **21**: 23–34.

23. Nemanichvili, N., Tomris, I., Turner, H. L., McBride, R., Grant, O. C., van der Woude, R., Aldosari, M. H., Pieters, R. J., Woods, R. J., Paulson, J. C., Boons, G. J., Ward, A. B., Verheije, M. H. and de Vries, R. P. 2019. Fluorescent trimeric hemagglutinins reveal multivalent receptor binding properties. *J Mol Biol*. **431**: 842–856.

24. Kawaoka, Y. and Webster, R. G. 1985. Evolution of the A/chicken/Pennsylvania/83 (H5N2) influenza virus. *Virology*. **146**: 130–137.

25. Bosch, F. X., Orlich, M., Klenk, H. D. and Rott, R. 1979. The structure of the hemagglutinin, a determinant for the pathogenicity of influenza viruses. *Virology*. **95**: 197–207.

26. Bogs, J., Veits, J., Gohrbandt, S., Hundt, J., Stech, O., Breithaupt, A., Teifke, J. P., Mettenleiter, T. C. and Stech, J. 2010. Highly pathogenic H5N1 influenza viruses carry virulence determinants beyond the polybasic hemagglutinin cleavage site. *PLoS One*. **5**: e11826.

27. Maruyama, J., Okamatsu, M., Soda, K., Sakoda, Y. and Kida, H. 2013. Factors responsible for pathogenicity in chickens of a low-pathogenic H7N7 avian influenza virus isolated from a feral duck. *Arch Virol*. **158**: 2473–2478.

28. Matrosovich, M., Zhou, N., Kawaoka, Y. and Webster, R. 1999. The surface glycoproteins of H5 influenza viruses isolated from humans, chickens, and wild aquatic birds have distinguishable properties. *J Virol*. **73**: 1146–1155.

29. Munier, S., Larcher, T., Cormier-Aline, F., Soubieux, D., Su, B., Guigand, L., Labrosse, B., Cherel, Y., Quéré, P., Marc, D. and Naffakh, N. 2010. A genetically engineered waterfowl influenza virus with a deletion in the stalk of the neuraminidase has increased virulence for chickens. *J Virol*. **84**: 940–952.

30. Stech, O., Veits, J., Abdelwhab, E. S. M., Wessels, U., Mettenleiter, T. C. and Stech, J. 2015. The neuraminidase stalk deletion serves as major virulence determinant of H5N1 highly pathogenic avian influenza viruses in chicken. *Sci Rep*. **5**: 13493.

31. Banks, J., Speidel, E. S., Moore, E., Plowright, L., Piccirillo, A., Capua, I., Cordioli, P., Fioretti, A. and Alexander, D. J. 2001. Changes in the haemagglutinin and the neuraminidase genes prior to the emergence of highly pathogenic H7N1 avian influenza viruses in Italy. *Arch. Virol.* **146**: 963–973.

32. Criado, M. F., Leyson, C. M., Youk, S., DeBlois, S., Olivier, T., Killian, M. L., Torchetti, M. L., Parris, D. J., Spackman, E., Kapczynski, D. R., Suarez, D. L., Swayne, D. E. and Pantin-Jackwood, M. J. 2021. The pathobiology of H7N3 low and high pathogenicity avian influenza viruses from the United States outbreak in 2020 differs between turkeys and chickens. *Viruses*. **13**: 1851.

33. Zinyakov, N., Andriyasov, A., Zhestkov, P., Kozlov, A., Nikonova, Z., Ovchinnikova, E., Grekhneva, A., Shcherbakova, L., Andreychuk, D., Sprygin, A., Prokhvatilova, L. and Chvala, I. 2022. Analysis of avian influenza (H5N5) viruses isolated in the southwestern European part of the Russian Federation in 2020–2021. *Viruses*. **14**: 2725.

34. Li, J., Dohna, H. zu, Cardona, C. J., Miller, J. and Carpenter, T. E. 2011. Emergence and genetic variation of neuraminidase stalk deletions in avian influenza viruses. *PLoS One*. **6**: e14722.

35. Giannecchini, S., Clausi, V., Di Trani, L., Falcone, E., Terregino, C., Toffan, A., Cilloni, F., Matrosovich, M., Gambaryan, A. S., Bovin, N. V., Delogu, M., Capua, I., Donatelli, I. and Azzi, A. 2010. Molecular adaptation of an H7N3 wild duck influenza virus following experimental multiple passages in quail and turkey. *Virology*. **408**: 167–173.

36. Li, J., Dohna, H. Z., Anchell, N. L., Adams, S. C., Dao, N. T., Xing, Z. and Cardona, C. J. 2010. Adaptation and transmission of a duck-origin avian influenza virus in poultry species. *Virus Res*. **147**: 40–46.

37. Sorrell, E. M., Song, H., Pena, L. and Perez, D. R. 2010. A 27-amino-acid deletion in the neuraminidase stalk supports replication of an avian H2N2 influenza A virus in the respiratory tract of chickens. *J Virol*. **84**: 11831–11840.

38. Yamada, S., Shinya, K., Takada, A., Ito, T., Suzuki, T., Suzuki, Y., Le, Q. M., Ebina, M., Kasai, N., Kida, H., Horimoto, T., Rivailler, P., Chen, L. M., Donis, R. O. and Kawaoka, Y. 2012. Adaptation of a duck influenza A virus in quail. *J Virol*. **86**: 1411–1420.

39. Arai, Y., Elgendy, E. M., Daidoji, T., Ibrahim, M. S., Ono, T., Sriwilaijaroen, N., Suzuki, Y., Nakaya, T., Matsumoto, K. and Watanabe, Y. 2020. H9N2 influenza virus infections in human cells require a balance between neuraminidase sialidase activity and hemagglutinin receptor affinity. *J Virol*. **94**: e01210-20.

40. Chen, S., Quan, K., Wang, D., Du, Y., Qin, T., Peng, D. and Liu, X. 2020. Truncation or deglycosylation of the neuraminidase stalk enhances the

pathogenicity of the H5N1 subtype avian influenza virus in mallard ducks. *Front Microbiol*. **11**: 583588.

41. Matsuoka, Y., Swayne, D. E., Thomas, C., Rameix-Welti, M. A., Naffakh, N., Warnes, C., Altholtz, M., Donis, R. and Subbarao, K. 2009. Neuraminidase stalk length and additional glycosylation of the hemagglutinin influence the virulence of influenza H5N1 viruses for mice. *J Virol*. **83**: 4704–4708.

42. Palese, P., Tobita, K., Ueda, M. and Compans, R. W. 1974. Characterization of temperature sensitive influenza virus mutants defective in neuraminidase. *Virology*. **61**: 397–410.

43. Matrosovich, M. N., Matrosovich, T. Y., Gray, T., Roberts, N. A. and Klenk, H. D. 2004. Neuraminidase is important for the initiation of influenza virus infection in human airway epithelium. *J Virol*. **78**: 12665–12667.

44. Ohuchi, M., Asaoka, N., Sakai, T. and Ohuchi, R. 2006. Roles of neuraminidase in the initial stage of influenza virus infection. *Microbes Infect*. **8**: 1287–1293.

45. Guo, H., Rabouw, H., Slomp, A., Dai, M., van der Vegt, F., van Lent, J. W. M., McBride, R., Paulson, J. C., de Groot, R. J., van Kuppeveld, F. J. M., de Vries, E. and de Haan, C. A. M. 2018. Kinetic analysis of the influenza A virus HA/NA balance reveals contribution of NA to virus-receptor binding and NA-dependent rolling on receptor-containing surfaces. *PLoS Pathog*. **14**: e1007233.

46. Sakai, T., Nishimura, S. I., Naito, T. and Saito, M. 2017. Influenza A virus hemagglutinin and neuraminidase act as novel motile machinery. *Sci Rep*. **7**: 45043.

47. Huang, I. C., Li, W., Sui, J., Marasco, W., Choe, H. and Farzan, M. 2008. Influenza A virus neuraminidase limits viral superinfection. *J Virol*. **82**: 4834–4843.

48. Sims, A., Tornaletti, L. B., Jasim, S., Pirillo, C., Devlin, R., Hirst, J. C., Loney, C., Wojtus, J., Sloan, E., Thorley, L., Boutell, C., Roberts, E. and Hutchinson, E. 2023. Superinfection exclusion creates spatially distinct influenza virus populations. *PLoS Biol*. **21**: e3001941.

49. von Itzstein, M., Wu, W. Y., Kok, G. B., Pegg, M. S., Dyason, J. C., Jin, B., van Phan, T., Smythe, M. L., White, H. F., Oliver, S. W., Colman, P. M., Varghese, J.

N., Ryan, D. M., Woods, J. M., Bethell, R. C., Hotham, V. J., Cameron, J. M. and Penn, C. R. 1993. Rational design of potent sialidase-based inhibitors of influenza virus replication. *Nature*. **363**: 418–423.

50. Kim, C. U., Lew, W., Williams, M. A., Liu, H., Zhang, L., Swaminathan, S., Bischofberger, N., Chen, M. S., Mendel, D. B., Tai, C. Y., Laver, W. G. and Stevens, R. C. 1997. Influenza neuraminidase inhibitors possessing a novel hydrophobic interaction in the enzyme active site: Design, synthesis, and structural analysis of carbocyclic sialic acid analogues with potent anti-influenza activity. *J Am Chem Soc.* **119**: 681–690.

51. Li, T., Spruit, C. M., Wei, N., Liu, L., Wolfert, M. A., de Vries, R. P. and Boons, G. J. 2024. Chemoenzymatic synthesis of tri-antennary *N*-glycans terminating in sialyl-Lewis X reveals the importance of glycan complexity for influenza A virus receptor binding. *Chemistry*. **30**: e202401108.

52. Sauter, N. K., Bednarski, M. D., Wurzburg, B. A., Hanson, J. E., Whitesides, G. M., Skehel, J. J. and Wiley, D. C. 1989. Hemagglutinins from two influenza virus variants bind to sialic acid derivatives with millimolar dissociation constants: a 500-MHz proton nuclear magnetic resonance study. *Biochemistry*. **28**: 8388–8396.

53. Landers, J. J., Cao, Z., Lee, I., Piehler, L. T., Myc, P. P., Myc, A., Hamouda, T., Galecki, A. T. and Baker, J. R., Jr. 2002. Prevention of influenza pneumonitis by sialic acid–conjugated dendritic polymers. *J Infect Dis*. **186**: 1222–1230.

54. Li, Y., Cao, H., Dao, N., Luo, Z., Yu, H., Chen, Y., Xing, Z., Baumgarth, N., Cardona, C. and Chen, X. 2011. High-throughput neuraminidase substrate specificity study of human and avian influenza A viruses. *Virology*. **415**: 12–19.

55. Matrosovich, M. N., Mochalova, L. V., Marinina, V. P., Byramova, N. E. and Bovin, N. V. 1990. Synthetic polymeric sialoside inhibitors of influenza virus receptor-binding activity. *FEBS Lett*. **272**: 209–212.

56. Matsuoka, K., Kaneshima, T., Adachi, R., Sasaki, J., Hashiguchi, T., Koyama, T., Matsushita, T. and Hatano, K. 2021. Preparation of glycopolymers having sialyl α2→3 lactose moieties as the potent inhibitors for mumps virus. *Bioorg Med Chem Lett*. **52**: 128389.

57. Adachi, R., Matsushita, T., Koyama, T., Hatano, K. and Matsuoka, K. 2023. Synthetic assembly of a series of glycopolymers having sialyl α2-3 lactose moieties connected with longer spacer arms. *Bioorg Med Chem*. **81**: 117209.

58. Sakoda, Y., Sugar, S., Batchluun, D., Erdene-Ochir, T. O., Okamatsu, M., Isoda, N., Soda, K., Takakuwa, H., Tsuda, Y., Yamamoto, N., Kishida, N., Matsuno, K., Nakayama, E., Kajihara, M., Yokoyama, A., Takada, A., Sodnomdarjaa, R. and Kida, H. 2010. Characterization of H5N1 highly pathogenic avian influenza virus strains isolated from migratory waterfowl in Mongolia on the way back from the southern Asia to their northern territory. *Virology*. **406**: 88–94.

59. Kikutani, Y., Okamatsu, M., Nishihara, S., Takase-Yoden, S., Hiono, T., de Vries, R. P., McBride, R., Matsuno, K., Kida, H. and Sakoda, Y. 2020. E190V substitution of H6 hemagglutinin is one of key factors for binding to sulfated sialylated glycan receptor and infection to chickens. *Microbiol Immunol*. **64**: 304–312.

60. Reeves, P. J., Callewaert, N., Contreras, R. and Khorana, H. G. 2002. Structure and function in rhodopsin: High-level expression of rhodopsin with restricted and homogeneous *N*-glycosylation by a tetracycline-inducible *N*-acetylglucosaminyltransferase I-negative HEK293S stable mammalian cell line. *Proc Natl Acad Sci*. **99**: 13419–13424.

61. Hiono, T., Okamatsu, M., Igarashi, M., McBride, R., de Vries, R. P., Peng, W., Paulson, J. C., Sakoda, Y. and Kida, H. 2016. Amino acid residues at positions 222 and 227 of the hemagglutinin together with the neuraminidase determine binding of H5 avian influenza viruses to sialyl Lewis X. *Arch Virol*. **161**: 307–316.

62. de Vries, R. P., de Vries, E., Bosch, B. J., de Groot, R. J., Rottier, P. J. M. and de Haan, C. A. M. 2010. The influenza A virus hemagglutinin glycosylation state affects receptor-binding specificity. *Virology*. **403**: 17–25.

63. Adachi, R., Matsushita, T., Koyama, T., Hatano, K. and Matsuoka, K. 2023. Use of a longer aglycon moiety bearing sialyl α(2→3) lactoside on the glycopolymer for lectin evaluation. *Polymers*. **15**: 998.

64. Hiono, T., Okamatsu, M., Nishihara, S., Takase-Yoden, S., Sakoda, Y. and Kida, H. 2014. A chicken influenza virus recognizes fucosylated α2,3 sialoglycan receptors

on the epithelial cells lining upper respiratory tracts of chickens. *Virology*. **456–457**: 131–138.

65. Tzarum, N., de Vries, R. P., Zhu, X., Yu, W., McBride, R., Paulson, J. C. and Wilson, I. A. 2015. Structure and receptor binding of the hemagglutinin from a human H6N1 influenza virus. *Cell Host Microbe*. **17**: 369–376.

66. Motohashi, Y., Igarashi, M., Okamatsu, M., Noshi, T., Sakoda, Y., Yamamoto, N., Ito, K., Yoshida, R. and Kida, H. 2013. Antiviral activity of stachyflin on influenza A viruses of different hemagglutinin subtypes. *Virol J*. **10**: 118.

67. Mammen, M., Choi, S. K. and Whitesides, G. M. 1998. Polyvalent interactions in biological systems: Implications for design and use of multivalent ligands and inhibitors. *Angew Chem Int Ed Engl*. **37**: 2754–2794.

68. Bandlow, V., Liese, S., Lauster, D., Ludwig, K., Netz, R. R., Herrmann, A. and Seitz, O. 2017. Spatial screening of hemagglutinin on influenza a virus particles: Sialyl-LacNAc displays on DNA and PEG scaffolds reveal the requirements for bivalency enhanced interactions with weak monovalent binders. *J Am Chem Soc.* **139**: 16389–16397.

69. Takemoto, D. K., Skehel, J. J. and Wiley, D. C. 1996. A surface plasmon resonance assay for the binding of influenza virus hemagglutinin to its sialic acid receptor. *Virology*. **217**: 452–458.

70. Nycholat, C. M., McBride, R., Ekiert, D. C., Xu, R., Rangarajan, J., Peng, W., Razi, N., Gilbert, M., Wakarchuk, W., Wilson, I. A. and Paulson, J. C. 2012. Recognition of sialylated poly-*N*-acetyllactosamine chains on *N*- and *O*-Linked glycans by human and avian influenza A virus hemagglutinins. *Angew Chem Int Ed Engl*. **51**: 4860–4863.

71. Dam, T. K. and Brewer, C. F. 2010. Lectins as pattern recognition molecules: The effects of epitope density in innate immunity. *Glycobiology*. **20**: 270–279.

72. Nagao, M., Kurebayashi, Y., Seto, H., Tanaka, T., Takahashi, T., Suzuki, T., Hoshino, Y. and Miura, Y. 2016. Synthesis of well-controlled glycopolymers

bearing oligosaccharides and their interactions with influenza viruses. *Polym J*. **48**: 745–749.

73. Ichikawa, T., Hiono, T., Okamatsu, M., Maruyama, J., Kobayashi, D., Matsuno, K., Kida, H. and Sakoda, Y. 2024. Hemagglutinin and neuraminidase of a non-pathogenic H7N7 avian influenza virus coevolved during the acquisition of intranasal pathogenicity in chickens. *Arch Virol*. **169**: 207.

74. Els, M. C., Air, G. M., Murti, K. G., Webster, R. G. and Laver, W. G. 1985. An 18-amino acid deletion in an influenza neuraminidase. *Virology*. **142**: 241–247.

75. Durrant, J. D., Bush, R. M. and Amaro, R. E. 2016. Microsecond molecular dynamics simulations of influenza neuraminidase suggest a mechanism for the increased virulence of stalk-deletion mutants. *J Phys Chem B*. **120**: 8590–8599.

76. Harris, A., Cardone, G., Winkler, D. C., Heymann, J. B., Brecher, M., White, J. M. and Steven, A. C. 2006. Influenza virus pleiomorphy characterized by cryoelectron tomography. *Proc Natl Acad Sci*. **103**: 19123–19127.

77. Soda, K., Asakura, S., Okamatsu, M., Sakoda, Y. and kida, H. 2011. H9N2 influenza virus acquires intravenous pathogenicity on the introduction of a pair of di-basic amino acid residues at the cleavage site of the hemagglutinin and consecutive passages in chickens. *Virol J*. **8**: 64.

78. Yamamoto, N., Soda, K., Sakoda, Y., Okamatsu, M. and Kida, H. 2013. Proteins of duck influenza virus responsible for acquisition of pathogenicity in chickens. *Virus Res*. **173**: 294–298.

79. Lee, H. S., Qi, Y. and Im, W. 2015. Effects of *N*-glycosylation on protein conformation and dynamics: Protein Data Bank analysis and molecular dynamics simulation study. *Sci Rep*. **5**: 8926.

80. Wagner, R., Heuer, D., Wolff, T., Herwig, A. and Klenk, H. D. 2002. *N*-Glycans attached to the stem domain of haemagglutinin efficiently regulate influenza A virus replication. *J Gen Virol*. **83**: 601–609.

81. Soda, K., Sakoda, Y., Isoda, N., Kajihara, M., Haraguchi, Y., Shibuya, H., Yoshida, H., Sasaki, T., Sakamoto, R., Saijo, K., Hagiwara, J. and Kida, H. 2008.

Development of vaccine strains of H5 and H7 influenza viruses. *Jpn J Vet Res*. **55**: 93–98.

82. Reed, L. J. and Muench, H. 1938. A simple method of estimating fifty per cent endopoints. *Am J Epidemiol*. **27**: 493–497.

83. Hoffmann, E., Neumann, G., Kawaoka, Y., Hobom, G. and Webster, R. G. 2000. A DNA transfection system for generation of influenza A virus from eight plasmids. *Proc Natl Acad Sci*. **97**: 6108–6113.

84. Fujii, Y., Goto, H., Watanabe, T., Yoshida, T. and Kawaoka, Y. 2003. Selective incorporation of influenza virus RNA segments into virions. *Proc Natl Acad Sci*. **100**: 2002–2007.

85. Hiono, T. and Kuno, A. 2020. C-terminally tagged NA in replication-competent influenza A viruses reveals differences in glycan profiles between NA and HA. *Analyst*. **145**: 5845–5853.

86. Hoffmann, E., Stech, J., Guan, Y., Webster, R. G. and Perez, D. R. 2001. Universal primer set for the full-length amplification of all influenza A viruses. *Arch Virol*. **146**: 2275–2289.

87. Ip, H. S., Uhm, S., Killian, M. L. and Torchetti, M. K. 2023. An evaluation of avian influenza virus whole-genome sequencing approaches using nanopore technology. *Microorganisms*. **11**: 529.

88. Hew, L. Y., Isoda, N., Takaya, F., Ogasawara, K., Kobayashi, D., Huynh, L. T., Morita, T., Harada, R., Zinyakov, N. G., Andreychuk, D. B., Chvala, I. A., Irza, V. N., Watanabe, Y., Fujita, H., Saito, K., Hiono, T. and Sakoda, Y. 2024. Continuous introduction of H5 high pathogenicity avian influenza viruses in Hokkaido, Japan: characterization of viruses isolated in winter 2022–2023 and early winter 2023–2024. *Transbound Emerg Dis*. **2024**: 1199876.

89. Sakabe, S., Sakoda, Y., Haraguchi, Y., Isoda, N., Soda, K., Takakuwa, H., Saijo, K., Sawata, A., Kume, K., Hagiwara, J., Tuchiya, K., Lin, Z., Sakamoto, R., Imamura, T., Sasaki, T., Kokumai, N., Kawaoka, Y. and Kida, H. 2008. A vaccine prepared from a non-pathogenic H7N7 virus isolated from natural reservoir conferred

protective immunity against the challenge with lethal dose of highly pathogenic avian influenza virus in chickens. *Vaccine*. **26**: 2127–2134.

90. Ohgane, K. and Yoshioka, H. 2019. Quantification of gel bands by an Image J macro, band/peak quantification tool. dx.doi.org/10.17504/protocols.io.7vghn3w

91. Kaji, H., Saito, H., Yamauchi, Y., Shinkawa, T., Taoka, M., Hirabayashi, J., Kasai, K., Takahashi, N. and Isobe, T. 2003. Lectin affinity capture, isotope-coded tagging and mass spectrometry to identify *N*-linked glycoproteins. *Nat Biotechnol*. **21**: 667–672.

92. Kaji, H., Yamauchi, Y., Takahashi, N. and Isobe, T. 2006. Mass spectrometric identification of *N*-linked glycopeptides using lectin-mediated affinity capture and glycosylation site–specific stable isotope tagging. *Nat Protoc*. **1**: 3019–3027.

93. Reid, S. M., Brookes, S. M., Núñez, A., Banks, J., Parker, C. D., Ceeraz, V., Russell, C., Seekings, A., Thomas, S. S., Puranik, A. and Brown, I. H. 2018. Detection of non-notifiable H4N6 avian influenza virus in poultry in Great Britain. *Vet Microbiol*. **224**: 107–115.

94. Lorenz, R., Bernhart, S. H., Höner zu Siederdissen, C., Tafer, H., Flamm, C., Stadler, P. F. and Hofacker, I. L. 2011. ViennaRNA Package 2.0. *Algorithms Mol Biol*. **6**: 26.

95. Sato, K., Akiyama, M. and Sakakibara, Y. 2021. RNA secondary structure prediction using deep learning with thermodynamic integration. *Nat Commun*. **12**: 941.

96. Castrucci, M. R. and Kawaoka, Y. 1993. Biologic importance of neuraminidase stalk length in influenza A virus. *J Virol*. **67**: 759–764.

97. DuBois, R. M., Zaraket, H., Reddivari, M., Heath, R. J., White, S. W. and Russell, C. J. 2011. Acid stability of the hemagglutinin protein regulates H5N1 influenza virus pathogenicity. *PLoS Pathog*. **7**: e1002398.

98. García, M., Crawford, J. M., Latimer, J. W., Rivera-Cruz, E. and Perdue, M. L. 1996. Heterogeneity in the haemagglutinin gene and emergence of the highly pathogenic

phenotype among recent H5N2 avian influenza viruses from Mexico. *J Gen Virol*. **77**: 1493–1504.

99. Nao, N., Yamagishi, J., Miyamoto, H., Igarashi, M., Manzoor, R., Ohnuma, A., Tsuda, Y., Furuyama, W., Shigeno, A., Kajihara, M., Kishida, N., Yoshida, R. and Takada, A. 2017. Genetic predisposition to acquire a polybasic cleavage site for highly pathogenic avian influenza virus hemagglutinin. *mBio*. **8**: e02298-16.

100. Rowe, C. L., Fleming, J. O., Nathan, M. J., Sgro, J. Y., Palmenberg, A. C. and Baker, S. C. 1997. Generation of coronavirus spike deletion variants by high-frequency recombination at regions of predicted RNA secondary structure. *J Virol*. **71**: 6183–6190.

101. Park, S., Kim, J. I., Lee, I., Bae, J. Y., Yoo, K., Nam, M., Kim, J., Sook Park, M., Song, K. J., Song, J. W., Kee, S. H. and Park, M. S. 2017. Adaptive mutations of neuraminidase stalk truncation and deglycosylation confer enhanced pathogenicity of influenza A viruses. *Sci Rep*. **7**: 10928.

102. Danwen, Q., Code, C., Quan, C., Gong, B. J., Arndt, J., Pepinsky, B., Rand, K. D. and Houde, D. 2016. Investigating the role of artemin glycosylation. *Pharm Res*. **33**: 1383–1398.

103. Lee, S. M., Jeong, Y., Simms, J., Warner, M. L., Poyner, D. R., Chung, K. Y. and Pioszak, A. A. 2020. Calcitonin receptor *N*-glycosylation enhances peptide hormone affinity by controlling receptor dynamics. *J Mol Biol*. **432**: 1996–2014.

104. Ramakrishnan, K., Johnson, R. L., Winter, S. D., Worthy, H. L., Thomas, C., Humer, D. C., Spadiut, O., Hindson, S. H., Wells, S., Barratt, A. H., Menzies, G. E., Pudney, C. R. and Jones, D. D. 2023. Glycosylation increases active site rigidity leading to improved enzyme stability and turnover. *FEBS J*. **290**: 3812–3827.

105. Seitz, C., Deveci, İ. and McCammon, J. A. 2023. Glycosylation and crowded membrane effects on influenza neuraminidase stability and dynamics. *J Phys Chem Lett.* **14**: 9926–9934.

106. Zhou, B., Donnelly, M. E., Scholes, D. T., St. George, K., Hatta, M., Kawaoka, Y. and Wentworth, D. E. 2009. Single-reaction genomic amplification accelerates

sequencing and vaccine production for classical and swine origin human influenza A viruses. *J Virol*. **83**: 10309–10313.

107. Kawasaki, Y., Abe, H. and Yasuda, J. 2023. Comparison of genome replication fidelity between SARS-CoV-2 and influenza A virus in cell culture. *Sci Rep*. **13**: 13105.

108. Palese, P. and Compans, R. W. 1976. Inhibition of influenza virus replication in tissue culture by 2-deoxy-2,3-dehydro-*N*-trifluoroacetylneuraminic acid (FANA): Mechanism of action. *J Gen Virol.* **33**: 159–163.

109. Stanley, P., Moremen, K. W., Lewis, N. E., Taniguchi, N. and Aebi, M. 2022. *N*-glycans. *Essentials of Glycobiology. 4th edition*, Cold Spring Harbor Laboratory Press.

110. Nordén, R., Samuelsson, E. and Nyström, K. 2017. NFκB-mediated activation of the cellular FUT3, 5 and 6 gene cluster by herpes simplex virus type 1. *Glycobiology*. **27**: 999–1005.

111. Nyström, K., Nordén, R., Muylaert, I., Elias, P., Larson, G. and Olofsson, S. 2009. Induction of sialyl-Le^X expression by herpes simplex virus type 1 is dependent on viral immediate early RNA-activated transcription of host fucosyltransferase genes. *Glycobiology*. **19**: 847–859.

112. Watanabe, Y., Shiratsuchi, A., Shimizu, K., Takizawa, T. and Nakanishi, Y. 2002. Role of phosphatidylserine exposure and sugar chain desialylation at the surface of influenza virus-infected cells in efficient phagocytosis by macrophages. *J Biol Chem*. **277**: 18222–18228.

113. Opitz, L., Zimmermann, A., Lehmann, S., Genzel, Y., Lübben, H., Reichl, U. and Wolff, M. W. 2008. Capture of cell culture-derived influenza virus by lectins: Strain independent, but host cell dependent. *J Virol Methods*. **154**: 61–68.

114. Hiono, T., Matsuda, A., Wagatsuma, T., Okamatsu, M., Sakoda, Y. and Kuno, A. 2019. Lectin microarray analyses reveal host cell-specific glycan profiles of the hemagglutinins of influenza A viruses. *Virology*. **527**: 132–140.

115. Opitz, L., Salaklang, J., Büttner, H., Reichl, U., Wolff, M. W. 2007. Lectin-affinity chromatography for downstream processing of MDCK cell culture derived human influenza A viruses. *Vaccine*. **25**: 939–947.

116. Pralow, A., Hoffmann, M., Nguyen-Khuong, T., Pioch, M., Hennig, R., Genzel, Y., Rapp, E. and Reichl, U. 2021. Comprehensive *N*-glycosylation analysis of the influenza A virus proteins HA and NA from adherent and suspension MDCK cells. *FEBS J*. **288**: 4869–4891.

117. Milland, J., Taylor, S. G., Dodson, H. C., McKenzie, I. C. and Sandrin, M. S. 2001. The cytoplasmic tail of α1,2-fucosyltransferase contains a sequence for Golgi localization. *J Biol Chem*. **276**: 12012–12018.

118. Fullmer, J. M., Riedl, M., Williams, F. G., Sandrin, M. and Elde, R. 2007. Enzymes that synthesize the IB4 epitope are not sufficient to impart IB4 binding in dorsal root ganglia of rat. *J Comp Neurol*. **501**: 70–82.

119. Soda, K., Ozaki, H., Sakoda, Y., Isoda, N., Haraguchi, Y., Sakabe, S., Kuboki, N., Kishida, N., Takada, A. and Kida, H. 2008. Antigenic and genetic analysis of H5 influenza viruses isolated from water birds for the purpose of vaccine use. *Arch Virol*. **153**: 2041–2048.

120. Manzoor, R., Sakoda, Y., Sakabe, S., Mochizuki, T., Namba, Y., Tsuda, Y. and Kida, H. 2008. Development of a pen-site test kit for the rapid diagnosis of H7 highly pathogenic avian influenza. *J Vet Med Sci*. **70**: 557–562.

121. Hiono, T., Kobayashi, D., Kobayashi, A., Suzuki, T., Satake, Y., Harada, R., Matsuno, K., Sashika, M., Ban, H., Kobayashi, M., Takaya, F., Fujita, H., Isoda, N., Kimura, T. and Sakoda, Y. 2023. Virological, pathological, and glycovirological investigations of an Ezo red fox and a tanuki naturally infected with H5N1 high pathogenicity avian influenza viruses in Hokkaido, Japan. *Virology*. **578**: 35–44.

122. Suda, T., Kamiyama, S., Suzuki, M., Kikuchi, N., Nakayama, K., Narimatsu, H., Jigami, Y., Aoki, T. and Nishihara, S. 2004. Molecular cloning and characterization of a human multisubstrate specific nucleotide-sugar transporter homologous to *Drosophila fringe* connection. *J Biol Chem*. **279**: 26469–26474.

123. Niwa, H., Yamamura, K. and Miyazaki, J. 1991. Efficient selection for high-expression transfectants with a novel eukaryotic vector. *Gene*. **108**: 193–199.

124. Yen, H. L., Hoffmann, E., Taylor, G., Scholtissek, C., Monto, A. S., Webster, R. G. and Govorkova, E. A. 2006. Importance of neuraminidase active-site residues to the neuraminidase inhibitor resistance of influenza viruses. *J Virol.* **80**: 8787–8795.

125. Zhu, X., McBride, R., Nycholat, C. M., Yu, W., Paulson, J. C. and Wilson, I. A. 2012. Influenza virus neuraminidases with reduced enzymatic activity that avidly bind sialic acid receptors. *J Virol*. **86**: 13371–13383.

126. Richard, M., Ferraris, O., Erny, A., Barthélémy, M., Traversier, A., Sabatier, M., Hay, A., Lin, Y. P., Russell, R. J. and Lina, B. 2011. Combinatorial effect of two framework mutations (E119V and I222L) in the neuraminidase active site of H3N2 influenza virus on resistance to oseltamivir. *Antimicrob Agents Chemother*. **55**: 2942–2952.

127. Tsuchiya, M., Kong, W., Hiraoka, Y., Haraguchi, T. and Ogawa, H. 2023. TBK1 inhibitors enhance transfection efficiency by suppressing p62/SQSTM1 phosphorylation. *Genes Cells*. **28**: 68–77.

128. Schneider, C. A., Rasband, W. S. and Eliceiri, K. W. 2012. NIH image to ImageJ: 25 years of image analysis. *Nat Methods*. **9**: 671–675.

129. Kanda, Y. 2013. Investigation of the freely available easy-to-use software 'EZR' for medical statistics. *Bone Marrow Transplant*. **48**: 452–458.

130. Kamiki, H., Murakami, S., Nishikaze, T., Hiono, T., Igarashi, M., Furuse, Y., Matsugo, H., Ishida, H., Katayama, M., Sekine, W., Muraki, Y., Takahashi, M., Takenaka-Uema, A. and Horimoto, T. 2022. Influenza A virus agnostic receptor tropism revealed using a novel biological system with terminal sialic acid knockout cells. *J Virol*. **96**: e00416-22.

131. Kuno, A., Uchiyama, N., Koseki-Kuno, S., Ebe, Y., Takashima, S., Yamada, M. and Hirabayashi, J. 2005. Evanescent-field fluorescence-assisted lectin microarray: a new strategy for glycan profiling. *Nat Methods*. **2**: 851–856.

132. Menezes-Souza, D., Corrêa-Oliveira, R., Guerra-Sá, R., Giunchetti, R. C., Teixeira-Carvalho, A., Martins-Filho, O. A., Oliveira, G. C. and Reis, A. B. 2011. Cytokine and transcription factor profiles in the skin of dogs naturally infected by *Leishmania (Leishmania) chagasi* presenting distinct cutaneous parasite density and clinical status. *Vet Parasitol*. **177**: 39–49.

133. Noro, E., Matsuda, A., Kyoutou, T., Sato, T., Tomioka, A., Nagai, M., Sogabe, M., Tsuruno, C., Takahama, Y., Kuno, A., Tanaka, Y., Kaji, H. and Narimatsu, H. 2021. *N*-glycan structures of *Wisteria floribunda* agglutinin-positive Mac2 binding protein in the serum of patients with liver fibrosis. *Glycobiology*. **31**: 1268–1278.

134. Fukao, K., Ando, Y., Noshi, T., Kitano, M., Noda, T., Kawai, M., Yoshida, R., Sato, A., Shishido, T. and Naito, A. 2019. Baloxavir marboxil, a novel cap-dependent endonuclease inhibitor potently suppresses influenza virus replication and represents therapeutic effects in both immunocompetent and immunocompromised mouse models. *PLoS One*. **14**: e0217307.

135. Noshi, T., Kitano, M., Taniguchi, K., Yamamoto, A., Omoto, S., Baba, K., Hashimoto, T., Ishida, K., Kushima, Y., Hattori, K., Kawai, M., Yoshida, R., Kobayashi, M., Yoshinaga, T., Sato, A., Okamatsu, M., Sakoda, Y., Kida, H., Shishido, T. and Naito, A. 2018. In vitro characterization of baloxavir acid, a first-in-class cap-dependent endonuclease inhibitor of the influenza virus polymerase PA subunit. *Antiviral Res*. **160**: 109–117.

136. Amano, K., Kurebayashi, Y., Takahashi, T., Narimichi, Y., Otsubo, T., Ikeda, K., Minami, A. and Takeuchi, H. 2024. Visualizing intracellular sialidase activity of influenza A virus neuraminidase using a fluorescence imaging probe. *J Virol Methods*. **323**: 114838.

137. Takashima, S. and Tsuji, S. 2011. Functional diversity of mammalian sialyltransferases. *Trends Glycosci Glycotechnol*. **23**: 178–193.

138. Ogawa, H. and Galili, U. 2006. Profiling terminal *N*-acetyllactosamines of glycans on mammalian cells by an immuno-enzymatic assay. *Glycoconj J*. **23**: 663–674.

139. Ohtsubo, K. and Marth, J. D. 2006. Glycosylation in cellular mechanisms of health and disease. *Cell*. **126**: 855–867.

140. Matlin, K. S., Reggio, H., Helenius, A. and Simons, K. 1981. Infectious entry pathway of influenza virus in a canine kidney cell line. *J Cell Biol*. **91**: 601–613.

141. de Vries, E., Tscherne, D. M., Wienholts, M. J., Cobos-Jiménez, V., Scholte, F., García-Sastre, A., Rottier, P. J. M. and de Haan, C. A. M. 2011. Dissection of the influenza A virus endocytic routes reveals macropinocytosis as an alternative entry pathway. *PLoS Pathog*. **7**: e1001329.

142. Sempere Borau, M. and Stertz, S. 2021. Entry of influenza A virus into host cells — recent progress and remaining challenges. *Curr Opin Virol*. **48**: 23–29.

143. Broich, L., Wullenkord, H., Osman, M. K., Fu, Y., Müsken, M., Reuther, P., Brönstrup, M. and Sieben, C. 2025. Single influenza A viruses induce nanoscale cellular reprogramming at the virus-cell interface. *Nat Commun*. **16**: 3846.

Summary in Japanese（和文要旨）

インフルエンザ A ウイルスは哺乳動物および鳥に広範な宿主域を持ち、主に急性の呼吸器感染症を引き起こす。本ウイルスの表面にはヘマグルチニン（HA）とノイラミニダーゼ（NA）の 2 種類の表面糖タンパク質が存在する。HA は標的細胞表面上のシアロ糖を認識しウイルス感染を惹起する一方、NA は糖鎖から末端のシアル酸を切断しウイルスの細胞からの遊離を促進する。したがって、HA と NA の相反する機能のバランスはインフルエンザ A ウイルスの感染環の維持に重要である。

鳥インフルエンザはインフルエンザＡウイルスに起因する家禽のウイルス性疾病である。カモを含む野生の水禽類からはすべての血清亜型のインフルエンザ A ウイルスが分離されることから、野生水禽はインフルエンザＡウイルスの自然宿主と考えられる。カモの有する非病原性の鳥インフルエンザウイルスがアヒルなどの水生家禽やニワトリ以外の陸生家禽に伝播する過程を経るとニワトリへの感染性を獲得することがある。また、ウイルスが鶏群内で感染伝播を繰り返すと、HA 亜型が H5 あるいは H7 のウイルスではニワトリに対して致死的な病原性を示す、高病原性鳥インフルエンザウイルスが出現することがある。そのため、本疾病の制御のためには鳥インフルエンザウイルスの宿主間伝播およびニワトリにおける病原性獲得機構の解明が必須である。

野生のカモ類で維持伝播している非病原性の鳥インフルエンザウイルスは主に α2,3 シアロ糖を受容体として認識する。一方、α2,6 シアロ糖を受容体として認識するヒト由来インフルエンザウイルスの HA には、α2,6 シアロ糖を提示する糖鎖の幹部分の伸長や分岐に特異性を示すものがあるが、鳥インフルエンザウイルスではこれらに対する特異性が明らかになっていない。本稿第一章では、鳥インフルエンザウイルスの組換え HA とウイルス粒子を用いて、長さと局所

密度の異なる α2,3 シアロ糖に対する結合特異性を比較した。様々な長さと局所密度を持つ α2,3 シアロ糖を合成糖鎖ポリマーにより再現するため、糖鎖の伸長は末端のシアリルラクトースに長さの異なるポリエチレングリコール鎖を結合し、糖鎖の密度は糖鎖モノマー間に重合するアクリルアミドの数を変えることで模倣した。組換え HA は糖鎖密度が高いポリマーに強く結合したものの、糖鎖密度が最も高いポリマーに対する結合性は低かった。この観察結果は、ポリマー上の多くの α2,3 シアロ糖が HA との結合に関与していないと考えられ、著しく高い密度の糖鎖は HA との結合を弱めると考えられる。一方、ウイルス粒子は低い密度の糖鎖に対しても高い結合性を示した。これはウイルス粒子上に存在する複数の HA が糖鎖と多価相互作用することにより低い密度の糖鎖に対する結合性を補う、クラスター効果に起因すると考えられた。本手法を用いることにより、ウイルス粒子と糖鎖の結合における複雑な相互作用や糖鎖密度によるクラスター効果の評価を可能にした。

鳥インフルエンザウイルスの NA の酵素活性部位を含む頭部と膜貫通領域をつなぐ、ストーク領域はニワトリ由来株においてアミノ酸欠失を認めることがある。先行研究では、非病原性鳥インフルエンザウイルスから遺伝子改変（rgVac2-P0）とニワトリでの接種継代を経て、ニワトリに致死的な病原性を示す株（Vac2-P3L4）が得られ、この株は NA ストーク領域のアミノ酸が 5 か所の *N* 型糖鎖付加部位を含む形で欠失していた。そのため、本稿第二章では NA ストーク領域の糖鎖の欠損およびアミノ酸の欠失が本ウイルスのニワトリに対する病原性を高める分子基盤を明らかにすることを目的とした。まず、アミノ酸置換により糖鎖のみを欠損した NA 遺伝子をクローニングし、他の遺伝子分節は継代後の株を由来に持つ組換えウイルス（rgVac2-P3L4/P0NAΔGlyco）を作出した。このウイルスを接種したニワトリは様々な転機を示し、またウイルス遺伝子の不安定性が認められた。遺伝子の不安定性を代償するアミノ酸置換を加

えた変異株を用いてニワトリに対する病原性を比較したところ、糖鎖欠損ウイルスは糖鎖を持つ親株と比較してニワトリに対して高い病原性を示した。ストーク領域の糖鎖付加部位における糖鎖占有率を解析したところ、継代前のウイルスの NA ストーク領域には 3–4 か所に糖鎖が付加しており、この NA を持つウイルスの赤血球遊離能が高い一方、糖鎖欠損ウイルスはアミノ酸欠失ウイルスと同様に赤血球遊離能が低かった。以上より、NA ストーク領域の糖鎖欠損はアミノ酸欠失と同様に NA の機能を低下させ、ウイルスのニワトリに対する病原性を増強させることを明らかにした。

インフルエンザ A ウイルスの NA はウイルス粒子上でシアル酸を遊離する機能を持つが、細胞内での成熟過程や機能は明らかになっていない。本稿第三章では NA の細胞内での機能を調べるため、インフルエンザ A ウイルスに感染した犬腎臓由来株化細胞（MDCK 細胞）の表面の糖鎖構造をレクチンにより解析した。その結果、ウイルスに感染した MDCK 細胞では非感染細胞と比較して、末端にガラクトースや α1-2 フコースを持つ糖鎖が増加していた。α1-2 フコース転移酵素はゴルジ体内に局在し、シアル酸転移酵素と拮抗することから、ウイルス感染細胞内で NA はシアル酸を遊離する機能を持つことが示唆された。また、ウイルス感染細胞上の糖鎖の経時的変化を観察したところ、感染 5 時間以降、脱シアリル化と α1-2 フコースの転移を認め、感染細胞内でのウイルスタンパク質の発現と経時的に一致した。これらの観察結果より、NA が粒子形成前の感染細胞内ですでに活性を有しており、脱シアリル化によりシアル酸転移酵素と拮抗する α1-2 フコース転移酵素に糖鎖修飾の機会を与えていることを示した。また、NA の細胞内での機能は感染細胞から出芽するウイルスのシアロ糖との相互作用を減らし、ウイルス放出を促進していると考えられる。さらに、NA の細胞内機能は細胞外での機能に加えて、感染細胞表面のシアロ糖を減らし、インフルエンザ A ウイルスの重感染の阻害に寄与していると考えられる。

以上、本研究により明らかになった知見は、インフルエンザ A ウイルスの生態と病原性発揮機構の解明に貢献するとともに、抗ウイルス薬の開発に対して新たな視点を提供するものである。本研究成果がインフルエンザ A ウイルス感染症の制圧および制御に資することが期待される。